Visualization of Exon Junction Complex (EJC) and related factors at transcription sites of *Drosophila* polytene chromosomes

Subhendu Roy Choudhury

Supervised by Dr. Saverio Brogna

A thesis submitted to

The University of Birmingham

For the degree of

DOCTOR OF PHILOSOPHY

School of Biosciences

College of Life and
Environmental Sciences

The University of Birmingham

September 2015

Summary

It was long believed that cytoplasmic events like translation and mRNA degradation are not linked to nuclear events such as pre-mRNA splicing. This view has been challenged in recent years by the discovery that pre-mRNA splicing can affect cytoplasmic processes such as nonsense-mediated mRNA decay (NMD). The current explanation is that this nucleus/cytoplasm communication is mediated by the exon junction complex (EJC), a multiprotein complex deposited during splicing in the nucleus and which remains associated with the mRNA during export to the cytoplasm. The consensus is that the EJC is deposited exclusively on spliced mRNA, 20-24 nucleotides upstream of the exon-exon junction. Splicing appears to deposit the EJC similarly in *Drosophila melanogaster*, yet it has also been reported that, in contrast to mammalian cells, the EJC might be required for splicing, suggestive of an earlier association with the pre-mRNA. The EJC appears to have an important role in the localization *oskar* mRNA to the posterior of the *Drosophila* oocyte. My PhD project aimed to visualize the assembly of the EJC on nascent RNA at polytene chromosome transcription sites. The main conclusion of these studies is that, contrary to current predictions, EJC components are recruited at transcription sites corresponding to both intron-containing and intron-less genes. A similar conclusion was reached in *Drosophila* S2 cells, where chromatin immunoprecipitation coupled with high-throughput sequencing (ChIP-seq) data indicate that the core EJC protein Y14 associates to transcription sites independently of the gene having introns. Additionally, here I also report the results of two parallel projects aimed at testing whether ribosomal proteins and the NMD protein UPF1 also associate with Pol II transcription sites. My results confirm the presence of additional ribosomal proteins at transcription sites and also indicate the presence of UPF1 at these sites.

Acknowledgements

Firstly, I would like to thank my supervisor Dr. Saverio Brogna for accepting me as a PhD student in his laboratory. His guidance and supervision allowed me to finish my PhD work on time. Secondly, I would like to thanks the Indian Government for providing a studentship for my PhD living expense in the United Kingdom.

I would also like to thank Dr. Alicia Hidalgo for her useful suggestion in my experiment, Dr. Paul Badenhorst for helping me to carry out the ChIP-seq experiments at IBR and also Dr. Aditi Kanhere for analysing the ChIP-seq data. I am also thankful to other PIs and other people on the 6th floor of Biosciences, who let me use their equipment, reagents and gave useful suggestions. I would like to express my thanks to Saverio's lab past members, particularly Preethi Ramanathan, Kim Piechocki and Dr. Jikai Wen for their valuable time and help during the initial stage of my PhD study. I am also grateful and thankful to the present lab members, particularly Tina McLeod and Marija Petrick for the time they put in helping me with the writing of thesis, and also Jianming Wang for being a good friend throughout the PhD. Thanks to the School of Biosciences, and University of Birmingham different events they organized for PhD students to fulfill my PhD study.

Last but not least, a special gratitude goes to my family for their patience and support throughout the whole four years and their sacrifice for me to complete my study.

SUBHENDU ROY CHOUDHURY

Dedication

This work is dedicated to my dearest parents Satyajit Roy Choudhury and Gita Roy Choudhury and my family members.

Table of Contents

List of Abbreviations

EJC	Exon Junction Complex
NMD	Nonsense-mediated mRNA decay
PTC	Premature termination codon
UPF	Up-frame shift
40S	Eukaryotic small ribosomal subunit
60S	Eukaryotic large ribosomal subunit
80S	Eukaryotic ribosomes
BSA	Bovine serum albumin
CBC	Cap binding complex
ChIP	Chromatin immunoprecipitation
DAPI	4’-6-diamidino-2-phenylinodole
DDAB	Dimethyl dioctadecyl ammonium bromide
EDTA	Ethylenediaminotetra-acetic acid
eEF1 / eEF2/ eEF3	Eukaryotic translation elongation factors
eIF3/eIF4AIII/eIF4G	Eukaryotic translation initiation factors
eRF1/eRF3	Eukaryotic release factor 1 and 3
FBS	Fetal bovine serum
FITC	Fluorescein isothiocyanate
GFP	Green fluorescent protein

RFP	Red fluorescent protein
HRP	Horseradish peroxidase
PABPC	Poly(A) binding protein, cytoplasm
Pol (I, II, and III)	RNA polymerases (I, II, and III).
RPs	Ribosomal proteins
SDS	Sodium dodecyl sulfate
TBS	Tris-buffered saline
TRIS	Tris(hydromethyl-amino)ethane
UAS	Upstream activating sequences
UTR	Untranslated region
WT	Wild-type
YFP	Yellow fluorescent protein
RNA	Ribonucleic acid
DNA	Deoxyribonucleic acid
RpL	Ribosomal protein large subunit
RpS	Ribosomal protein small subunit
PBS	Phosphate buffered saline
PMSF	Phenylmethylsulfonyl fluoride

Chapter 1

1.0 Introduction

1.1 Summary of eukaryotic gene expression

Gene expression of protein-coding genes is a process in which genetic information contained in DNA is transcribed into messenger RNA (mRNA) which is then translated into protein. This process is different between eukaryotic and prokaryotic organisms. In prokaryotes, transcription and translation are a coupled process and transcripts start to translate during their transcription. However, eukaryotes possess a nuclear envelope which separates the transcription that occurs in the nucleus, from translation which takes place in the cytoplasm. Whilst within the nucleus, the primary transcripts (pre-mRNAs) must undergo post-transcriptional modifications including 5'end capping, 3'end processing, and intron splicing (Figure 1.0). Following these processing the mature mRNA is then exported from the nucleus to the cytoplasm where it is translated by the ribosome.

1.1.1 Pre-mRNA processing

The first step of pre-mRNA processing is 5' capping during which a guanine nucleotide is added to the 5' end of pre-mRNA which is subsequently methylated to produce 7-methylguanosine (m^7G) (Shuman, 2001). This cap structure is recognized by the cap-binding complex (CBC), consisting of two proteins, cap-binding protein 80 (CBP80) and CBP20. The 5' cap protects the mRNA from 5'-3' exonuclease degradation, thus playing an important role in mRNA stabilization (Beelman and Parker, 1995). The 3' end processing reaction, which involves cleavage of the pre-mRNA and addition of a poly (A) tail at the 3'end (Colgan and Manley, 1997), results in transcription termination and release of RNA Polymerase II (Pol II) from the DNA template. The majority of eukaryotic protein-coding

genes contain non-coding sequences, termed introns, that are removed from the primary transcript, in a process called splicing, to produce a functional mRNA. Segments of the pre-mRNA that are retained in the mature mRNA are called exons. The splicing reaction is carried out by a large macromolecular complex, the spliceosome (Zhou et al., 2002). Additionally, transcripts of eukaryotic genes can undergo alternative splicing, which results in the production of different functional mRNAs from a single pre-mRNA molecule (Berget et al., 2000). Therefore, alternative splicing has the potential to produce several protein variants from a single gene and is partly responsible for increased diversity of proteins in higher eukaryotes (Hui, 2009). Moreover, in eukaryotes, some of the RNA such as tRNA, rRNA, mRNA also undergoes RNA editing process (Su and Randau, 2011). Although, RNA editing is rare compared to normal RNA processing as mentioned earlier, yet RNA editing responsible for great molecular diversity by addition, deletion or substitution of nucleotide bases within the RNA molecule.

Once the processing of pre-mRNA is complete, mature mRNA is then exported from nucleus to the cytoplasm through the nuclear pore complex (NPC). By the time the mRNA is exported, it associates with several proteins to form an mRNA-protein complex (mRNP) – the formation of the mRNP starts cotranscriptionally, possibly with the binding of the CBC to the cap as it emerges from Pol II, it involves a large number of proteins and depends, as detailed in the sections below, on pre-mRNA processing. The mRNPs undergo extensive remodelling as enter in the cytoplasm, yet some components which associated in the nucleus persist so that the structure and composition of the nuclear mRNPs influence downstream processes such as export, localization and translation and mRNA stability (Brodsky and Silver, 2000).

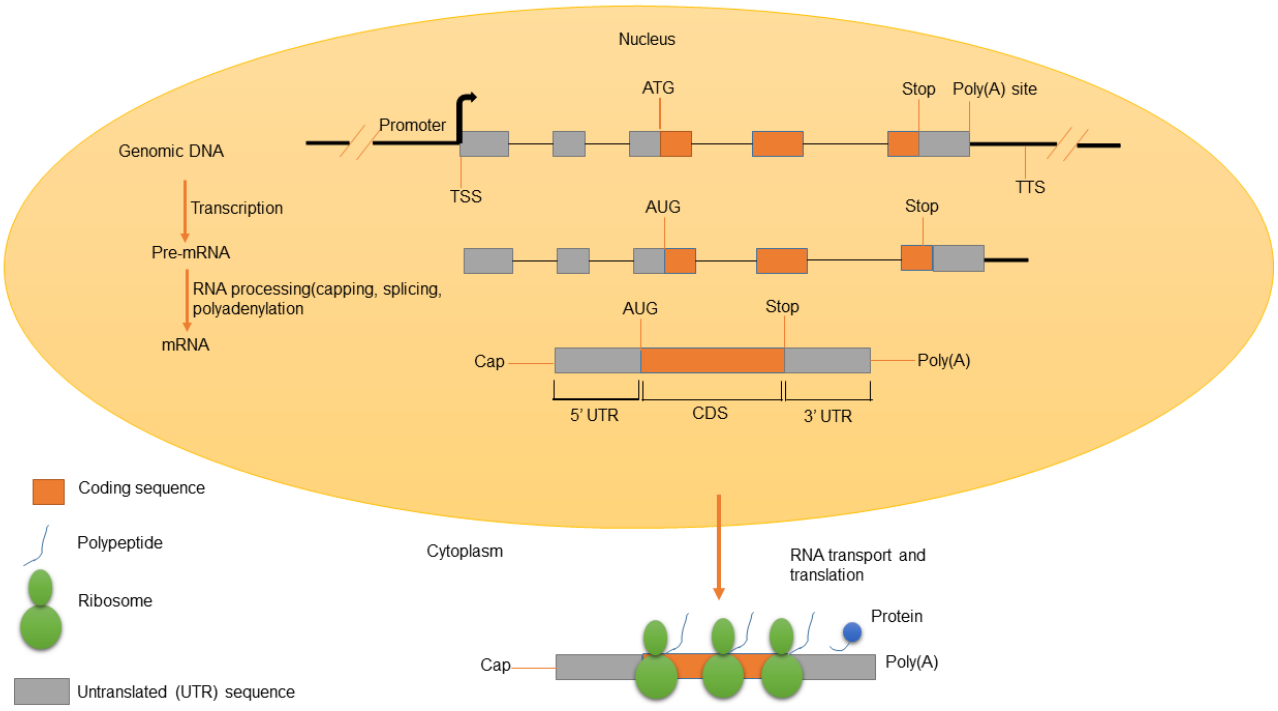

Figure 1.0 Schematic representation of eukaryotic gene expression. Gene expression in eukaryotes involves transcription of genomic DNA into pre-mRNA, which further undergoes several steps of processing, including 5' capping, splicing, and 3' polyadenylation, to produce mature RNA. Mature mRNA is then transported through the nuclear pore complex to the cytoplasm where it is translated into protein by the ribosome. This model is adapted from Zhang (2002).

1.1.2 Coupling of transcription and pre-mRNA splicing

Splicing is a multistep process catalysed by the spliceosome which consists of five small nuclear ribonucleoprotein complexes (snRNPs) each of which is composed of a small nuclear RNA (snRNA - U1, U2, U4, U5 or U6) and a number of associated proteins. Up to 300 different proteins have been identified to be associated with the spliceosome (Nilsen, 2003). Some of these proteins are specific to a certain snRNP while others are present in all (Will and Luhrmann, 2001). The first step in splicing is recognition of the 5' and 3' splice sites (SS); this is mediated by the U1 and U2 snRNP U1 binds to the 5'end of the intron, while U2 associates with the adenosine in the pyrimidine rich region known as the branch point (20-50nt upstream of the 3'SS). This binding occurs in an ATP-dependent manner and, as a result, the pre-spliceosomal A complex is formed. Subsequent binding of U4, U5 and U6 snRNPs as a tri-snRNP complex gives rise to the complex B or complete spliceosome (Sharma et al., 2008). Further structural arrangements are required to form the catalytically active spliceosome (C complex) which includes dissociation of U1 and U4 (Figure 1.1). However, in metazoan the second type of intron with different splice sites recognized by the second class of U12 spliceosome or minor spliceosomes. The minor spliceosome consists of U11, U12, U4atac and U6atac which are functionally analog of U1, U2 and U4/U6 of the major spliceosome (Hall and Padgett, 1996). Although minor spliceosome contains U12 snRNP instead of U2 snRNP, yet U12 dependent spliceosome follows the same splicing pathway as U2 dependent or major spliceosome.

Although it was believed that pre-mRNA processing is independent from transcription, it is now clear that all these reactions are in fact coupled to this process. Most introns are spliced while the 3' end of the pre-mRNA is still being synthesized by the RNA Pol II. Studies

performed by Carrillo Oesterreich (2010), using high-density tiling arrays for nascent RNA, indicate that splicing in yeast predominantly occurs co-transcriptionally. This is supported by additional chromatin immunoprecipitation (ChIP) experiments (Abruzzi et al., 2004; Gornemann et al., 2005). The carboxy-terminal domain (CTD) of RNA Pol II plays a key role in the coupling of splicing and other pre-mRNA processing reactions to transcription. The CTD serves as a platform for assembly of the pre-mRNA processing machinery and it is necessary for the efficiency of these processes (Phatnani and Greenleaf, 2006; Shatkin and Manley, 2000). The heptad repeats of Pol II CTD (26 in yeast and 52 in mammals) with the consensus sequence YS2PTS5PS7 undergo phosphorylation and dephosphorylation at several positions in such a way that enables RNA Pol II to associate with appropriate factors in different phases of the transcription cycle. Moreover, another *in vitro* study showed that CTD increases the rate of 5' capping and 3' end formation by functioning as a "landing pad" for processing factors, therefore facilitating their association with the nascent transcript or the correct assembly of these in multisubunit complexes (Carrillo Oesterreich et al., 2011; Perales and Bentley, 2009). One early study reported that deletion of CTD results in defects in 3' end processing, splicing and transcription in human cells (McCracken et al., 1997). Co-transcriptional splicing was first observed in *Drosophila* embryos by electron microscopy (Beyer and Osheim, 1988) as well as in further biochemical experiments in *Drosophila* salivary glands (LeMaire and Thummel, 1990). Moreover, an *in vitro* study in HeLa cells revealed that the assembly of the spliceosome on RNA Pol II transcript is proportional to the rate of its synthesis therefore, immediate spliceosome assembly, increased yields of spliced mRNA and increase in the kinetics of splicing spliceosome (Das et al., 2006). Pol II elongation rate also appears to be a critical factor for co-transcriptional splicing, as mutation which induces lower Pol II elongation rate results in increased co-transcriptional splicing efficiency. In yeast and mammals, alternative splicing depends on the Pol II elongation rate

(de la Mata et al., 2010; Kadener et al., 2001). Also, it has been suggested that efficient cotranscriptional splicing may require a pause in Pol II elongation around the 3'SS (Alexander et al., 2010). Transcriptional pause release is recognized as an important step of gene expression regulation in mammals (Adelman and Lis, 2012). The transition from this paused state to elongation state requires the recruitment of positive transcription elongation factor b (P-TEFb), a cyclin-dependent kinase that is normally localized in an inhibitory complex containing 7SK noncoding RNA (Peterlin and Price, 2006). A recent report indicates that a splicing factor, specifically serine/arginine–rich splicing factor 2 (SRSF2), is a part of 7SK complex assembled at gene promoters and has a direct role in transcriptional pause release (Ji et al., 2013). Thus, the function of SRSF2 in transcription activation further indicates co-regulation of gene expression at both transcriptional and posttranscriptional levels in mammalian cells. SR proteins are a family of RNA-binding proteins that play an important role in splicing (Lin and Fu, 2007) and colocalize with 7SK in nuclear speckles, specific nuclear domains that are enriched in splicing factors. Additionally, previous studies have reported that a delay in transcript release may be required for complete processing in yeast (Schmid and Jensen, 2010).

Recent studies of nascent transcripts in *Drosophila* indicate that fifty percent of introns are spliced co-transcriptionally, while the remaining ones are either poorly spliced or retained in the mature mRNA (Khodor et al., 2011). Co-transcriptional splicing also depends on factors such as intron length, intron number, exon length (Neugebauer, 2002). Several lines of evidence also suggest that the longer the gene is, the greater the chance of splicing of the nascent transcript (Beyer and Osheim, 1988). In addition, a recent cotranscriptional splicing study in mouse suggest that gene length and position strongly affects the efficiency of cotranscriptional splicing (Khodor et al., 2012).

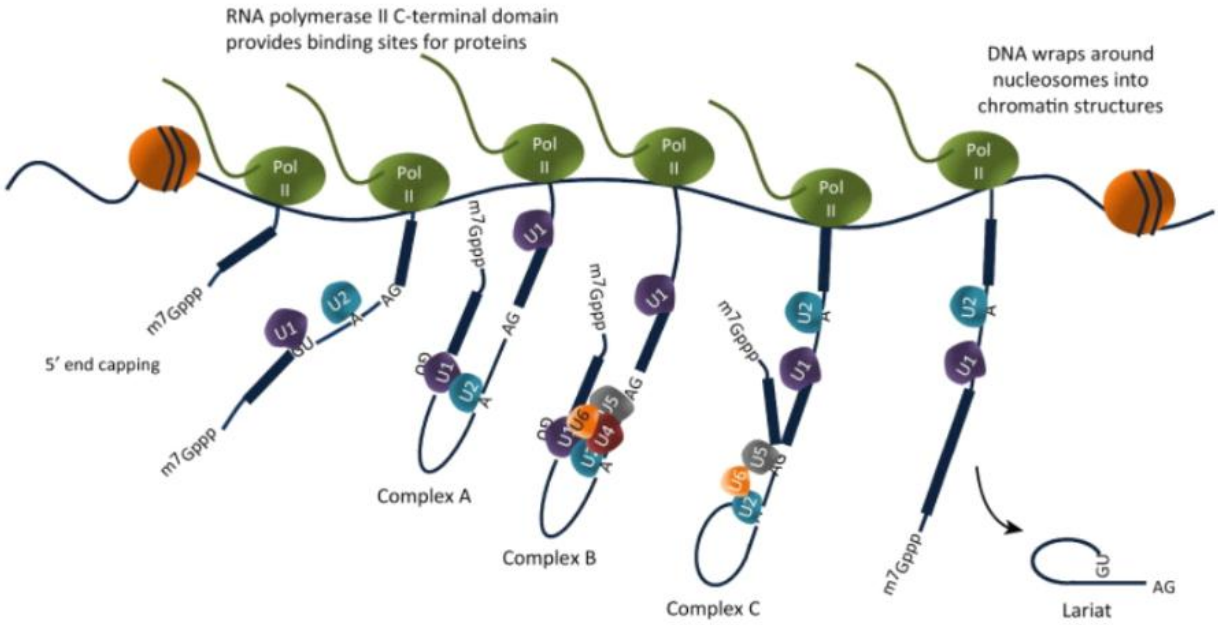

Figure 1.1 Schematic representation of co-transcriptional splicing. During transcription C-terminal domain of Pol II acts as a binding platform for several other proteins involved in pre-mRNA processing, splicing and export of mature mRNA. Pre-mRNA transcribed by Pol II associates with spliceosome components (U1, U2, U4, U5, and U6 snRNPs) in a step-wise manner so that introns are removed in a process called splicing. The first step involves the formation of complex A in which U1 and U2 are recruited to the 5' splice site and the branch point A respectively. In the subsequent step recruitment of U4, U5 and U6 leads to the formation of complex B, which undergoes further rearrangements to form active complex C. These rearrangements cause two exons to ligate while intron is released in the form of a lariat. This figure was taken from Mandy S. Wong and Collaborators (2014).

1.2 Eukaryotic cell compartmentalization and the bridge between transcription and translation

The distinctive feature of eukaryotic gene expression is that translation occurs only in the cytoplasm. However, coordination between transcription and translation is required to express genes accurately and efficiently. In case of prokaryotes, this is achieved directly, by physical coupling between the RNA polymerase and ribosomes which are loaded on the nascent transcript (Proshkin et al., 2010). Since in eukaryotes the nuclear envelope separates the nucleus from the cytoplasm, such direct coordination does not occur; transcription and RNA processing take place in the nucleus and translation in the cytoplasm. However, some studies indicate that pre-mRNA splicing, as a nuclear process, enhances cytoplasmic events such as nonsense mediated mRNA decay (NMD), outlined in the next section, which is coupled to translation (Carter et al., 1996). These studies suggest that there must be some means by which mRNAs that have been spliced are differentiated from otherwise identical transcripts generated from intron-less genes. The discovery of the exon junction complex (EJC), a number of proteins deposited on mRNA during splicing and transported along with it to the cytoplasm, provides an explanation. Next I will review the NMD phenomenon and published data that provide a model of how the EJC could coordinate splicing and NMD.

1.2.1 Nonsense Mediated Decay (NMD)

NMD is a translation dependent process found in all eukaryotes that rapidly destroys mRNA containing a premature translation termination codon (PTC) (Muhlemann et al., 2008). NMD is thought to reduce the accumulation of proteins derived from PTC-containing mRNAs that could be detrimental to survival. NMD targets are originally identified as point mutations in the DNA which generated PTCs, but have since been found to arise from errors during transcription or pre- mRNA processing (Chang et al., 2007). NMD has been more intensely studied in *Saccharomyces cerevisiae, D. melanogaster, Caenorhabditis elegans* and mammalian cells (Amrani et al., 2004; Le Hir et al., 2001). All these studies indicate that NMD is an active process which requires mRNA translation and specific trans-acting factors. These include the up-frameshift proteins (UPF) encoded by the *upf1, upf2,* and *upf3* genes, which were first discovered in a genetic suppressor screen in *S. cerevisiae* (Cummins et al., 1980). A similar study also identified seven genes encoding NMD factors (SMG1-7) in *C. elegans*, The NMD factors UPF1, UPF2, and UPF3 are homologous to SMG-2, SMG-3 and SMG-4 in *C. elegans*. These three proteins are highly conserved in all eukaryotic organisms and deletion of one of these genes, particularly UPF1 or UPF2, result in stabilization of PTC-containing mRNAs (Conti and Izaurralde, 2005; Perlick et al., 1996).

UPF1 is considered to be the key component of NMD and current models suggest that it forms a surveillance complex by interacting with eukaryotic translation release factors (eRF1 and eRF3) together with UPF2, UPF3 and exon junction complex (EJC) proteins to degrade PTC-containing mRNAs in the cytoplasm (Leeds et al., 1991). The UPF proteins associate

together to form an active complex which carries out NMD from yeast to humans (Conti and Izaurralde, 2005). However, a key outstanding question is how the cell distinguishes between those mRNAs that contain PTCs and those which possess normal stop codons. One model, known as faux 3'UTR model, predicts that this distinction depends on the distance between the stop codon and the 3' end of the mRNA (Amrani et al., 2004; Behm-Ansmant et al., 2007). The other model, as reviewed below, predicts that the PTC can be recognized by the presence of one or more downstream introns, which instead are typically not present in standard 3'UTRs.

1.2.2 EJC stimulates NMD in mammalian cells

Studies in mammalian cells indicate that a PTC is distinguished from a normal stop codon by its position relative to an exon-exon junction (Zhang et al., 1998). When a PTC is located more than 50-55 nucleotides upstream of last exon-exon junction the mRNA is targeted for rapid degradation (Zhang et al., 1998). This has been explained by the presence of EJC proteins, which are deposited on a spliced mRNA ~20-24 nucleotides (nt) upstream of the exon-exon junction; this binding is sequence independent, but position dependent (Figure 1.2) (Le Hir et al., 2000a). This model provides a very plausible account of how splicing and NMD are linked. According to this model, during translation, when a ribosome reaches a stop codon upstream of the EJC, it serves as a binding platform for NMD factors which initiate mRNA degradation (Figure 1.3).

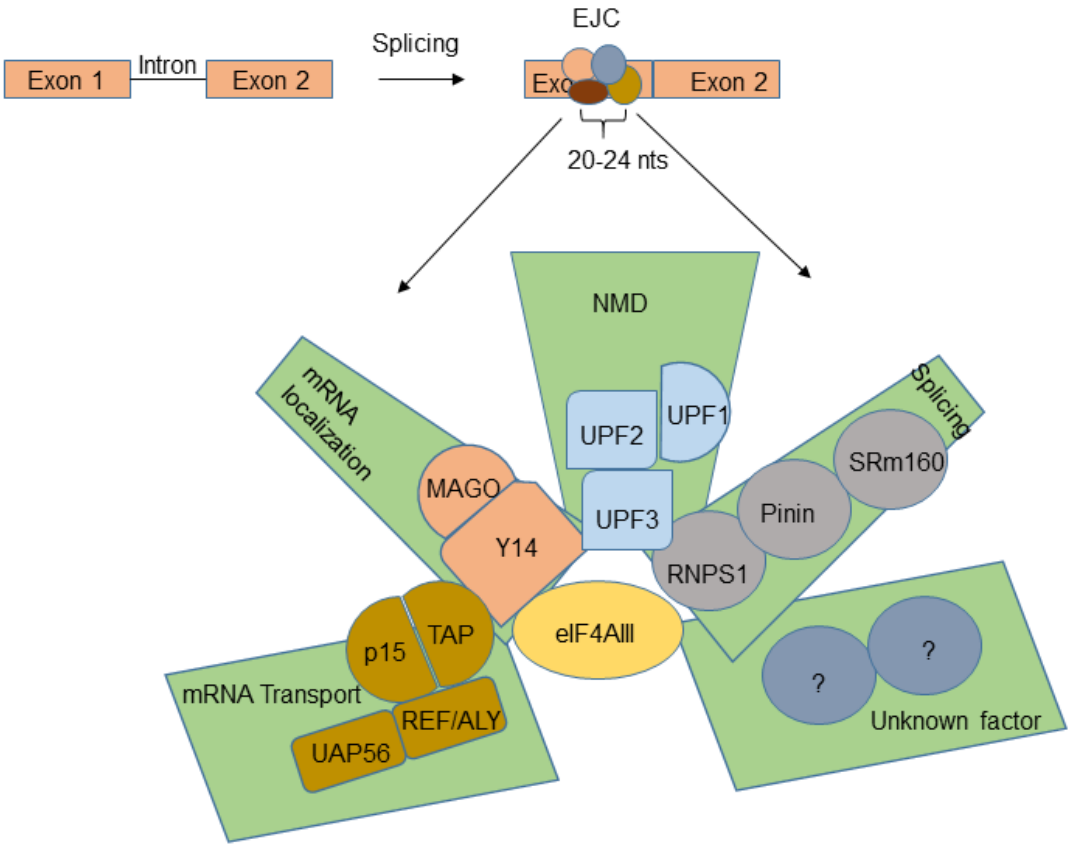

Figure 1.2 Association of the EJC with spliced mRNA enables interaction with associated factors. The EJC is deposited 20-24 nt upstream of an exon-exon junction during splicing. The EJC bound to a spliced mRNA creates a platform for other peripheral factors to assemble. Most of these factors are transiently associated with the EJC and their functions include NMD, mRNA transport, splicing, and mRNA localization. This image was modified from Tange and Collaborators (2004).

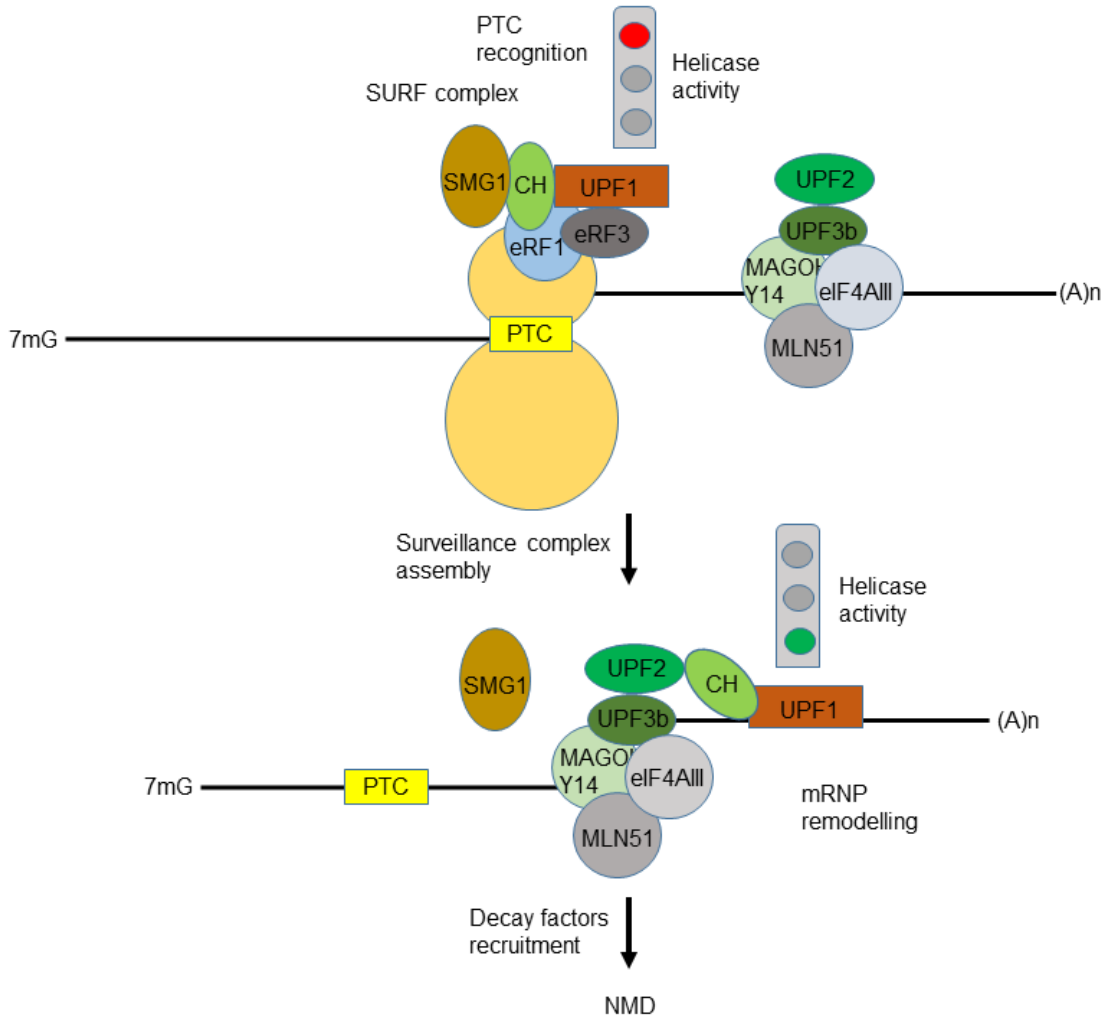

Figure 1.3 The EJC forms a surveillance complex with NMD factors to degrade PTC-containing mRNAs. During translation, the ribosome stalls at a PTC, allowing recruitment of UPF1 along with eRF1, eRF3, and SMG-1, forming the SURF complex. SURF then interacts with a downstream EJC, leading to SMG-1 mediated phosphorylation of UPF1 and further intecration with EJC-bound UPF2, leading to the formation of a surveillance complex, which degrades the PTC-containing mRNA. This image was modified from Chamieh and Collaborators (2008).

The EJC contains four proteins at its core: Y14 and MAGO, which form a heterodimer, eukaryotic translation initiation factor 4AIII (eIF4AIII) (Tange et al., 2004) and metastatic lymph node 51 (MLN51) (Barentsz or Btz in *Drosophila*) (Degot et al., 2004). These core EJC components allow it to interact in a dynamic manner with peripheral factors involved in splicing, mRNA localization, EJC assembly and the latter stages of mRNA metabolism (Figure 1.2). In the cytoplasm, apart from having a role in NMD, EJC components Y14, MAGO and RNPS1, when tethered to an artificial reporter, enhance the translation yield from intronless mRNAs (Nott et al., 2004). In *Xenopus* oocytes, spliced mRNAs yield more protein than identical mRNAs produced from intronless genes. Thus, it has been concluded that splicing can enhance translation (Matsumoto et al., 1998).

It has been proposed that eIF4AIII is the only component of the EJC in direct contact with the RNA, and it is with this that Y14 and MAGO interact before export to the cytoplasm (Ballut et al., 2005). eIF4AIII is a DEAD-box protein and belongs to the subgroup of DExH/D-box family of RNA-dependent ATPases, which bind to the RNA directly (Shibuya et al., 2004). The crystal structure of the three-dimensional core of the EJC explains how these components are organized into a complex (Bono et al., 2006). The structure of the EJC core is L- shaped with eIF4AIII and Btz at the base and the Y14-MAGO heterodimer arranged perpendicularly to it (Figure 1.4) (Bono et al., 2006). In the presence of ATP eIF4AIII adopts a closed conformation and binds to the RNA. Y14–MAGO forms a stable heterodimer with a molecular mass of about 40 kDa on spliced mRNAs and is considered to be a nuclear shuttle protein, which is imported back to the nucleus by Importin 13 (Imp13), a protein transport factor belonging the karyopherin-beta family (Bono et al., 2010). Although Y14 has an RNA recognition motif (RRM), its RNA binding site is buried when in association with MAGO (Fribourg et al., 2003). Thus, rather than binding to RNA, the main function of the Y14-

MAGO heterodimer is to inhibit ATP hydrolysis of eIF4AIII, so that eIF4AIII effectively locks onto the RNA. This explains the remarkable ability of the EJC to persist through nuclear export and cytoplasmic localisation (Ballut et al., 2005). As described above, the Y14-MAGO heterodimer has been shown to increase the translation of spliced mRNAs and both are also required for cell viability (Mohr et al., 2001). Additionally, a mutated form of Y14, which prevents its interaction with MAGO, leads to stabilization of NMD substrates. These observations suggest that Y14 and MAGO interaction is also crucial to elicit NMD (Kim et al., 2001).

It has been reported that eIF4AIII is recruited to the spliceosome during the early step of splicing rather than after splicing (Gehring et al., 2009). The mechanism of EJC loading during splicing was not clear until recent reports showed that the spliceosome component CWC22 interacts directly with eIF4AIII via a specific domain, which probably drives the splicing-dependent assembly of EJCs (Figure 1.5) (Barbosa et al., 2012; Steckelberg et al., 2012). CWC22 is an abundant component of the activated spliceosomal C complex (Bessonov et al., 2010).

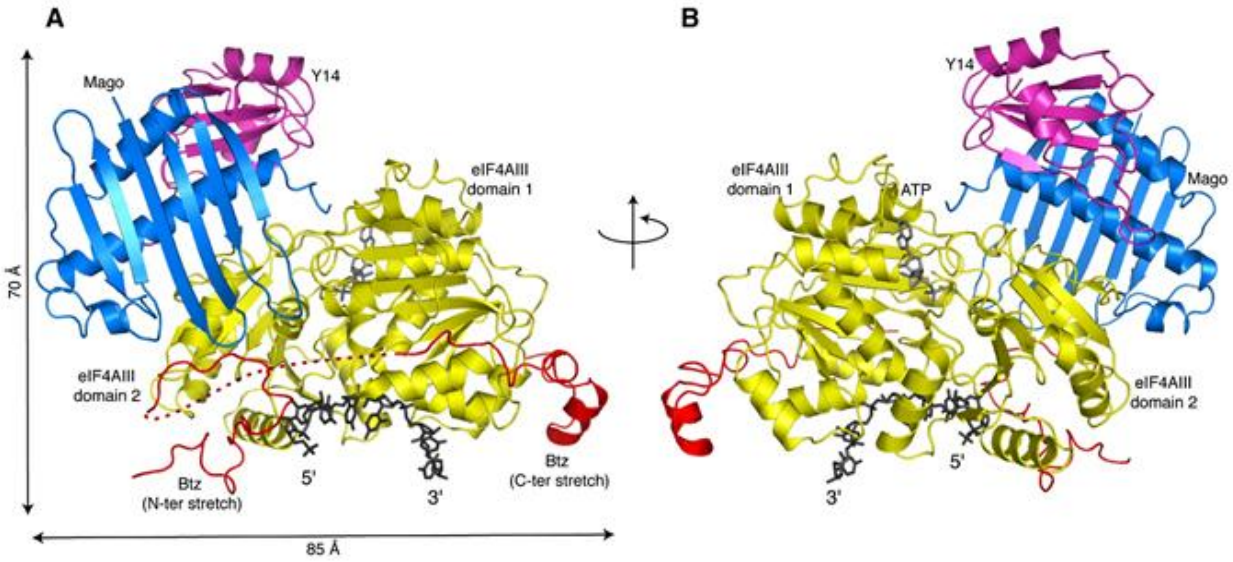

Figure 1.4 Three-dimensional representation of the arrangement of core EJC components. Human EJC seen here in two orientations rotated by 180^0 about a vertical axis. In this model, Btz, marked in red, stretches over eIF4AIII (yellow). RNA (black line) interacts with two RecA-like domains of eIF4AIII. MAGO (in blue) and Y14 (in magenta) bind to domain 2 of eIF4AIII, and this interaction surface also included domain 1 of eIF4AIII. The dotted red line indicates the approximate position of a region of Btz not present in the X-ray structure. This image was taken from Bono and Collaborators (2006).

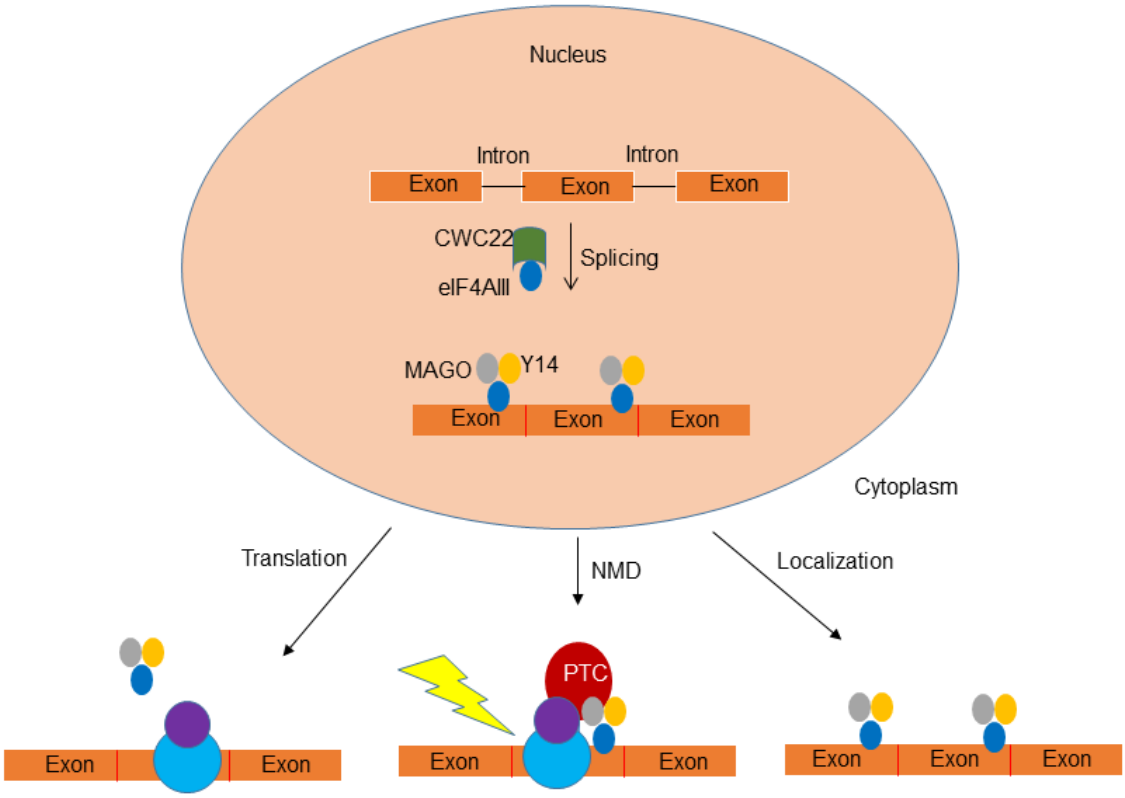

Figure 1.5 The EJC component eIF4AIII is deposited during early steps of splicing. The interaction of the EJC core component eIF4AIII with splicing factor CWC22 creates a platform for other core factors, Y14 and MAGO, enabling their deposition on spliced mRNAs. Once the EJC has associated with spliced mRNA, it assists in guiding the mRNA through the nuclear pore complex to the cytoplasm. In the cytoplasm, the EJC has a role in enhancing translation, degrading PTC-containing mRNAs and localizing mRNAs to their specific location.

1.2.3 Canonical and non-canonical form of EJC

Previously, most research into the mammalian EJC was conducted, either *in vitro* or *in vivo*, with artificially tethered reporter RNAs or expressed proteins (Bono and Gehring., 2011). However, the most recent studies into endogenous EJC proteins show that in fact EJCs multimerize together with numerous SR proteins to form mega-Dalton sized complexes, in which SR proteins are super-stoichiometric to the EJCs core factors (Singh et al., 2012). These complexes, termed high molecular weight (HMW) EJCs, probably protect long stretches of RNA from nuclease digestion. Immunoprecipitation experiments confirmed the presence of the SRSF1, SRSF3, and SRSF7 SR proteins within the HMW complex. In these studies, as expected, most of the EJC deposition sites were at the 24 nucleotide position upstream of the last exon-exon junction. EJCs located in this position are termed canonical EJCs (cEJCs), however, recent RNA seq data indicate EJC binding is not always at such sites and enrichment is also found at other exonic locations, termed non-canonical EJC (ncEJC) sites (Singh et al., 2012). Unlike cEJCs, whose binding is sequence independent, ncEJCs are mainly observed to bind specific sequences including CG-rich motif regions in the first exon, C-rich motifs regions which resemble high affinity binding sites for SRSF3 in internal exons and AG-rich motif regions resembling the binding site for SRSF1 (Singh et al., 2012).

In a similar cross-linking immunoprecipitation (CLIP) study, which was followed by high-throughput sequencing of eIF4AIII, one of the EJC's core components was found to occupy both canonical and non-canonical regions (Sauliere et al., 2012). Remarkably, cEJCs and ncEJCs share similar features. There is no enrichment of either cEJCs or ncEJCs on the exons of intron-less mRNAs, while they are found in the CDS of spliced mRNAs and specifically

associated with exons flanked by long introns (Sauliere et al., 2012). Moreover, both CLIP-seq and mRNA-seq data of two spliced mRNAs showed that eIF4AIII occupancy varies between the exon junctions from the same transcript, raising the question of whether other factors influence the presence of the EJC on spliced mRNAs (Sauliere et al., 2012). Analysis of the sequence motif region for eIF4AIII indicates enrichment associated with a GAAGA region at both canonical and non-canonical sites. Interestingly, GAAGA regions are higher affinity binding sites for SR proteins. This observation suggests that the binding of the EJC is not uniform across exon-exon junction, as reported earlier. In addition, the EJC forms a tight molecular bond with SR proteins, as previously reported in an *in vitro* study (Le Hir et al., 2000b). Therefore, it is possible that SR proteins, or other RNA binding factors, directly or indirectly modulate the binding of the EJC to a particular site.

1.2.4 The EJC is deposited at splice junctions also in *Drosophila*

The EJC core proteins are well conserved in *Drosophila*; where Y14, MAGO and MLN51 are also known as Tsunagi, Mago Nashi and Barentsz (BTZ) respectively (Macchi et al., 2003; Mohr et al., 2001; Palacios et al., 2004). The core components eIF4AIII, Y14 and MAGO are mostly localized in the nucleus (Le Hir et al., 2001; Palacios et al., 2004). Although BTZ considered as a core EJC component, evidence suggests that BTZ associates with the EJC after mRNA export to the cytoplasm (Macchi et al., 2003). As described above eIF4AIII interact with splicing factor CWC22 and recruited early step of splicing, whereas MAGO and Y14 bind during excision of intron and exon ligation (Ballut et al., 2005). Association of BTZ further stabilizes the EJC core on the mRNA in the cytoplasm (Bono and Gehring, 2011). A study into the Y14-MAGO heterodimer carried out in *Drosophila*, showed that it is required for the localization of *oskar* mRNA, a gene involved in *Drosophila* embryonic development, to the posterior pole of the oocyte (Hachet and Ephrussi, 2001). In

addition, mutant forms of either of the two proteins lead to mislocalization of *oskar* mRNA in *Drosophila* oocytes (Mohr et al., 2001). Recent findings reported that partner of Y14 and MAGO (PYM), a cytoplasmic protein in *Drosophila*, enables the dissociation of the EJC from *oskar* mRNA, which leads to its mislocalization and female infertility (Ghosh et al., 2014). Additionally, Y14 and MAGO are also required for germline stem cell differentiation and oocyte maturation (Parma et al., 2007). Unlike the mammalian heterodimer, *Drosophila* Y14-MAGO does not have any role in NMD (Gatfield et al., 2003).

Although the majority of research focuses on the EJC's role in post-splicing events, some recent data in *Drosophila* has shown that it could exist initially as a pre-EJC which influences the splicing process itself (Ashton-Beaucage et al., 2010; Roignant and Treisman, 2010). Evidence from these studies suggests that the pre-EJC plays an important role in splicing of a specific subset of primary transcripts, including mitogen activated protein kinases (MAPK) pre-mRNA, and in the absence of pre-EJC subunits, MAPK mRNA levels are significantly reduced. Based on their model, binding of the EJC occurs before splicing, and loss of the EJC from those sites results in exon skipping during splicing (Figure 1.6). This demonstrates another role for the EJC, that of influencing the processing of a specific set of transcripts in the nucleus. Moreover, it has also been proposed that pre-mRNA having large introns are more sensitive to depletion of pre-EJC, which result in exon exclusion indicates that the EJC has a role in exon definition of long intron-containing genes (Ashton-Beaucage et al., 2010). In a similar study it has been reported that the EJC is required for splicing of intron 4 of the piwi transcript, (a small non-coding RNA) and lack of the EJC results in splicing defects of this intron (Hayashi et al., 2014) .

In summary, the EJC seems to have diverse functions, both in the nucleus and the cytoplasm, which further indicates that it plays an important role in coupling nuclear and cytoplasmic events in gene expression.

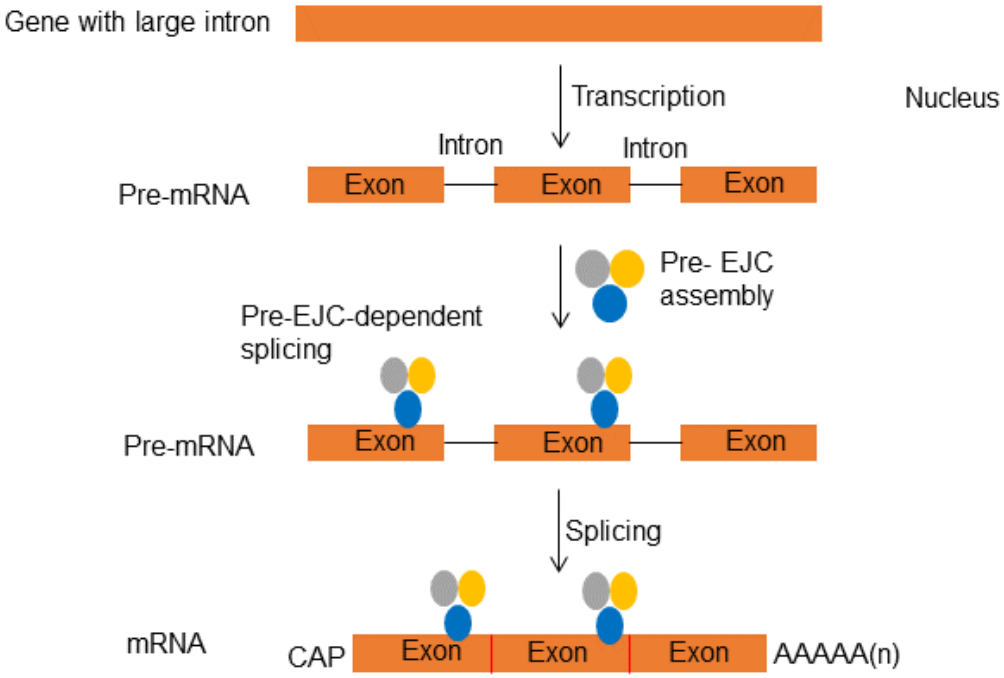

Figure 1.6 Pre-EJC dependent splicing. The EJC binds to pre-mRNA before splicing and aids in splice site selection. A lack of the pre-EJC from that site results in exon skipping. This image was modified from Roignant and Collaborators (2010).

1.3 Nuclear Translation

1.3.1 PTC recognition in the nucleus

Although the EJC model provides a reasonable explanation of how splicing could affect NMD, and translation, other data from the NMD field indicate that PTC-containing mRNAs might also be degraded in the nucleus. Early studies suggest that many mammalian mRNAs are down-regulated by NMD in the nuclear fraction (Belgrader et al., 1994; Chang and Kan, 1979; Urlaub et al., 1989). Additionally, it has also been reported that scanning of mRNA occurs either in the nucleus or when it is still associated with the nucleus before entering the cytoplasm (Maquat and Carmichael, 2001). Earlier evidence that nonsense mutations in the human triosephosphate isomerase (TPI) gene lead to the reduction of 25% of normal mRNA in the nucleus further support the suggestion that NMD is a nucleus-associated event (Belgrader et al., 1994). In addition, there is evidence from mammalian systems suggesting that NMD may take place in the nucleus (Chang and Kan, 1979).

The discovery of the cap binding complex (CBC) further supports the idea that NMD occurs on newly synthesized mammalian mRNAs. The cap binding complex (CBC) consists of the CBP20 and CBP80 subunits that bind to the 5' cap of nascent mRNAs during transcription and are required for stability of the mRNA (Leeds et al., 1992). During the pioneer round of translation, CBP80 is replaced by cytoplasmic translation initiation factor eIF4E (Maquat et al., 2010). However, the study suggests that PTC recognition occurs while mRNA still bound with CBP80 before replace with cytoplasmic eIF4E, therefore NMD does occur with CBP80 associated mRNA not with eIF4AE associated mRNA (Ishigaki et al., 2001). Therefore, CBP80-bound mRNAs harbouring a PTC are the primary targets of NMD, rather than eIF4E-

bound mRNAs during the pioneer round of translation. In addition, NMD factors UPF2 and UPF3 are also observed to associate with spliced mRNPs when immunopurified with an anti-CBP80 antibody (Ishigaki et al., 2001). However, this may suggest that nuclear NMD occurs during a pioneer round of translation of mRNAs which have not yet been released from the nuclear envelope. Moreover, in a parallel study it was also reported that EJC components co-immunopurified with CBP80 but not with eIF4E (Lejeune et al., 2002). In addition, it is also reported that the level of mRNAs bound by the CBP80 subunit decreases in the presence of PTC. In contrast, there is no such decrease in mRNA levels observed when bound by eIF4E, further indicating that NMD acts only on CBP80-bound mRNAs (Cui et al., 1995).

However, it is also proposed that PTC recognition occurs on nascent transcript and this idea is supported by experiments showing that PTCs can affect specific nuclear events, such as alternative splicing and 3' end formation (Brogna, 1999; Wang et al., 2002) . Moreover, a ChIP study indicated that SMG6 and UPF1 associate with transcription sites of both PTC+ and PTC– reporter genes in mammalian cells, suggesting that NMD may occur co-transcriptionally (de Turris et al., 2011). Taken together, the evidence suggests that PTC recognition, and therefore translation, might also occur in the nucleus, possibly close to sites of pre-mRNA synthesis.

1.3.2 Controversial issue with nuclear translation

The hypothesis that some translation occurs in the nucleus remains debated. The debate has been re-opened following the observation that some NMD also occurs in the nucleus. Thus, it has been proposed that NMD mechanism utilizes active nuclear ribosomes (Wilkinson and Shyu, 2002). More recently, direct evidence for nuclear translation was provided by experiments that allow visualization of translation sites in mammalian cells (Iborra et al., 2001). It was reported that fluorescently labelled amino acids could be incorporated into nascent peptides in highly purified nuclei. In this assay, putative translation sites were readily

visible under a fluorescence microscope and appeared as distinct fluorescent dots. The occurrence of this nuclear fluorescence was prevented by translation inhibitor drugs.

In *Drosophila*, similar observations were reported and found that [35S] methionine/cysteine was rapidly incorporated at active transcription sites of polytene chromosomes and also in the nucleolus; this incorporation is sensitive to translation inhibitor drugs (Brogna et al., 2002). In addition, many ribosomal proteins and some translation factors are found associated with transcription sites, and an in-situ hybridization study showed that rRNAs are also present at these chromosomal sites (Brogna et al., 2002). It was argued, that the nuclear translation reported by Iborra et al (2001) may be an artefact of over-permeabilization that allowed entry of cytoplasmic ribosomes into the nucleus (Nathanson et al., 2003). Additionally, it was also argued that the antibodies used by Brogna et al to detect ribosomal proteins were not sufficiently specific. However, one study in yeast suggests that ribosomal proteins also present at chromosomal sites (De et al., 2011; Schroder and Moore, 2005). In addition, fluorescent protein tagging recently confirmed the presence of ribosomal proteins at *Drosophila* polytene chromosomes (Rugjee et al., 2013). This further observation is consistent with previous observations made by Brogna et al (2002). Furthermore, it has very recently been reported that puromycin can be incorporated into the nucleus and nucleolus of mammalian cells, and it was concluded that translation therefore must occur at these sites (David et al., 2012). In this study, they developed a novel technique known as ribopuromycylation in which the usually released puromycylated peptide is immobilized on ribosome by translation elongation inhibitor drugs, followed by detection of these nascent chains with an antibody specific to puromycin. It has however been argued that puromycylation is an indicator of peptidyl transferase activity, and not necessarily of 80S engaged in translation (Dahlberg and Lund, 2012). The question of whether translation can occur in the nucleus was therefore, unanswered at the start of my PhD.

1.0 Aims, and research plan

I would like to advance our understanding of the mechanism that links pre-mRNA splicing with NMD. The results of a number of studies across organisms show that pre-mRNA splicing, a strictly nuclear process, affects NMD, a process expected to be restricted to the cytoplasm. It has been proposed that this link is mediated by the exon junction complex (EJC), a multiprotein complex deposited during splicing in the nucleus, which remains associated with the mRNA during export to the cytoplasm. Some observations are not consistent with this function attributed to the EJC. For example, all of the proteins that constitute the EJC are well conserved in *Drosophila*, yet these proteins are not required for NMD in this organism. Since splicing is a co-transcriptional process in *Drosophila*,

- I aimed to visualize the association of EJC proteins at the sites of transcription at which nascent RNA is present, in the polytene chromosome. If these proteins do associate with transcription sites, I will then directly test key predictions of current models such as that EJC proteins are recruited selectively at intron-containing genes and will also assess whether EJC assembly differs depending on specific intron features.

- In my second project I will investigate whether there are functional ribosomes and ribosomal proteins at transcription sites and whether there is a link between these ribosomes and NMD. I plan to investigate the presence of both ribosomes and ribosomal proteins at transcription sites by using the same approach as used for EJC proteins. In parallel, I will use a similar experimental approach to visualize nascent

RNPs and pre-mRNA splicing at the site of transcription, which will give us a better understanding of the proteins associated during splicing such as the EJC.

Chapter 2

2.0 Materials and Methods

2.1 Solutions and buffers

All buffers, solutions, and media were prepared according to standard protocols described in Molecular Cloning 4th edition (Sambrook et al., 2012). Molecular biology kits were used as directed by the company, unless otherwise stated. All solutions were prepared with analytical grade reagents (Sigma-Aldrich, Fisher Scientific or VWR) in double distilled water and subsequently sterilized by autoclaving or by filtration through a 0.22 µm filter (Pall Corporations). Solutions used for RNA experiments were treated with diethylpyrocarbonate (DEPC, 0.1% v/v), incubated overnight in a laminar flow hood and subsequently sterilized by autoclaving the next morning.

2.2 *Drosophila* Schneider 2 cells (S2 cells) culture and maintenance

The S2 cell line derives from a primary culture of late stage (20-24 h old) *Drosophila melanogaster* embryos (Schneider, 1972). S2 cells are easy to maintain as they normally grow at room temperature without CO_2 and form a semi-adherent monolayer in tissue culture flasks. S2 cells were maintained in T25 tissue culture flasks in Insect–XPRESS medium (Lonza) supplemented with 10% (v/v) fetal bovine serum (FBS) and 1% (v/v) Penicillin-Streptomycin-Glutamine (P/S/G) (Invitrogen), incubated at 27°C without CO_2. S2 cells were normally split in a 1:5 ratio of cells to media into a fresh tissue culture flask every two days until the confluence reached ~70%-80%.

2.2.1 Transfection of S2 cells

To carry out transfection, cells were seeded at a 3 X 10^6 cells/well in a 6 well plate with complete media (10% v/v FBS and 1% v/v P/S/G) and were grown at 27ºC. The following day, transfection was carried out by mixing plasmid DNA (2.5 µg/ml per well) with 5µl of 4 mg/ml of the transfection reagent dimethyldioctadecylammoniumbromide (DDAB, Sigma-Aldrich) as described in Ramanathan and collaborators (2008). DNA was thoroughly mixed with DDAB and incubated for 30 min at room temperature. Meanwhile, cells were washed twice with 1 ml serum-free media (no FBS and P/S/G). Following incubation, the whole transfection mix was diluted with serum-free media to a final volume of 1 ml shaken vigorously to ensure thorough mixing, then transferred into the well of the cell culture plate. The cell culture plates were kept in the 27^0C incubator for 2 h and 30 min. After incubation, the transfection mix was carefully removed from the well and replaced with 2 ml 10% (v/v) complete media (10% v/v FBS and 1% v/v P/S/G,) and returned it is only similar with those with to 27^0C incubator for a further two days.

2.3 Chromatin Immunoprecipitation (S2 cells)

2.3.1 Cross-linking and sonication

S2 cells were grown in a T75 tissue culture flask at 27°C in 15 ml of Insect–XPRESS medium (Lonza) supplemented with 10% (v/v) fetal bovine serum (FBS) and 1% v/v P/S/G (Invitrogen) for 2 days. The cells were counted with a haemocytometer and 10^7 cells were used for each ChIP. Cells were fixed by adding formaldehyde (10% EM grade, Polyscience) to a final concentration of 1% (v/v) and incubated at 25°C for 15 min. After fixation, glycine was added to the cell mixture at a concentration of 125mM, followed by incubation another 5 min at 25°C to stop the cross-linking reaction. Next the cells were pelleted by centrifugation

at 3000 rpm/ 835 g (Eppendorf) for 5 min at 4°C. The cell pellet was resuspended in 500 µl of 1X PBS with one tablet of EDTA-free Complete Protease Inhibitor Cocktail (Roche) and washed for two times. After washing, the supernatant was discarded, and cell pellets were stored at -80°C for further used in a ChIP experiment.

2.3.2 Sonication optimization

Sonication is one of the key steps for successful ChIP as it renders the chromatin soluble and dictates the resolution of the assay. Normally the DNA fragment size used in a ChIP experiment is 200 – 1000 bp. Sonication conditions should be optimized for different cell lines, and the sonication efficiency depends on the cell line, cell density, and the extent of cross-linking. Sonication was performed with Biorupture (Diagenode). Conditions were optimized using S2 cells with different time intervals and a pulse of 15 seconds on and 15 seconds off, to produce DNA fragments in the range of 0.5-1.0 kb in size. The fragment sizes were checked by agarose gel electrophoresis (Figure 2.1). Judging from the gel, sonication carried out between 8 and 16 minutes produced the desired sized fragments. Therefore, sonication was performed for 12 minutes to achieve optimal fragment size.

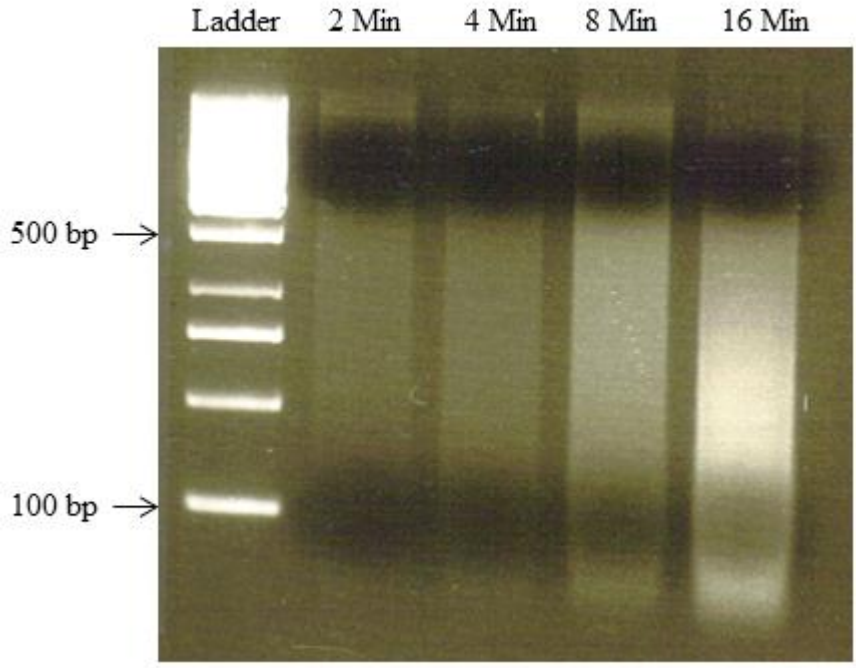

Figure 2.1 Optimization of sonication time

Sonication of chromatin samples for different time intervals (2 min, 4 min, 8 min and 16 min) using a Biorupture sonicator. The samples were run on a 1% agarose gel (w/v), and the size of the fragment was determined by comparison with a 100 bp DNA marker (Thermo Scientific) run in parallel.

2.3.3 Chromatin immunoprecipitation

ChIP was performed using 40 µL of Dynabeads®Protein-G beads, per sample. The 40µL of beads was split into two tubes, 25µL of which were coated with the desired antibody (+Ab) and 15 µL of which were pre-absorbed (-Ab). The beads were then washed four times in LoBind microcentrifuge tubes (Eppendorf) with 1ml of 1X PBS containing 5 mg/ml bovine serum albumin (BSA). Washing steps were carried out by rotating the tubes six times in a magnetic stand. After each wash the beads were allowed to migrate to the back of the magnetic stand so that the supernatant could be discarded completely.

After the final wash, beads were resuspended again in 500 µL of 1 X PBS with 5mg/ml BSA. Typically, 2µg of anti-Y14 antibody (see section 2.8.10) were added to the tube derived from 25 µL of beads. Both +Ab and –Ab tubes were incubated overnight at 4^0C with rotation. The next day pellets of cross-linked cells (section 2.3.1) were thawed on ice and resuspended in 100 µl of SDS lysis buffer (1% w/v SDS, 10 mM EDTA). The cell suspension was then sonicated at high intensity for 12 min with 15 sec on/off in a Bioruptor sonicator. Samples were diluted in 1 ml ChIP dilution buffer (0.01% w/v Sodium dodecyl sulfate (SDS), 1.1% v/v Triton X-100, 1.2 mM EDTA, 16.7 mM Tris-HCl pH 8.1, 167 mM NaCl) and centrifuged at 13000 rpm/ 15682 g (Eppendorf) for 10 min at 18°C (n.b. SDS will precipitate at 4^0C) to pellet insoluble material. The supernatant (soluble chromatin) was kept in LoBind microcentrifuge tubes at 4^0C. In the meantime, both +Ab and -Ab beads were washed four times with 1 ml of 1 X PBS with 5mg/ml BSA to remove unbound antibody, using a magnetic stand as before. +Ab beads were then resuspended in 40 µl of 1X PBS with 5mg/ml BSA, whereas -Ab beads were resuspended in 25 µL and added to prepared before. Next 1 ml of the soluble chromatin was added to the -Ab beads and incubated for 15 min at room

temperature with rotation. The mixture was then spun briefly, the beads were pelleted in a magnetic stand and the supernatant was transferred into a fresh LoBind microcentrifuge tube. Approximately 50-100µL of the soluble chromatin was kept as an input control and stored at -20°C. The 40µL+Ab beads sample was added to the remainder of the soluble chromatin and incubated for two and a half hours at room temperature with rotation to allow the formation of antibody-antigen immune complexes on the beads.

2.3.4 Washing steps

The beads were separated from the supernatant using a magnetic stand, as previously explained. Beads were then sequentially washed with rotation at room temperature for 5 min with 1 ml of each of the following buffers: low salt wash (0.1% w/v SDS, 1% v/v Triton X-100, 2 mM EDTA, 20 mM Tris-HCL pH 8.1, 150 mM NaCl); high salt wash (0.1% w/v SDS, 1% v/v Triton X-100, 2 mM EDTA, 20 mM Tris-HCL pH 8.1, 500 mM NaCl); LiCl wash (0.25M LiCl, 1% v/v IGEPAL-CA630, 1% w/v deoxycholic acid, 1 mM EDTA, 10 mM Tris-HCL (pH 8.1); two 5 min washes in 1mL of TE buffer (10 mM Tris-HCL (pH 8.0), 1 mM EDTA). Beads were vortexed in each washing buffer and collecting on a magnetic stand, as previously described. The supernatant was discarded after each wash.

2.3.5 Elution steps and reverse cross-links

Protein-DNA complexes were eluted from the beads by washing them twice with 75µl of freshly prepared 0.1M $NaHC0_3$ solution containing 1% w/v SDS. The mix was then vortexed, briefly spun and incubated with rotation at a room temperature for 15 min. The tube was spun briefly and the beads were separated from the supernatant using a magnetic stand. The supernatant was transferred to a new LoBind microcentrifuge tube and the beads were resuspended with a further 75 µl of elution buffer and the process was repeated, resulting in a

final volume of 150 µl. More elution buffer was added to the input sample to bring it up to the same volume as the ChIP sample (150 µl). Protease K was added to all samples (2 µl of 50 mg/ml) which were then incubated overnight at 65^0C on a dry heat block to digest proteins and to reverse crosslinks.

2.3.6 Purification steps

Following overnight incubation, DNA samples (both the input and ChIP samples) were purified using AMPure XP beads (Beckman Coulter). 1.8 volumes of AMPure XP bead slurry was added to each DNA sample. Samples were mixed by vortexing thoroughly and were incubated with rotation for 10 min at room temperature to allow the DNA to bind to the beads. Once the incubation was completed, samples were briefly spun, and beads were recovered using a magnetic stand while the supernatant was discarded. Beads were then washed three times with 300 µL of freshly prepared 70% v/v ethanol (EtOH), using a magnetic stand as previously described, ensuring all EtOH was removed. The pellet was air-dried in a magnetic stand until cracks were visible in the beads slurry. DNA was eluted by resuspending the beads in 30µL of 10 mM Tris elution buffer (pH 8.0). The tube was placed back into the magnetic stand to separate the beads from the eluate. This process was repeated three times until all the beads were removed.

2.3.7 Solid ChIP-Seq library preparation

Library preparation and sequencing of ChIP DNA were performed by Dr. Paul Badenhorst at the Institute of Biomedical Research (IBR), University of Birmingham, UK, using the SOLID system Fragment Library protocol from Applied Biosystems.

2.4 S2 cells RNA interference (RNAi)

A primer pair for the gene of interest was obtained from an online tool - fly RNAi Updated Targets of RNAi Reagents (UP-TORR) - www.flyrnai.org/up-torr, and the desired gene Y14 and eIF4AIII was PCR amplified from FLAG-tagged plasmid (Appendix IV) and MAGO from fly cDNA plasmid library (available in Dr. Brogna lab). PCR fragments were purified with a QIAquick PCR Purification Kit (QIAGEN) according to the provided protocol. All the primer pairs used were tagged with the T7 promoter sequence (5'-TTAATACGACTCACTATAGGGGAGA-3') at the 5' end. The dsRNAs were synthesized using the T7 RiboMAX express RNAi system (Promega) according to the manufacturer's instructions: 1µg of DNA was used as a template in a 20µl reaction containing 10µl RiboMAX Express T7 2X buffer and 2µl Enzyme Mix T7 express. The final volume was adjusted to 20µl with diethylpyrocarbonate (DEPC) treated water. The tube was gently mixed and incubated for 2 h at 37^0C. The mix was then incubated for 20 min at 70^0C in a dry heating block to inactivate the enzyme and to allow the RNA strands to anneal. 1µl of DNase I (Promega) was added to the mix to remove the DNA template and the sample was further incubated for 30 min at 37^0C.

2.4.1 Purifying dsRNA

To purify dsRNA, 2.5 volumes of 95% v/v EtOH and 0.1 volumes of 3M sodium acetate (pH 5.2) were added to the mix and incubated for 30 min at -20^0C. The RNA was then pelleted by centrifugation at 13,000 rpm/ 15682 g (Eppendorf) for 15 min at 4^0C, and the supernatant was discarded. The pellet was washed in 70% v/v EtOH and air dried for 15 min at room temperature, then resuspended in 100µl of DEPC treated water. Nanodrop spectrophotometer was used to measure the concentration of dsRNA, and its integrity was checked by running 1µl on a 1% w/v agarose gel.

2.4.2 S2 cells siRNA

S2 cells were grown for two days in T25 culture flasks with 5 ml of Insect–XPRESS medium (Lonza) supplemented with 10% v/v fetal bovine serum (FBS) and 1% v/v P/S/G (Invitrogen) media. On the day of the RNAi treatment, cells confluency were checked by phase contrast microscopy and subsequently transferred into a 50 ml falcon tube. The cell culture was then centrifuged at 1000 rpm/ 92 g (Eppendorf) for 3 min at room temperature, the supernatant was discarded and the cell pellet was diluted with serum-free media (without FBS and P/S/G) to a final concentration of 10^6 cells/ml. Next 1 ml of cell culture was transferred to each well of a six-well cell culture plate and 15µg of dsRNA was added to each. The cell culture and dsRNA were mixed by moving the plate back and forth several times and were incubated for a further hour at room temperature. After incubation, 2 ml of complete media (10% v/v FBS and 1% v/v P/S/G) was added to the plate, mixed and placed in the 27^0C incubator. The plate was then incubated for a further four days to allow depletion of the pre-existing targeted protein. After four days, cells were treated with 1µM ecdysone without changing the media and incubated for 2 h at room temperature. RNA was then extracted from all the samples.

2.4.3 RNA extraction and complementary DNA synthesis (cDNA)

RNA extraction from S2 cells was carried out using the RNeasy Mini Kit (QIAGEN) according to the manufacturer's instructions. 700ng of total RNA was used for cDNA synthesis using a qScript Kit (Quanta Biosciences). Synthesized cDNA was kept at -20^0C for later usage.

2.4.4 Quantitative Real-Time PCR

Quantitative real-time PCR was carried out using the SensiFAST SYBR Hi-ROX Kit (Bioline). Real-time PCR was carried out in 96 well plates in an Applied Biosystems Prism (ABI PRISM) 7000. The qPCR reaction was a two-step cycle with an initial denaturation at 95^0C for 2 min, followed by 40 cycles of denaturation at 95^0C for 15 s and annealing and extension at 60^0C for 1 min. The primer pairs used to check transcript levels of various genes are listed in Appendix II. The threshold cycle (Ct) was set at a point where all samples were in the exponential stage of amplification. This value was used to measure transcript levels of target genes and was normalized by dividing by the level of the reference RpL32 control transcript for each sample.

2.5 Purification of nuclear and cytoplasmic fractions from S2 cells

To separate nuclear and cytoplasmic fractions, a protocol based on one published by Parker and Topol (1984) was used. S2 cells were grown in a T75 tissue culture flask at 27°C in 15 ml of Insect – XPRESS medium (Lonza) supplemented with 10% v/v fetal bovine serum (FBS) and 1% v/v penicillin/streptomycin/glutamine mix (Invitrogen) for 2 days. Cells were then pelleted by centrifugation at 2500 rpm/ 580 g (Eppendorf) at for 5 min and washed with ice cold PBS twice (a 1 ml aliquot of the culture was pelleted and kept as whole cell extract). The cell pellet was resuspended in five times its volume in buffer A (15 mM KCL, 10 mM HEPES (pH 7.6), 2mM $MgCl_2$, 0.1 mM EDTA) and was centrifuged at 5000 rpm/ 2319 g (Eppendorf) for 5 min at 4^0C. Supernatant was discarded, and the pellet was resuspended in the same volume of buffer A with the addition of DTT to the concentration of 1mM. The cells were then homogenized using a Dounce glass homogenizer (a 2 ml homogenizer with a

tight (B) pestle) and checked under a phase contrast microscope to confirm that at least 85% of the cells were broken. The cell suspension was then mixed with 1/10 volume of buffer B (1 M KCl, 50 mM HEPES (pH 7.6), 30mM $MgCl_2$, 0.1mM EDTA, 1mM DTT) and centrifuged at 10000 rpm/ 9279 g (Eppendorf) at 4^0C or 10 min. After centrifugation the supernatant was kept as a cytoplasmic fraction (1ml) and the pellet was considered a crude nuclear extract which was dissolved in 400µl of 9 parts buffer A and 1part buffer B. 100µl of the crude nuclear extract was transferred to a new tube and 4 M ammonium sulfate (pH 7.9) was added to the remainder at a final concentration of 0.36 M. The mix was gently rotated at 4^0C for 30 min to lyse the nuclei and then centrifuged at 16000 rpm/ 23755 g (Eppendorf) at 4^0C for 1h 30 min to pellet the DNA. To the supernatant ammonium sulfate was added at 0.25 g/ml, followed by centrifugation at 16000/ 23755 g (Eppendorf) rpm for 15 min at 4^0C and pellet was kept as soluble precipitated protein.

2.6 S2 cells and salivary glands Western blotting

2.6.1 Sample preparation

Salivary glands (20-30 pairs) were dissected from mid-3rd instar larvae in Shields and Sang M3 insect medium consist of inorganic salt, amino acid, vitamins, sugar and yeast extract (Sigma-Aldrich). All glands were then transferred to 2x SDS loading dye supplemented with 5% v/v β-mercaptoethanol and 1mM PMSF and homogenized with a plastic pestle grinder in a 2ml microcentrifuge tube. The lysate was boiled for 6 min in a heat block which was followed by cooling for 1 min on ice. Samples were centrifuged at the highest speed at 4^0C for 2 min in a microcentrifuge and either loaded on SDS-PAGE gels or stored at -20^0C.

S2 cells were grown in six-well plates to a density of $3x10^6$ cells/ml, as described above (section 2.2.1). 1 ml of cells was collected in a 1.5 ml microcentrifuge tube and centrifuged at 5000 rpm/ 2319 g (Eppendorf) at 4^0C for 3 min. Cells were washed twice with 500 µl of ice-

cold PBS and the pellet was dissolved in 100 µl of 2X SDS loading dye. Samples were then boiled in a heat block for 6 min which was followed by cooling for 1 min on ice. The protein mixture was then centrifuged at the highest speed at 4^0C for 2 min and used directly for loading on SDS-PAGE gels or stored at -20^0C.

2.6.2 Western Blotting

Protein extracts were typically loaded on a 12% v/v SDS-PAGE gel which was run for 90 min at room temperature. The prestained protein marker, broad range (7-175 kDa) from New England Biolabs (NEB) was used as a ladder in the gel. Proteins were then transferred to a nitrocellulose membrane (Protran BA-85, Geneflow) using a wet blotting apparatus (BioRad). The transfer was carried out at 350 mA in transfer buffer (25 mM Tris, 192 mM glycine and 10% v/v methanol) at 4^0C for 2 h. The membrane was then stained with Ponceau S to check that the proteins were transferred on the membrane uniformly. The membrane was blocked in Tris-buffered Saline containing 0.05% v/v Tween-20 (TBST) containing 5% w/v milk (Marvel) on a rocker for 1 h at room temperature. The membranes were incubated with primary antibody diluted in 1X TBST overnight at 4°C (dilution dependant on the concentration of the antibody). The membrane was washed five times with 1X TBST prior to secondary antibody incubation. The secondary antibody was HRP conjugated specific for the species and Ig class of the primary antibody (Chemicon), typically diluted 1:10000 in 1X TBST and incubated for 1 h on a rocker at room temperature. The membranes were washed again as before and incubated with Amersham ECL Prime Western Blotting Detection Reagent (GE Healthcare Life Science) for 5 min and then visualized with a GelVue Dual UV Transilluminator using the Gene Snap Software (Syngene).

2.6.3 Reprobing of Western blot membranes

Membranes were stripped using the Abcam stripping protocol. The membrane was washed with mild stripping buffer (15 g glycine, 1 g SDS and 10 ml Tween-20 in a 1L volume of water, pH 2.2) two times for 10 min each at room temperature. The membrane was then further washed with 1X PBS two times for 10 min followed by two times washed with 1X TBST for 5 min each at room temperature. The same membrane was blocked again with TBST containing 5% w/v milk and then re-probed with a different primary antibody as described above. As a loading control, membranes were typically incubated with a tubulin primary antibody (Sigma-Aldrich, T5168 1:4000) with the appropriate HRP conjugated secondary antibody.

2.7 Fly genomic DNA extraction and Polymerase Chain Reaction

A single male fly was first frozen at -20°C for 30 min in a PCR tube, then squashed against the tube wall using a pipette tip, in 50 µL 'squishing' buffer (10 mM Tris pH 8.0, 1 mM EDTA, 25 mM NaCl,). The sample was placed in a thermocycler for 30 min at 37°C followed by 2 min incubation at 95°C. It was then centrifuged and the supernatant was kept as genomic DNA and stored at 4°C.

The PCR reaction was carried out in a 50 µL volume using Phusion® high-fidelity DNA polymerase (Biolabs) with the following parameters: 2 min at 98°C followed by 32 cycles of 10 s at 98°C, 30 s at 58°C and 1 min at 72°C and a final extension of 10 min at 72°C.

2.7.1 DNA Sequencing

PCR products were purified using a QIAquick Gel Extraction Kit (QIAGEN) and were subsequently checked by running on a 1% w/v agarose gel. The purified PCR product was then sent, with appropriate primers, to GATC Biotech (London) for sequencing (see Appendix V).

2.8 Salivary gland dissection and polytene chromosome squashing

2.8.1 Salivary gland dissection

D. melanogaster larvae were grown at 18^0C in bottles containing dry yeast. To obtain well-squashed polytene chromosomes, larvae must be healthy. Salivary glands were dissected from wandering third instar larvae. Larvae were collected from the bottles and transferred into a dissecting glass dish filled with water which was placed on ice for 5 min for washing purposes and for the larvae to be put to sleep. Larvae were then dissected using sharp tweezers in 20 µl of solution A or the dissection buffer (100 µl 10x Buffer A, 100 µl 10% v/v Triton X-100, 800 µl distilled water; buffer A (1X): 15 mM HEPES pH 7.4, 60 mM KCl, 15 mM NaCl, 1.5 mM spermine, 1.5 mM spermidine). For the fixation, salivary glands were kept for 1 min in 20 µl of solution B or the fixative (100 µl 10x Buffer A, 100 µl 10% v/v Triton X-100, 250µl 4% v/v formaldehyde, 550µl distilled water). Salivary glands were further washed for a few seconds in 20 µl of solution G (500 µl glacial Acetic acid, 250 µl 4% v/v formaldehyde and 250 µl distilled water) and then transferred to a siliconized glass coverslip containing 13 µl of solution G and incubated for a further 3 min. After that, the microscopic slide was gently put on top of the coverslip. It was also necessary to ensure that solution G was evenly spread between the slide and the coverslip.

2.8.2 Squashing

Salivary glands were first broken by tapping a few times on top of the coverslip with a blunt tip of a brush, dissecting needle or a similar implement. A piece of folded tissue paper was placed on top of the coverslip and then pressed using the thumb on a flat surface. The spreading of the chromosomes was checked under a phase contrast microscope. If satisfactory, the position of the coverslip was lightly marked with a diamond pencil on both sides of the coverslip and the slide was frozen by dipping into liquid nitrogen for 60 seconds. The coverslip was then quickly removed from the slide using a razor blade and put in a Coplin jar filled with 95% v/v EtOH and stored at -20°C. It could be used for immunostaining the following day.

2.8.3 Immunostaining

Slides with chromosome spreads were washed twice in a Coplin jar with 1X TBST (150 mM NaCl, 10 mM Tris-Cl pH 7.0-7.5, 0.05% v/v Tween). Each washing was performed at room temperature for 10 min. Slides were then transferred to a Coplin jar filled with blocking solution (TBS, 10% v/v Fetal Bovine Serum (FBS) and 0.05% w/v sodium azide (NaN3) and kept at room temperature for 30 min. Primary antibody was diluted in blocking solution (typically 1:100 dilution, depending on the antibody) and, as such, was used for immunostaining. A 20 µl drop of diluted antibody was placed on the coverslip and the slide with the chromosome was carefully placed on top of the drop, making sure that no air bubbles were formed between the slide and the coverslip. Slides were then placed in a humid chamber saturated with TBS and incubated overnight at 4^0C.

Slides were removed from the chamber the following day and submerged into a beaker containing TBST in order to detach the coverslip from the slide without breaking the chromosomes. Slides were then washed twice with TBST at room temperature for 10 min. Secondary antibody staining was carried out in the same way as primary antibody but the dilution was typically 1: 250, as detailed in figures legend. The incubation with secondary antibody was performed in a humid chamber for 1 h at room temperature. In order to stain DNA, slides were first washed with TBST containing 0.1 µg/ml 4-6-diamidino-2-phenyl indol (DAPI, from Sigma-Aldrich) which was followed by a second wash in TBST for 10 min. Slides were subsequently dried at room temperature for around 20 min, covered with aluminium foil to protect the secondary antibody-fluorophore from light. Once the slides were dried, they were mounted using a single drop of fluorescence Antifade medium (PromoFluor, Promokine) which was placed on a coverslip and carefully fitted on the slide allowing it to settle by capillary force. Slides could be either viewed immediately using a fluorescence microscope or stored at 4^0C for future use.

2.8.4 Fluorouridine (FU) labelling of polytene chromosome nascent RNA

Salivary glands were dissected in M3 media and incubated with 2mM 5-fluorouridine (FU, Sigma-Aldrich) at room temperature for 15 min. The cell membrane was then permeabilized by transferring the glands to solution A containing 1% v/v Triton X-100 and incubated at a room temperature for 2 min. Glands were subsequently transferred to solution A containing 0.1% v/v Triton X-100 and incubated at room temperature for 10 min either with or without 1µg/µl ribonuclease (RNAse, Invitrogen) treatment. All glands were then fixed in solution B for 1 min and squashed in solution G as described above. Immunostaining was carried out by following the protocol explained above.

2.8.5 Salivary gland RNase treatment

Salivary glands were dissected in Solution A containing 1% v/v Triton X-100 and kept at room temperature for 2 min. Glands were then transferred to a 50 µl of solution A with 0.1% v/v Triton and incubated at room temperature for a further 10 min either with or without 1µg/ µl RNAse (Invitrogen). Glands were then fixed in solution B for 1 min and squashed in solution G. Immunostaining was carried out as described above.

2.8.6 Acid-free polytene chromosome squashing

To preserve the green fluorescent protein (GFP) signal, polytene chromosome squashing was carried out in 50% v/v glycerol instead of in acetic acid since the latter could destroy fluorescent signals. Salivary glands were routinely dissected in PBS and fixed in PBS containing 4% v/v formaldehyde (Agar Scientific) for 1 min. The glands were transferred to a 50 µl of 50% v/v glycerol containing DAPI (0.1µg/ml) and incubated at room temperature for 30 min. The salivary glands were squashed in a slide containing 20-30 µl of 50% v/v glycerol and DAPI (0.1µg/ml) (Johansen et al., 2009).

2.8.7 Salivary glands heat shock induction

To induce heat shock protein genes on polytene chromosomes, larvae were placed in a standard fly food vial and immersed in a water bath at 37^0C for 45 min to just below the rim of the vial. Larvae were dissected in solution A and processed following the standard immunostaining protocol.

2.8.8 Salivary glands ecdysone treatment protocol

Incubation with 20-hydroxyecdysone (Sigma-Aldrich) was used to express ecdysone-regulated genes in polytene chromosomes. Salivary glands were dissected in M3 media and incubated with 1µM ecdysone at room temperature for different time intervals (15 min, 30 min, 1 h and 2 h). Salivary glands were then incubated for 1 min in solution A , followed by fixation for further 1 min in solution B and both squashing, immunostaining was carried out using the explained protocol in section 2.8.1-2.8.3.

2.8.9 Antibodies

Antibodies against the EJC proteins - MAGO, Y14 and eIF4AIII - were all rabbit IgG generated by our collaborator Dr. Marco Blanchet (Stower Institute of Medical Research, USA). A 1:100 dilution was used per incubation. Primary antibodies against fluorouridine, Sm proteins and FLAG-tagged EJC proteins were mouse anti-BrdU (Sigma-Aldrich, 1:200 dilution), mouse anti-Y12 (Thermo Fisher Scientific, 1:100 dilution) and anti-FLAG M2 (Sigma-Aldrich, 1: 200 dilution) respectively. The secondary antibody used for the detection of the EJC primary antibodies was either Cyanine 3 (Cy3) conjugated goat anti-rabbit IgG (1:250 dilution), or fluorescein isothiocyanate (FITC) conjugated goat anti-rabbit IgG (1:200 dilution). Secondary antibodies against Sm proteins, fluorouridine and FLAG tagged EJC proteins were detected by Alexa Fluor 647 conjugated goat anti-mouse IgG (Invitrogen, 1:200 dilution). The primary antibody against RNA Pol II was mouse anti-Pol II H5 (Covance, 1:250 dilution) which was subsequently detected by Cyanine 3 (Cy3) conjugated goat anti-mouse IgM (1:250 dilution). All the secondary antibodies were from Jackson Immuno Research Technologies and Life Technologie**s.**

2.8.10 Fluorescence microscopy

A Nikon Eclipse Ti epifluorescence microscope was used to view the stained polytene chromosomes using a 40X objective dry lens while the images were captured with an ORCA-R2 camera (Hamamatsu Photonics).

2.9 Whole salivary glands immunostaining

Larvae were grown at 18°C in a glass bottle containing dry yeast to get well-fed larvae with big salivary glands. Larvae were dissected in M3 insect media and 4 to 5 pairs of glands were used for each experiment. All glands were fixed in a PBS solution containing 4% v/v formaldehyde (from 10% EM grade, Polyscience) and incubated on ice for 30 min. After fixation, salivary glands were washed with 0.3% v/v Triton in PBS three times for 10 min each at RT. All glands were then transferred to blocking solution (10% v/v FBS and 0.3% v/v Triton in 1X PBS) at room temperature for 1 h. After blocking glands were incubated with primary antibody (dilution depending on the antibody used) in a blocking solution overnight at 4°C. The following day glands were washed in PBS with 0.3% v/v Triton three times, 10 min each, at room temperature. Glands were subsequently incubated with the appropriate secondary antibody (dilution depending on the antibody used) in blocking solution at room temperature for 2 h. Glands were washed again for 10 min in a PBS solution containing 0.3% v/v Triton, followed by staining with 0.1µg/ml of DAPI in the washing solution at room temperature for another 20 min. Glands were then incubated in the washing solution for 10 min and then transferred to 50 µl of 50% v/v glycerol and incubated for 10 min at room temperature. All the glands were mounted in Antifade media (PromoFluor, Promokine) and viewed using a Leica SP2-AOBS confocal microscope. Images were further processed with ImageJ software (http://imagej.nih.gov/ij/).

2.10 Puromycin labelling of nascent peptides on polytene chromosomes

2.10.1 Polytene chromosome squashing and ribo-puromycylation

Optimization of puromycin labelling was carried out in two-steps. In the first step, salivary glands were dissected from 3rd instar larvae in M3 insect medium and kept in fresh media for up to 10 min. Salivary glands were then incubated with 50 µg/ml puromycin and 100 µg/ml emetine in M3 media at room temperature for 15 min. After labelling, glands were washed three times for 5 min each in ice cold PBS with 100 µg/ml emetine. In the second optimization step, 10 µg/ml actinomycin D was added in both the labelling and the washing buffers. Salivary glands were then incubated in solution A with 100 µM aurintricarboxylic acid (ATA) and EDTA-free Complete Protease Inhibitor Cocktail (Roche) at room temperature for 2 min. Glands were then fixed for approximately 1 min in solution B and subsequently squashed in solution G. Slides were stored at 4°C in 95% v/v ethanol.

2.10.2 Immunostaining and antibody

Before immunostaining, slides were washed twice in TBS (150 mM NaCl, 10 mM Tris-Cl pH 7.0-7.5, 0.05% v/v Tween) for 10 min. Slides were incubated in a TBS blocking solution containing 10% v/v Fetal Bovine Serum (FBS) and 0.05% w/v sodium azide (NaN_3) at room temperature for 30-60 min. All chromosome spreads were stained with 0.1 µg/ml DAPI for 20 min. The antibody used was an Alexa 488-conjugated 2A4 monoclonal antibody (from Dr. John Yewdell, NIH, USA) (David et al., 2012) and was diluted 1:200 in blocking buffer. The slides were mounted with a drop of fluorescence Antifade medium (PromoFluor, Promokine). Stained polytene chromosomes were viewed using an epifluorescence Nikon microscope with a 40X objective lens and images were captured using a CCD camera.

2.11 Incorporation of puromycin in whole salivary glands of *D. melanogaster*

2.11.1 Puromycin and emetine labelling

Salivary glands from 3rd instar larvae were dissected in M3 media. Glands were incubated in M3 media either containing both 50 μg/mL puromycin and 100 μg/mL emetine or 50 μg/mL puromycin only. The incubation was at room temperature for 15 min and followed by three 5 min washes in ice cold PBS containing 100 μg/mL emetine. This was followed by a 1 min incubation of a pair of glands in emetine (100 μg/mL), 60 mM KCl, 15 mM NaCl, 15 mM HEPES pH 7.4, 1.5 mM spermine, 1.5 mM spermidine, 100 μM aurintricarboxylic acids (ATA), 1% v/v Triton X-100, and EDTA-free Complete Protease Inhibitor Cocktail (Roche) at room temperature.

As a control, glands were pre-incubated with 2μM harringtonine in M3 media at room temperature for 15 min, before the previously explained puromycin/emetine treatment. All subsequent steps were carried out as above.

2.11.2 Immunostaining

After labelling, salivary glands were fixed in a PBS solution containing 4% v/v formaldehyde for 30 min on ice. Glands were then washed twice in PBS containing 0.3% v/v Triton X-100 for 10 min each at room temperature. Salivary glands were then incubated with 10% v/v FBS in PBS and 0.3% v/v Triton X-100 for 1 h at room temperature which was followed by incubation with the Alexa 488 conjugated 2A4 monoclonal antibody (1:200 dilution) at 4°C overnight. Glands were subsequently washed in PBS containing 0.3% v/v Triton X-100 and 0.1 μg/ml DAPI at room temperature for 20 min. A further wash without DAPI was carried out at room temperature for another 10 min and glands were mounted on the slide with anti-fade media. Sample was either viewed immediately or stored at 4°C.

2.11.3 Confocal microscopy/image processing

A Leica confocal inverted microscope (DMIRE2) with a 40X and 63X oil objective lenses was used to view glands and images were captured using Leica Confocal Software Suite.

2.12 Genetics

D. melanogaster was used in all of the above experiments. Fly stocks were kept in standard fly food plastic or glass vials with dry yeast. Fly stocks were maintained either at 18°C or 25°C depending on the required experimental purpose. Fly stocks kept at 18°C were normally transferred to fresh vials after 28 days, while those at 25°C stock were transferred every 14 days.

2.12.1 Virgin collection

To collect virgin female flies, fly vials were emptied in the evening and kept at 18°C. Virgin female flies were collected the following morning, vials were kept at 25°C and virgins were collected as they emerged throughout the day. Virgin females were identified by the presence of meconium in the gut. The lower temperature (18°C) delays the emergence of flies. Virgin females were kept at 18°C until required.

2.12.2 Setting up crosses

To set up a cross, four virgin females were typically crossed with two males in glass vials with freshly sprinkled dry yeast. The vials were kept at 25°C for two days and then transferred to fresh fly foods vials. To get well-fed larvae with big salivary glands, vials were kept at 18°C. Third instar larvae could then be dissected on the 10th day after egg laying.

2.12.3 GAL4/UAS expression system

The GAL4/UAS system is one of the most well-known systems used in *Drosophila* which provides tissue-specific transgene expression. The yeast transcription activator, Gal4, binds to yeast upstream activating sequences (UAS) and induces transcription of corresponding genes (Duffy, 2002). Gal4 serves as a driver in this system and acts on any gene flanked by the UAS sequence. To express UAS-regulated transgenes in specific tissue/cells, the UAS line was crossed with a specific Gal4 driver line.

2.12.4 Generation of a fly strain expressing both LacI-GFP and MCP-RFP

To produce LacI-GFP and MCP-RFP on the same transgenic flies, a genetic cross was set up as following: flies strain with MCP-RFP y[1] w[67c23]; P{w[+mC]=Hsp83-MCP-RFP}12a/TM3, Sb[1] on the 3rd chromosome and strain with lacI-GFP 6(4:1)/ Cyo hsp83.GFP-Lac I on the 2nd chromosome were crossed using standard genetics protocols (Figure 2.2). In the G0 cross, a homozygous red eyed male with [Cyo-Hsp83. GFP-Lac I] (see Appendix III) on the 2nd chromosome (cross a) and P W[+mc]= Hsp83-Mcp RFP (see Appendix III) on the 3rd chromosome (cross b) were crossed with double balancer virgin females. Red eye males from the F1 (a) progeny, with IF and TM6B markers, were crossed with red-eye virgin females with Cyo and MKRS of the F1(b) progeny. Then F2 flies with the indicated genotypes were crossed to produce F3 flies homozygous for both inserts, which were selected for the absence of both Cyo and TM6B dominant markers. The strain was initially verified by observing the larvae on fluorescence microscope and by inspecting the presence of GFP and RFP fluorescence in the salivary glands of 3rd instar larvae.

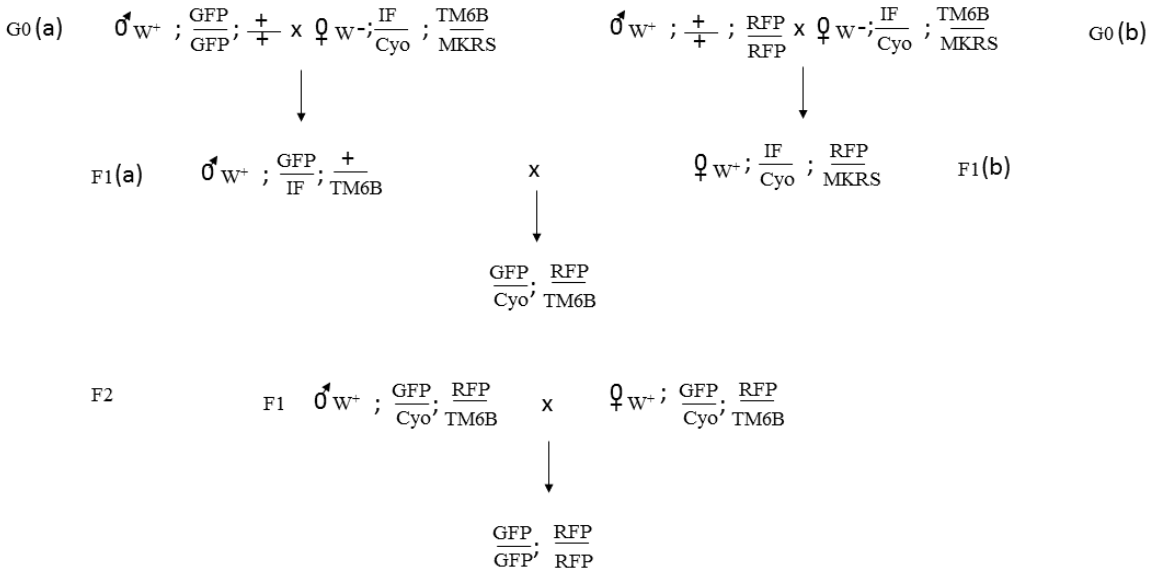

Figure 2.2 Schematic representation of genetic cross of LacI - GFP and MCP-RFP - In the G0 (a) and G0 (b) phase LacI-GFP and MCP-RFP cross with double balancer lines. F1 (a) and F1 (b) generation were collected by observing the above phenotype and were further crossed to give rise to GFP-RFP transgenic lines in the F2 generation.

2.13 Parameters used to select target epitopes for UPF1 and UPF2

Abmart SEAL technology was used to produce the monoclonal antibody against UPF1 and UPF2 protein (Figure 2.3). The protein amino acid sequence for UPF1 and UPF2 were given in Table 2.1 and 2.2. Abmart Bioinformatics tools and algorithm antigen software were used to design the protein secondary structure and potential epitopes. Following is the most important parameter considered in algorithm to design the epitopes

1. Secondary structure-Loop/helix/sheet
2. Special region- N-terminal, C-terminal, signal peptide, Trans-membrane, Solvent accessibility.
3. Blast- Query species and Mouse
4. Amino Acid property- Antigenic enhancement amino acid Flexibility
5. Evolution- Positive selection, Discrimination
6. Specificity- Protein specificity, Region specificity

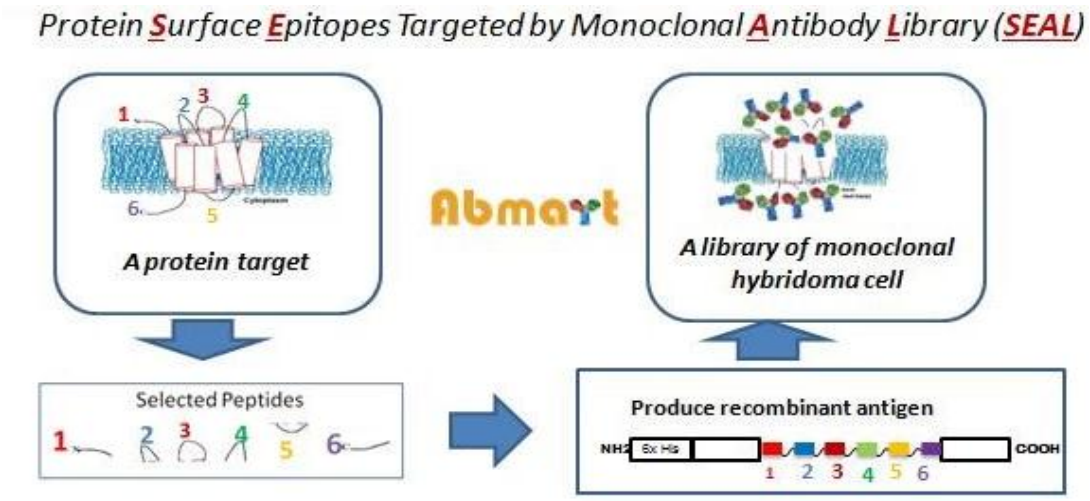

Figure 2.3 Abmart SEAL technology for antibody production

Abmart designs potential epitopes by using specific algorithm antigen software. The potential epitopes then integrated into the Abmart expression vector to produce recombinant antigen, subsequently the antigen then used for immunization in mice. This image was taken from Abmart (http://www2.abmart.com/index.php?&controller=SealPerformanceLibrariesTechnology).

Table 2.1

```
MSVDTYAPSSALSFLDMDDNELLPGADTQPTQYDYRDFTMPSTSQSQTQNDQLEIAQRCSAGDSHPRLASITNDL
ADLQFEEEDDEPGSSYVKELPPHACKYCGIHDPATVVMCNNCRKWFCNGRGSTSGSHIINHLVRAKHREVTLHGE
GPLGETILECYSCGVRNVFVLGFIPAKADSVVVLLCRQPCAAQNSLKDMNWDQEQWKPLIADRCFLAWLVKQPSE
QGQLRARQISAAQINKLEELWKENIEATFQDLEKPGIDSEPAHVLLRYEDGYQYEKTFGPLVRLEAEYDQKLKES
ATQENIEVRWDVGLNKKTIAYFTLAKTDSDMKLMHGDELRLHYVGELYNPWSEIGHVIKVPDNFGDDVGLELKSS
TNAPVKCTSNFTVDFIWKCTSFDRMTRALCKFAIDRNSVSNFIYSRLLGHGRADSNDEVLFRGPQPKLFSAPHLP
DLNRSQVYAVKHALQRPLSLIQGPPGTGKTVTSATIVYQLVKLHGGTVLVCAPSNTAVDQLTEKIHRTNLKVVRV
CAKSREAIDSPVSFLALHNQIRNMETNSELKKLQQLKDETGELSSADEKRYRNLKRAAENQLLEAADVICCTCVG
AGDGRLSRVKFTSILIDESMQSTEPECMVPVVLGAKQLILVGDHCQLGPVVMCKKAARAGLSQSLFERLVVLGIR
PFRLEVQYRMHPELSQFPSNFFYEGSLQNGVCAEDRRLKLDFPWPQPERPMFFLVTQGQEEIAGSGTSFLNRTEA
ANVEKITTRFLKAGIKPEQIGIITPYEGQRAYLVQYMQYQGSLHSRLYQEIEIASVDAFQGREKDIIIMSCVRSN
ERQGIGFLNDPRRLNVALTRAKFGIIIVGNPKVLAKQQLWNHLLNFYKDRKVLVEGSLNNLKESLIHFQKPKKLV
NSMNIGAHFMSTIIADAKEVMVPGSIYDRSGGYGQGRQMVGQSMNGGQYGGSGGGPYGNSPLGYGTPSSNSMVGF
GLGNGGNGAAGGNNNFGGAGPSWAAAHLHHDSIGYISNEHGAAALGNMPVPVGMFMNMSNIPPRFYNQHQQAIMA
VKQNRAIQQQTGNFSPGNSGPGVTGVGVGRSATPGGNKKTNKLGKSRVTGGGTGGAPLTQGSSVCNAAPYSQHPM
PLSLQMTQPSGFALSQQPELSQDFGQISQMDGLLSQDVAFNASGERSLNQFSQPY
```

Table 2.2

```
MLANDSATTDSEVSTPPSSRKDLADGVAEGDNDNDIDTGDTDANADEDVDAAAAIALEAEEREELQQFISELREK
IESKRQLRLQNSTIELPGEEYFAKLDSNLKKNTAFVKKLKLFTATQLDGLLREISALNLSKYISEICAALVEAKL
KMTDVPAVVTLASRLHCTYADFDVHFLEAWQKALNIKATEKIGNPSKLRVDLRLFAELVSSGVIQMKPGLAQLGV
VLVHLIALDKDDHSNFSIILSFCRHCGEEYAGLVPQKMQQLATKYGVEVPKSDFLTADKQLNLRTMLKGYFKALC
KHVLAEQAELMNMTKNIRRTMECKGEISTEKREKCELMQAGFDKLLASAQSLSELLGEPLPELAKESEGCNPGTV
IDNMLDSASFGVLDPWGDEETRAFYTDLPDLRQFLPNFSAPKVDLETLEEPSELTEEAIDANLDAEMDLDDPPST
TSDTTPENPIEEQPTTPVAAAEDLKPQKMGNALMELGRQQQQQSQLNQNPIQIQNQMRQQFDGFLVNLFNCVNKE
LIDSAAIEFLLNFNTKHQRKKLTRTIFSVQRTRLDILPYLSRFVAIVHMCNTDVATDLAELLRKEFKWHIHKKNQ
LNIETKLKIVRFIGELVKFGLFKKFDALGCLKMLLRDFQHHQIEMACAFVEVTGVYLYNCRDARLLMNVFLDQML
RLKTATAMDSRHAAQIESVYYLVKPPESSKREPMVRPAMHEYIRYLIFEELCKQNVDRCIKMLRRIDWQDPETNC
YAIKCLSKAYLLRFQLIRCLADLVSGLSSYQPRAVTIVIDNVFEDIRAGLEIHSPRMAQRRIAMAKYLGEMYNYK
LVESTNILNTLYSIISLGVSNDQNVVSPLDPPDSLFRLKLACMLLDTCAPYFTSQATRKKLDYFLVFFQHYYWFK
KSHPVFSKTENTSDLFPILMDHTYRDCLLNVRPKLKIYKSLEQAKAAIDHLQEKLYPQLKTTNNAQDPSLGTISE
ISEIDEGGTDEDSGSSNDQRERQVSGQEQDQSNDWTENEAEPPLPPLPPPEKSKEDLEFEQLYEKMTTDSYQERL
KEPIKATAKDIPVPMMARLQKKSYDQITGAQTIGPGINNMSQISKSVPNQDGTPGSPGADSPDGNGKSGGGVGGS
DVGAAGAAGASGATSVPFVLMVRGHKGGKQQFKSFVAPSDSHLATNLKRQEQMIREEKEKVKRLTLNITERIEEE
DYQESLMPPQHRNFTQSYYQKPNKHKFKHQKGAPDADLIFH
```

Table 2.1 & 2.2 Represents the amino acid sequence of UPF1 and UPF2 used to produce potential epitope against the target protein, source (FlyBase ID FBgn0030354 and FBgn0029992).

2.13.1 Step wise Antibody production from Abmart

The selected Protein immunogen was over-expressed in *E. coli*, and Ni-affinity chromatography was used to further purify the immunogen. Purified immunogen were then immunized to three 8 to 12-week old laboratories- bred strain of house mouse (BALB/C mice, female). After immunization, the mouse that shows the desired immune-response were selected for hybridoma production. To produce the hybridoma, SP2/0 myeloma cells fused with selected mouse spleen cells. Next both cell mixtures were diluted, and hypoxanthine-aminopterin-thymidine (HAT) were used to grow the clone from single parent cells on microtitre wells. Secreted antibodies were then assayed by enzyme - linked immunosorbent assay (ELISA) based on their binding affinity towards antigen from different clones. Once the desired clone selected, the hybridoma cells were injected into the peritoneal cavity of mice. These produced tumors in mice after 10-14 days of injection and these tumors filled with an antibody-rich fluid called ascites fluid. These ascites fluids were then used for screening the best antibody. Once the desired clone was chosen, the Protein A/G affinity chromatography used to purify further the antibody.

2.14 Statistical analysis

Analysis of variance (ANOVA) one-way test was used to check the mean values among the RNAi treatment groups with the control group. Statistical significance calculated with Power of performed test with alpha = 0.050: 1.000. $P < 0.05$ indicates difference is statistically significant, whereas, $P > 0.05$ denotes the difference is due to random sampling variability; there is not a statistically significant difference.

Chapter 3

3.0 EJC components associate with transcription sites on *Drosophila* polytene chromosomes

3.1 Summary or Introduction

The Exon Junction Complex (EJC) is a multi-protein complex that binds to the mRNA after splicing in the nucleus, and is one of the best characterised components of messenger ribonucleoprotein particles (mRNPs). Binding of the EJC assists with the passage of an mRNA through the nuclear pore to the cytoplasm, where it determines the fate of mosts mRNAs. To date, most evidence stipulates that this complex has a significant role in downstream events. EJC has a crucial role in NMD, where it contributes to recognition and degradation of mRNAs containing premature translation termination codons (PTCs) in the cytoplasm of mammalian cells. In addition, this complex also has a prime role in enhancing translation and localization of the mRNA (Mohr et al., 2001; Nott et al., 2004). However, more recent studies show that this complex is required for the splicing of genes that contain long introns, and loss of this complex results in abnormally spliced transcripts (Ashton-Beaucage et al., 2010; Ruiz-Echevarria et al., 1998). Since splicing is typically a co-transcriptional event, I aimed to visualize the recruitment of EJC proteins at transcription sites on *Drosophila melanogaster* polytene chromosomes, providing a unique system to visualize transcription, pre-mRNA processing and associated factors. I used indirect immunostaining to localize three proteins that constitute the core of the EJC. Here I report that association of these proteins with gene loci is transcription dependent, but surprisingly, RNA independent. Notably, their association with both intron-containing and intron-less genes, arguing against current predictions that the EJC binds only spliced mRNAs or intron

containing pre-mRNAs. To further characterise the role of EJC proteins at transcription sites, I carried out chromatin immunoprecipitation, followed by high-throughput sequencing (ChIP-seq), of the EJC proteins and found that the core EJC component Y14 accumulates at transcription start sites. I also showed experimental evidence that Y14 and MAGO might be involved in regulating transcription of ecdysone inducible genes.

3.2 Results

3.2.1 The core EJC proteins are abundant in both nucleus and cytoplasm

The core EJC proteins, Y14, MAGO, and eIF4AIII, are present in both the nucleus and cytoplasm of cells across organisms and cell types. This feature is apparent in salivary glands, which are composed of large cells with polytenic nuclei, providing a good cell model to visualize the subcellular localization of the proteins (Hochstrasser and Sedat, 1987). Immunostaining of whole salivary glands show that all three EJC proteins are present in both the nucleus and cytoplasm (Figure 3.1 A). While the signal appears more intense in the nucleus, particularly around the chromosomes, a strong signal is visible in the cytoplasm, although not in the vesicles, which are abundant at this stage of larval development, prior to the peak of secretion of glue protein (Biyasheva et al., 2001). Moreover, knockdown of Y14 and MAGO in salivary glands significantly reduced the signal compared to control glands (Figure 3.1 B). The knockdown experiment was carried out by crossing fkh-Gal4 lines with Y14 RNAi and MAGO RNAi lines, described later in this chapter. These findings suggest that antibodies are specific against the *Drosophila* endogenous Y14 and MAGO. In addition, specificity of these antibodies was also checked in S2 cell extracts by Western blotting. From the western blot, all antibodies show a single band corresponding to endogenous proteins, with minimal cross-reactivity (Figure 3.1 C). These antibodies were raised in rabbit and affinity purified by our collaborator Dr. Marco Blanchette (Stowers Institute for Medical Research, USA). To provide a more quantitative estimate of the levels of EJC proteins in the nucleus compared to cytoplasm, I assayed the three proteins by Western blotting of nuclear and cytoplasmic fractions of *Drosophila* S2 cells. I found these proteins to be equally distributed between the two compartments (Figure 3.1 D). As the volume of the cytoplasm is larger, the proteins will be more concentrated in the nucleus of these cells.

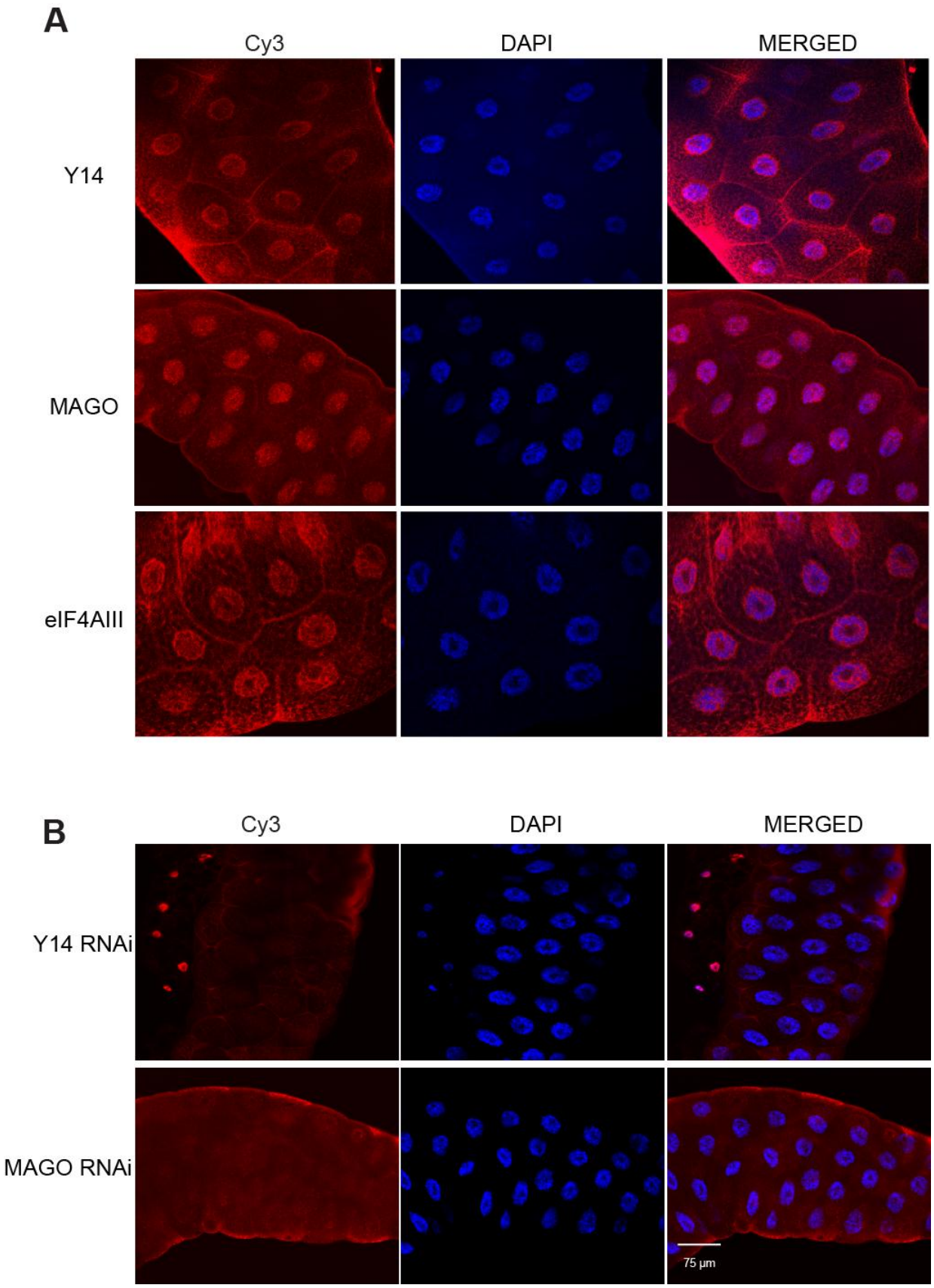
A
Cy3
DAPI
MERGED
Y14
MAGO
eIF4AIII
B
Cy3
DAPI
MERGED
Y14 RNAi
MAGO RNAi
75 µm

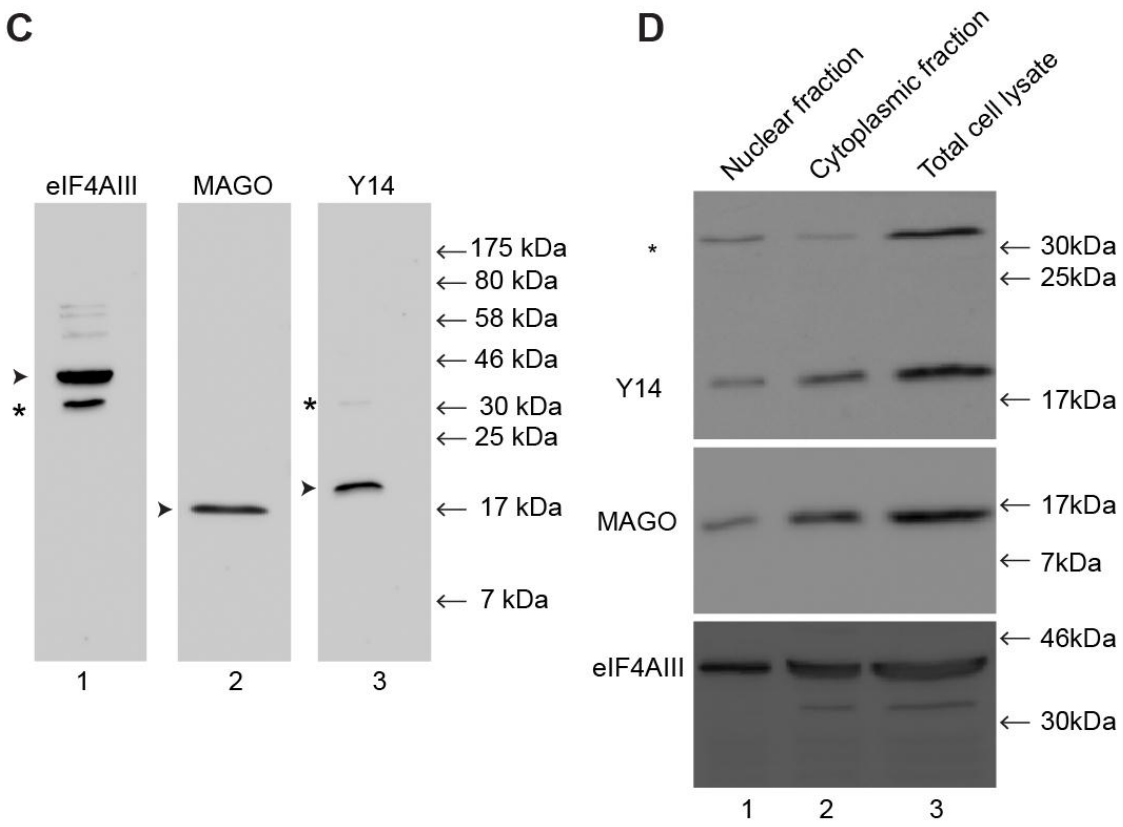

Figure 3.1 Subcellular localization of EJC proteins in salivary glands

(A) Indirect immunostaining of whole salivary glands with anti-Y14, anti-MAGO and anti-eIF4AIII antibodies, and detected with Cy3 conjugated (red signal) secondary antibody, showed a signal in both the nucleus and cytoplasm. Glands were counterstained with DAPI (middle panels), and rightmost panels show the merged channels of Cy3 and DAPI. (B) Y14 RNAi (S-305, ID-36585, see Appendix III) and MAGO RNAi (S-252,ID-28132, see Appendix III) lines were crossed with fkh-Gal4, to express dsRNA against the endogenous Y14 and MAGO in salivary glands, and stained with anti-Y14 and anti-MAGO antibodies. (C) Western blot of whole S2 cell extract, immunoblotted with Y14 (lane 3, 19.01 kDa), MAGO (lane 2, 17.31 kDa) and eIF4AIII (lane 1, 45.65 kDa). (*) denotes might be the

degradation product of eIF4AIII in lane 1 and isoform of Y14 at lane 3. (D) Distribution of Y14, MAGO and eIF4AIII in the nuclear fraction (lane 1) cytoplasmic fraction (lane 2) of S2 cells and of whole cell lysate (lane 3), detected with anti-Y14, anti-MAGO and anti-eIF4AIII via Western blot.

3.2.2 Visualization of EJC components at polytene chromosome transcription sites

The polytene chromosomes of *Drosophila melanogaster* are expanded interphase chromosomes, each locus containing around a thousand copies of each gene, therefore providing an effective system to analyse the association of individual proteins with sites of transcription and nascent pre-mRNA (Hochstrasser and Sedat, 1987; Matunis et al., 1993). Pre-mRNA splicing is typically co-transcriptional in *Drosophila* (Khodor et al., 2012); so I used the polytene chromosomes to gain insights into why the EJC seems to associate only with a subset of transcripts in *Drosophila* (Sauliere et al., 2010). I performed indirect immunostaining with antibodies for the three EJC core proteins, Y14, MAGO, and eIF4AII. All three antibodies predominantly stain the interbands of the polytene chromosome, which are decondensed segments containing one or more actively transcribed gene loci (Figure 3.2 A). The signals from all three EJC proteins colocalize with that of hyperphosphorylated RNA polymerase II (Pol II^{Ser2}) (Figure 3.2 B), which is a marker of active transcription elongation (O'Brien et al., 1994). As expected from the observation that Y14 and MAGO form a stable heterodimer *in vitro* (Lau et al., 2003), the staining patterns of Y14 and MAGO are very similar; this is most apparent at the cytological regions 58E, 56E, 50C and 53D which can be mapped using the DAPI banding pattern (further evidence that Y14 and MAGO colocalize will be show further below). However, as exemplified by position 60E, other sites show intense eIF4AIII signals yet Y14 and MAGO signals are either absent or very faint (Figure 3.2 A). This difference in staining pattern is more apparent by comparison to parallel Pol II^{Ser2} immunostaining; eIF4AIII is observed at every Pol II transcription site, but the Y14 and MAGO signals are either absent or weak at intense Pol II^{Ser2} sites (Figure 3.2 B, indicated by arrows). In contrast, at some other sites I detected relatively strong EJC protein signals but weak Pol II^{Ser2} (Figure 3.2 B, indicated by lines).

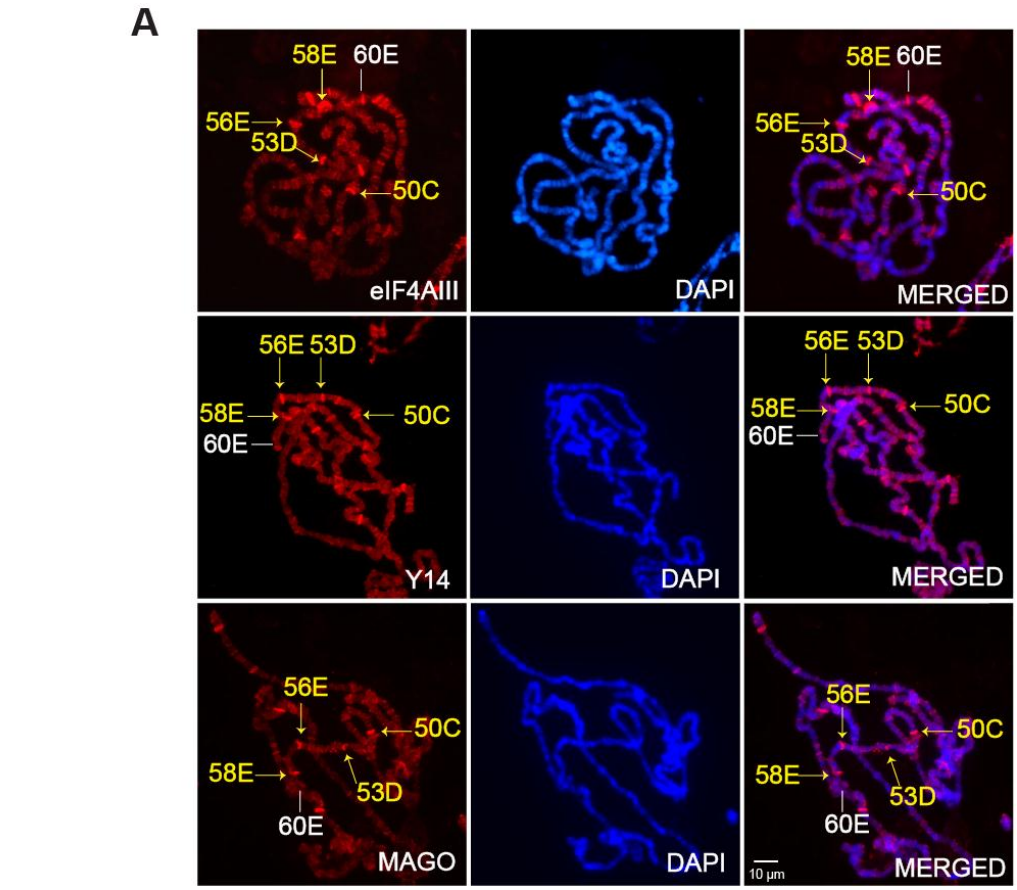
A
58E
60E
56E
53D
50C
eIF4AIII
DAPI
MERGED
56E 53D
58E
60E
50C
Y14
DAPI
MERGED
56E
50C
58E
53D
60E
MAGO
DAPI
10 µm
MERGED

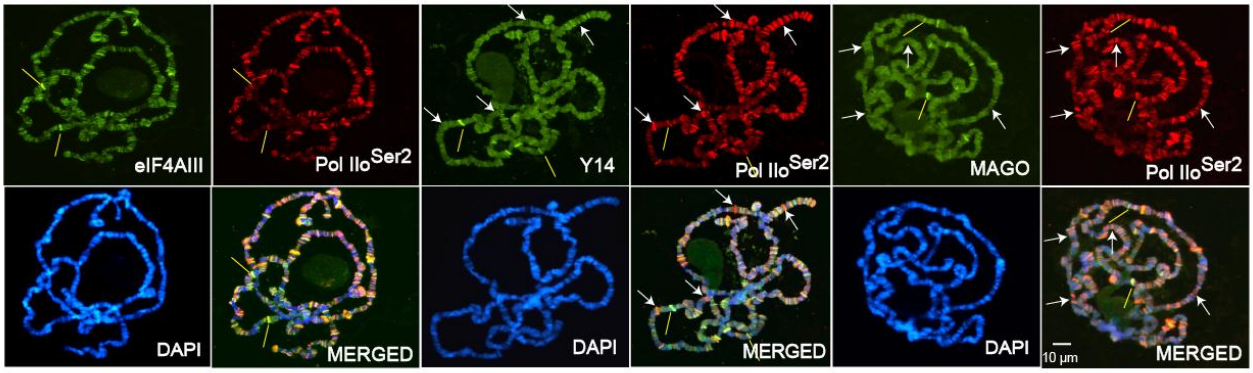
B
eIF4AIII
Pol IIo Ser2
Y14
Pol IIo Ser2
MAGO
Pol IIo Ser2
DAPI
MERGED
DAPI
MERGED
DAPI
10 µm
MERGED

Figure 3.2 EJC core components are at transcription sites of polytene chromosomes

(A) Indirect immunostaining of chromosome squashes with anti-eIF4AIII (top panel), anti-Y14 (middle panel) and anti-MAGO (bottom panel) primary antibodies, subsequently detected using a Cy3-conjugated (red signal) secondary antibody. The yellow arrows indicate the positions of the most apparent interbands in all channels, while the white line shows the position of a highly intense eIF4AIII signal that is faint in Y14 and MAGO staining. The middle panels show DAPI (blue) to mark DNA, whereas the top right channels are the merged images of DAPI and Cy3.

(B) Double immunostaining was performed with antibodies against each of the three EJC components and against hyperphosphorylated RNA Pol II^{Ser2} (H5). EJC proteins were detected with a FITC-conjugated secondary antibody (green) while Pol II was detected with a Cy3-conjugated secondary antibody (red signal). White arrows indicate the position of a strong Pol II^{Ser2} signal but weak EJC signals, whereas the yellow line shows a strong EJC but weak Pol II signal. All images were counterstained with DAPI to show the DNA. Images were captured using an epifluorescence microscope with a 40X objective.

3.2.3 Colocalization confirms Y14 and MAGO might form a heterodimer at same transcription sites

As shown above, immunostaining of polytene chromosomes gives similar banding patterns for both Y14 and MAGO, consistent with the proteins forming a stable heterodimer. To directly investigate the extent of Y14 and MAGO colocalization at the chromosomes, and in general to characterise more in detail the association of EJC proteins with transcription sites, I made use of transgenic fly lines encoding Y14 and eIF4AIII, double tagged at their C-termini with 2x FLAG and 2x HA epitopes (these strains were generated by our collaborator Dr Marco Blanchette). The transgenes are under the control the UAS promoter, so can be expressed in salivary glands by crossing them with the forkhead-Gal4 driver, which is highly expressed salivary glands (Henderson and Andrew, 2000). Western blotting of salivary gland extracts shows that the double-tagged Y14 and eIF4AIII proteins migrate as predominantly a single band of the expected size (Figure 3.3 A & B). These tagged proteins appear to be functional, since immunostaining revealed a chromosomal banding pattern very similar to that of endogenous Y14 and eIF4AIII (Figure 3.3 C). Specifically, both FLAG-tagged Y14 and endogenous Y14 give the same pattern on chromosomal sites when I carried out double immunostaining with antibodies against the FlAG-tagged Y14 and endogenous Y14 (Figure 3.4 A). The same approach was also used for FlAG-tagged eIF4AIII and endogenous eIF4AIII (Figure 3.4 B). Next, to directly assess the extent of co-localization of Y14 and MAGO, I crossed the FLAG-tagged transgenic lines with the forkhead-Gal4 driver, dissected salivary glands from mid-3rd instar larvae and stained the polytene chromosome with anti-FLAG and anti- MAGO to detect tagged-Y14, and endogenous MAGO. The immunostaining signals of the two proteins show complete colocalization along the chromosomes and in the nucleolus (Figure 3.5). Chromosomes were also stained with DAPI and the co-localization

signal was comparable in the merged channel at transcribed gene loci. The above results strongly indicate that Y14 and MAGO might form a constitutive heterodimer at transcription sites, consistent with observations made in previous *in vitro* studies.

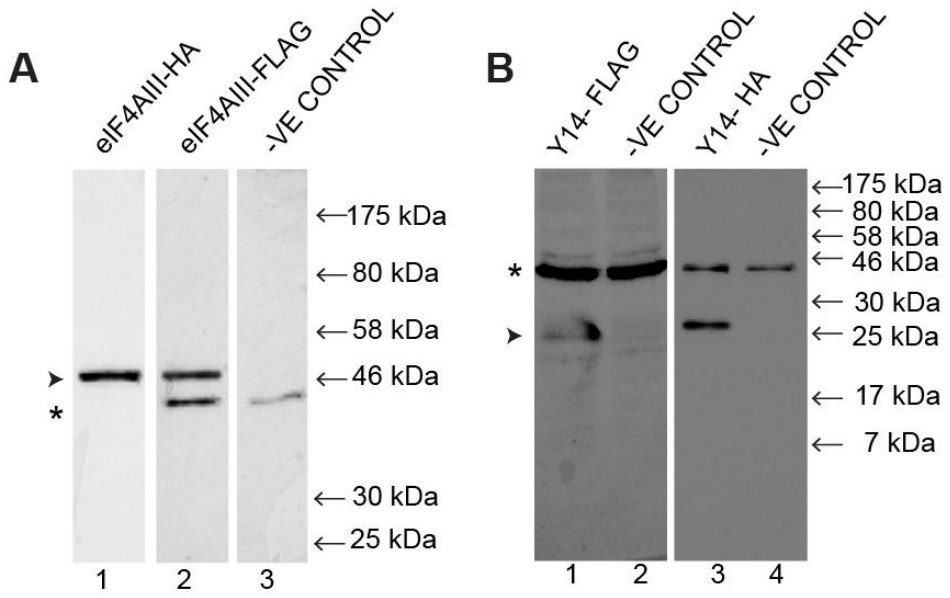
A
eIF4AIII-HA
eIF4AIII-FLAG
-VE CONTROL
175 kDa
80 kDa
58 kDa
46 kDa
30 kDa
25 kDa
1
2
3
B
Y14- FLAG
-VE CONTROL
Y14- HA
-VE CONTROL
175 kDa
80 kDa
58 kDa
46 kDa
30 kDa
25 kDa
17 kDa
7 kDa
1
2
3
4

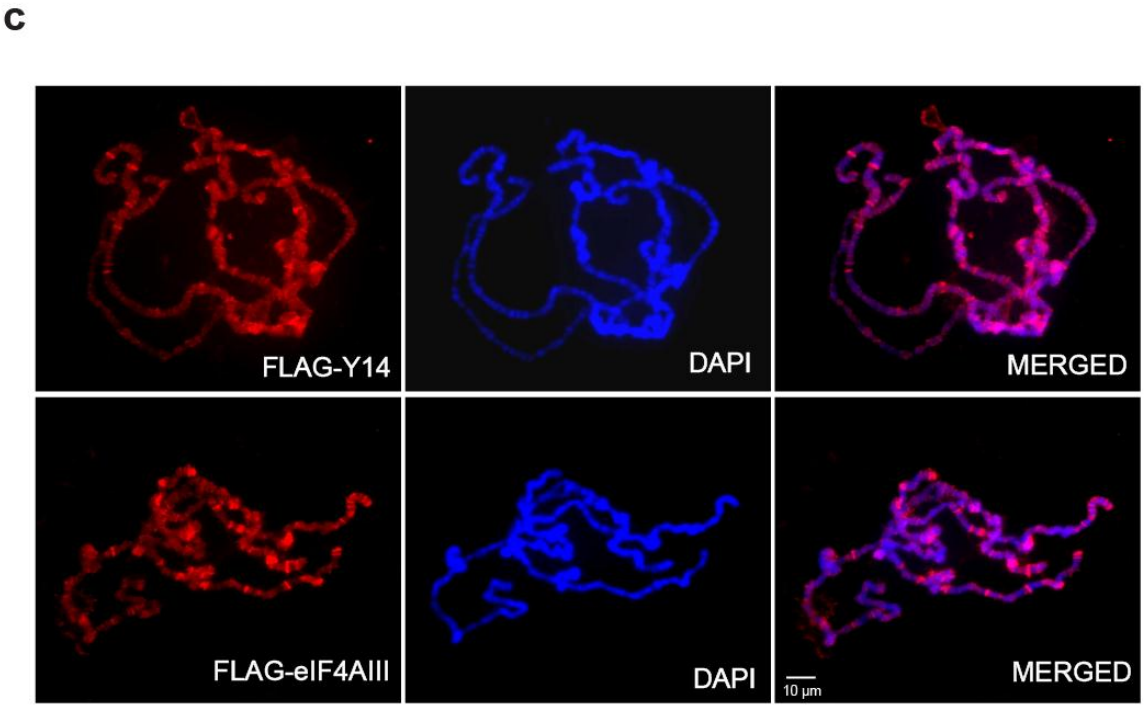
c
FLAG-Y14
DAPI
MERGED
FLAG-eIF4AIII
DAPI
MERGED
10 µm

Figure 3.3 FLAG-tagged EJC protein shows identical signal patterns throughout the polytene chromosome. (A) & (B) Western blot of salivary glands from eIF4AIII FLAG/HA-tagged (S-259, see Appendix III) and Y14 FLAG/HA-tagged (S-253, see Appendix III) transgenic lines and immunoblotted with anti-FLAG M2 and anti-HA antibodies. Lane 1(A): HA-tagged eIF4AIII (50.15 kDa), lane 2: FLAG-tagged eIF4AIII (50.15 kDa) and lane 3 used as a negative control. Lane 1(B): FLAG-tagged Y14 (24 kDa), lane 3: HA-tagged Y14 (24 kDa) and lane 2 and 4 used as a negative control. (C) FLAG/HA-tagged Y14 and FLAG/HA-tagged eIF4AIII transgenic lines were crossed with an fkh-Gal4 driver (see Appendix III) and immunostained with an anti-FLAG M2 antibody (leftmost panels). A Cy3-conjugated (red signal) secondary antibody was used to detect FLAG-Y14 (top panel) and FLAG-eIF4AIII (bottom panel). The middle panels show DAPI (blue) staining to mark DNA, whereas the right channels are the merged images of DAPI and Cy3. The images were taken under a standard epifluorescence microscope with a 40X objective lens. (*) denotes nonspecific band.

A

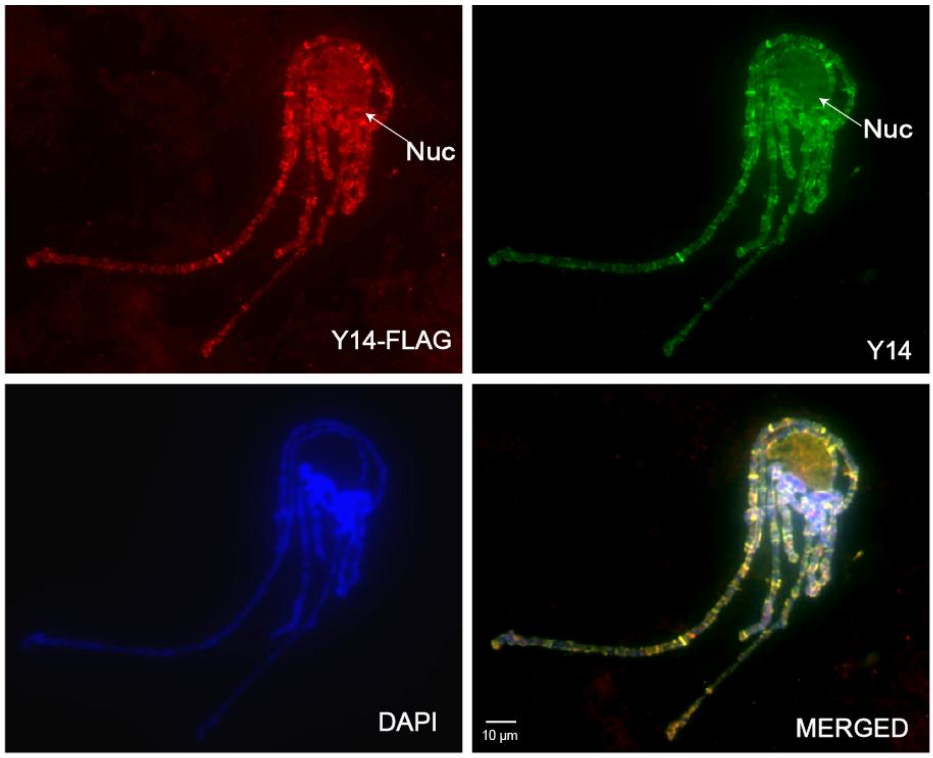
Nuc
Y14-FLAG
Nuc
Y14
DAPI
10 µm
MERGED

B

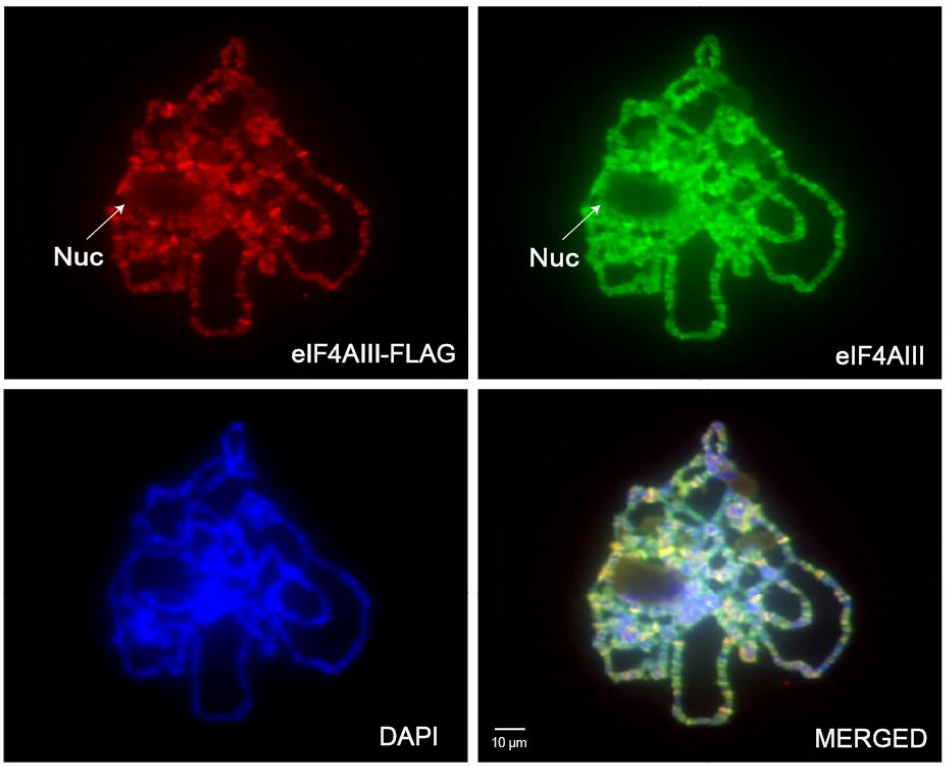
Nuc
eIF4AIII-FLAG
Nuc
eIF4AIII
DAPI
10 µm
MERGED

Figure 3.4 Expressed EJC proteins colocalize with endogenous EJC in the polytene chromosome. (A) & (B) Colocalization of FLAG-tagged Y14 (S-253, see Appendix III) with endogenous Y14 and FLAG-tagged eIF4AIII) (S-259, see Appendix III) with endogenous eIF4AIII. Expressed FLAG-tagged proteins were detected with an anti-FLAG M2 antibody (top-left panels in A&B) and endogenous Y14 and eIF4AIII were detected with anti-Y14 and anti-eIF4AIII (top-right panels in A&B). Subsequently, an Alexa Fluor 647-conjugated secondary antibody (red signal) and FITC-conjugated secondary antibody (green) were used against FLAG and endogenous Y14 and eIF4AIII. Arrows indicate the nucleolus. DAPI (blue) was used to stain the DNA (bottom-left panels in A&B), and rightmost panels are a merged image of blue, red and green channels. Images were captured with an epifluorescence microscope with a 40X objective.

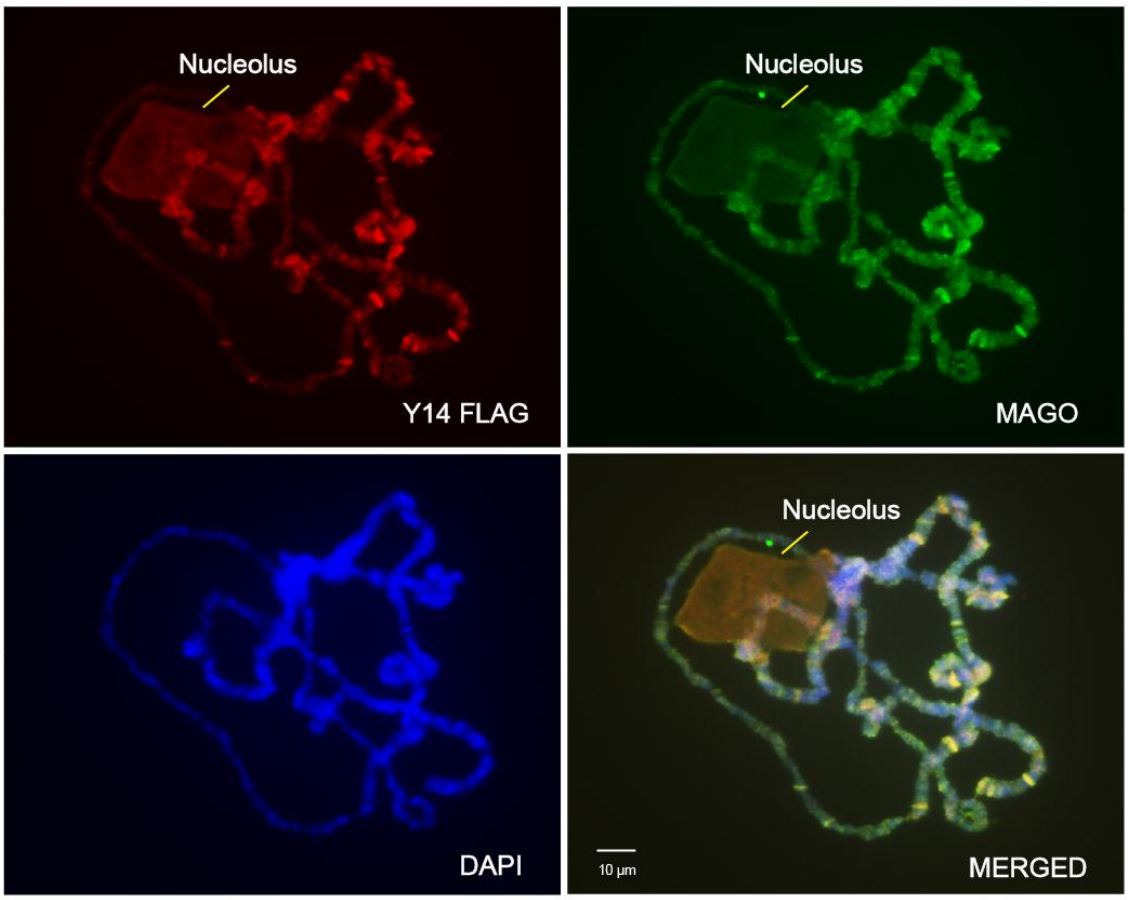

Figure 3.5 Y14 and MAGO localize at same transcription sites.

Double immunostaining with an anti-FLAG antibody to detect expressed FLAG-tagged Y14 (top-left) (S-253, see Appendix III) and anti-MAGO to detect endogenous MAGO (top-right). Subsequently, an Alexa Fluor 647 conjugated secondary antibody and a FITC-conjugated secondary antibody were used to detect FLAG-tagged Y14 (in red) and endogenous MAGO (green). The yellow arrows indicate MAGO and FLAG-tagged Y14 signals in the nucleolus. The chromosome was also stained with DAPI (bottom-left panel); the colocalization signals more apparent in the merged channels (bottom-right). Images were visualized using an epifluorescence microscope with a 40X objective.

3.2.4 Association of Y14 and MAGO with transcription sites differs from that of eIF4AIII

The EJC component eIF4AIII is thought to be the nucleating component of the complex. The protein is the first to be recruited at a splice junction by its direct interaction with the spliceosomal protein CWC22. Current models envisage that Y14 and MAGO bind eIF4AIII at the exon junction upon the latter dissociating from CWC22 (Barbosa et al., 2012; Steckelberg et al., 2012). The banding pattern of eIF4AIII at polytene chromosomes is different from that of Y14-MAGO. As shown above (Figure 3.2 B), the most apparent difference is that while eIF4AIII is at essentially every Pol II transcription site, there are many sites at which Y14 and MAGO signals are either absent or very faint, compared to both eIF4AIII and Pol II. To investigate this unexpected observation further, I performed a double immunostaining for endogenous Y14 and FLAG-tagged eIF4AIII using the transgenic line described above. These experiments clearly demonstrate that Y14 (and by inference, MAGO) are absent from sites in which a very strong eIF4AIII signal is detected (Figure 3.6). These results suggest that the association of Y14/MAGO at transcription sites is not directly linked to that eIF4AIII. The results indicate that the EJC may not be recruited at many active transcription sites, even though eIF4AIII is.

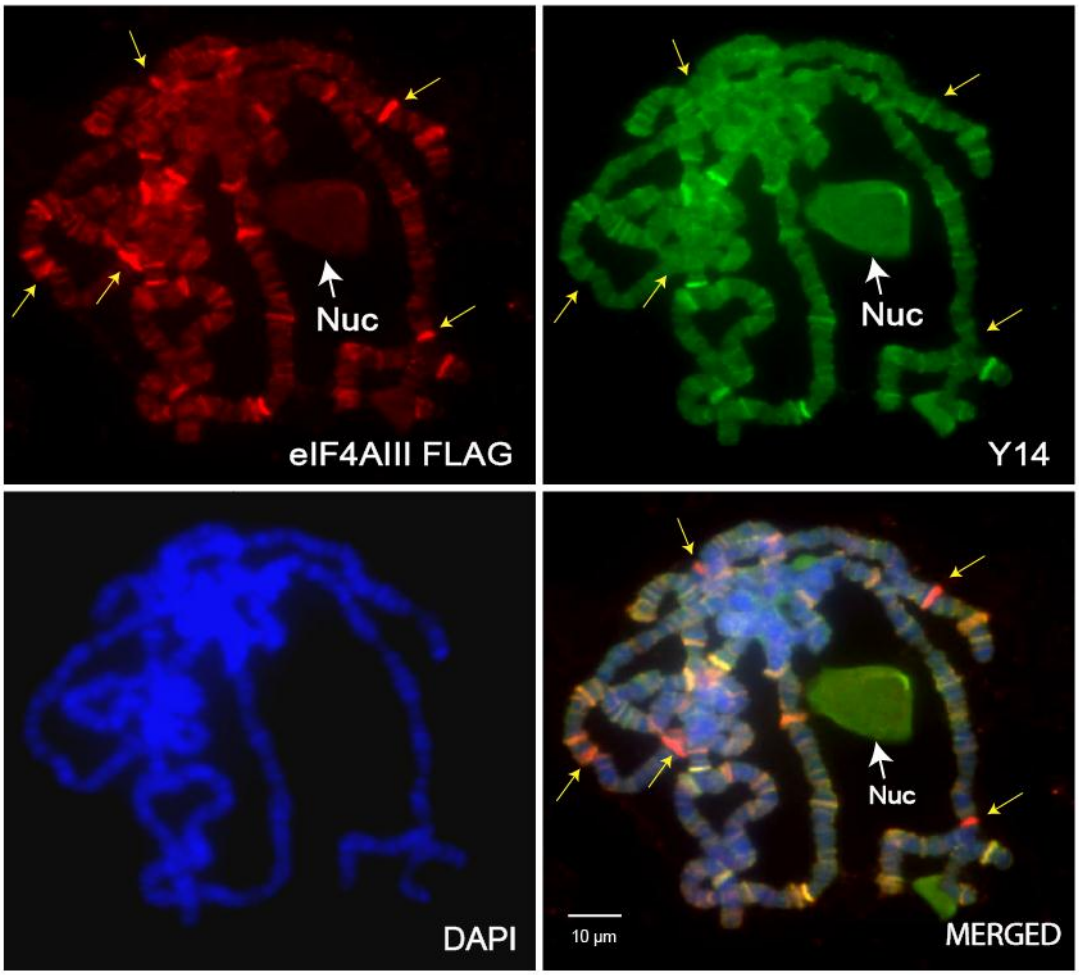

Figure 3.6 Association of eIF4AIII poorly correlates with Y14

Double immunostaining with an antibody against FLAG to detect expressed FLAG-tagged eIF4AIII (top-left) (S-259, see Appendix III) and anti-Y14 to detect endogenous Y14 (top-right) in polytene chromosomes. An Alexa Fluor 647-conjugated secondary antibody was used to detect FLAG-tagged eIF4AIII (in red) and a FITC-conjugated secondary antibody (green) was used against endogenous Y14. The white arrow indicates the nucleolus. Yellow arrows highlight locations where there is a positive FLAG-tagged eIF4AIII but where the Y14 signal absent. Chromosomes were also stained with DAPI (bottom-left panel), and the

bottom-right panel is a merged image of the DAPI, red and green channels. Images were captured using an epifluorescence microscope with a 40X objective.

3.2.5 Knockdown of the core EJC component eIF4AIII affects the development of *Drosophila* salivary glands *in vivo*

In order to study the mechanism of EJC recruitment at transcription sites, I used an *in vivo* approach to knockdown each EJC components (Y14, MAGO and eIF4AIII) in salivary glands. To knockdown these proteins we obtained Y14 and eIF4AIII RNAi lines from Bloomington (see Appendix III) and a MAGO RNAi (see Appendix III) from Vienna. These RNAi lines were all under the control of the GAL4/UAS system, therefore, a forkhead-Gal4 driver was used to express dsRNA against the target protein in salivary glands. The RNAi lines were crossed with forkhead-Gal4 lines and salivary glands were dissected from mid-3rd instar larvae. Knockdown of Y14 and MAGO does not have any obvious phenotypic effect in salivary glands compared to control condition (Figure 3.7 A). However, knockdown of eIF4AIII makes the glands significantly smaller in size compared to the Y14 and MAGO knockdowns. Additionally, in a parallel study, in which the *nucampholin* (*ncm*) gene was knocked down, a similar phenotype was observed in salivary glands (Figure 3.7 A). *Drosophila* NCM is a homologue of human pre-mRNA splicing factor CWC22, which interacts with eIF4AIII during early stages of splicing (Alexandrov et al., 2012; Barbosa et al., 2012). Although it is not yet clear whether CWC22 and eIF4AIII are recruited as a heterodimer during splicing, the observation that knockdown of both ncm and eIF4AIII give a similar phenotype suggests that eIF4AIII possibly has a role in splicing in conjugation with CWC22. Additionally, these studies also indicate that eIF4AIII has an independent role in salivary gland development and functions beyond the EJC complex. A similar observation was reported in mice, where knockdown of MAGO reduced both body and brain size by

regulating neural stem cell division (Silver et al., 2010). These findings demonstrate that the EJC core components function independently, besides have a role in post transcriptional events of mRNA. The knockdown efficiency of both Y14 and MAGO were confirmed in salivary glands by Western blot (Figure 3.7 B) and was found to be comparable to that in S2 cells (shown below).

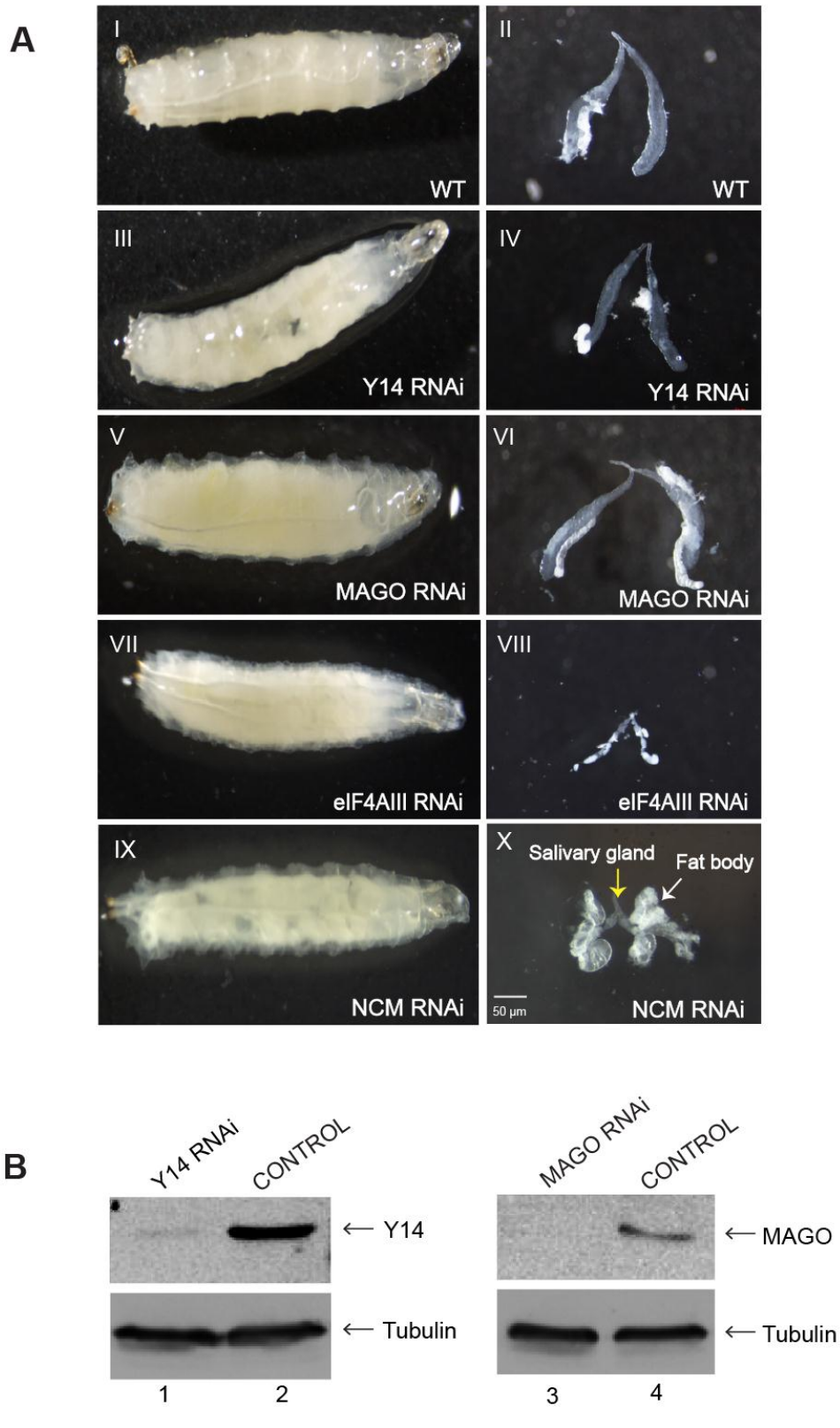
A
I
WT
II
WT
III
Y14 RNAi
IV
Y14 RNAi
V
MAGO RNAi
VI
MAGO RNAi
VII
eIF4AIII RNAi
VIII
eIF4AIII RNAi
IX
NCM RNAi
X
Salivary gland
Fat body
50 µm
NCM RNAi
B
Y14 RNAi
CONTROL
← Y14
← Tubulin
1
2
MAGO RNAi
CONTROL
← MAGO
← Tubulin
3
4

Figure 3.7 eIF4AIII is required for salivary gland development in *Drosophila*

(A) Y14, MAGO, eIF4AIII and NCM were selectively knocked down in salivary glands using RNAi lines. RNAi lines received from Bloomington include Y14 RNAi (ID-36585, S-305) and eIF4AIII RNAi (ID-32444, S-307) while MAGO RNAi (ID-28132, S-252) and NCM RNAi (S-314, ID-17304) (See Appendix III for all RNAi lines) lines were from Vienna. Each of these RNAi lines was expressed in salivary glands by crossing with the fkh-Gal4 driver. Knockdown of eIF4AIII and NCM makes the gland significantly small (bottom right panel VIII &X)) compared to the control wild-type (top right), Y14 RNAi and MAGO RNAi. Yellow arrows show salivary gland size, while the white arrow indicates the fat body upon knockdown of NCM (bottom right panel, X). However, there were no such changes observed in 3rd instar larvae size (left panels). (B) Western blot analysis to check the knockdown efficiency of Y14 and MAGO in the salivary gland. Lanes 1 and 2 show immunoblotting with Y14 and lanes 3 and 4 show immunoblotting with MAGO. Knockdown efficiency compares with the control (lanes 2 and 4) and tubulin was used as a reference control.

3.2.6 Y14 is required for the association of MAGO with transcription sites *in vivo*

While eIF4AIII knockdown makes glands too small for preparing chromosome squashes, neither RNAi of Y14 nor MAGO hinders larval development or polytenization, therefore it was possible to directly assess whether knockdown of Y14 affects recruitment of MAGO at transcription sites, and whether either of them is involved in eIF4AIII chromosomal association. To address this issue, I first analysed Y14 RNAi lines crossed with forkhead-Gal4 lines and salivary glands dissected from mid-3rd instar larvae. Staining with a Y14 antibody shows drastically reduced the Y14 signal from the chromosomal sites, (Figure 3.8 A). The MAGO signal however, was completely gone from both chromosomes and the nucleolus. Notably, knockdown of Y14 has no effect on the association of eIF4AIII with transcription sites, as signals are still present at transcriptional loci (Figure 3.8 A). The results from these data suggest that Y14 is required for the recruitment of MAGO at actively transcribed gene loci, but that Y14 is not required for eIF4AIII chromosomal association. Secondly, I analysed the effect of MAGO knockdown of the association of Y14. Consistent with Western blotting results (Figure 3.7B), the MAGO signal is drastically reduced (Figure 3.8 B); however, that of Y14 was only partially reduced at the chromosomes, and was very intense in the nucleolus (Figure 3.8 B). MAGO is therefore not necessary for Y14 association with transcription sites. The partial reduction in the Y14 signal might be the result of destabilization of the protein rather than MAGO being required for recruitment and association with the chromosomes. As observed earlier for Y14, MAGO knockdown does not affect eIF4AIII association with transcription sites (Figure 3.8 B).

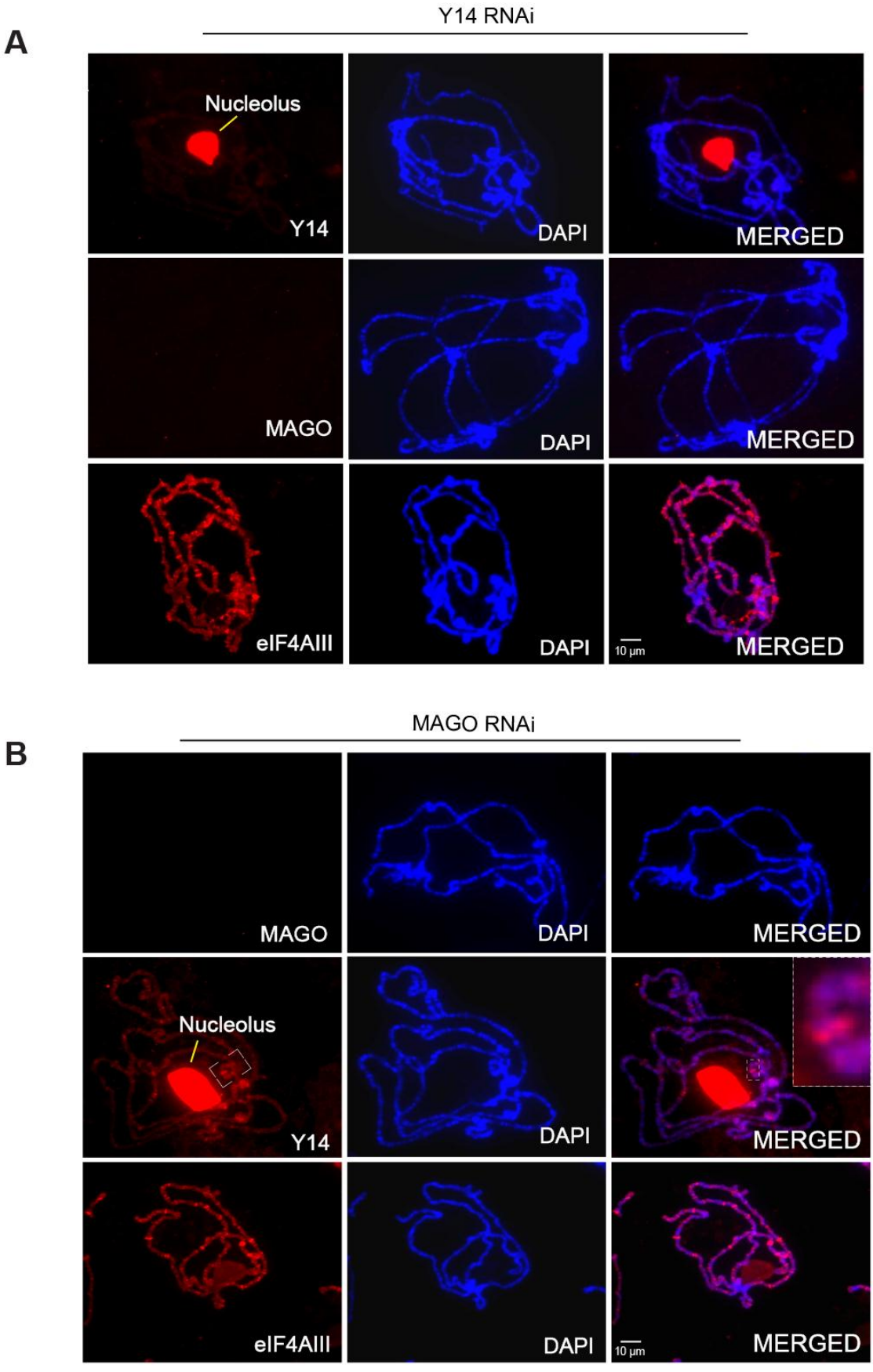
A
Y14 RNAi
Nucleolus
Y14
DAPI
MERGED
MAGO
DAPI
MERGED
eIF4AIII
DAPI
10 µm
MERGED
B
MAGO RNAi
MAGO
DAPI
MERGED
Nucleolus
Y14
DAPI
MERGED
eIF4AIII
DAPI
10 µm
MERGED

Figure 3.8 Y14 recruitment does not require MAGO but MAGO recruitment does require Y14

(A) Y14 RNAi lines from Bloomington (ID-36585, S-305), were crossed with an fkh-Gal4 driver to knockdown Y14 in salivary glands which were subsequently immunostained with Y14 (top-left) MAGO (middle-left) and eIF4AIII (bottom-left). A Cy3-conjugated (red signal) secondary antibody was used to detect EJC proteins. An arrow (in yellow) indicates a strong Y14 signal in the nucleolus (top-left panel). Y14 knockdown eliminates the MAGO signal from transcription sites, whereas there was no effect on the eIF4AIII signal. All images were also stained with DAPI, and the rightmost panels are the merged images of DAPI and Cy3 signals. (B) In a similar way, MAGO RNAi lines from Vienna (ID-28132, S-252) were used to knockdown MAGO in salivary glands which were subsequently stained with MAGO (top-left), Y14 (middle-left) and eIF4AIII (bottom-left). These proteins were again detected with Cy3-conjugated (red signal) secondary antibody. MAGO knockdown partially eliminates the Y14 signal, and this was more apparent in the magnified inserts of the main image (indicated by the box) in the merged channels. All slides were counterstained with DAPI and merged images are shown in the rightmost panels. The images were taken under a standard epifluorescence microscope.

3.2.7 Dimerization stabilizes Y14 and MAGO

The results shown above, as well as published data, suggest that Y14 and MAGO form a heterodimer, but why this heterodimer is important for these two proteins is poorly understood. To further investigate the role of Y14 and MAGO heterodimerization, I selectively knocked down the core EJC components Y14, MAGO and eIF4AIII, in *Drosophila* S2 cells. Knockdown efficiency was verified by both Western blotting and q-RT-PCR. A significant level of knockdown was achieved for Y14, and was almost complete for MAGO. However, the knockdown level of eIF4AIII was less compared to Y14 and MAGO (Figure 3.9 A). Notably, Y14 knockdown also drastically reduces MAGO expression, as determined by the observation that the MAGO signal was completely gone when carrying out Western blotting (Figure 3.9 B). In the same way I investigated the effect of knocking down MAGO and then blotting for Y14, however, the signal for Y14 although reduced, was not depleted completely (Figure 3.9 C). In both cases, eIF4AIII was affected to a lesser extent compared to Y14 and MAGO. This raises the possibility that Y14 might affect MAGO transcript levels. To evaluate this possibility, I checked the transcript levels of both Y14 and MAGO knockdowns in S2 cells. The result was that knockdown of Y14 does not affect transcript levels of MAGO and neither does knockdown of MAGO affect those of Y14 (Figure 3.9 D & E). These results therefore suggest that Y14 and MAGO heterodimerization is required for the stability of this complex *in vivo*.

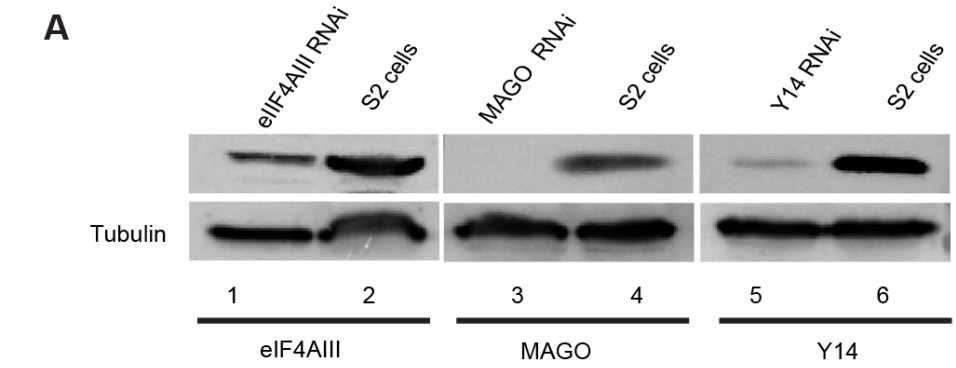
A
eIIF4AIII RNAi
S2 cells
MAGO RNAi
S2 cells
Y14 RNAi
S2 cells
Tubulin
1
2
3
4
5
6
eIF4AIII
MAGO
Y14

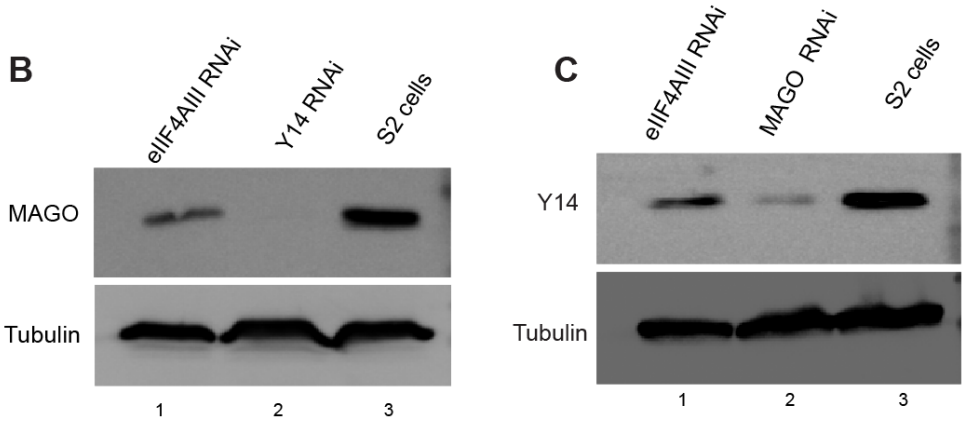
B
eIIF4AIII RNAi
Y14 RNAi
S2 cells
MAGO
Tubulin
1
2
3
C
eIIF4AIII RNAi
MAGO RNAi
S2 cells
Y14
Tubulin
1
2
3

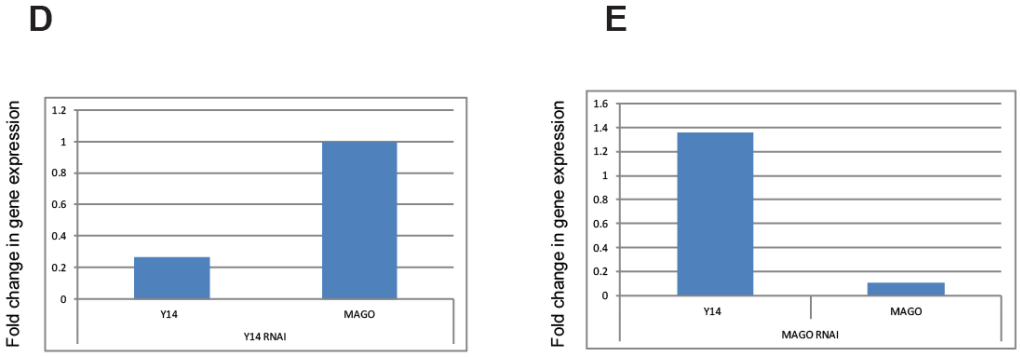
D
Fold change in gene expression
1.2
1
0.8
0.6
0.4
0.2
0
Y14
MAGO
Y14 RNAI
E
Fold change in gene expression
1.6
1.4
1.2
1
0.8
0.6
0.4
0.2
0
Y14
MAGO
MAGO RNAI

Figure 3.9 Y14 and MAGO dimerization is required for the stability of this complex

A) Y14, MAGO and eIF4AIII were selectively knocked down in S2 cells by expressing dsRNA against the endogenous proteins. Knockdown efficiency was checked by Western blot with antibodies against eIF4AIII (lanes 1 and 2), MAGO (lanes 3 and 4) and Y14 (lanes 5 and 6). (B) Western blot to check the protein levels of MAGO upon knockdown of eIF4AIII (lane 1), Y14 (lane 2) and in control S2 cells (lane 3). (C) Western blot to check the protein levels of Y14 upon knockdown of eIF4AIII (lane 1), MAGO (lane 2) and in control S2 cells (lane 3). Tubulin was used as a reference control in all of the above experiments. (D) & (E) qRT-PCR to check transcript levels of Y14 and MAGO in S2 cells upon knockdown of Y14 and MAGO. The fold enrichment method was used for calculation and normalized to reference control RpL32 See Appendix II (S 78 to S 81) for the Y14 and MAGO primer pairs.

3.2.8 Association of EJC core components at transcription sites seems RNA independent

As described above, all three EJC core proteins (Y14, MAGO and eIF4AIII) are present at transcription sites. Current observations predict that the association is primarily with nascent RNA. To test the prediction, I treated the polytene chromosome with RNase A (see details in Material and Methods and figure legends). As a positive control I made use of Sm proteins, which are core shared components of the small nuclear ribonucleoproteins (snRNPs) that form the spliceosome (Will and Luhrmann, 2001). An antibody specific for Sm proteins stains polytene chromosome transcription sites and the signal is characteristically highly sensitive to RNase A treatment (Matunis et al., 1993). As predicted by the observations described above (Figure 3.2A.), I found that Y14 is present at many but not all transcription sites, some of which are Sm-positive while others are not (Figure 3.10 A). Notably, while RNase treatment completely removed the Sm signal in all chromosome squashes treated, that of Y14 was reproducibly indistinguishable from that in control squashes (Figure 3.10 B). These data suggest that the association of Y14 with transcription sites might not be via RNA. The same result was also observed with the other core protein, eIF4AIII (Figure 3.10 C-D). Although RNase sensitivity was not tested for MAGO, since is constitutively paired with Y14, we predict that its chromosomal association is equally resistant to RNase treatment.

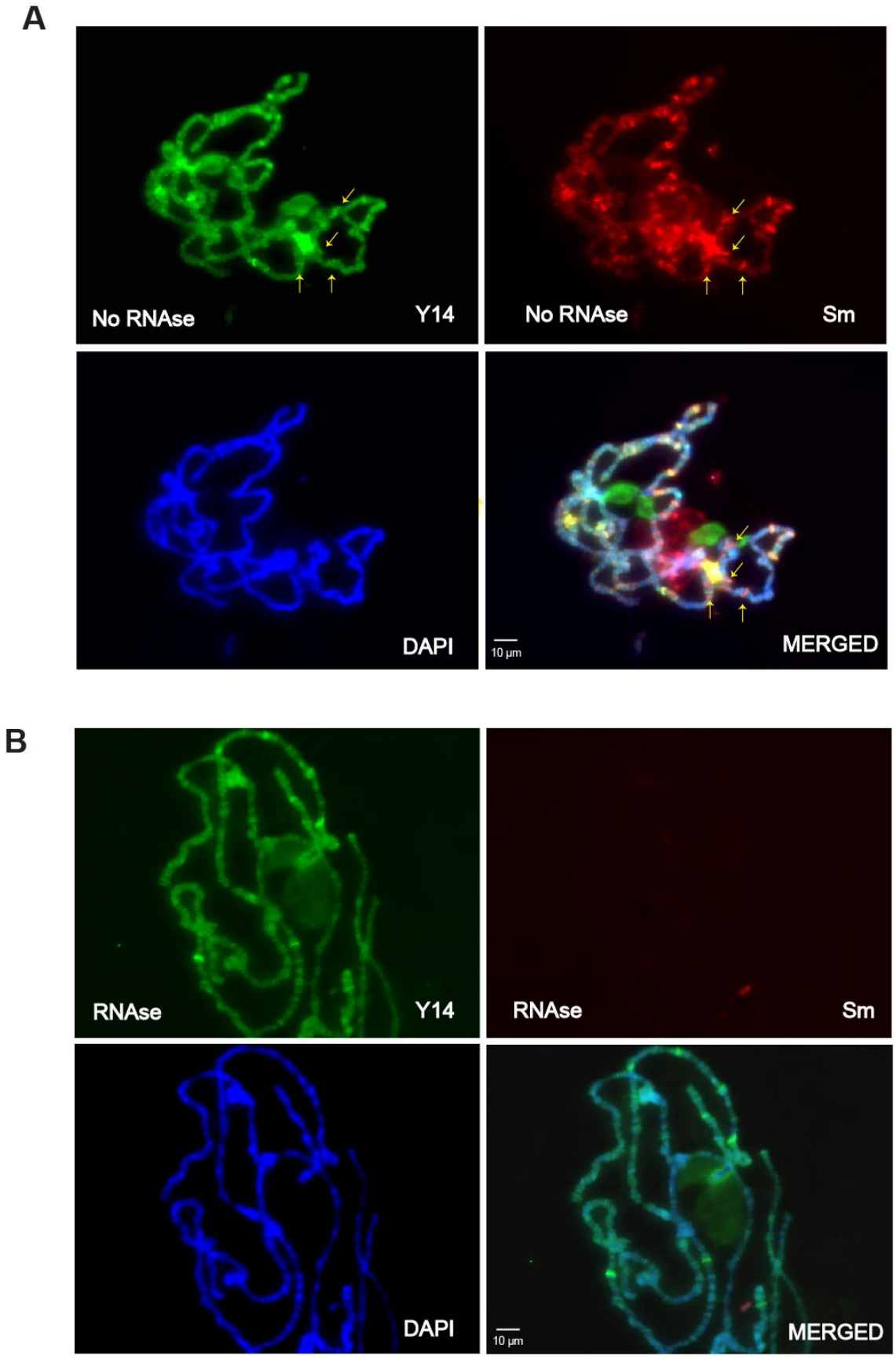
A
No RNAse
Y14
No RNAse
Sm
DAPI
10 µm
MERGED
B
RNAse
Y14
RNAse
Sm
DAPI
10 µm
MERGED

C

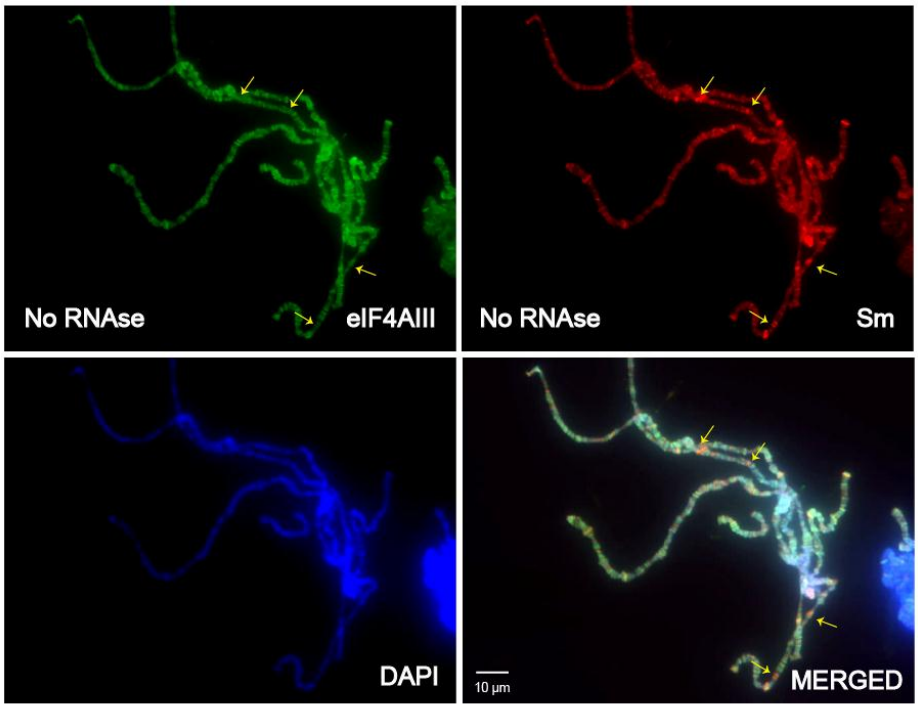
No RNAse
eIF4AIII
No RNAse
Sm
DAPI
10 µm
MERGED

D

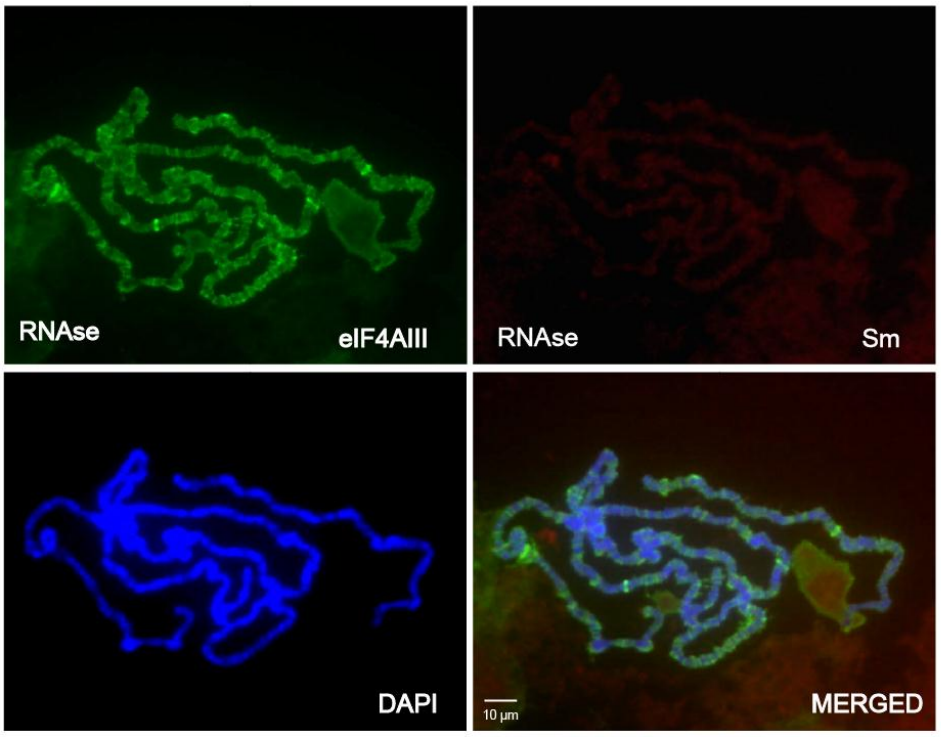
RNAse
eIF4AIII
RNAse
Sm
DAPI
10 µm
MERGED

Figure 3.10 Association of EJC proteins is RNA-independent (A) Top panel indicates double immunostaining with anti-Y14 and anti-Y12 (Sm) and (C) anti-eIF4AIII and anti-Y12 in the polytene chromosome shows the Y14, eIF4AIII and Sm signals to be present at most transcription sites in the absence of RNase. Subsequently, anti-Y14, anti-eIF4AIII and anti-Y12 were detected with a FITC-conjugated secondary antibody (green) and an Alexa Fluor 647-conjugated secondary antibody (red signal). Arrows indicate sites where the Sm signal did not colocalize with Y14 and eIF4AIII. Bottom (B) and (D) panel shows that following treatment with 1 µg/µl RNase A, the Y14, and eIF4AIII signals persist, whereas the Sm signal is absent from transcription sites. All samples were also counter stained with DAPI (blue) and the rightmost bottom panels show the merged images of DAPI, red and green channels. Images were taken using a standard epifluorescence microscope with a 40X objective lens.

3.2.9 Nascent RNA labelling indicates EJC core proteins are not primarily associated with pre-mRNA

Having observed that Y14 and eIF4AIII resist RNase treatment, it is possible that the recruitment of core EJC proteins at transcription sites is independent of RNA. While the snRNAs to which Sm proteins are bound could be more sensitive to RNase than nascent RNA, these observations suggest that the protein components of nascent RNA, such as the EJC, can make RNA-independent secondary contacts with chromatin or DNA directly. To address this issue, I labelled nascent RNA with fluorouridine. The function of fluorouridine is comparable to bromouridine as both are uridine derivatives used to label nascent RNA (Chang et al., 2000). To label the nascent RNA in this way, polytene chromosomes were first incubated with fluorouridine for 15 minutes prior to RNase A treatment, and a parallel control sample was prepared without RNase treatment (see details in Material and Methods). As expected, signals for both Y14 and fluorouridine are seen at many interbands in the control (Figure 3.11 A.). RNase treatment drastically reduced the fluorouridine signal, but not that of Y14 (Figure 3.11 B). Similar observations were made with eIF4AIII (Figure 3.11 C-D). Therefore, these observations indicate that the EJC core proteins are not primarily recruited to transcription sites by binding nascent RNA. However, it is feasible that the recruitment of these proteins at these sites occur via other proteins present at these sites, or with DNA directly.

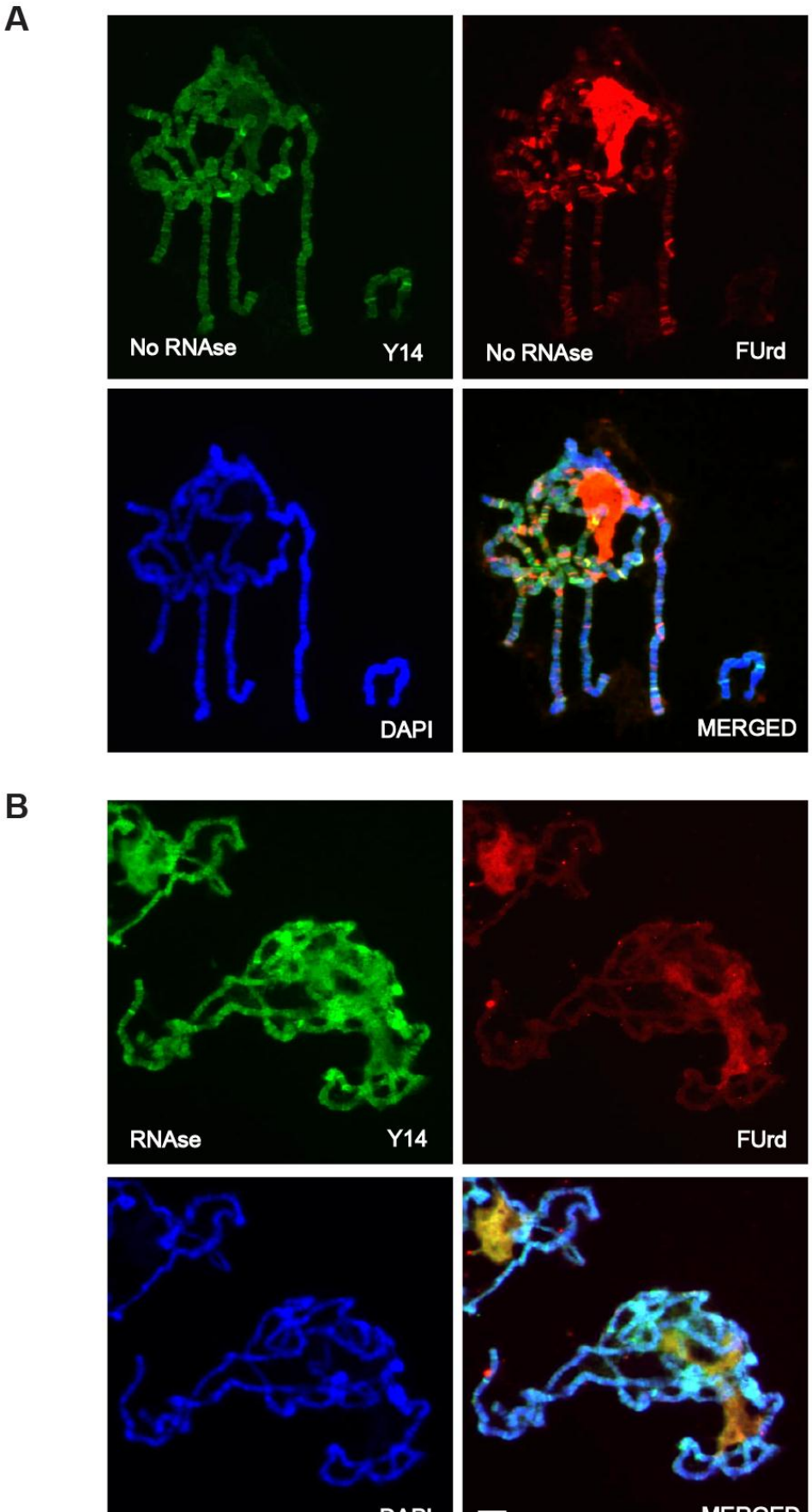
A
No RNAse
Y14
No RNAse
FUrd
DAPI
MERGED
B
RNAse
Y14
FUrd
DAPI
10 µm
MERGED

C

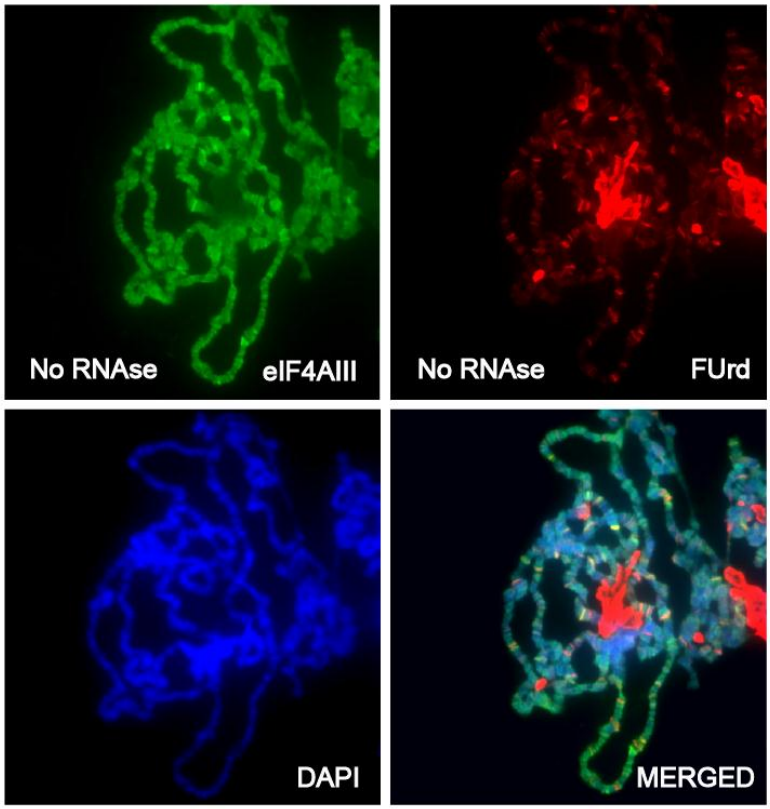
No RNAse
eIF4AIII
No RNAse
FUrd
DAPI
MERGED

D

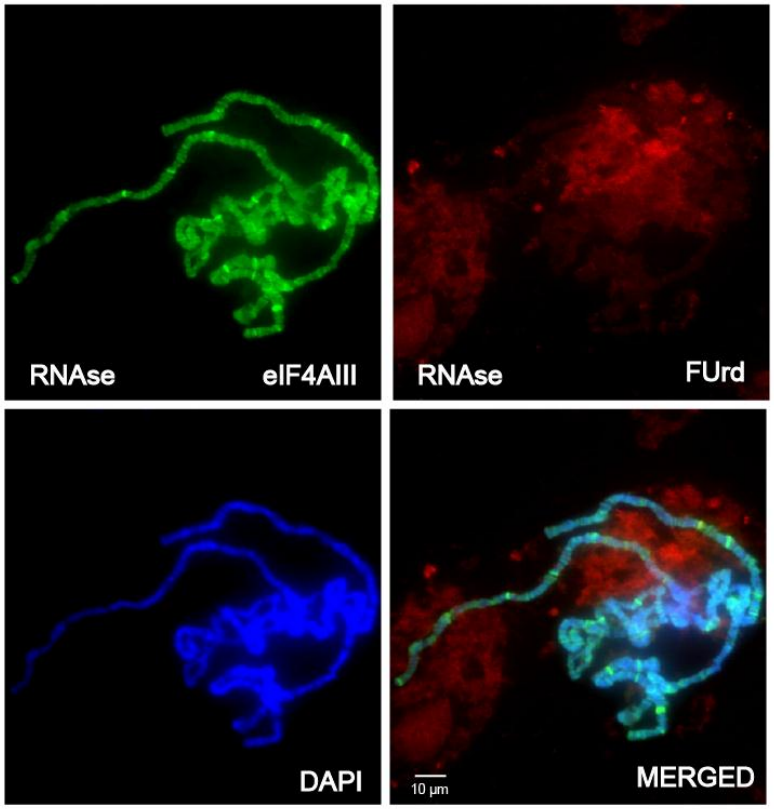
RNAse
eIF4AIII
RNAse
FUrd
DAPI
10 µm
MERGED

Figure 3.11 FUrd labelling indicates EJC proteins is not associated with nascent mRNA

(A) Top panel shows double immunostaining with anti-Y14 and anti-BrdU and (C) anti-eIF4AIII and anti-BrdU in the polytene chromosome. The Y14, eIF4AIII and FUrd signals are present at most transcription sites in the absence of RNase. Anti-Y14, anti-eIF4AIII and anti-BrdU were detected with a FITC-conjugated secondary antibody (green) and Alexa Fluor 647-conjugated secondary antibody (red signal). Bottom (B) and (D) panel shows that following treatment with 1 µg/µl RNase A, the Y14 and eIF4AIII signals persist, whereas FUrd signal has gone from transcription sites, seen more clearly in merged channels. All the images were also prepared with DAPI to indicate DNA. Images were captured with an epifluorescence microscope with a 40X objective.

3.2.10 EJC core components are recruited at transcription sites independently of introns

One of the key predictions of current models is that EJC proteins bind mRNA after splicing. To test this prediction *in vivo,* I used the polytene chromosome on which specific intron and intronless transcription sites can be cytologically mapped. Well characterised intron-less loci are the heat shock genes and heat shock generates prominent puffs at these loci. A puff is a highly transcribed decondensed region of the chromosome which appears as bulge at a specific location of the chromosome. The most apparent heat shock puffs are at cytological positions 87A and 87C, both of which encode the heat shock protein 70 (Hsp70) and both do not have introns. Other prominent heat-shock puffs are visible at 93D and 95D (Lis et al., 1981). 95D encodes heat shock protein 68 (Hsp68) and also has no introns. 93D on the other hand is an intron-containing gene which encodes the long non-coding RNA (hsr-ω-n). Immunostaining shows that all three EJC core proteins (Y14, MAGO and eIF4AIII) are recruited to the intron containing 93D region, as well as also at the intron-less 87A, 87C and 95D regions (Figure 3.12 A, B & C). In summary, recruitment of EJC proteins at heat shock loci, which are characteristically intron-less, indicates that their association does not depend on the splicing features of genes.

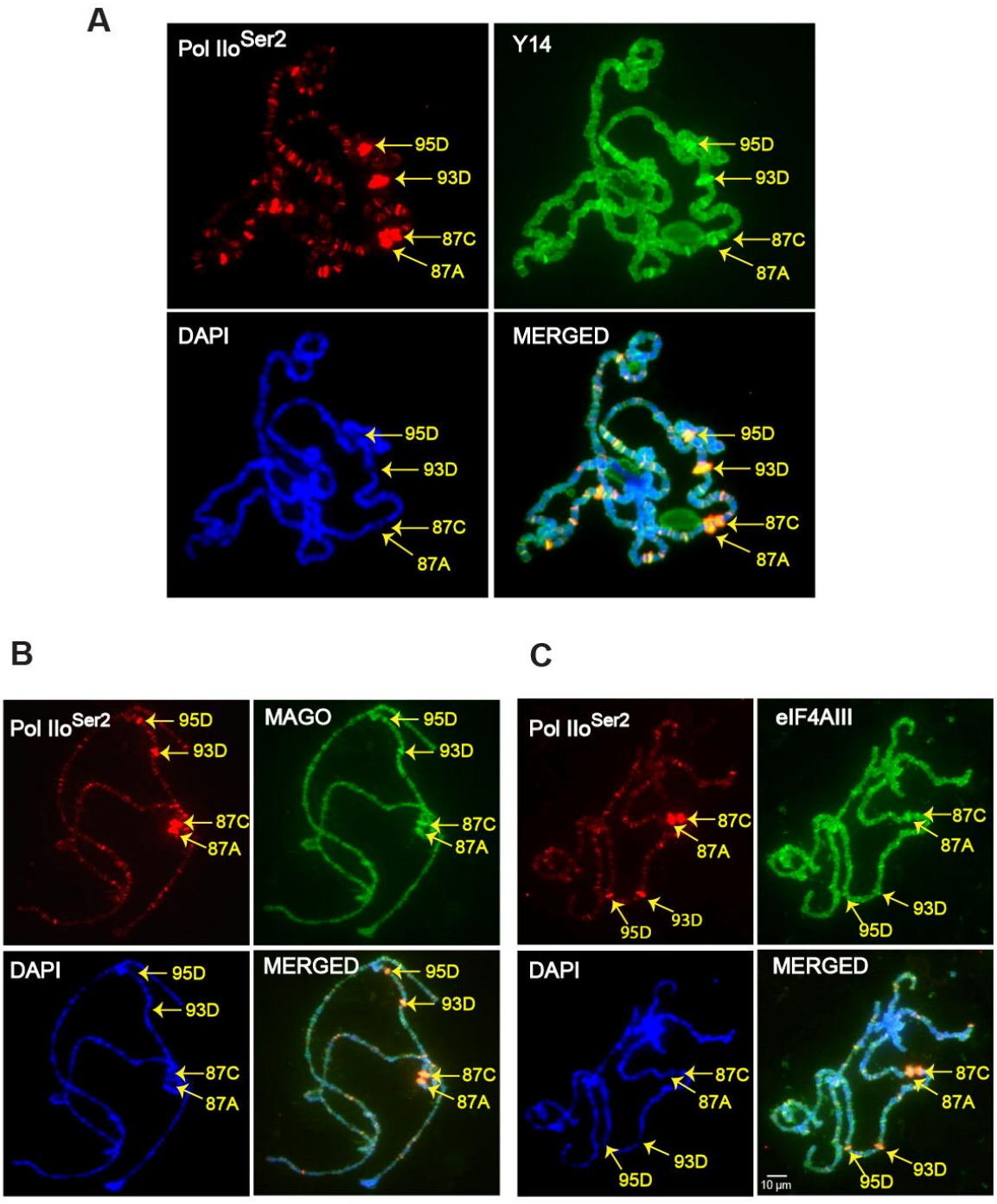
A
Pol IIo Ser2
Y14
DAPI
MERGED
95D
93D
87C
87A
B
Pol IIo Ser2
MAGO
DAPI
MERGED
C
Pol IIo Ser2
eIF4AIII
DAPI
MERGED
10 µm

Figure 3.12 EJC proteins are recruited to both intron-containing and intron-less genes.

(A) Larvae were heat shocked at 37^0C for 45 minutes and squashed polytene chromosomes were immunostained with anti-Y14 and hyperphosphorylated RNA Pol II^{Ser2} (H5). Y14 was subsequently detected with a FITC-conjugated secondary antibody (top-right panel, green signal) and Pol II with a Cy3-conjugated secondary antibody (top-left panel, red signal). Arrows (yellow) indicate recruitment of Y14 and Pol II^{Ser2} at the heat shock loci 87A & 87C, 93D, and 95D respectively. (B) & (C) Immunostaining with MAGO and eIF4AIII shows a similar pattern of recruitment at all mentioned heat shock loci. All samples were also stained with DAPI (blue) and the colocalization signal is more apparent in the merged channels of blue, green and red. Images were captured by an epifluorescence microscope with a 40X objective.

3.2.11 Transcription dependent recruitment of EJC components at ecdysone induced puffs

To assess further the transcription dependence of the EJC association with chromosomal loci, I studied the association of EJC proteins with two well-known puffs, 74EF and 75B, at which transcription is induced by ecdysone. Ecdysone is a *Drosophila* moulting hormone produced from prothoracic glands of these insects, and has a role in metamorphosis by inducing transcription of specific genes (Truman and Riddiford, 2002). Ecdysone directly induces transcription of 74EF and 75B, which are two of the longest *Drosophila* genes at 60 kb and 108 kb respectively (Burtis et al., 1990; Segraves and Hogness, 1990). Both genes have very long introns, the largest intron for 74EF is about 30 Kb and for 75B is 60 Kb. As a consequence, it takes about 60 minutes for 74EF and 90 minutes for 75B to complete transcription at the estimated rate of 1.1kb/minute and for the first mature mRNA to be produced (LeMaire and Thummel, 1990). The presence of very long introns provides a good model for studying the recruitment of the EJC at these gene loci. Salivary glands were dissected from mid-3rd instar larvae and treated with ecdysone for 1 hr before fixation. Immunostaining was carried out with EJC core components and the same squash was also stained for Pol II^{Ser2}. A clear enrichment in the signal was observed at both the 74EF and 75B loci for all three EJC proteins, which colocalizes well with Pol II^{Ser2} (Figure 3.13 A).

Notably, the signal intensity for the EJC core proteins at the 75B locus is higher compared to 74EF. This might suggest that EJC recruitment at these two loci behaves differently. Binding of EJC proteins at both 74EF and 75B puffs further indicates that their recruitment is transcription-dependent. As predicted from an earlier study, the association of the EJC occurs after splicing, therefore recruitment of EJC proteins at these loci does not confirm whether

this recruitment occurs at the beginning of transcription with Pol II^{Ser2}. As mentioned earlier, genes at both of these loci contain a very long intron, therefore, they take a longer time to produce the first mature mRNA. To further address the possibility of whether there is delay in the recruitment of Y14 at these loci I performed a time course ecdysone treatment in parallel with RNA Pol II^{Ser2}. Prior to adding ecdysone, there was no Y14 recruitment at either loci, however, after 15 min the Y14 signal accumulates at the 75B locus and a very weak signal is seen at the 74EF loci, in parallel with Pol II^{Ser2} (Figure 3.13 B). After 30 minutes, 1 h and 2 h, the enrichment of Y14 increases at both loci, but particularly at 75B. The results of the above observations suggest that the recruitment of Y14 occurs as early as after 15 min ecdysone treatment, before splicing is completed.

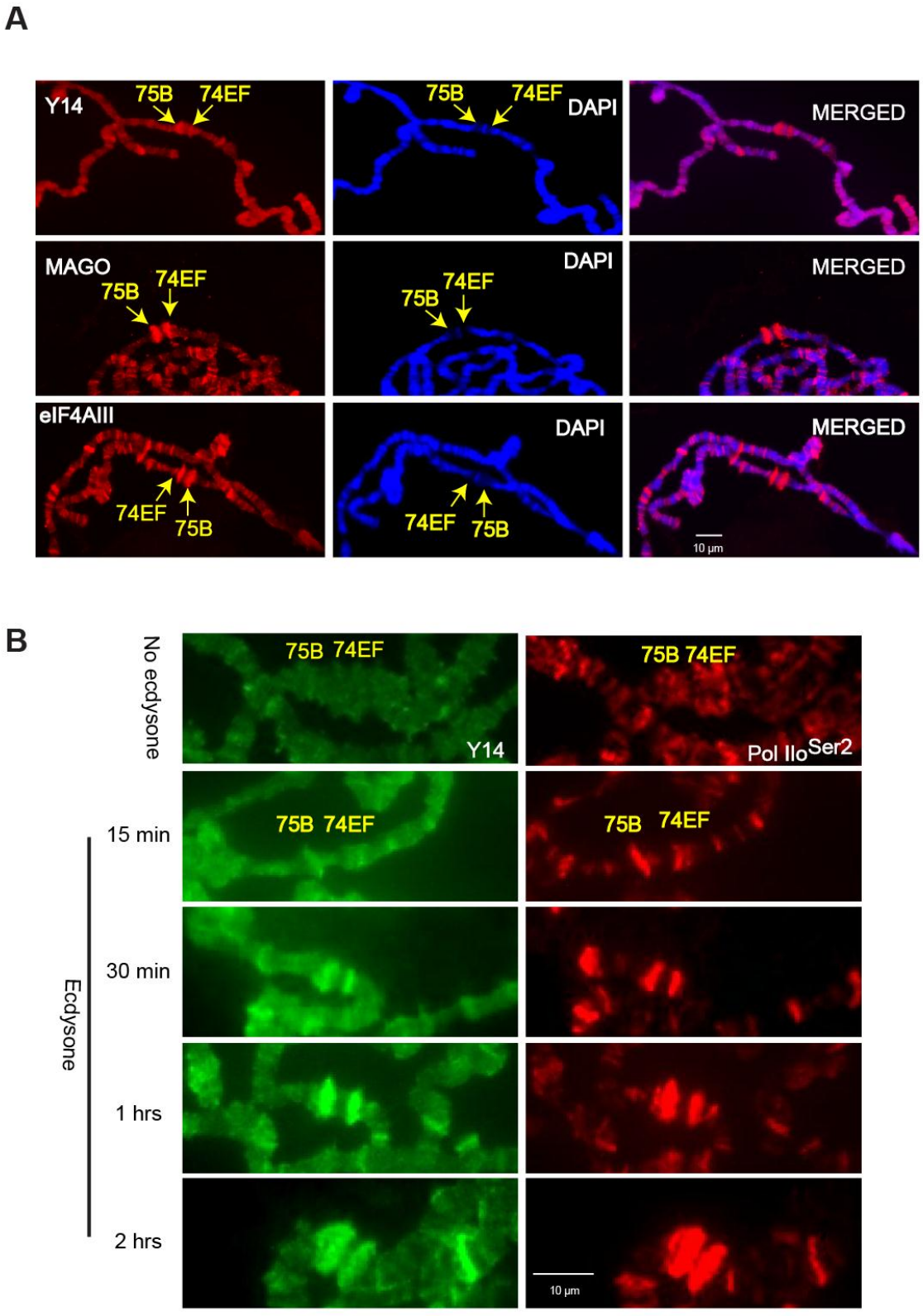
A
Y14
75B
74EF
DAPI
MERGED
MAGO
eIF4AIII
10 µm
B
No ecdysone
15 min
30 min
1 hrs
2 hrs
Ecdysone
75B 74EF
Y14
Pol IIoSer2
10 µm

Figure 3.13 EJC proteins recruitment is transcription dependent

(A) Salivary glands were treated with 1µM ecdysone for 1 h, the squashed polytene chromosome was immunostained with anti-Y14, anti-MAGO and anti-eIF4AIII, which were subsequently detected using a Cy3-conjugated secondary antibody (red). Arrows indicate recruitment of all three EJC proteins (left panels) on the ecdysone induced 74EF and 75B puffs. Middle panels show the DAPI images (blue), and right panels are the merged red and blue channels. (B) Time interval recruitment of Y14 (left panel) and Pol II^{Ser2} (right panels) on ecdysone-induced puffs (74EF and 75B) with a no ecdysone control in the top panels. Y14 was detected with a FITC-conjugated secondary antibody (green signal) and Pol II^{Ser2} with a Cy3-conjugated secondary antibody (red signal). The images were taken under a standard epifluorescence microscope with a 40X objective lens.

3.2.12 Y14/MAGO might regulate expression of ecdysone induced genes

Having observed that EJC proteins associate with the 75B and 74EF puffs upon ecdysone induction, the question remained as to what their function was at these sites. To investigate further, I knocked down both Y14 and MAGO by RNAi in S2 cells. As previously shown, knockdown is efficient as both transcript and protein levels are drastically reduced (Figure 3.9). In this later experiments we also observed EJC recruitment at the BR-C puff, upon ecdysone treatment (Figure 3.14 A). BR-C is a protein-coding gene with a long intron. Transcription of all three genes is rapidly induced upon ecdysone treatment in S2 cells; the induction reaches its highest peak after 2 h incubation (optimization data not shown). I observed that upon knockdown of either Y14 or MAGO, the transcript levels of 75B and BR-C were significantly increased compared to control S2 cells upon ecdysone induction (Figure 3.14 C). Notably, the level of this enhanced induction seems to correlate negatively with the level of of Y14 and MAGO at the gene, this is most apparent at 75B, which is the more affected than 74EF, yet shows higher levels of Y14 and MAGO. The data therefore suggest that the Y14/MAGO heterodimer might act as a transcriptional repressor specifically of the 75B gene.

A

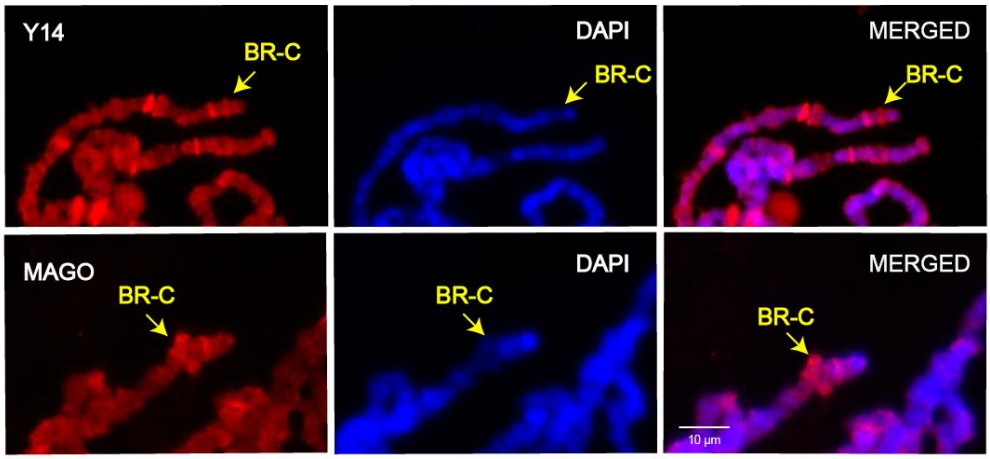
Y14
BR-C
DAPI
BR-C
MERGED
BR-C
MAGO
BR-C
DAPI
BR-C
MERGED
BR-C
10 µm

B

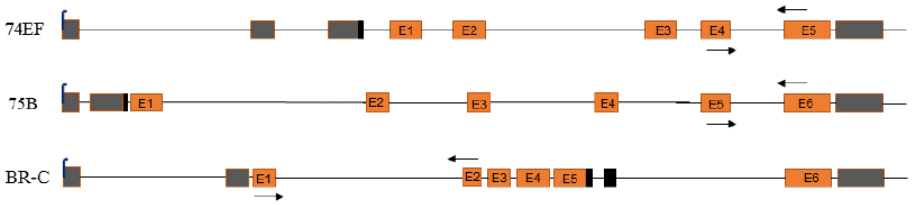
74EF
E1
E2
E3
E4
E5
75B
E1
E2
E3
E4
E5
E6
BR-C
E1
E2
E3
E4
E5
E6

C

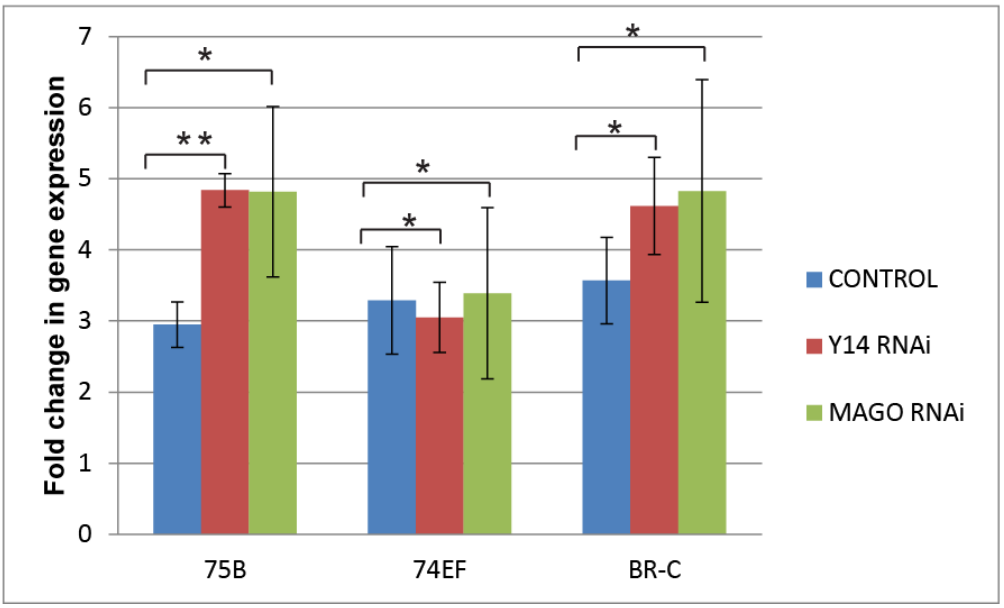
Fold change in gene expression
0
1
2
3
4
5
6
7
75B
74EF
BR-C
CONTROL
Y14 RNAi
MAGO RNAi

Figure 3.14 Y14 and MAGO effects the expression of ecdysone-induced genes

(A) Immunostaining with Y14 and MAGO of polytene chromosomes treated with 1 µM ecdysone, subsequently detected using a Cy3-conjugated secondary antibody (red). Arrows show the recruitment of Y14 and MAGO at BR-C loci. Middle panels indicate DAPI and rightmost panels are the merged images of DAPI and red channels. (B) Schematic representation of 74EF, 75B and BR-C genes, where arrows (black) indicate the location of primer pairs used for real-time RT-PCR (see Appendix II for list of primers, S-50 to S-55). (C) qRT-PCR was used to measure the transcript levels of 74EF, 75B and BR-C genes upon knockdown of Y14 and MAGO in S2 cells. The fold enrichment method was used for calculation and normalized to reference control RpL32. Error bar indicates the standard deviation between the three biological repeats. (**) indicates statistically significant difference (P=0.001) between the control and Y14 RNAi treated sample, whereas, (*) denotes the difference between control and RNAi treated samples is insignificant (P>0.05), (see Material and Methods for details, section 2.14)

3.2.13 ChIP-seq data indicates recruitment of Y14 predominantly at transcription start sites

To gain more detailed information on the distribution of the EJC throughout the genome, I carried out chromatin immunoprecipitation (ChIP) followed by high-throughput DNA sequencing (ChIP-seq). ChIP-seq is a widely used advanced technique to analyse the interaction between protein and DNA and is followed by DNA sequencing to map the binding sites of protein throughout the genomic region. ChIP experiments were performed with *Drosophila* S2 cells. Before performing ChIP, I optimized sonication conditions of the samples (see Material and Methods). ChIP experiments were carried out for all three EJC core factors, Y14, MAGO and eIF4AIII. However, only the Y14 antibody performed well and produced informative sequencing data (the sequencing and its analysis was carried out in collaboration with Dr. Paul Badenhorst at the Institute of Biomedical Research (IBR), and Aditi Kanhere in our school here at University of Birmingham, UK. Unexpectedly, ChIP-seq analysis revealed enrichment at transcription start sites (Figure 3.15 A & B). Similar analysis, using the Cis-regulatory Element Annotation System (CEAS) also shows that Y14 associates particularly at the promoter region of the gene (Figure 3.15 C & D). As an example, the enrichment at the TSS is apparent at the super sex comb gene (*sxc*) (Figure 3.15 E). This data might explain why the Y14 signal at the chromosomes is resistant to RNase treatment; Y14 might be recruited to transcription sites directly or indirectly via an interaction with either DNA or DNA associated proteins. This analysis identified a list of putative Y14 associated genes, which includes both protein-coding and other RNA coding genes. Notably, the protein associates with intron-less genes (see Appendix VIII), consistent with the pattern on the polytene chromosomes which showed that Y14, similarly to the other two EJC proteins, associates also with intron-less heat shock genes.

A

Enrichment of Y14 Across the Whole Genebody

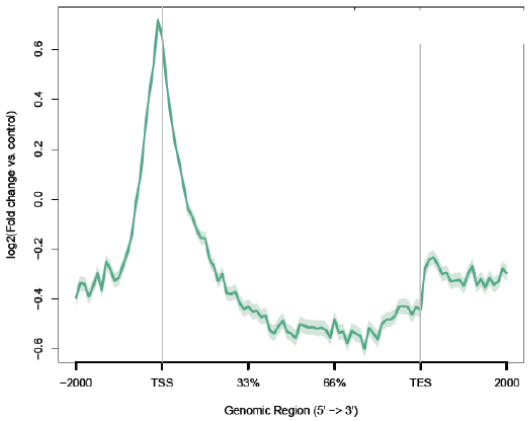

B

Enrichment of Y14 at Transcription Start Site (TSS)

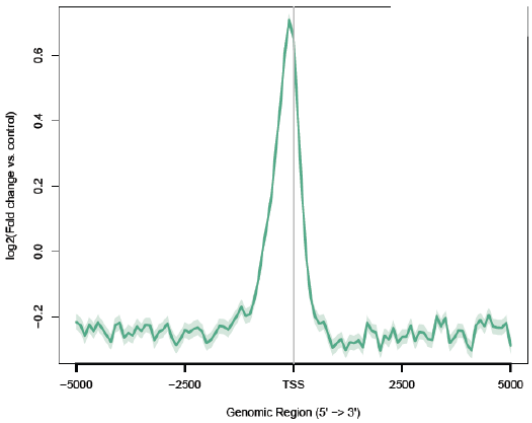

C

Enrichment of Y14 in the Promoter Region (1KB)

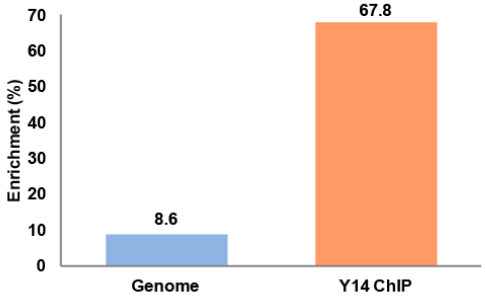

D

Enrichment of Y14 Downstream of TSS

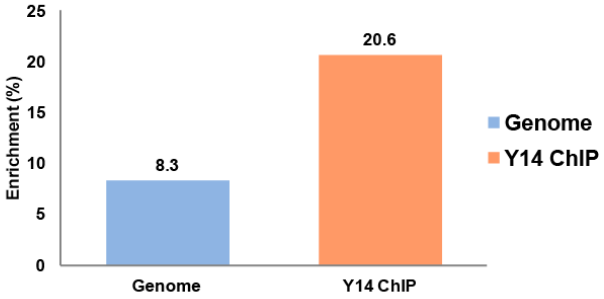

E

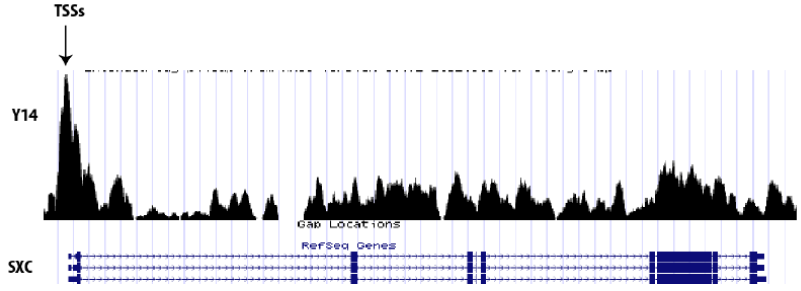

Figure 3.15 Y14 is associated with transcription start sites (TSS)

(A) & (B) Enrichment of Y14 across the whole genome body, indicates Y14 mainly associated at the transcription start sites. Plots were produced using next generation sequencing plot (ngs.plot, https://code.google.com/p/ngsplot/). (C) & (D) Plots showing Y14 enrichment at either the promoter region or downstream of the TSS. Plots were produced using the Cis-regulatory Element Annotation System (CEAS) by Dr Aditi Kenhere. (E) A snapshot of a reference gene, sxc, in which Y14 enrichment at TSSs is apparent, indicated by the arrow. Chip-seq was carried out in two biological replicates, and each time the Y14 peak was found in the promoter region, further indicating that the result is reproducible.

3.3 Discussion

Based on the contemporary model, the association of the EJC at spliced junction occurs simultaneously with splicing. Pre-mRNA splicing is typically co-transcriptional in *Drosophila* (Khodor et al., 2012); I therefore took advantage of the polytene chromosomes to gain insights into why the EJC seems to associate only with a subset of transcripts in *Drosophila* (Sauliere et al., 2010). The core EJC proteins Y14, MAGO, and eIF4AII localize mostly to the nucleus in mammalian cells (Baguet et al., 2007; Custodio et al., 2004; The Human Protein Atlas - www.proteinatlas.org). In *Drosophila*, the proteins also appear to be mostly nuclear in the cells analysed, however, as demonstrated by the *oskar* mRNA localization studies cited earlier, in the oocyte they are most abundant within the cytoplasm. I reported here that the EJC proteins are present in both the nucleus and the cytoplasm in salivary glands. Quantitative estimation to compare the nuclear and cytoplasmic levels of all three EJC proteins in *Drosophila* S2 cells found the proteins to be equally distributed between the two compartments. To assess their distribution in the nucleus more directly, I carried out indirect immunostaining and report that the core EJC proteins Y14, MAGO and eIF4AIII associate with transcription sites of the *Drosophila* polytene chromosome. This localization with transcription sites is confirmed by double-immunostaining of the EJC proteins and $PolII^{Ser2}$. This association with transcription sites was also observed using transgenic flies expressing tagged version of these proteins. My observation shows a complete overlap of the Y14 and MAGO signals, consistent with these proteins forming a stable heterodimer *in vitro* (Lau et al., 2003). The Y14 and MAGO signals are expected to match that of eIF4AIII at transcription sites, however, I found the distribution of eIF4AIII poorly correlates with that of Y14 and MAGO. This difference in staining pattern is more

apparent with parallel PolI^{Ser2} immunostaining, in which eIF4AIII is well colocalized with PolI^{Ser2}, whereas, Y14 and MAGO signals are either absent or weak at intense PolI^{Ser2} sites. Specifically, double immunostaining of tagged eIF4AIII and endogenous Y14 further verified that there are sites at which the eIF4AIII signal is strong but Y14 is absent. Knockdown of Y14 also completely eliminated MAGO from transcription sites, while MAGO knockdown only partially reduced Y14. This suggests that Y14 can be recruited at transcription sites independently of MAGO. Y14 or MAGO knockdown does not have visible phenotypic effects, however, knockdown of eIF4AIII drastically impairs the growth of glands. This observation indicates that eIF4AIII might have additional roles, which are independent of EJC assembly. The observation that, after RNase treatment, EJC signals remain at transcription sites, suggests that EJC proteins might indirectly contact chromatin or DNA-associated proteins. An unexpected finding is the recruitment of all EJC proteins at heat shock gene loci (87A & 87C). An association of EJC components at these loci further concludes that their association does not depend on the intronic features of genes, as these genes do not have introns. Moreover, EJC recruitment was also observed at other heat shock loci, for instance at 95D, which encodes heat shock protein 68 (Hsp68) and also has no introns, and the 93D region that encodes non-protein coding gene hsr-ω-n (Lakhotia and Tapadia, 1998). Similar observations were made with ChIP-seq of Y14, which showed that this protein associates with genes both with or without introns. This latter analysis also showed a preferential association with transcription start sites, suggestive of a role for Y14 at the promoter. My observations contradict previous conclusions that EJC association is splicing-dependent in *Drosophila*. Additionally, I show evidence that Y14/MAGO knockdown affects expression of ecdysone inducible genes, suggesting a role for these proteins in transcription.

Chapter 4

4.0 Visualization of ribosomes, translation and the NMD factor UPF1 at transcription sites

4.1 Summary

Evidence from past indicates that NMD may occur in the nucleus. NMD is a strictly translation dependent process, and the ribosome is the only cell component capable of reading the mRNA coding sequence and allowing recognition of a premature translation termination codon (PTC). Therefore, ribosomes may be functional in the nucleus. Here I describe a side project of my PhD in which I aimed to visualize ribosomal proteins and ribosome activity at transcription sites of the polytene chromosomes, following a strategy similar to that used for EJC proteins (Chapter 3). Firstly, to investigate whether ribosomal proteins are present at transcription sites, I used several transgenic *Drosophila* lines, that endogenously express yellow fluorescent protein (YFP)-tagged ribosomal proteins, to analyse their sub-cellular localization. This analysis confirmed that ribosomal proteins (RPs) accumulate in both the cytoplasm and the nucleus, and associate with transcription sites on polytene chromosomes, which was consistent with that previously reported (Brogna et al., 2002). Identification of RPs at transcription sites is not sufficient to distinguish between fully assembled translating ribosomes and ribosomal proteins undertaking translation-unrelated functions. To differentiate between the two, I applied the ribopuromycylation (RPM) technique recently described for mammalian cells, which allows visualisation of translation (David et al., 2012). By using this technique, I found evidence of ribosomal activity at transcription sites on *Drosophila* polytene chromosomes. These findings indicate that nascent RNAs are translated, suggesting that there is a link between ribosomal scanning and RNA processing. This observation is consistent with the view that NMD may occur co-

transcriptionally. To assess this hypothesis directly, we used antibodies against endogenous UPF1, a key NMD factor, to determine its presence on the polytene chromosomes. Notably, I found that UPF1 associates with majority of transcription sites. In summary, the data provide evidence that both ribosomes and UPF1 are at transcription sites. These observations are consistent with the view that NMD is initiated at transcription sites.

4.2 Results

4.2.1 Characterization of YFP tagged ribosomal protein expression in salivary glands

Transgenic lines carrying YFP tagged ribosomal proteins used in this study were received from *Drosophila* Genomics and Genetic Resources (DGGR), Kyoto Stock Centre (see Appendix III) (www.dgrc.kit.ac.jp). These trap lines carry the YFP coding region inserted into an intron of an endogenous gene, thus keeping the endogenous promoter activity (Morin et al., 2001). The YFP trapping cassette was inserted using a construct based on the piggyback transposable element and it was flanked by splice acceptor (SA) and donor sites (SD)(Figure 4.1A) (More details can be found at http://kyotofly.kit.jp/stocks/documents/CPTI.html). These constructs produce chimeric proteins in which YFP is added at variable positions of the trapped protein, therefore providing a potentially good system to target proteins in tissues. Detailed information about each fly line and their source is given in Table 4.1, while a schematic diagram of each construct has been shown in Figure 4.1.

Gene Name	Clone Name	Cambridge Protein Trap Line	Kyoto DGRC Number	CG Number	Break Points/Insertion Site	YFP Insert Location on Chromosome
RpS9	PBac{602.P.SVS-1}RpS9[CPTI000493]	CPTI000493	115034	CG3395	3L (67B11)	9503969
RpS9	PBac{602.P.SVS-1}RpS9[CPTI000785]	CPTI000785	115504	CG3395	3L (67B11)	9504066
RpL10Ab	PBac{802.P.SVS-2}RpL10Ab[CPTI003957]	CPTI003957	115462	CG7283	3L (68E1)	11816014
RpL41	PBac{754.P.FSVS-0}RpL41[CPTI002881]	CPTI002881	115344	CG30425	2R (60E5)	20791354

Table 4.1 YFP tagged transgenic lines.

Details of the transgenic lines RpS9-034, RpS9-504, RpL10Ab and RpL 41 which were used to characterize YFP expression.

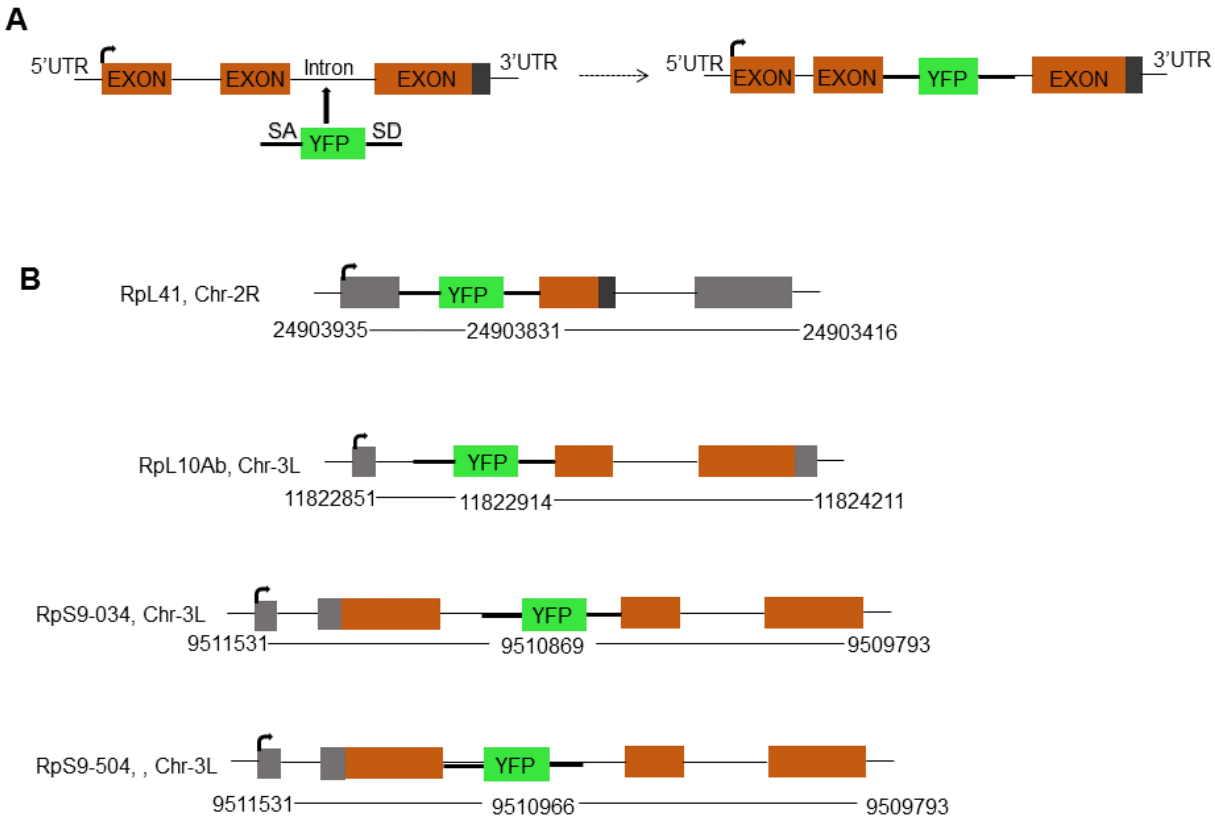

Figure 4.1 Schematic representation of YFP tagged ribosomal proteins.

(A) Schematic of the principle of the YFP protein trap strategy in which the YFP coding sequence, flanked by acceptor (SA) and donor (SD) splice sites, gets randomly inserted into an intron. (B) A simplified representation of different tagged RpL41, RpL10Ab, RpS9 034, and RpS9 504 proteins which are expressed from their endogenous promoter. Black line indicates an intron, whereas boxes represent exons. Length of each gene and location is indicated by the nucleotide base number (source flyBase).

4.2.2 Confirmation of the transgene inserts of each fly strain

To validate the transgenic lines by PCR, primers were designed to amplify part of the YFP sequence and downstream exons (Figure 4.2 A). This work was done in collaboration with Sarah Taylor (a Masters student in our lab). Fly genomic DNA was used as a template and PCR products were visualised by agarose gel electrophoresis (Figure 4.2 B). PCR of RpL41-YFP and RpL10Ab-YFP produced the right size fragment of 189 bases and 1393 bases respectively, confirming the right constructs. However, line 034 of RpS9-YFP produced a larger fragment than expected which was 740 bases and no PCR products were amplified for line 504 of RpS9-YFP, suggesting the latter does not carry the desired construct (4.2 B). Having confirmed the fragment size by PCR, we also further verified the tagging construct of RpL41-YFP and RpL10Ab-YFP and RpS9-YFP (034) by DNA sequencing. Corresponding PCR fragments were gel purified and sent to GATC Biotech Ltd (London) for sequencing. The sequence was also matched with a BLAST search for all transgene constructs (http://blast.ncbi.nlm.nih.gov/Blast.cgi) (see Appendix V). Confirmation of the constructs suggests that fluorescence observed in immunostaining comes from the YFP tagged proteins.

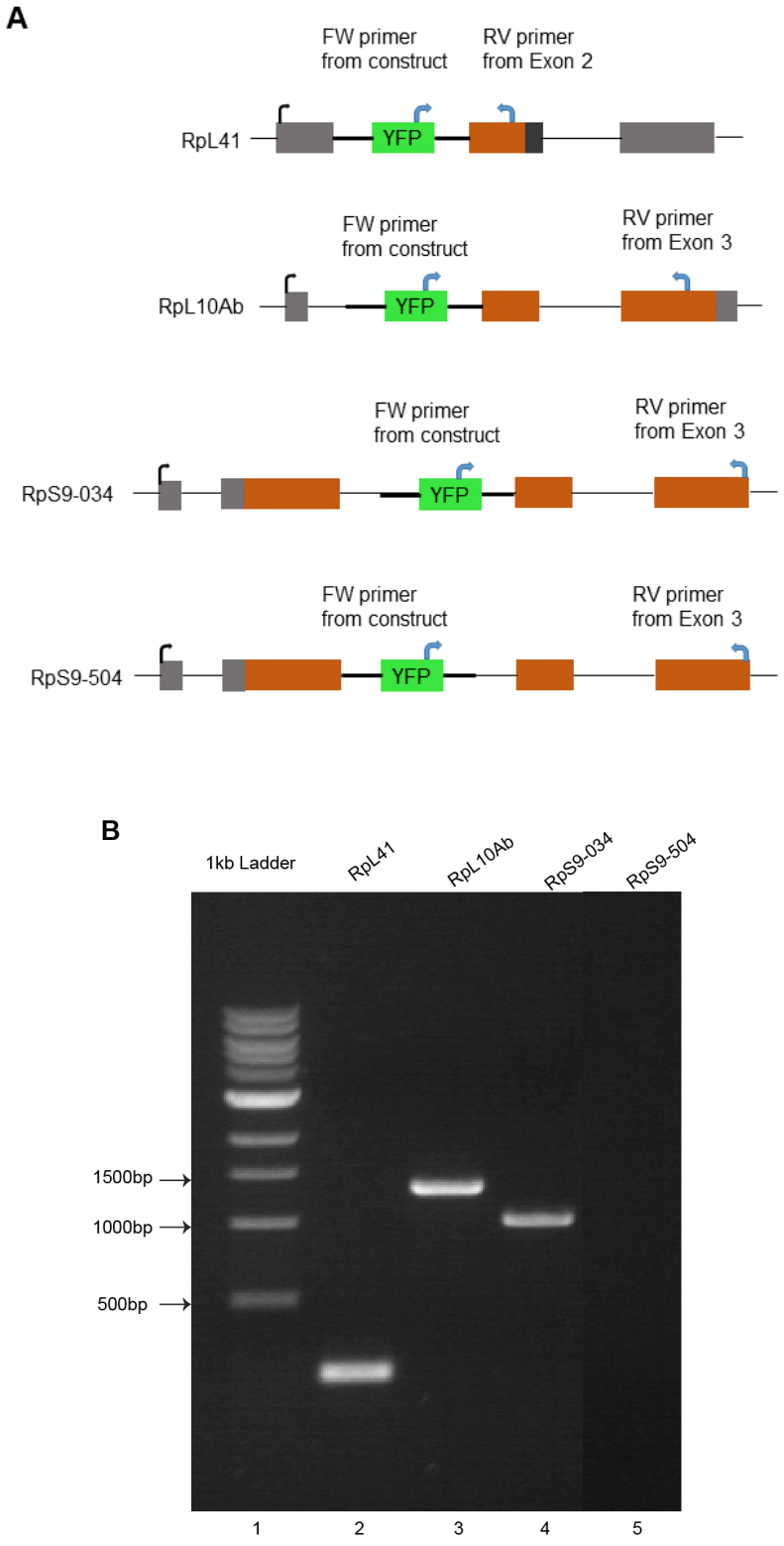

Figure 4.2 Confirmation of transgene constructs by gel electrophoresis. (A) Representation of primer location within the each construct. (B) PCR products were run in

1% agarose gel. Lane 1 indicates 1kb DNA ladder whereas lanes 2 and 3 show PCR products of RpL41-YFP and RpL10Ab-YFP. Lanes 4 and 5 represent PCR products of RpS9 034-YFP and RpS9 504-YFP.

4.2.3 Localization of ribosomal proteins in whole salivary glands

I visualized YFP tagged ribosomal proteins in the salivary glands of 3rd instar larvae. Microscopy imaging of RpL41-YFP shows a strong YFP signal in the nucleus, particularly intense in the nucleolus, and a relatively weaker signal in the cytoplasm. Instead, RpL10Ab–YFP, as expected for a RP shows a strong signal in both the cytoplasm and the nucleolus, but a weak signal in the rest of the nucleus. The RpS9-YFP (034) lines show a signal mostly in the cytoplasm with no apparent nucleolar signal. The second RpS9-YFP (504) line produced no fluorescent signal above background (Figure 4.3 A). After these initial results, I focused on better characterizing the subcellular localization of RpL41 as it shows an unexpectedly strong signal in the nucleus. RpL41 is a very small protein (only 25 amino acid) that it is associated with the intersubunit surface of the 80S (Klinge et al., 2012). In *Drosophila,* the RpL41 gene is present as a single copy in the genome and is essential for viability (Marygold et al., 2007). Confocal imaging of RpL41-YFP confirmed that the signal is most concentrated in the nucleus, particularly in the nucleolus (Figure 4.3 B). We published these observations along with similar data, which show that other fluorescently tagged ribosomal proteins also accumulate in the nucleus and are present at transcription sites of the polytene chromosome (Rugjee et al., 2013).

A

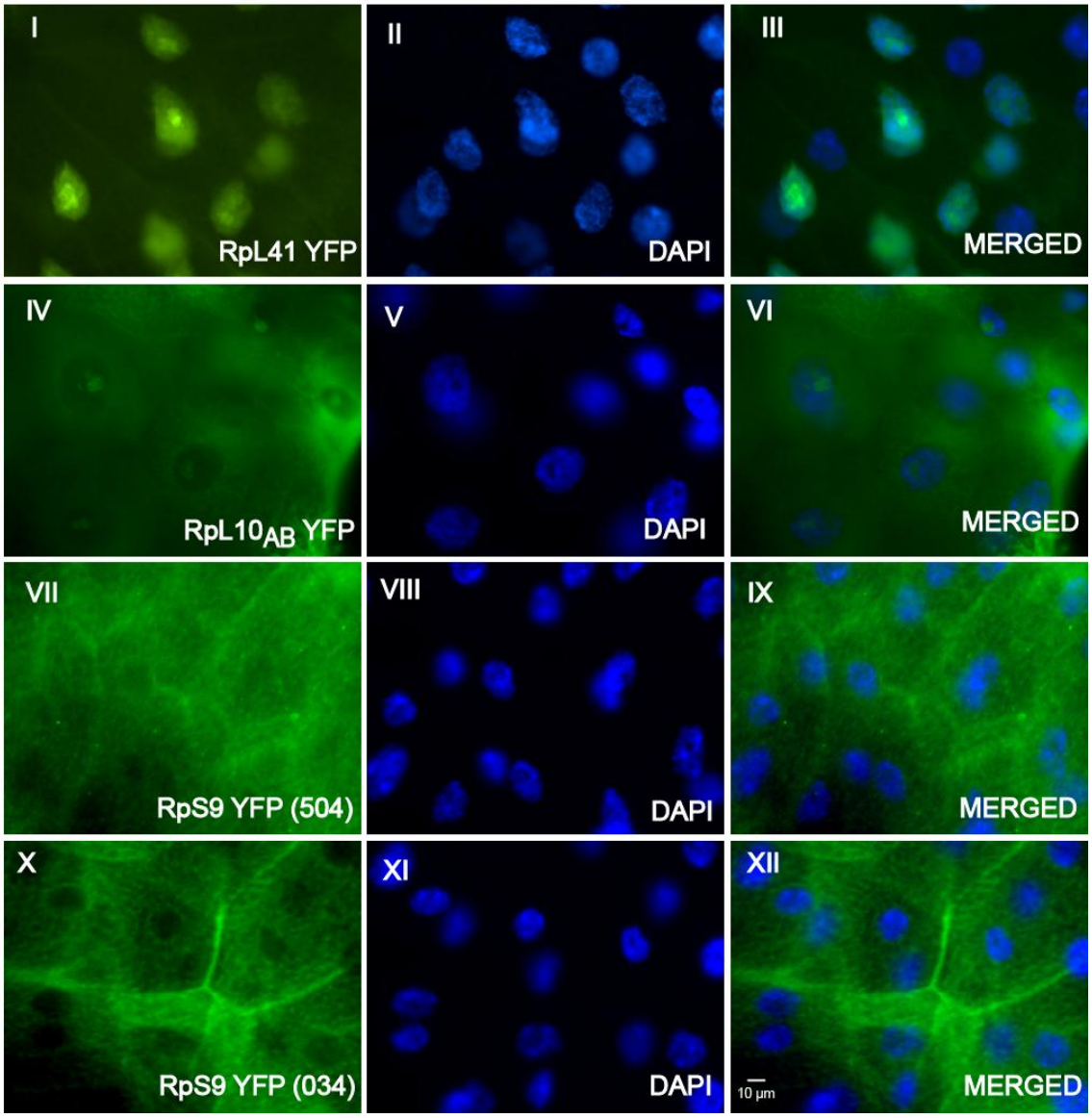
I
RpL41 YFP
II
DAPI
III
MERGED
IV
RpL10AB YFP
V
DAPI
VI
MERGED
VII
RpS9 YFP (504)
VIII
DAPI
IX
MERGED
X
RpS9 YFP (034)
XI
DAPI
XII
10 µm
MERGED

.

B

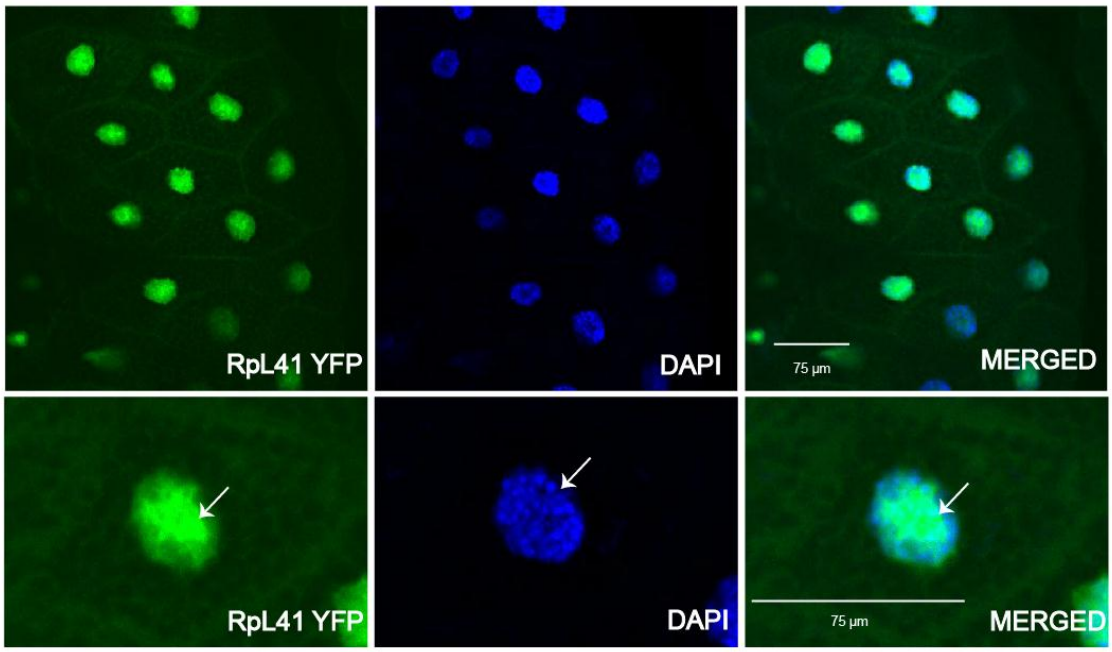

Figure 4.3 Expression of endogenously tagged ribosomal proteins in salivary glands.

(A) Top left panel (I) shows the subcellular localization of YFP tagged RpL41 in salivary gland cells. Panel (IV) indicates expression of YFP-RpL10Ab and bottom two panels (VII & X) show localization of RpS9 (504) and RpS9 (034) under native promoter control. Middle panel shows DAPI staining to indicate the nucleus and the right panel shows the merged channels of DAPI and YFP. All images were taken using an epifluorescence microscope with a 40X objective. (B) Top left panel shows a confocal section of RpL41-YFP fluorescence signal in salivary gland cells. The nucleus is stained with DAPI in the middle panel while the top right panel is a merged image of DAPI and YFP fluorescence. The bottom panel shows a magnified view of a single cell in the top panel, with the arrow indicating the nucleolus. (Parts of this data (B) were published in Rugjee et al. 2013, see appendix IX).

4.2.4 Endogenously tagged RpL41-YFP associates with transcription sites

To test directly whether RpL41 associates with transcription sites, I stained the polytene chromosomes for YFP. However, this produced a very faint signal at the chromosome which was difficult to interpret (Figure 4.4 A). To further assess the association of RpL41 with the chromosomes, I analysed polytene chromosomes squashed in native conditions to preserve YFP fluorescence (in the standard procedure, the presence of acetic acid destroys fluorescent signals). Although it is difficult to achieve good chromosomal spreads with this procedure, these squashes clearly show that RpL41-YFP specifically associates with interband regions (Figure 4.4 B) (see Materials and Methods for detailed information on this acid-free squashing procedure). These squashes were also prepared with DAPI to stain the DNA and it is clear from the merged channel that tagged RpL41-YFP associates with transcription sites of gene loci.

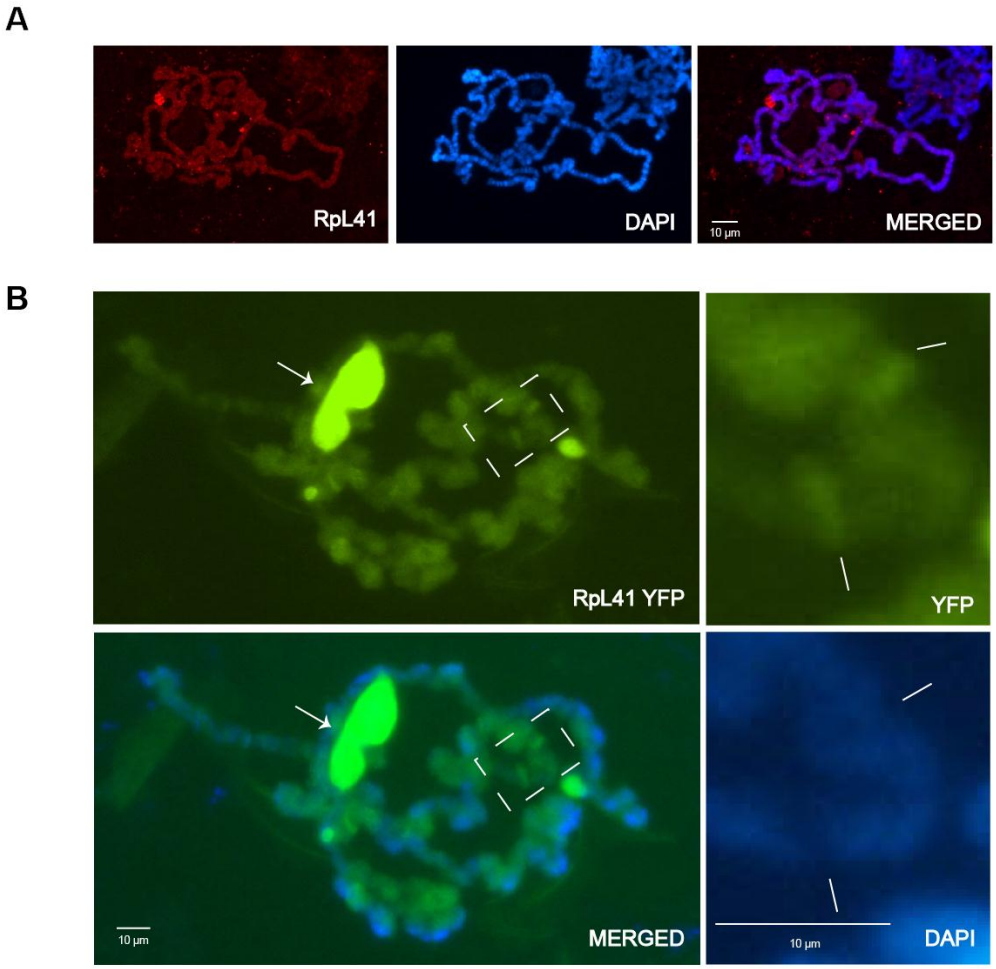

Figure 4.4 Tagged RpL41 associates with transcription sites of the polytene chromosome

Top row (A) shows a polytene chromosome from a strain expressing RpL41-YFP, indirectly immunostained with an anti-GFP primary antibody, which was subsequently detected with a Cy3-conjugated secondary antibody. DAPI staining is shown in the middle panel, while the top right panel is a merged image of Cy3 and DAPI. (B) A polytene chromosome under native conditions shows the YFP fluorescence signal corresponding to YFP-RpL41 in the top left panels, whereas the bottom left panel is a merged image of the YFP and DAPI channels. The top rightmost panel is a magnified view of the box indicated in the main image; lines denote the fluorescence signals in the interband positions and that of DAPI in the bottom right panels. (Parts of this figure (B) were published in Rugjee et al. 2013, see appendix IX)

4.2.5 Ribopuromycylation allows visualisation of translation sites *in vivo*

To assess whether translating ribosomes are present in the nucleus in *Drosophila*, I utilised a new technique known as ribopuromycylation (RPM), which was first used to detect translation sites in mammalian cells (David et al., 2012) (Figure 4.5). Puromycin is an aminonucleoside antibiotic, mainly derived from the Streptomyces alboniger bacterium and is an analog of the 3' end of an aminoacylated tRNA (Yarmolinsky and Haba, 1959). Puromycin enters the A site of the translating ribosome and is incorporated into the newly synthesized peptide chain, causing its premature release (Tscherne and Pestka, 1975). It was reported by David and Collaborators (2012) that elongation inhibitors such as emetine or cycloheximide (CHX) prevent the release of puromycylated peptide chains, which remain bound to the ribosome. An antibody specific to puromycin can thus be used to detect the translating ribosome in both fixed and permeabilized cells (David et al., 2012). The RPM technique was successfully applied by David and Collaborators (2012) to visualize translating ribosomes, which notably were seen both in the cytoplasm and in the nucleolus of mammalian cells (David et al., 2012).

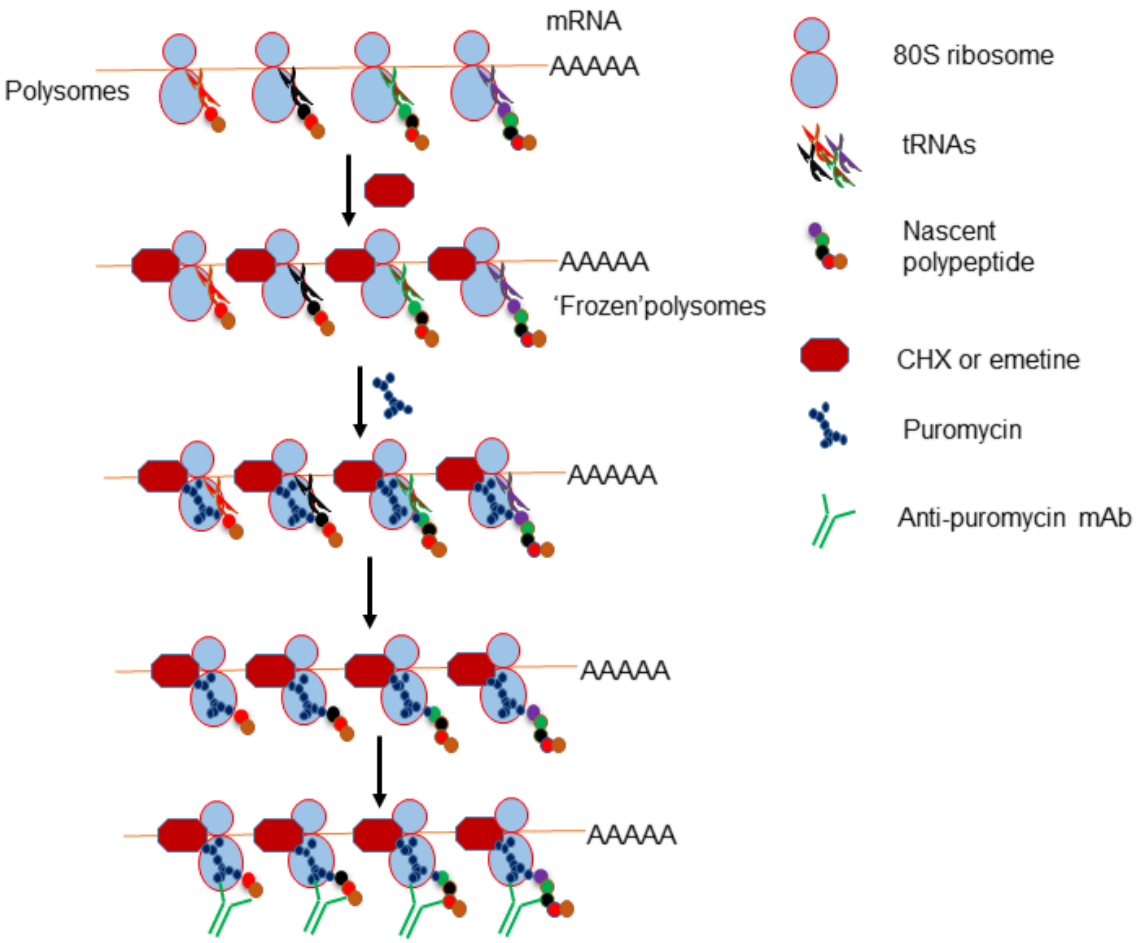

Figure 4.5 Schematic of the RPM procedure

Polysomes were immobilized on mRNAs by one of two elongation inhibitors, CHX or emetine. Puromycin was added, which is then incorporated into nascent polypeptide chains and subsequently detected by anti-PMY mAb. This figure is a modified from David and Collaborators (2012).

4.2.6 Puromycylation observed in salivary glands and S2 cells

To test the feasibility of the puromycylation technique, I used both salivary glands and S2 cells, which were treated with puromycin alone, or in combination with translation elongation inhibitors and other translation inhibitors, as described for mammalian cells (David et al., 2012). My Western blotting results clearly indicate that puromycin incorporation was observed in both S2 cells and salivary glands, in either the presence or absence of translation inhibitors drugs, but no signal was observed in the absence of puromycin, which further indicates the specificity of the antibody in *Drosophila* (Figure 4.6). Moreover, in the presence of translation initiation inhibitors such as harringtonine or anisomycin, puromycin incorporation was significantly reduced compared to the untreated samples, which is as expected and as shown by David et al. (2012). However, treatment with emetine reduces puromycylation in both S2 cells and salivary glands, suggesting that the drug can partially inhibit puromycylation in these cell types (Figure 4.6, lanes 1 and 2).

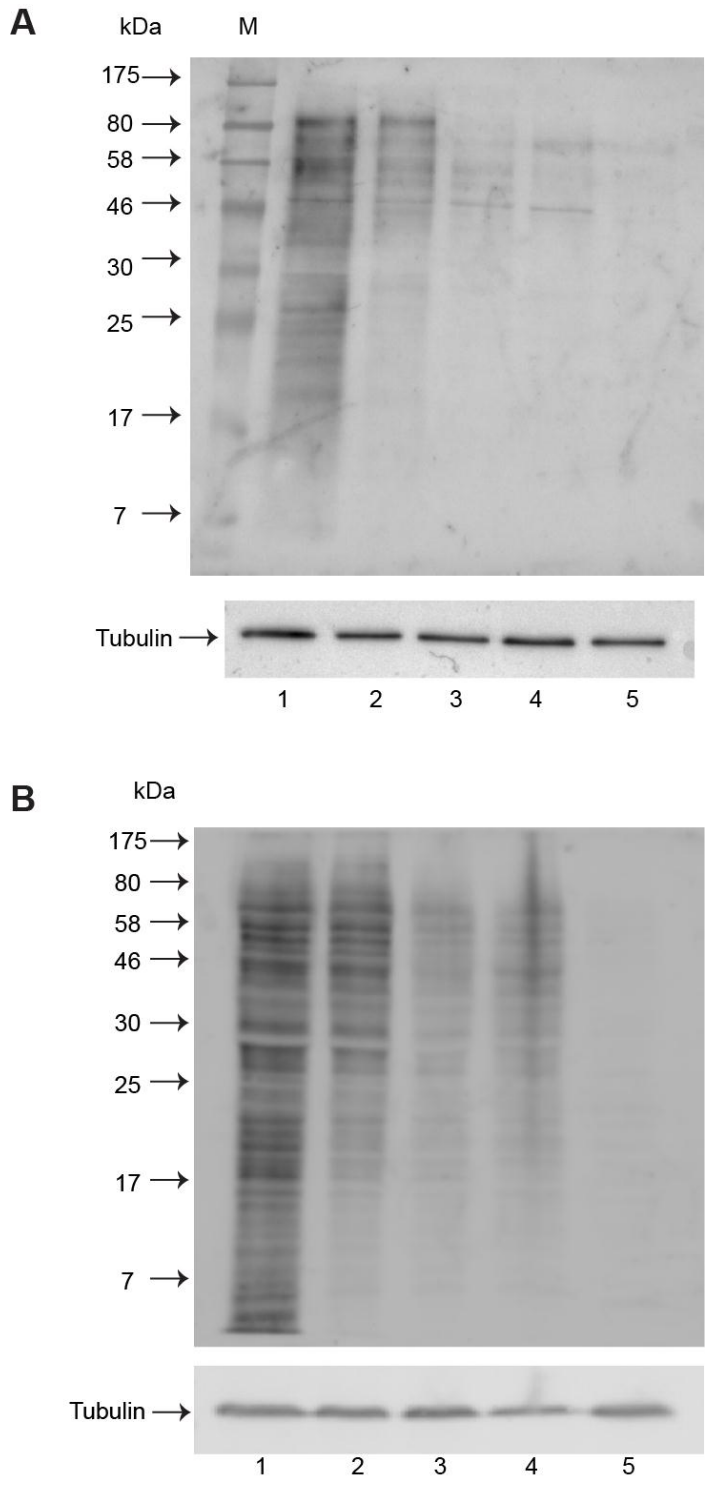

Figure 4.6 Western blot shows puromycin incorporation in both S2 cells and salivary glands

(A) The top panel shows puromycin incorporation in salivary glands. Lane 1 shows a sample treated with 50 µg/ml puromycin only and lane 2 with both 50 µg/ml puromycin and 100

µg/ml emetine. Lanes 3 and 4 were pretreated with 2µm harringtonine and 20 µg/ml anisomycin followed by puromycin. Lane 5 represents a no drug control to check the specificity of the antibody. (B) Bottom panel: the same drug treatments were used in S2 cell extracts (see Materials and Methods for details). The same membrane was also re-probed with tubulin which was used as a loading control for both Western blots. (This figure were published in Al-jubran et al. 2013, see appendix IX).

4.2.7 Puromycin incorporation in intact whole salivary glands

To assess whether the RPM technique can be used to detect translating ribosomes *in vivo*, intact salivary glands were dissected from mid-3rd instar larvae and pre-treated with different drug combinations as in S2 cells. The results suggest that puromycylation occurs both in the cytoplasm and in the nucleus (Figure 4.7 A). In the larger cells of the lobe, puromycylation is also observed around the chromosomes. The signal is also apparent in the nucleolus, particularly in the smaller cells that make the proximal portion of the gland. (Figure 4.7 B). Notably, the relative signal intensity of the nucleus and nucleolus is higher after treatment with emetine, consistent with RPM reporting translation sites. Glands pretreated with the translation initiation inhibitor harringtonine, showed drastically reduced puromycylation, consistent with the Western blot results (Figure 4.6).

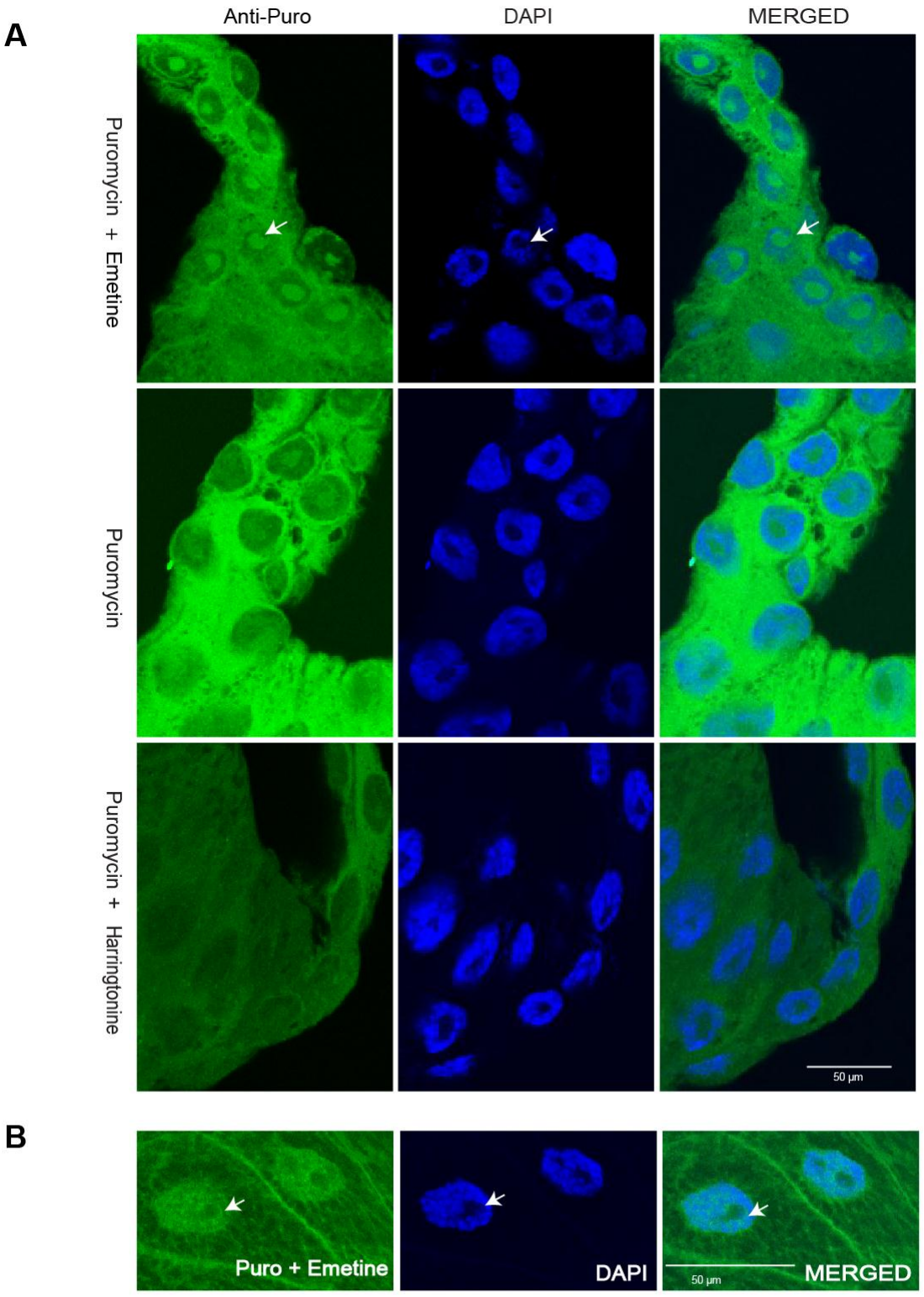
A
Anti-Puro
DAPI
MERGED
Puromycin + Emetine
Puromycin
Puromycin + Harringtonine
50 µm
B
Puro + Emetine
DAPI
50 µm
MERGED

Figure 4.7 Puromycylation in intact whole salivary glands

The first panel, Figure (A), shows a confocal image of salivary glands treated with puromycin and emetine and subsequently immunostained with an Alexa 488 conjugated 2A4 monoclonal antibody. Arrows indicate puromycin incorporation in the nucleolus. The middle panel shows glands treated with puromycin only and the last panel demonstrates pre-incubation with harringtonine followed by puromycin and emetine incubation. (B) Figure shows a magnified image of salivary gland cells treated with puromycin and emetine, where arrows indicate a ring-like structure around the nucleolus**.** All glands were also counterstained with DAPI to visualize the nucleus. The right panels show a merged image of the DAPI and the green channel. All images were taken with a Leica confocal microscope with a 63X oil immersion lens. (This figure were published in Al-jubran et al. 2013, see appendix IX).

4.2.8 Incorporation of puromycin at polytene chromosome transcription sites

To address the issue whether ribosomes are present at transcription sites, I applied the RPM technique to the polytene chromosomes (see Material and Methods). Puromycin incorporation was detected at the chromosomes and particularly in the interband regions (Figure 4.8 A). Although a faint signal was also observed in the band region (transcriptionally inactive region of chromatin) this was mostly weak compared to the interband (transcriptionally active region of gene). Moreover, the signal was particularly intense at specific interbands (indicated by the arrow in Figure 4.8 A., magnified insets). The signal appears to be specific at these sites, as in the absence of puromycin there was no such signal (shown below). Also I noted that treatment of the glands with aurintricarboxylic acid (ATA), an RNase inhibitor, significantly increased the intensity of the signal at interband regions (see Materials and Methods). In addition, pre-treatment of the glands with the DNA intercalating drug actinomycin D, significantly intensifies the signal at interband regions particularly at transcription puffs (highly active in transcription) (Figure 4.8 B). Furthermore, a weak puromycin signal was also observed around the nucleolus. To further test whether the signal is translation dependent, polytene chromosomes were pre-incubated with the translation initiation inhibitor harringtonine. Upon treatment with this inhibitor, the puromycin incorporation signal appears to be drastically reduced at interband regions (Figure 4.9). These results indicate that puromycin incorporation is translation dependent and is consistent with that observed in salivary glands and S2 cells in Western blotting. As mentioned above, the signal is RNase-sensitive: the addition of RNase inhibitors increases the puromycin signal and adding RNase completely abolishes it at the interband or puffs (Figure 4.9). The RPM

method provides evidence for the recruitment of actively translating ribosomes at transcription sites on *Drosophila* polytene chromosomes.

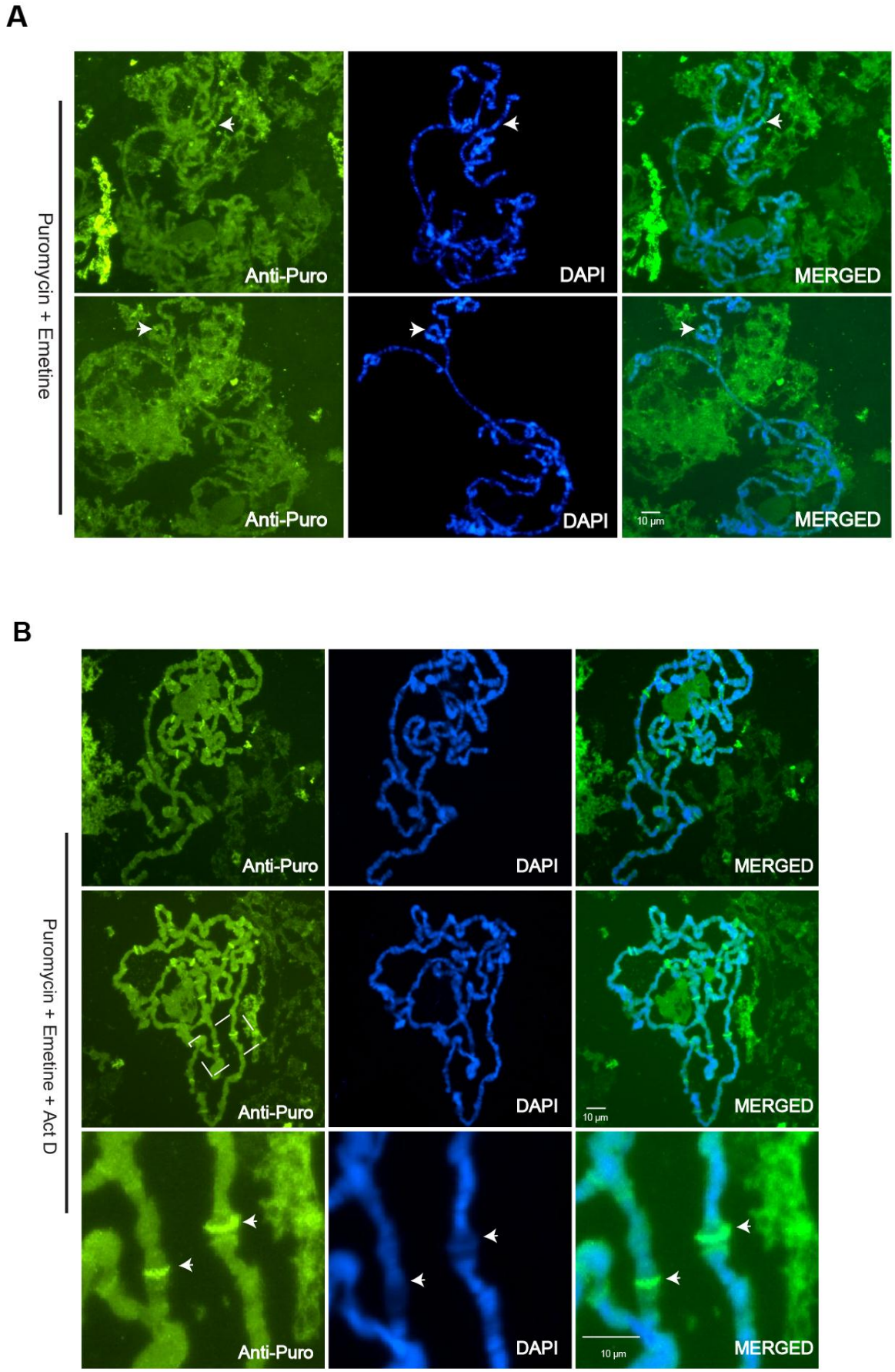
A
Puromycin + Emetine
Anti-Puro
DAPI
MERGED
Anti-Puro
DAPI
10 µm
MERGED
B
Puromycin + Emetine + Act D
Anti-Puro
DAPI
MERGED
Anti-Puro
DAPI
10 µm
MERGED
Anti-Puro
DAPI
10 µm
MERGED

Figure 4.8 Puromycin incorporation on transcription sites of *Drosophila* polytene chromosomes

(A) Top panels show salivary glands pre-incubated with 50 µg/ml puromycin and100 µg/ml emetine. White arrow indicates puromycin signal at the interband position. (B) Glands were incubated with 100 µg/ml emetine, 50 µg/ml puromycin and 10 µg/ml actinomycin D (Act D) (see Materials and Methods for details). Direct immunostaining with an Alexa488-conjugated anti-puromycin antibody shows puromycin signal all over the chromosome, particularly intense at the interband position. Bottom panels show a magnified section indicated by a white square from the panel above, with strong puromycin signal indicated by the white arrow at interband loci. (This figure were published in Al-jubran et al. 2013, see appendix IX).

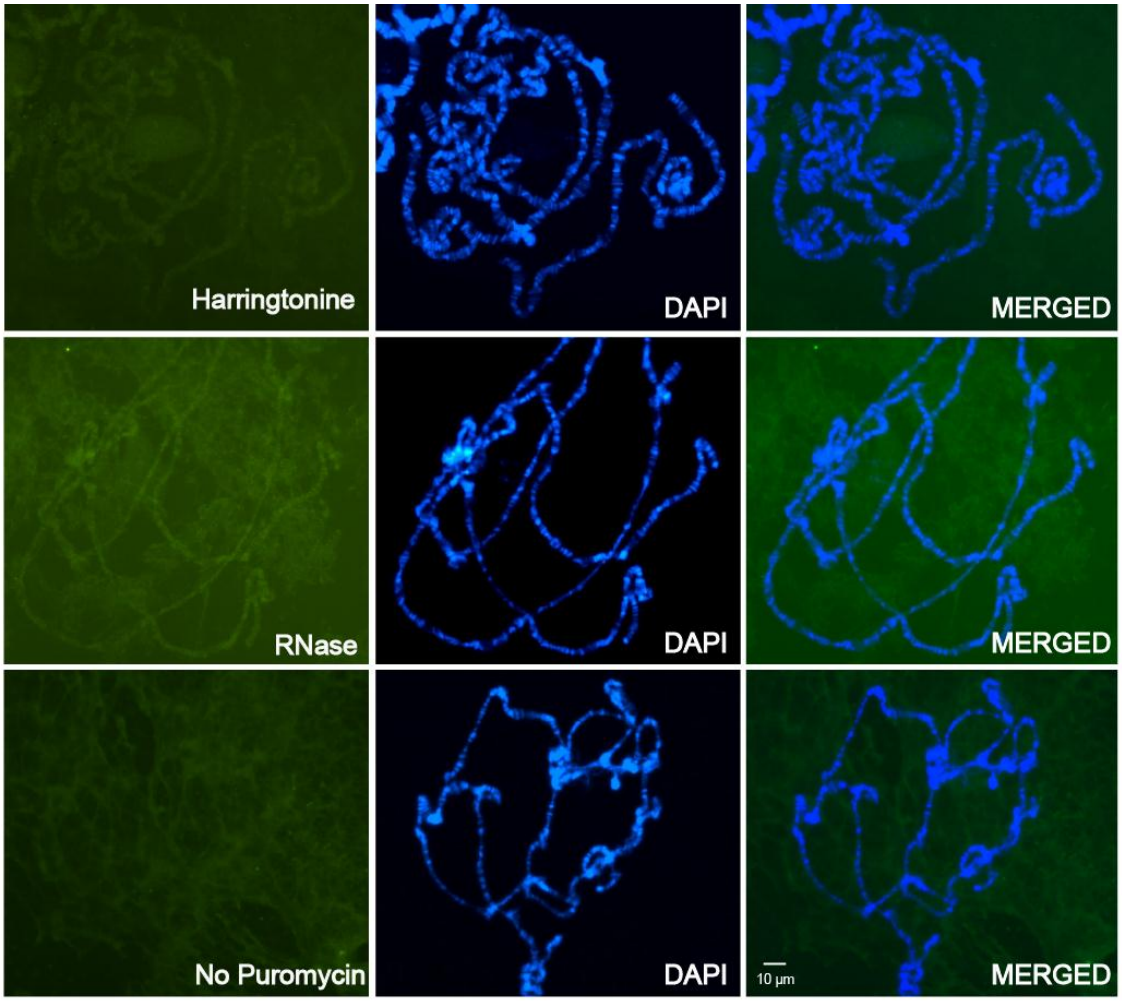

Figure 4.9 Puromycin signal is translation dependent

Immunostaining of chromosomes was performed as above. Top panel shows, 2 µM harringtonine was added for 30 minutes prior to incubation with puromycin, emetine and Act D. In the middle panel, 100 µg/ml RNase A was added to the first squashing step, prior to fixation, and the sample was incubated for 2 minutes at room temperature. Puromycin was omitted in the control (bottom panel), in which only faint background fluorescence can be detected. (This figure were published in Al-jubran et al. 2013, see appendix IX).

4.2.9 Generation of monoclonal antibodies against UPF1 and UPF2 of *Drosophila*

To produce the antibodies against the UPF1 and UPF2, protein amino acid sequences were retrieved from FlyBase (Table 2.1 & 2.2, see Material and Methods, section 2.13) and specific regions were selected by the company Abmart. Abmart uses its patented technology, Abmart Seal, which involves cloning of the selected epitopes into a specific vector to produce a recombinant protein incorporating several antigens. This is used for immunization of mice that then develop an immune response against the desired peptide, which is followed by production of hybridoma clones (a detailed description of the Abmart SEAL technology is given in Material and Methods, section 2.13). Twelve epitope sequences were selected for both UPF1 and UPF2 (Table 4.2 & 4.3 and Figure 4.10 & 4.11)

Table 4.2 Twelve potential epitopes for UPF1

Number	Start	End	Peptide
1	43	52	TSQSQTQNDQ
2	85	94	DEPGSSYVKE
3	1084	1093	PGGNKKTNKL
4	342	351	HYVGELYNPW
5	788	797	QYQGSLHSRL
6	27	36	DTQPTQYDYR
7	528	537	KSREAIDSPV
8	60	69	SAGDSHPRLA
9	1140	1149	SQQPELSQDF
10	259	268	KPGIDSEPAH
11	1060	1069	QTGNFSPGNS
12	1117	1126	AAPYSQHPMP

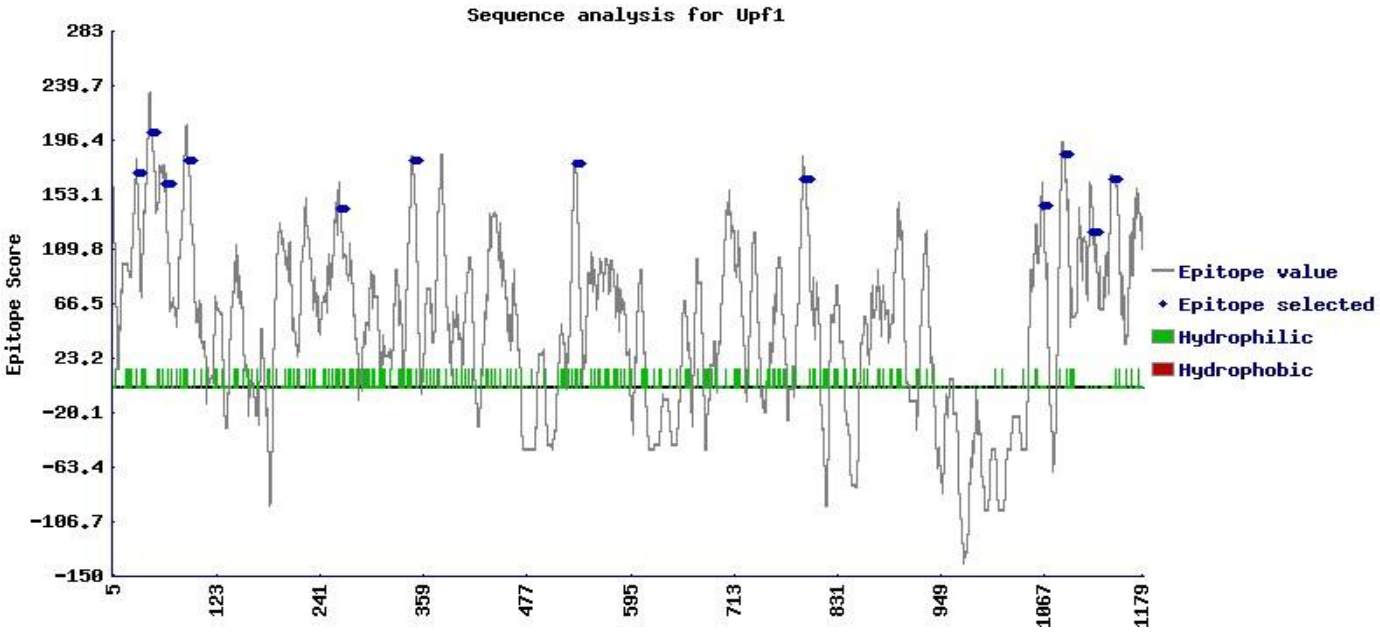

Figure 4.10 Prediction analysis of the UPF1 protein

This graph gives an overall view of the protein structure and the location of the selected peptides. The x-axis indicates the amino acids number in the protein, and y-axis is the value of the algorithm where the higher score indicates the higher probability of generation of the antibody against that epitope. The scores of each 10mer epitope are plotted with a grey line. Selected epitopes are highlighted in blue on the graph. Hydrophobic residues are shown using red bars under the x-axis. This graph was taken from Abmart.

Table 4.3 Twelve potential epitopes for UPF2

Number	Start	End	Peptide
1	1	10	MLANDSATTD
2	29	38	EGDNDNDIDT
3	13	22	VSTPPSSRKD
4	1220	1229	QKPNKHKFKH
5	445	454	DDPPSTTSDT
6	960	969	KTTNNAQDPS
7	703	712	SSKREPMVRP
8	999	1008	VSGQEQDQSN
9	461	470	EEQPTTPVAA
10	903	912	HPVFSKTENT
11	1098	1107	PNQDGTPGSP
12	980	989	DEGGTDEDSG

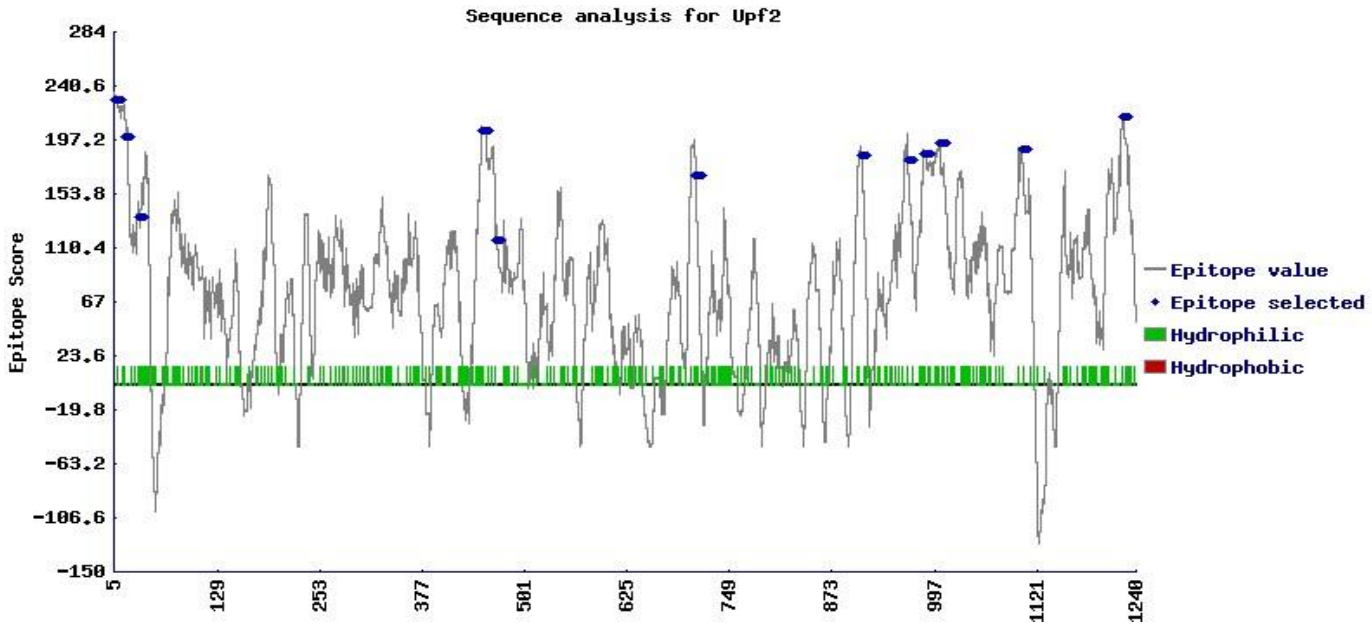

Figure 4.11 Prediction analysis of the UPF2 protein

This graph gives an overall view of the protein structure and the location of the selected peptides. The x-axis indicates the amino acids number in the protein, and y-axis is the value of the algorithm where the higher score indicates the higher probability of generation of the antibody against that epitope. The scores of each 10mer epitope are plotted with a grey line. Selected epitopes are highlighted in blue on the graph. Hydrophobic residues are shown using red bars under the x-axis. This graph was taken from Abmart.

4.2.10 Western blot analysis of UPF1 ascites identified three potential clones specific for UPF1

18 UPF1 hydridoma clones were received from Abmart (see Appendix VII for a list of all ascites and clone ID numbers) and we tested them for their specificity against UPF1 by Western blotting of *Drosophila* S2 cell extracts. The results showed a band of the expected size with several of the antibody clones, however, most of them also showed nonspecific bands. I chose three clones that showed minimal cross-reactivity with other proteins (Figure 4.12). These three clones were renamed based on the Western blot lane number: UPF1-1 (ID-10108-1-1M1/1C13-2_121113, epitope peptide 2, see table 4.2), UPF1-3 (ID-10108-1-7M1/7D17-11_121114, epitope peptide 12, Table 4.2) and UPF1-16 (ID-10108-1-7M1/7B12-12_121120, epitope peptide 10, Table 4.2). Based on these initial Western blot data, we (Dr. Brogna) requested Abmart to purify the above three monoclonal antibodies for further testing. Unfortunately, I was unable to detect any band of the correct molecular size for the UPF2 protein from any of the UPF2 ascites in the Western blot (see Appendix VI for details). UPF2 antibody production project was therefore terminated at this stage.

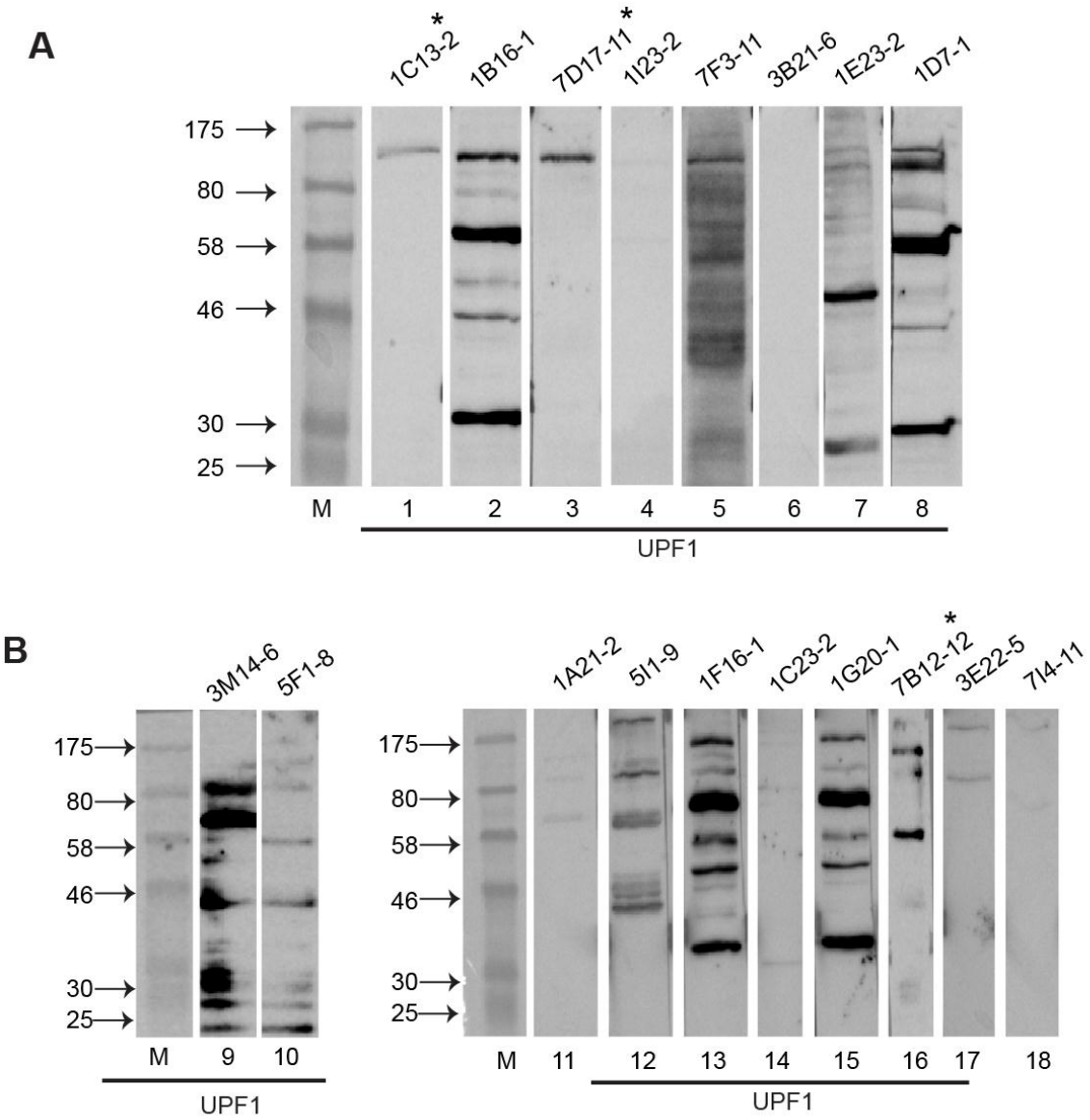
A
1C13-2*
1B16-1
7D17-11*
1I23-2
7F3-11
3B21-6
1E23-2
1D7-1
175
80
58
46
30
25
M
1
2
3
4
5
6
7
8
UPF1
B
3M14-6
5F1-8
1A21-2
5I1-9
1F16-1
1C23-2
1G20-1
7B12-12*
3E22-5
7I4-11
175
80
58
46
30
25
M
9
10
11
12
13
14
15
16
17
18
UPF1

Figure 4.12 Western blotting of S2 cell extracts with different UPF1 hybridoma clones (A) S2 cell extracts were immunoblotted with UPF1-1 to UPF1-8 ascites, in which two potential clones, UPF1-1 and UPF1-3 (lanes 1 & 3, marked by asterisk), identified by a band of the right molecular size (129.94 kDa) with no background signal, indicating the specificity against endogenous UPF1. Lanes are labelled with each UPF1 ascite's ID clone number. (B) Western blot of UPF1-9 to UPF1-18 ascites. Only UPF1-16 (lane 16, marked by asterisk) shows a band of the correct molecular size, corresponding to endogenous UPF1, although with some background signal of other molecular sizes.

4.2.11 Validation of potential UPF1 monoclonal antibodies

To further confirm that the three UPF1 antibodies we have selected can specifically detect the correct protein, I expressed GFP-tagged UPF1 in S2 cells (see Appendix IV) and assayed whole cell lysates by Western blotting. As expected, two bands were detected, one corresponding to endogenous UPF1 and the other to UPF1-GFP. All three UPF1 antibodies gave similar results. The top band corresponds to GFP-tagged UPF1 and the lower band is specific to endogenous UPF1 (Figure 4.13). The data thus show that all three monoclonal antibodies recognize endogenous UPF1 with minimal cross-reactivity.

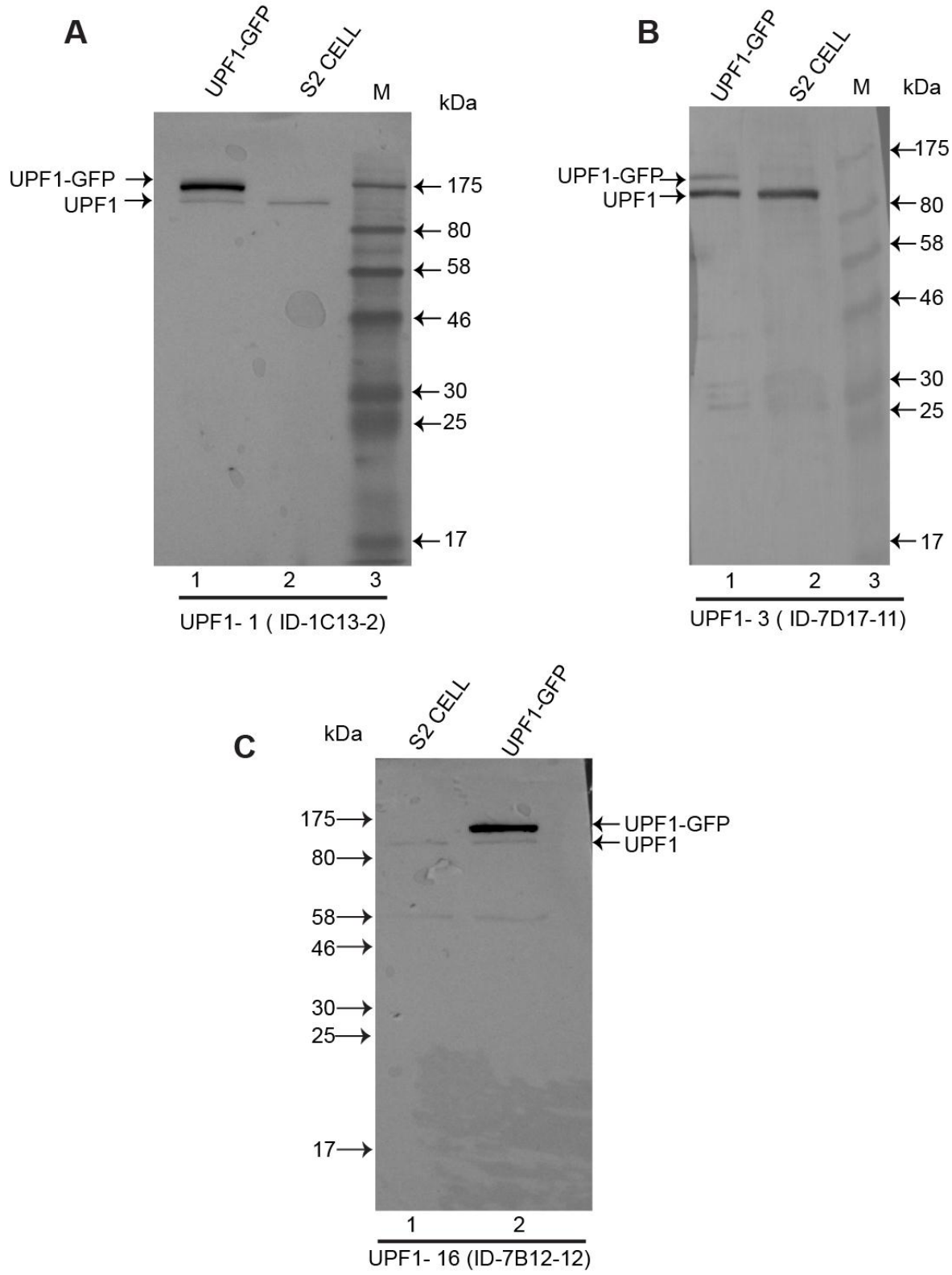
A
UPF1-GFP
S2 CELL
M
kDa
UPF1-GFP
UPF1
175
80
58
46
30
25
17
1
2
3
UPF1- 1 (ID-1C13-2)
B
UPF1-GFP
S2 CELL
M
kDa
UPF1-GFP
UPF1
175
80
58
46
30
25
17
1
2
3
UPF1- 3 (ID-7D17-11)
C
kDa
S2 CELL
UPF1-GFP
175
80
58
46
30
25
17
UPF1-GFP
UPF1
1
2
UPF1- 16 (ID-7B12-12)

Figure 4.13 Western blot analysis shows that UPF1 ascites detect both endogenous UPF1 and GFP-tagged UPF1

(A) S2 cells were transfected with UPF1-GFP and immunoblotted with UPF1-1 ascites in parallel with a control S2 cell extract. Lane 1 shows detection of both the expressed UPF1-GFP (156.94 kDa) (top) and endogenous UPF1 (bottom), whereas in lane 2 only endogenous UPF1 is detected. (B) and (C) UPF1-3 and UPF1-16 ascites were immunoblotted in a similar way, and both UPF1-GFP and endogenous UPF1 (lane 1 of (B) and lane 2 of (C)) were detected in the transfected extract, but only endogenous UPF1 was detected in the control S2 cell extract (lane 2 of (B) and lane 1 of (C)).

4.2.12 Purified UPF1 antibodies show specificity against endogenous UPF1

The first batch of UPF1-1, UPF1-3 and UPF1-16 antibodies (Table 4.4) received from Abmart were tested, after Protein A/G affinity chromatography and checked again by Western blotting (Figure 4.14). These purified antibodies produced similar results as the ascites but UPF1-1 sensitivity was low as only the UPF1-GFP band could be detected and UPF1-16 produced higher background than with the ascites. Two of the antibodies were purified again by Abmart. In this second batch (Table 4.5), UPF1-16 showed good specificity against both UPF1-GFP and endogenous GFP with little background signal (Figure 4.15), however UPF1-1 still detected only over-expressed UPF1-GFP but not the endogenous protein.

Table 4.4 First batch of purified UPF1 antibodies

Project ID	Target protein	Product name	Epitope peptide	Ig types	Antibody type	Company
14476-1	UPF1-1	10108-1-1M1/1C13-2_130510	DEPGSSYVKE	Mouse IgG Monoclonal	Powder	Abmart Inc
14476-1	UPF1-3	10108-1-7M1/7D17-11_130619	AAPYSQHPMP	Mouse IgG Monoclonal	Powder	Abmart Inc
14476-1	UPF1-16	10108-1-7M1/7B12-12_121120	KPGIDSEPAH	Mouse IgG Monoclonal	Powder	Abmart Inc

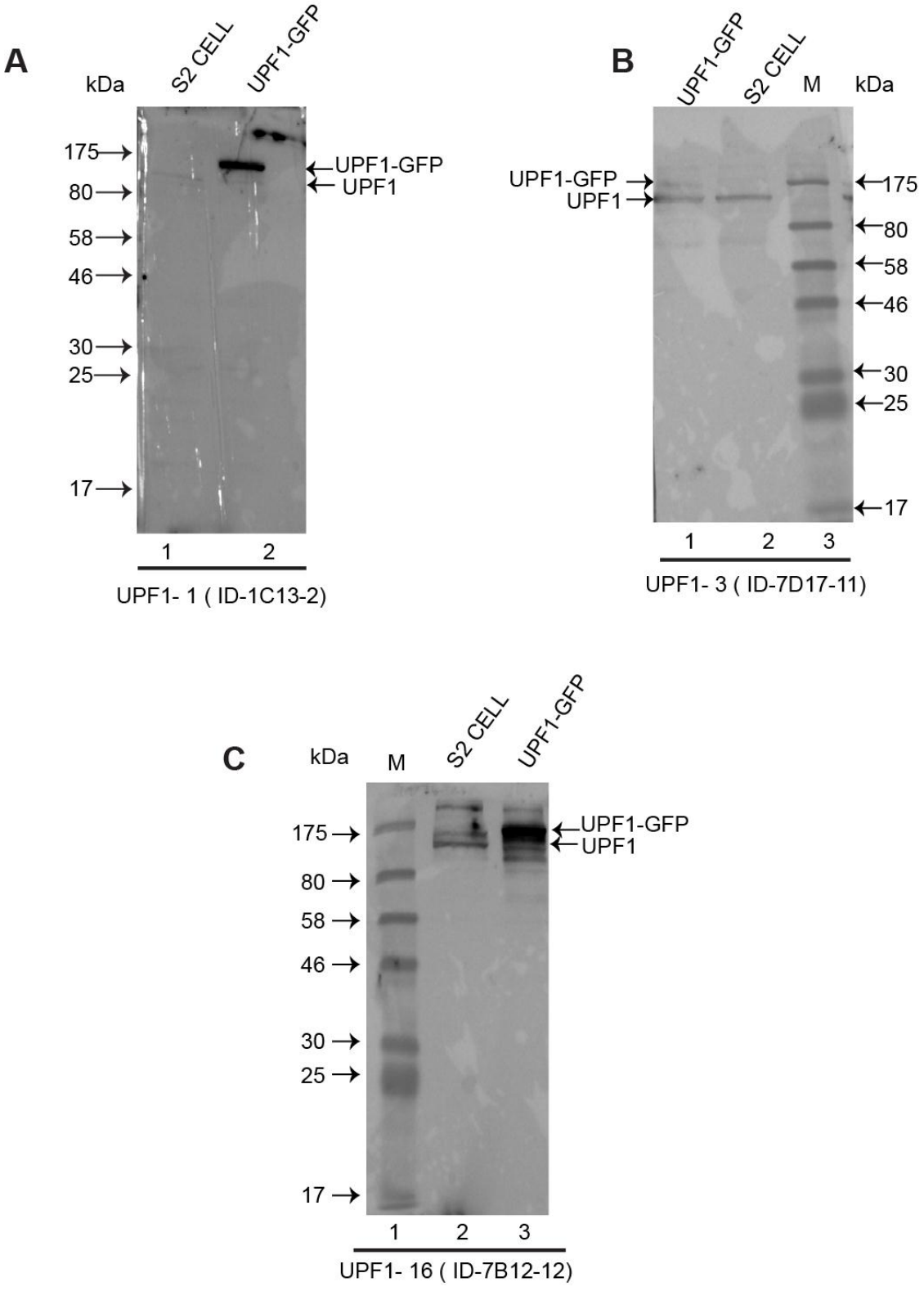

Figure 4.14 Western blot analysis of the first batch of purified UPF1 antibody detected endogenous UPF1 as well as GFP-tagged UPF1

(A) S2 cells were transfected with UPF1-GFP and immunoblotted with the UPF1-1 antibody in parallel with an S2 cell extract control. Lane 1 shows endogenous UPF1 and lane 2 shows both UPF1-GFP (156.94 kDa) (top) and endogenous UPF1 (bottom). (B) and (C) UPF1-3 and UPF1-16 antibodies were used in a similar way. These antibodies detected both UPF1-GFP and endogenous UPF1 (lane 1 of (B) and lane 3 of (C)) in the transfected cell extract while only endogenous UPF1 in the control S2 cell extract (lane 2 of (B) and lane 2 of (C)).

Table 4.5 Second batch of purified UPF1-1 and UPF1-16 antibodies

Project ID	Target protein	Product name	Epitope peptide	Ig types	Antibody type	Company
14476-1	UPF1-1	10108-1-1M1/1C13-2_130722	DEPGSSYVKE	Mouse IgG Monoclonal	Powder	Abmart Inc
14476-1	UPF1-16	10108-1-7M1/7B12-12_130821	KPGIDSEPAH	Mouse IgG Monoclonal	Powder	Abmart Inc

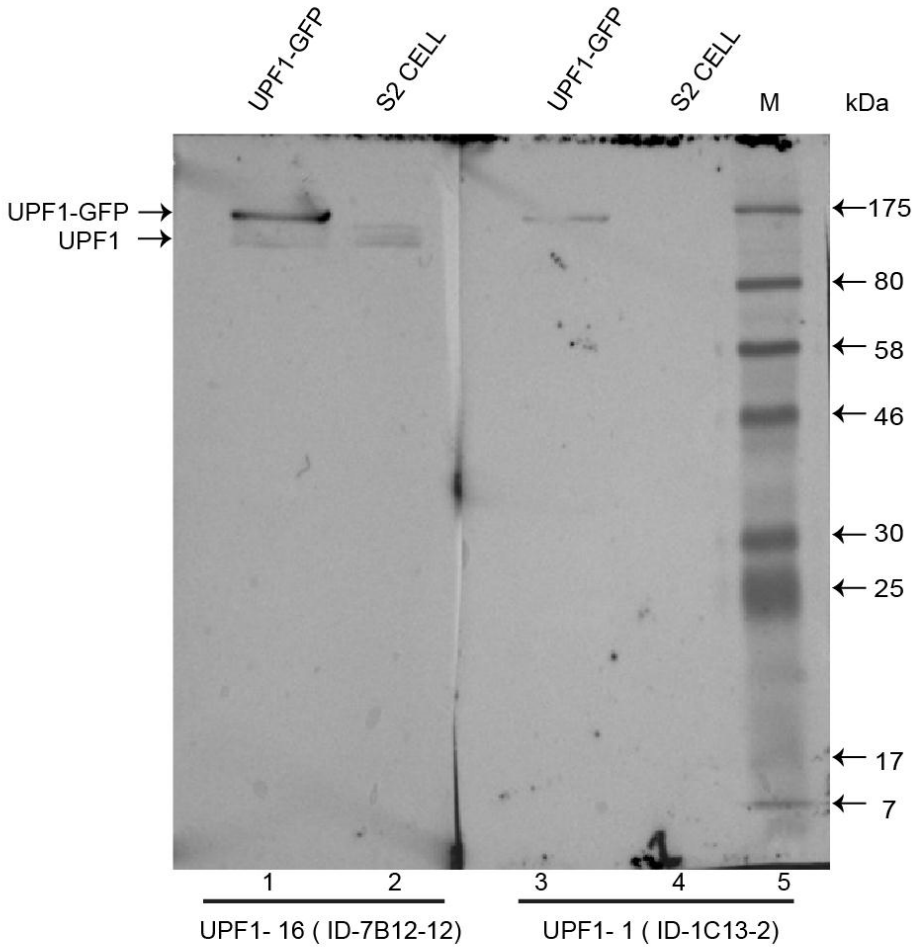

Figure 4.15 Western blot analysis of the second batch of purified UPF1 antibodies showed detection of both endogenous UPF1 and UPF1-GFP

(A) S2 cells were transfected with UPF1-GFP and immunoblotted with UPF1-1 and UPF1-16 antibodies in parallel with a control S2 cell extract. The Western blot with UPF1-16 antibody showed detection of both endogenous UPF1 and UPF1-GFP in lane 1, while only endogenous UPF1 in lane 2 (control). Immunoblot with UPF1-1 antibody detected UPF1-GFP in lane 3 but was unable to detect endogenous UPF1 in both lanes 3 and 4 (control).

4.2.13 UPF1 associates with most of the transcription sites of polytene chromosomes

The core NMD factor UPF1 not only functions in the cytoplasm to degrade PTC-containing mRNAs, but also has a nuclear role in telomere maintenance and cell cycle progression in mammalian cells. Here, I used a similar approach to that used for investigation of EJC proteins, to visualize UPF1 at transcription sites, using the antibodies we developed. To visualize the UPF1 protein at transcription sites, indirect immunostaining was carried out with all three available antibodies: UPF1-1, UPF1-3, and UPF1-16. Staining with the UPF1-3 and UPF1-16 antibodies showed a clear signal at polytene chromosomes (Figure 4.16). The signal is more specific to interband loci (transcriptionally active regions). Notably, the UPF1 signal was present at most of the transcription sites and counterstaining with DAPI showed a weak signal at the interbands. Both the UPF1-3 and UPF1-16 antibodies show similar patterns. Unfortunately, UPF1-1 did not show a clear signal around the chromosome (data not shown). The data from these results suggest that UPF1 associates with transcription sites of the polytene chromosome. I proceeded with using UPF1-3 and UPF1-16 for further experiments.

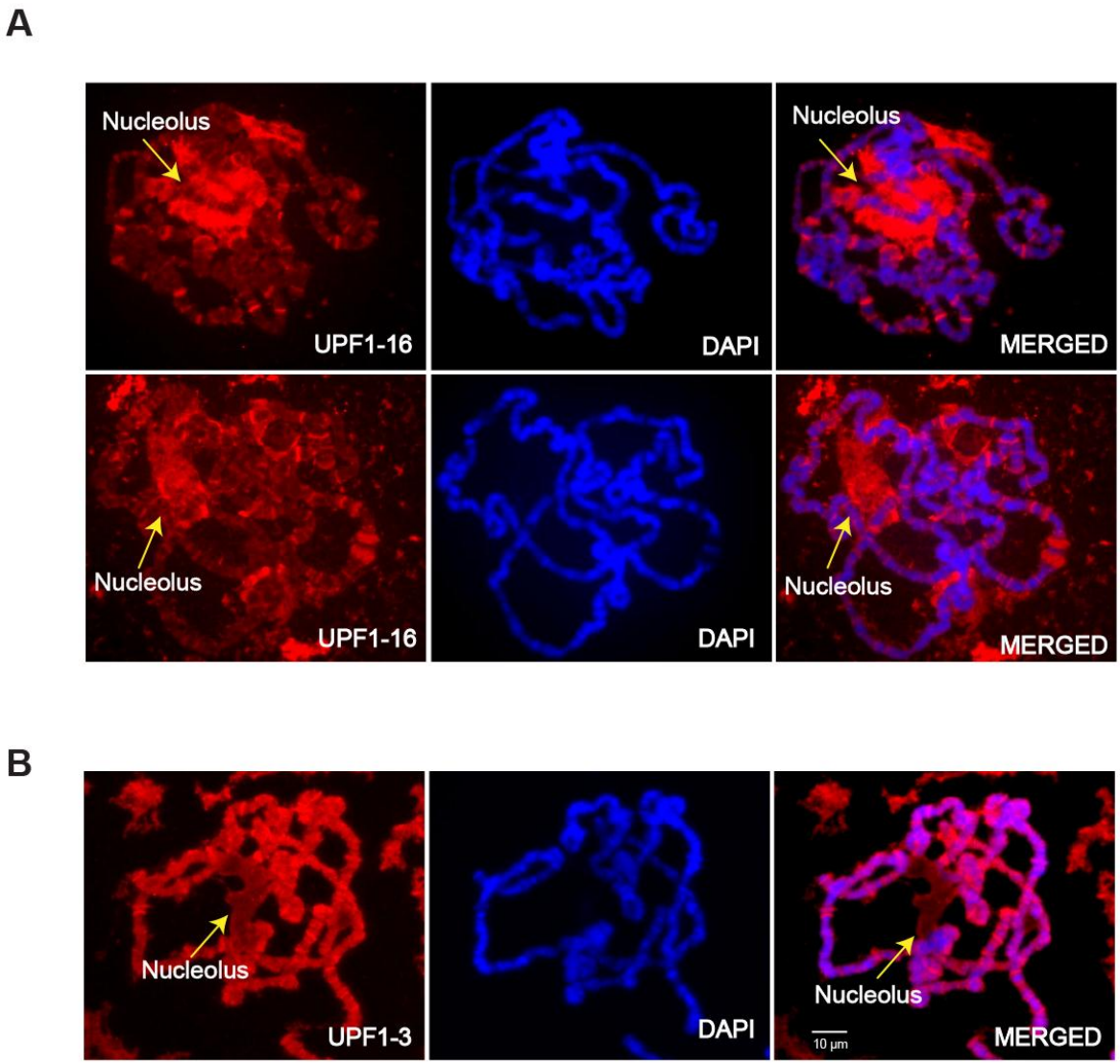

Figure 4.16 UPF1 associated with transcription sites of *Drosophila* polytene chromosome.

(A) Indirect immunostaining with the UPF1-16 antibody shows UPF1 recruitment at interband positions (top panel in red). The arrow indicates the nucleolus. DAPI is used to stain the banded regions of the chromosome (middle panel). The UPF1 signal is much clearer in the merged channel (right panel). (B) Indirect immunostaining with the UPF1-3 antibody, shows a similar pattern at interband regions as UPF1-16. Middle panel shows DAPI staining while the right panel is the merged image. UPF1 is detected using a Cy3 conjugated

secondary antibody. Micrographs were taken using an epifluorescence microscope with a 40X objective.

4.2.14 UPF1 accumulates in the nuclei of salivary gland cells

Whole salivary gland immunostaining was carried out with the UPF1-3 and UPF1-16 antibodies. As described earlier, whole salivary glands have large cells with polytenic nuclei, therefore they provide a good model to localize proteins in the subcellular compartment, and also give less variation between samples compared to polytene chromosome squash preparations. Salivary glands were dissected from 3rd instar larvae and analysed using a standard immunostaining protocol (see Material and Methods). Both antibodies show a signal in both the nucleus and cytoplasm (Figure 4.17). However, signal intensity is higher in the nucleus compared to the cytoplasm and specifically around the chromosomes, as indicated by DAPI counterstaining. To test the specificity of the antibodies further, I performed immunostaining of chromosomes from UPF1 RNAi lines (S-308, Bloomington, see Appendix III). The UPF1 signal was drastically reduced at the polytene chromosome compared to that in wild-type larvae (Figure 4.18). In summary, these results indicate that the UPF1 antibodies we have generated are specific, and UPF1 is abundant in the nucleus as well as the cytoplasm, and associates with the chromosomes.

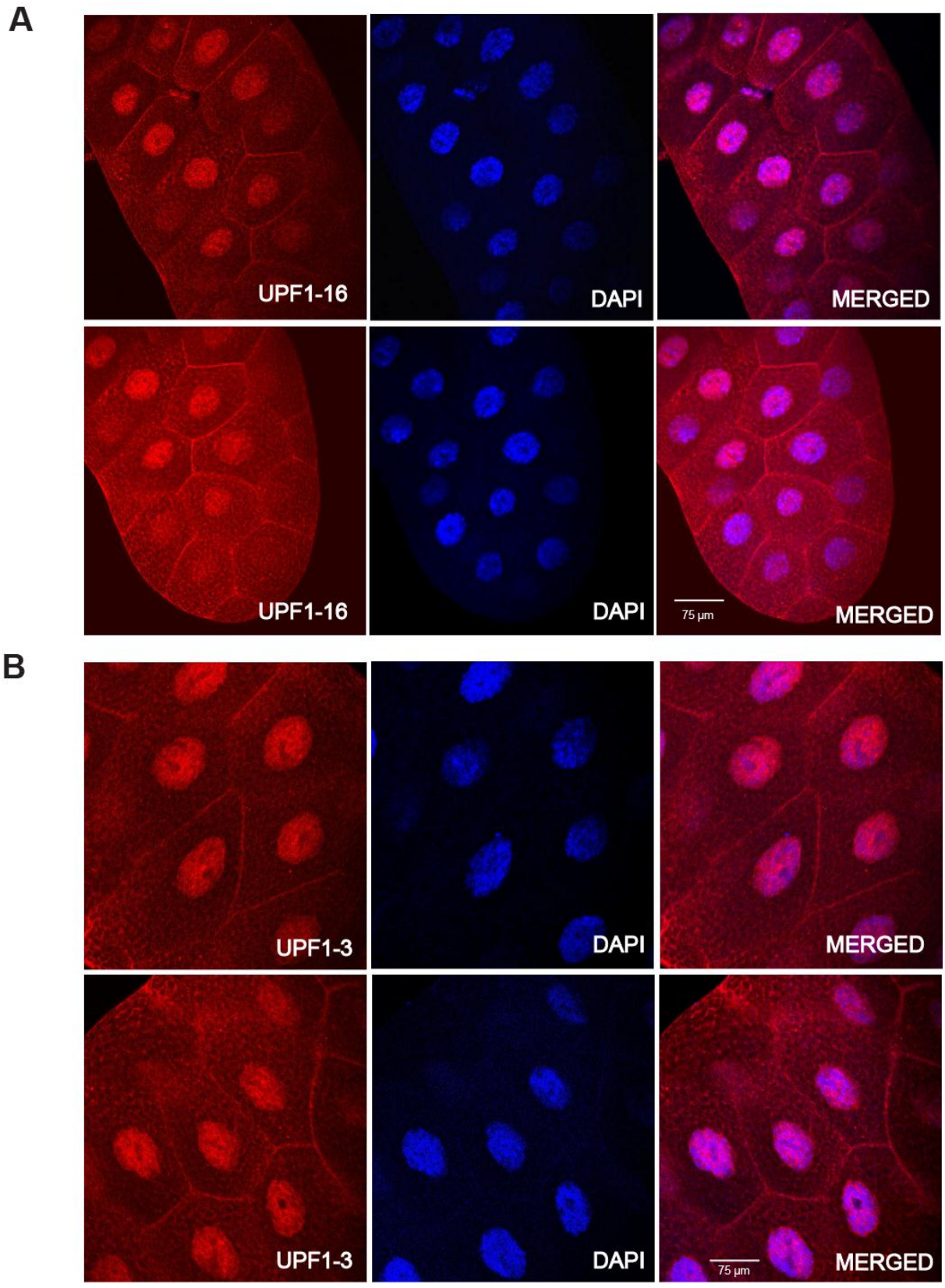
A
UPF1-16
DAPI
MERGED
UPF1-16
DAPI
75 µm
MERGED
B
UPF1-3
DAPI
MERGED
UPF1-3
DAPI
75 µm
MERGED

Figure 4.17 Visualization of UPF1 in whole salivary glands

(A) Confocal image of whole salivary glands stained with UPF1-16 showed a UPF1 signal in both the cytoplasm and the nucleus. The signal is much more intense in the nucleus compared to the cytoplasm, as also observed in the polytene chromosomes. The middle panel shows DAPI staining while the right panel is the merged image. (B) A similar signalling pattern was also observed by staining with the UPF1-3 antibody. Cy3 conjugated secondary antibody was used to detect UPF1.

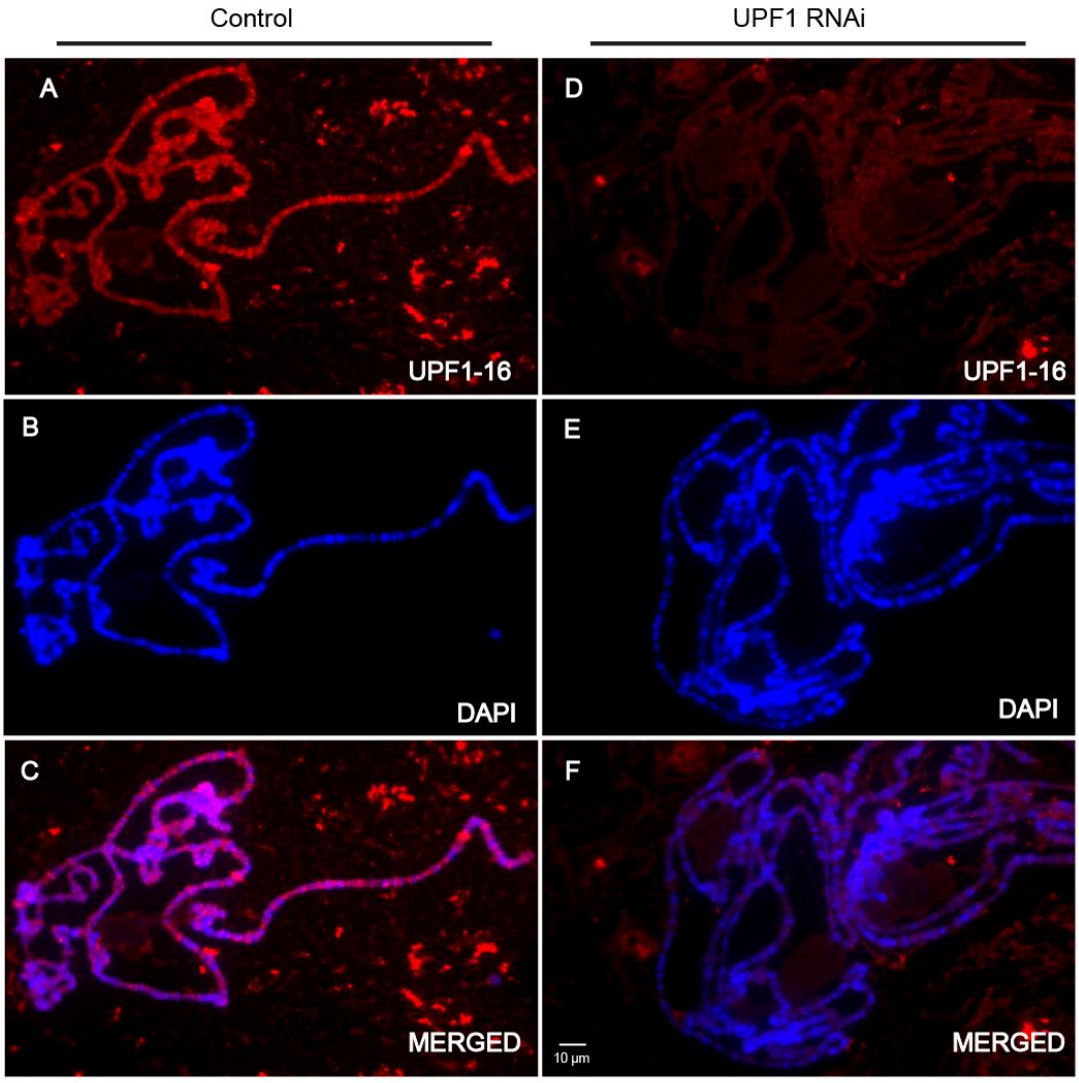

Figure 4.18 UPF1 knock down reduced the UPF1 signal from chromosomal sites

(A) Top left panel shows polytene chromosomes stained with UPF1-16 from wild-type larvae; the UPF1 signal is observed all over the chromosome, particularly at interband regions. This is much clearer in the merged channels (C). (B) DAPI staining of chromosomes. (D) Top right panel shows UPF1 RNAi lines (S-308, Bloomington, see Appendix III) which were crossed with the fkh-Gal4 driver, in which the UPF1 signal was

reduced from the chromosomal sites. (E) Middle panels show DAPI staining. (F) The UPF1 signal is more evident in the merged channel.

4.3 Discussion

Observations from the NMD field indicate that premature translation termination codons (PTCs) can be recognised while the transcript is still in the nucleus. NMD is a translation dependent process, and ribosomes are the only machinery able to scan the mRNA to recognize the PTC. If NMD were to take place in the nucleus, the expectation is that functional ribosomes and NMD factors will also be present in order for this scanning and PTC recognition to take place. Ribosomal proteins constitute an essential part of the ribosome and are also important for viability of all cell types. Therefore, I decided that a good starting point would be to localize tagged ribosomal proteins and their recruitment at transcription sites of the *Drosophila* polytene chromosome. Consistent with this view, here I report that analysis of several yellow fluorescent protein (YFP) -tagged ribosomal protein transgenic *Drosophila* lines, indicates that ribosomal proteins (RPs) accumulate in both the cytoplasm and the nucleus, specifically YFP-tagged RpL41. Moreover, the association of YFP-tagged RpL41 at transcription sites on polytene chromosomes further confirms their presence at these sites, which is consistent with that previously reported (Brogna et al., 2002). This result is also consistent with our report that several other fluorescently tagged ribosomal proteins are present at transcription sites in *Drosophila* polytene chromosomes (Rugjee et al., 2013). Although, it possible that the tagged ribosomal proteins observed are in a free state, and not incorporated into ribosomal subunits, my observations support the earlier conclusion that RPs might be recruited in the form of complexes at transcription sites (Brogna et al., 2002). The accumulation of YFP-tagged RpL41 in the nucleus, with the characteristic of nucleolar enrichment, and presence at transcription sites imply that these tagged RPs can be incorporated into ribosomes.

To assess whether there are translating ribosomes at these sites more directly, I applied the recently developed ribopuromycylation technique (David et al., 2012). The results of these experiments show puromycin incorporation at interband positions of highly transcribed regions of *Drosophila* polytene chromosomes. The puromycin signal seems to be transcription dependent, as RNase treatment depletes most of the signal from these transcription sites. In addition, puromycylation was also observed in intact salivary glands, mainly in the cytoplasm and nucleolus of smaller cells, and puromycylated peptides were observed around the chromosomes in larger cells. As reported earlier, following treatment with translation inhibitor drugs such as harringtonine, the signal appears to be drastically reduced, which suggests that the puromycin signal is translation-dependent, as previously concluded in mammalian cells by David et al 2012. These observations further suggest the presence of functional 80S ribosomes at these sites, providing additional evidence to support the possibility that PTC recognition can occur while the transcript is still nascent and that NMD may occur at the sites of transcription on newly synthesized mRNAs. Moreover, the observation that UPF1 is present at most of the transcription sites further strengthens the argument that NMD can occur in the nucleus. Future studies will have to investigate this further, and also test the alternative possibility that UPF1 is performing some other functions at transcription sites which could be unrelated to NMD. In addition, the antibodies we produced can be used for other experiments aimed at understanding how these protein function at the transcription sites.

Chapter 5

5.0 Visualization of co-transcriptional pre-mRNA splicing on polytene chromosomes of salivary glands

5.1 Summary

As reviewed in the Introduction, the coupling between transcription and pre-mRNA splicing is an essential step of gene expression. Co-transcriptional splicing is the process in which introns are spliced out of the nascent pre-mRNA that is still attached to the RNA polymerase. This coupling between transcription and pre-mRNA splicing is important in splice site selection. Here I describe the development of an experimental system that allows visualization of pre-mRNA splicing and mRNP assembly directly at transcription sites. This system uses reporter constructs based on the medfly *Ceratitis capitata Adh* gene, which is evolutionarily distantly related to *Drosophila melanogaster*. The first reporter construct (which was available in the Dr. Brogna lab) produces an mRNA carrying one or more repeats of the sequence-specific RNA binding sites for protein (MS2) sequence in the 3' UTR, which can be visualised by co-expression of fluorescently-tagged MS2 coat protein (MCP) that binds to the MS2 sequence with high specificity (Weil et al., 2010). The construct, denoted Adh-MS2 (Figure 5.1) (S-118, see Appendix III) is regulated by an ecdysone response element (ERE) in the promoter which enables its expression to be induced in the presence of ecdysone. Ecdysone is a steroidal prohormone whose increase in concentration induces the expression of protein coding genes. Moreover, this construct is also flanked by lac operator (lacO) repeats at the 5'end; the addition of the lacO repeats allows visualization of the locus

in cells expressing *lac* repressor tagged with GFP. A similar reporter construct was used to visualise spliced mRNA in which MS2 sequence was split between the 3' end of exon 1 and the 5' end of exon 2 which was denoted as Adh-split-MS2 (Figure 5.3).

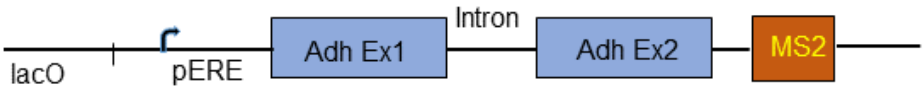

Figure 5.1 Schematic representation of Adh-MS2 reporter constructs. Reporter construct consists of two coding sequences (exons) of the medfly alcohol dehydrogenase (*Adh*) gene separated by an intron and flanked by 3'UTR containing MS2 binding sites. The promoter is regulated by an ecdysone response element (ERE) which is flanked by *lacO* repeats at the 5' side.

5.2 Result

5.2.1 Visualization of nascent RNA in *Drosophila* salivary glands

To test whether the approach I described above would allow visualisation of nascent mRNA, I crossed different available strains expressing MCP-GFP (Appendix III) with flies carrying the reporter construct Adh-MS2. As expected, I observed that MCP-GFP clearly generates a strong green fluorescence signal in correspondence to a specific interband, which most probably corresponds to the nascent mRNA of the Adh-MS2 transgene (Figure 5.2). Although the GFP signal is visible throughout the nucleus, as a result of background fluorescence, the signal is much stronger in correspondence to a specific interband. This observation indicates that this reporter can be further used to visualise specific nascent RNAs and its associated proteins.

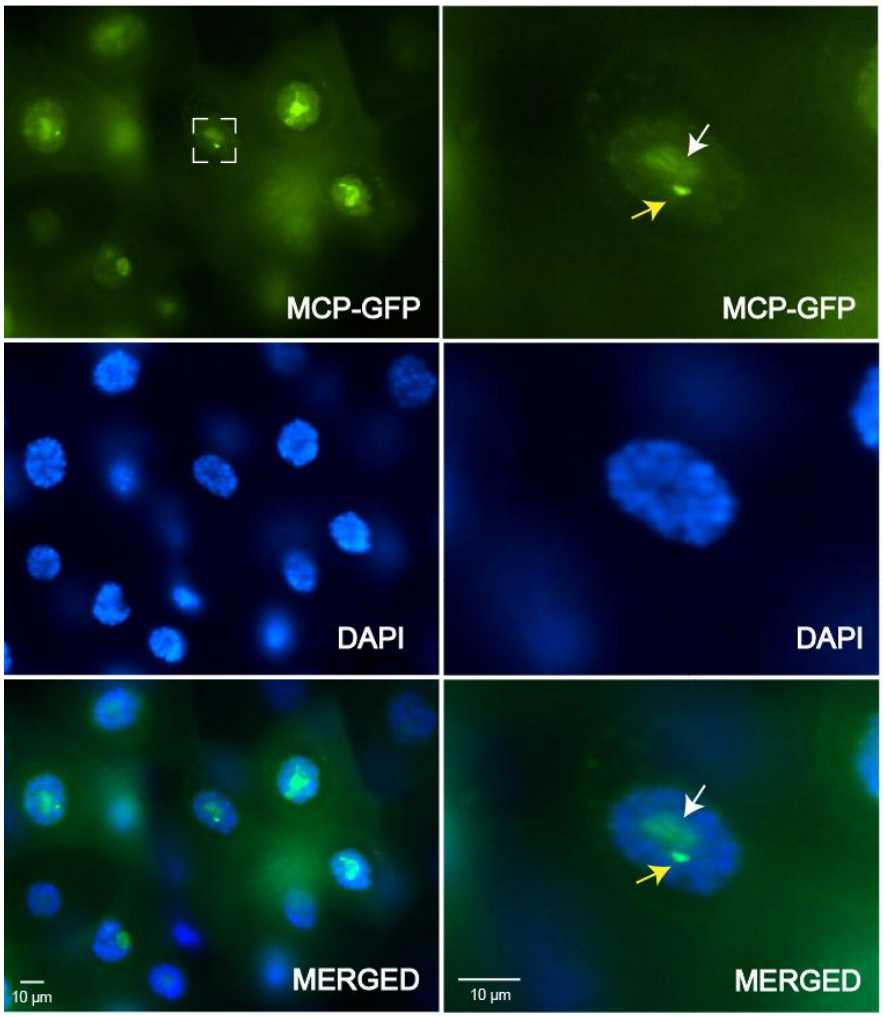

Figure 5.2 Visualisation of a specific reporter nascent RNA in the nuclei of salivary glands Left panel shows images of salivary glands from larval progeny of a cross between the reporter Adh-MS2 (S-118, see Appendix III) and the MCP GFP line flies (S-240, ID 7278, see Appendix III). GFP signal is visualized as a single dot in the nucleus. The signal is more apparent in the magnified insets of the original image (marked with a white box) in the right panels. Arrow indicates specific chromosomal position with an intense GFP signal. However, GFP also accumulates all over the cell and its signal is stronger in the nucleolus (white arrow). Glands were counterstained with DAPI to stain DNA (middle panel). Bottom panels show merged channel of both GFP and DAPI. Images were taken using an epifluorescence microscope equipped with a 40X objective.

5.2.2 Versatile gene reporter constructs allow visualisation of splicing

Having demonstrated that the above system allows visualisation of nascent RNA, I wanted to test whether it's feasible to specifically visualize spliced mRNA. To visualize spliced mRNA I used a transgenic line (Dr. Brogna lab, unpublished) carrying the Adh-split-MS2 construct (Figure 5.3), in which MS2 binding site was split between the end of the first and the beginning of the second exon. Therefore, a functional MS2 binding site is formed only upon ligation of the two exons, which can be visualized by co-expressing GFP or RFP-tagged MS2, as mentioned above. Additionally, the split Adh-MS2 reporter construct is flanked by ERE promoter at 5' UTR. This system is therefore expected to be effective in visualizing pre-mRNA splicing, fluorescently-tagged protein associated with the nascent pre-mRNA and mRNA.

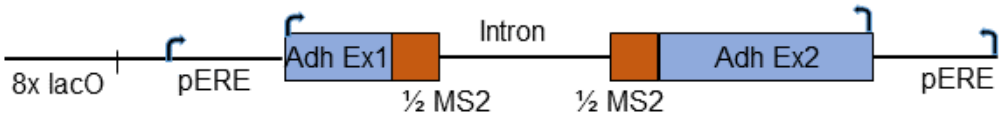

Figure 5.3 Simplified representation of the split Adh-MS2 reporter construct. The construct consists of Adh coding sequence split into two exons - each exon is flanked with two halves of the MS2 binding site. The Promoter is regulated by an ecdysone response element (pERE) at the 5'UTR which is further flanked by 8x *lacO* repeats.

5.2.3 Visualization of pre-mRNA splicing in nuclei of *Drosophila* salivary glands

To visualize splicing, I examined different *Drosophila* lines carrying the split-Adh1-MS2 construct (see Appendix III) at different chromosomal locations. I selected the best one by crossing them with MCP-GFP lines and inspecting which cross had the most defined GFP signal at the transgenic locus. The best Adh-split-MS2 line was then crossed again with the MCP-GFP line and salivary glands from 3rd instar larvae were used for *in vivo* imaging. Firstly, I examined glands which were not exposed to ecdysone in which, therefore, the expression of the reporter was not expected. In these glands, only background MCP-GFP signal was observed all over the cell, with particularly high intensity in the nucleolus (Figure 5.4). Several glands were inspected but no specific chromosomal signal could be detected. Salivary glands were then treated with 1μM ecdysone for 2.30 h prior to dissection to induce expression. After ecdysone treatment, a strong signal was observed in correspondence to a single chromosomal band (Figure 5.4). As demonstrated by the DAPI counterstaining, the signal is located at an interband on the chromosome. These observations suggest that this signal is due to the presence of a nascent spliced mRNA at this locus. Thus, this system allows visualisation of co-transcriptional splicing and studying selective docking of proteins onto a nascent spliced mRNA.

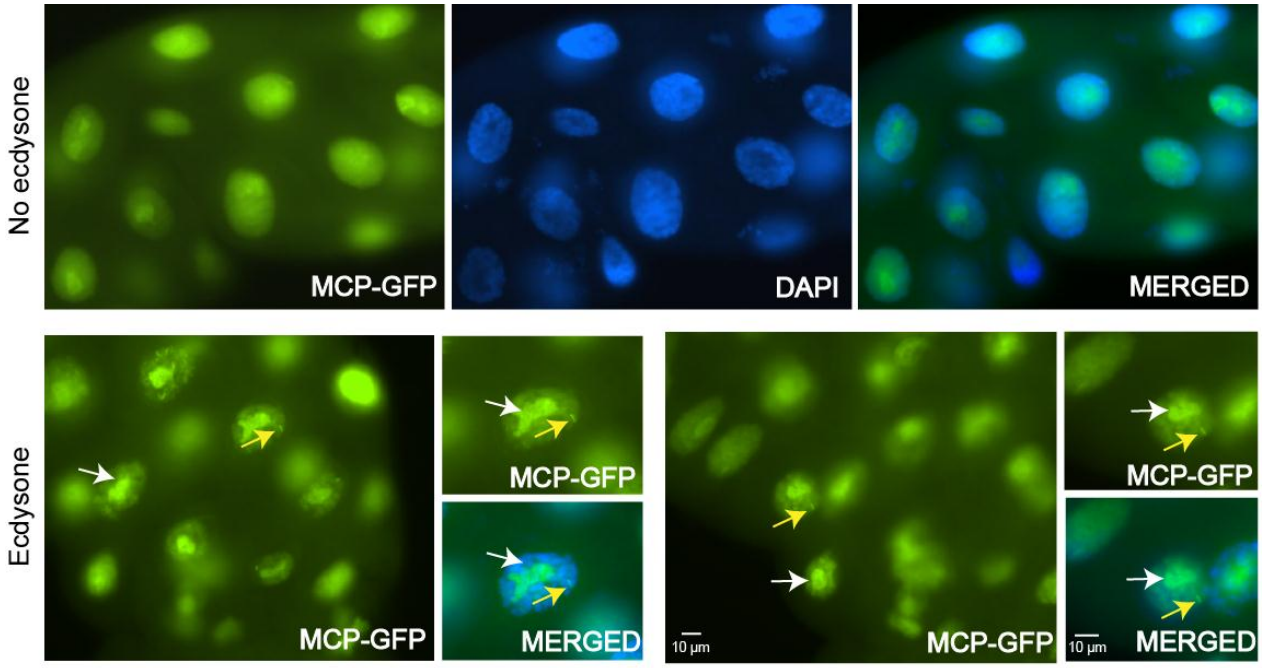

Figure 5.4 Visualisation of co-transcriptional splicing. Adh-split-MS2 line (S-90, see Appendix III) was crossed with MCP GFP Line (S-240. ID 7278, see Appendix III). The top left panel shows that there is no prominent chromosomal signal in the absence of ecdysone. Treatment with ecdysone (bottom panels) results in a prominent band at the chromosomes (arrow) which is shown clearer in the magnified inset showing a single nucleus. Another gland is viewed in the bottom right panel, which was similarly treated with ecdysone, as the one on the left. All images were captured by an epifluorescence microscope with a 40X objective.

5.2.4 Transgene visualisation using *lacI*-GFP

To facilitate visualization of specific mRNPs in intact nuclei without the need of chromosome spreading, lacO repeats were added to the reporter gene as described above. To verify the system, I combined *lacI*-GFP and MCP-RFP in order to be able to distinguish the locus and the mRNA signal, respectively (see Materials and Methods). Subsequently, I crossed the combined lines (*lacI*-GFP and MCP-RFP) with the one harbouring Adh-MS2 construct. The best line for MCP-RFP among four (see Appendix III), were selected by their crossing with the Adh-MS2 reporter line. The salivary glands were inspected as before and the line which produced the strongest MCP-RFP signal, in correspondence to a single interband (which is more apparent upon ecdysone treatment and most probably corresponds to the nascent mRNA of the transgene) was selected (Figure 5.5 A). Similarly, the best *lacI*-GFP (among three lines, see Appendix III) lines were selected after crossing with Adh-ERE reporters carrying lacO repeats flanking the transcribed region and the promoter (see Appendix III). The *lacI*-GFP lines are regulated by the heat shock promoter. Therefore, experiments were carried out with or without previous heat shock treatment. In the absence of heat shock, the signal is apparent at the transgene position (Figure 5.5 B, arrow). Upon heat shock, the signal becomes more prominent (Figure 5.5 C). The signal clearly located in the nucleus. These experiments demonstrated that the best *lacI*-GFP line is S-206, while the best MCP-RFP line is S-245 (Appendix III).

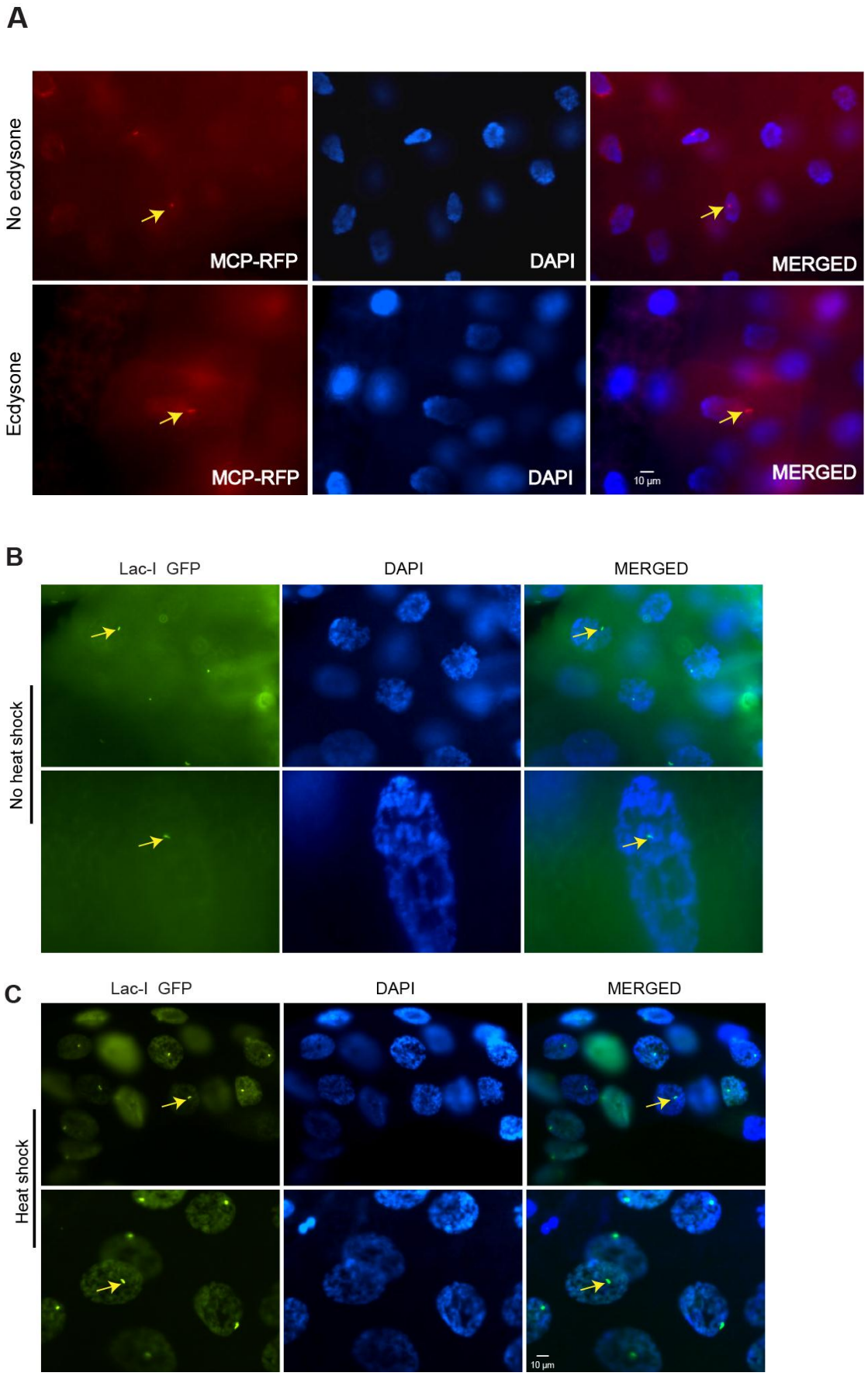
A
No ecdysone
MCP-RFP
DAPI
MERGED
Ecdysone
MCP-RFP
DAPI
10 µm
MERGED
B
Lac-I GFP
DAPI
MERGED
No heat shock
C
Lac-I GFP
DAPI
MERGED
Heat shock
10 µm

Figure 5.5 Visualisation of the transgene using lacI-GFP. (A) Visualization of the Adh-MS2 locus in salivary glands of flies expressing MCP-RFP (S-245, ID-9939, Appendix III). Top left panel shows weak RFP signal in the nuclei of glands which were not incubated with ecdysone. Bottom panels show stronger RFP signal in glands incubated with ecdysone. RFP signal at the putative transgene locus is indicated by the arrow. (B) Control glands in which transgenes were carrying several *lacO* repeats (S-133, Appendix III) are visualised by crossing with lacI-GFP (S-206, Appendix III) without previously being heat shocked. (C) The same as in B except larvae were heat shocked prior dissection. Middle panels show DAPI staining, while right panel represents merged channel with DAPI. Micrographs were taken using an epifluorescence microscope with a 40X objective.

5.2.5 Simultaneous visualisation of nascent RNP and transgenic locus

To verify that the MCP-RFP, reporting the nascent RNA, and lacI-GFP signal, reporting the Adh-MS2 transgene, are indeed co-localising, the strain carrying both *lacI*-GFP and MCP-RFP was crossed with the Adh-MS2 reporter carrying strain (Figure 5.1). As expected, the prominent RFP and GFP signals co-localize in the nucleus (Figure 5.6, arrows). These results confirm that MS2-RNA signal we detect is in fact at the transgene. Although both GFP and RFP fluorescence is visible throughout the nucleus, the signal is much stronger in correspondence to a single band. In summary, the results obtained so far make me confident that this system can be successfully used to investigate the docking of proteins on the spliced transcript as well as pre-mRNA processing *in vivo*.

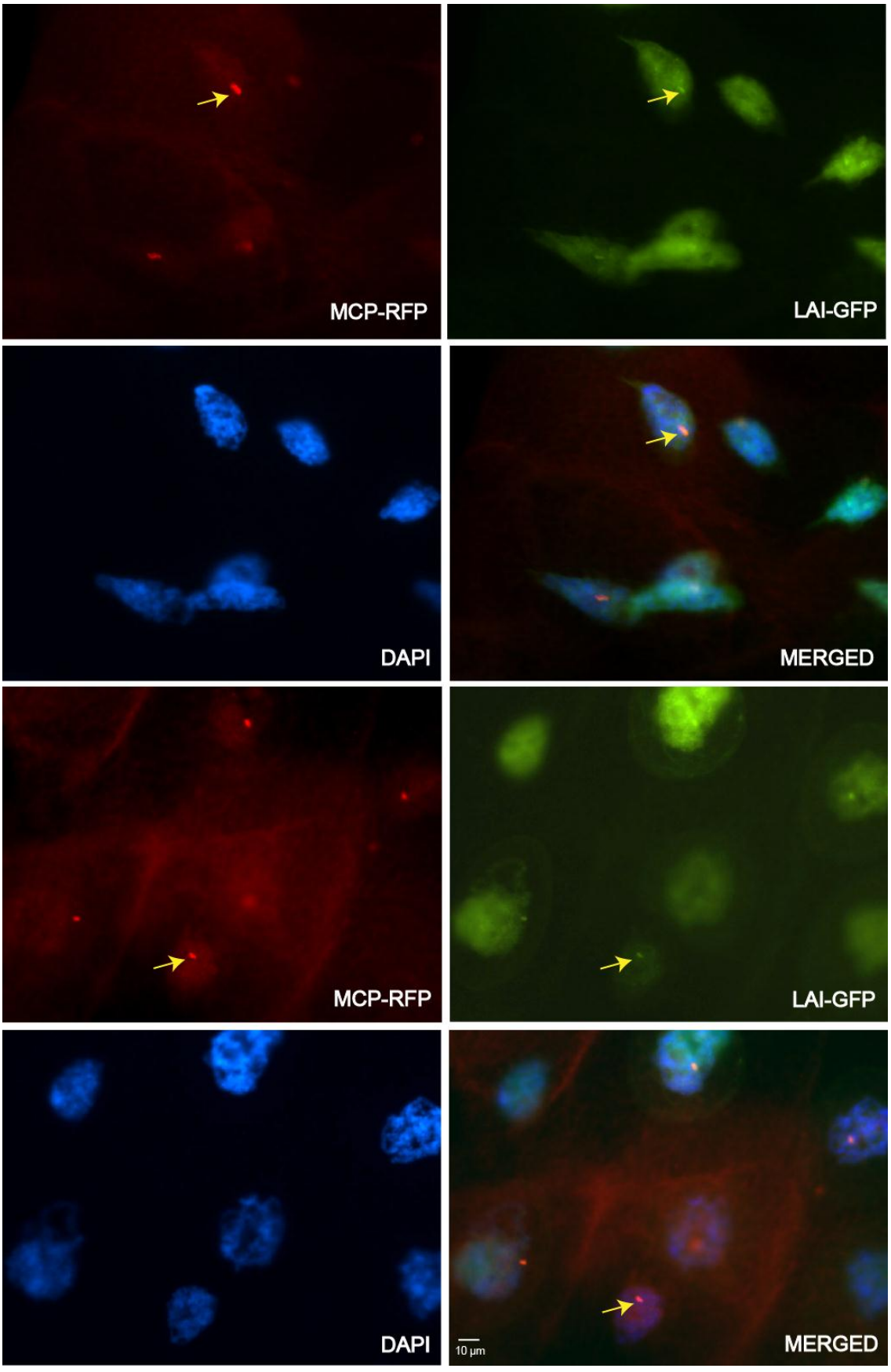
MCP-RFP
LAI-GFP
DAPI
MERGED
MCP-RFP
LAI-GFP
DAPI
10 µm
MERGED

Figure 5.6 Simultaneous visualization of the nascent RNA and the transgene locus

Visualisation of both the transgene locus (the *Adh-MS2* locus) and its nascent mRNA. *LacI*-GFP signal corresponds to the locus (carrying *lacO* repeats), while MCP-RFP binds to the MS2 repeats in the 3'UTR, therefore, MCP-RFP signal corresponds to the nascent RNA. Both GFP and RFP signals are detected at the same chromosomal site, denoted by an arrow. DAPI staining was also carried out in all samples in order to stain DNA. All images were taken using an epifluorescence microscope with a 40X objective.

5.3 Discussion

The physical coupling between transcription and pre-mRNA splicing has been shown to be important for accurate pre-mRNA splicing. The Pol II CTD may act as a platform for the localization of the splicing machinery near to the nascent transcript, as well as in helping define exons among intron sequences by exon tethering (Maniatis and Reed, 2002; Morris and Greenleaf, 2000). Here I reported that the MS2-GFP system is the most common *in vivo* approach to visualizing splicing and localization of mRNA in the cell. This system is based on the tethering of reporter mRNA with the MS2 sequence which is recognized by the GFP-tagged MS2 coat protein. Therefore, it is feasible that reporter mRNA can be visualized in the cell by simultaneously expression of the MS2 coat protein tagged with either RFP or GFP (Martin et al., 2013; Querido and Chartrand, 2008). The transgenic construct I used allows detection of specific RNAs, and visualization of DNA loci. The observation from the first study, based on this principle, shows a strong, clear GFP signal in the nucleus, which corresponds to the (Adh-MS2) reporter. Although, by using this system also produced some background fluorescence, but the GFP signal is much stronger in corresponding of a single fluorescent dot. Therefore, this system allows visualization of nascent mRNA in the cell. The latter split Adh-MS2 reporter is more complex as it relies on pre-mRNA splicing of the reporter mRNA which produces a functional MS2 site only after splicing. Observation from my data indicates that it is feasible to visualize spliced mRNA, as a GFP signal was produced in the nucleus, corresponding to the split Adh-MS2 reporter. Therefore, this construct provides an effective model to visualize splicing and spliced mRNA at the same sites. A key feature of all our reporter genes is that they are flanked by lacO repeats, which allows precise identification of the locus. Moreover, the reporter gene is also under the control of the ERE promoter, in which the signal becomes more apparent by treatment with ecdysone. To further verify the

GFP or RFP signal corresponds with the transgenic reporter locus would be required for independent identify the position the Adh-MS2 transgene in the intact nucleus, independent of the mRNP signal. To allow this, here I also produced a homozygous transgenic line, that expresses both *lacI*-GFP and MS2 coat protein MCP-RFP. The MCP-RFP will bind to the MS2 site of the reporter mRNA, which produces the red fluorescence signal, and *lacI*-GFP will bind to the LacO repeats corresponding to the locus of Adh-MS2 reporter to give the green fluorescent signal. As expected, observations of both RFP signals and GFP signals in the nucleus suggest that the MS2-RNA signal corresponds to the transgenic construct. Based on the above results, here I visualized co-transcriptional splicing in Drosophila for the first time. By using this system, future studies should be able to investigate in detail how pre-mRNA decoration is affected by splicing signals. Unfortunately, due to time constraints, this last stage of the project could not be initiated, nor I could use this system to visualize how EJC proteins are recruited at transcription sites and nascent transcripts, or investigate the dependence of this recruitment on splicing features, such as the presence of introns or intron length. However, the procedure to complete the experiment may involve using both transgenic lines (intron-containing and intron-less) and crosses with *lacI*-GFP lines (described above), then performing the double immunostaining in the polytene chromosome. The antibody against GFP will recognize the locus of the reporter transgene an antibody against the endogenous EJC protein allow us to detect whether the EJC signal is exactly at the same location as the GFP signal. If the EJC were to bind the transgene, this could provide further evidence that EJC recruitment is not only splicing-dependent, but also splicing independent.

Chapter 6

6.0 Discussion and Conclusion

6.1 Association of eIF4AIII at transcription sites distinct to that of Y14 and MAGO

Current models predict that the EJC binds an mRNA straight after pre-mRNA splicing (Kataoka et al., 2000; Le Hir et al., 2000a; Le Hir et al., 2000b). The EJC is best known for its role in NMD, but studies in yeast and *Drosophila* have concluded that it was not required for this process. However, EJC proteins are essential for survival in *Drosophila* and was known to be involved in mRNA localization. I wanted to understand how it performed this role and since it is a predominantly co-transcriptional process, I considered that a good starting point would be to visualise its recruitment at transcription sites of the *Drosophila* polytene chromosome. I also wanted to assess whether there are specific features of genes that promote EJC assembly.

My data indicate that the EJC core components Y14, MAGO and eIF4AIII are in fact present at most transcription sites. Although in mammalian cells EJC core components are localized primarily in the nucleus (Baguet et al., 2007; Custodio et al., 2004), in *Drosophila*, these proteins seem to be equally distributed between the nucleus and the cytoplasm, as observed from nuclear and cytoplasmic fractionation of S2 cells. Thus the abundance of these proteins in the cytoplasm is in agreement with an earlier observation that EJC proteins, particularly the Y14/MAGO heterodimer, are required for localization of *oskar* mRNA during embryonic development in *Drosophila* (Hachet and Ephrussi, 2001). It was reported that Y14/MAGO formed a tight heterodimer, therefore these two proteins are expected to colocalize at the same position on the chromosome. As I have demonstrated from chromosome mapping, both Y14 and MAGO are in fact co-localized precisely at the same loci; this observation is further

verified by co-localization of Flag-Y14 with endogenous MAGO and is consistent with the earlier observation that these two protein form heterodimer. However, recruitment of eIF4AIII poorly correlates with Y14 and MAGO, as most of the transcription sites associated with eIF4AIII and this observation most apparent upon colocalization with active Poll II ($PolI^{Ser2}$) – the antibody (H5) recognises the Ser2 hyperphosporylated CTD of the largest Pol II subunit, a marker of transcription elongation (Buratowski, 2009; O'Brien et al., 1994). Additionally, the observation that flag-tagged eIF4AIII is present at most transcription sites, and was not co-localized with Y14/MAGO, suggests that EJC assembly may not be a constitutive process in *Drosophila*. All previous studies reported that EJCs assemble on maturing mRNAs during splicing, however, it was not clear how it makes contact with the spliceosome. However, it was recently suggested that one splicing factor, CWC22, interacts directly with eIF4AIII via its MIF4AG domain, which allows for the splicing-dependent assembly of EJCs (Alexandrov et al., 2012; Barbosa et al., 2012). Therefore, this raises the possibility that most of the transcription sites are associated with eIF4AIII and that this association is independent of Y14 and MAGO.

6.1.1 MAGO is not essential for Y14 association with transcription sites

Although knockdown of eIF4AIII impairs the development of salivary glands and polytene chromosomes could not be prepared from them, knockdown of either Y14 or MAGO does not have any phenotypic effects, allowing me to further investigate these proteins in this tissue. Interestingly, analysis of these glands indicates that Y14 does not require MAGO to associate with the transcription sites, however, MAGO knockdown reduced that of Y14 at the chromosomes. Although the Y14 signal was apparently reduced at the chromosomes, however, the staining pattern around the chromosome remain the same with typical interband staining as in wild type. This observation indicates an independent function of Y14 that does not require

MAGO to associate with the transcription sites. However, the reduced intensity of the Y14 signal might solely be the result of the destabilization of the protein in the absence of MAGO. Additionally, it was recently reported that Y14 also functions as an inhibitor of mRNA decapping factor Dcp2 and modulates P body formation (Chuang et al., 2013). These observations are in further agreement with an earlier study that suggested Y14 functions in an independent manner that does not involve MAGO. To gain more detailed information about the role of their heterodimerization, I selectively knocked down Y14, MAGO and eIF4AIII in *Drosophila* S2 cells. Notably, and consistent with what was observed with the chromosome squashes, Y14 knockdown remarkably reduces MAGO recruitment and conversely, MAGO knockdown, reduces Y14, although not completely. In both cases, eIF4AIII was not visibly affected by either Y14 or MAGO knockdown, as is consistent with the polytene chromosome staining. This observation suggests that Y14 and MAGO heterodimerization is required for the stability of both proteins *in vivo*. However, Y14/MAGO heterodimerization stabilizes both proteins, arguing that their function is coupled.

6.1.2 The association of the EJC with transcription sites is splicing independent

All current models predict that the EJC is at transcription sites because it binds to nascent mRNA or pre-mRNA (Custodio et al., 2004; Le Hir et al., 2000a). Notably, I found that following treatment with RNase, the EJC signal remain at transcription sites while the signals from Sm proteins and fluorouridine labelled nascent mRNA were completely diminished. Therefore, these observations suggest that the EJC core proteins possibly are not recruited to transcription sites by binding to nascent RNA, but might make RNA-independent secondary contacts with chromatin or DNA directly. To address EJC binding at transcription sites more specifically, we carried out ChIP followed by high throughput sequencing (ChIP-seq). ChIP-seq of Y14 indicates that this protein mostly associates with transcription start sites and the

promoter region. These observations suggest that Y14, either individually or as a part of the EJC, may have a specific role at the promoter region. Moreover, It has been reported by yeast two-hybrid screening that Y14 directly interact with signal transducer and activator of transcription 3 (STAT3) (Ohbayashi et al., 2008). STAT3 belongs to STAT protein family and function as a transcription factor. Therefore, enrichment of Y14 at promoter region might indicate their function related to transcription sites. It was recently reported that core EJC factors of the interact with SR proteins (Singh et al., 2012) particularly SRSF2, which is a part of the 7SK, a complex which activates transcription by binding promoter–proximal nascent RNA (Ji et al., 2013).

So far, the pre-mRNA splicing is the only process that drives EJC with spliced mRNA. However, the recent finding concludes the function of pre-EJC that control the splicing of *mapk* and other long intron-containing genes which suggest that this complex has also a nuclear function (Ashton-Beaucage et al., 2010). It has been also proposed that knockdown of these proteins cause alternative splicing changes in mammalian cells (Wang et al., 2014). Therefore, these observations further raise the question of how does EJC core regulate splicing, given that it is deposited only after splicing? My data indicate that EJC core components are recruited to both intron-containing and intron-less genes. This is most apparent by the analysis of heat-shock puffs, which clearly show recruitment of EJC components at the intronless gene loci, 87A and 87C (encoding Hsp70), as well as at 93D which encodes the intron-containing, non-protein coding gene hsr-ω-n (Lakhotia and Tapadia, 1998). The Y14 ChIP-seq assay also shows enrichment independent of whether a gene has introns or not. The result from this study suggests that splicing is not a pre-requisite for binding of the EJC to transcription sites. Instead, my preliminary observations suggest a transcriptional role for EJC proteins. I observed that upon knockdown of Y14 and MAGO in S2 cells, the transcript levels of specific ecdysone inducible genes (75B) was significantly increased compared to the control. This raises the

possibility that Y14/MAGO might be function as transcriptional repressors of ecdysone-induced genes.

6.1.3 Nuclear translation visualized at transcription sites

Although the EJC is not essential for NMD in *Drosophila*, it has recently been reported that some introns are able to trigger EJC dependent NMD in *Drosophila* (Sauliere et al., 2010). This observation is the first indication that EJC might have a role in NMD in *Drosophila* as well. Although NMD is a general phenomenon of cytoplasmic events, there is substantial evidence indicating that PTC recognition occurs on mRNAs while they are still in the nucleus. Observing that most transcription sites are associated with EJC, I applied a similar approach to visualize translation associated factors, ribosomal proteins, ribosomes and NMD factors at the same sites, since the ribosome is the only machinery able to scan the mRNA for a PTC during translation.

Ribosomal proteins, together with rRNA make up the large molecular machine that serves as the site of protein synthesis. Earlier evidence indicates that at least 20 RPs and rRNAs bind to transcription sites of *Drosophila* polytene chromosomes (Brogna et al., 2002). Analysis of several *Drosophila* endogenously YFP tagged ribosomal proteins, particularly RpL41, show strong accumulation both in the cytoplasm and nucleus. Additionally, native polytene chromosome staining further confirmed their association at transcription sites. This observation is consistent with the fact that fluorescently tagged ribosomal proteins are present at transcription sites in *Drosophila* polytene chromosomes (Rugjee et al., 2013). However, it was earlier reported that RPs have extra-ribosomal functions and some of the RPs regulate their own expression by binding to their pre-mRNA or promoters (Warner and McIntosh, 2009). Therefore, observations of ribosomal proteins at transcription sites does not

necessarily confirm their presence as a complete ribosomal subunit at these sites. However, it might be that they are recruited at these sites as a complex, possibly ribosomal subunits, as previously proposed (Brogna et al., 2002; De et al., 2011). Additionally, it was recently reported in yeast that it is possible that these RPs are in ribosomal subunits or other ribosomal-like complexes (De et al., 2011).

To resolve the issue of whether there are functional ribosomes at transcription sites, I applied the ribopuromycylation technique (RPM) that was successfully developed to visualize puromycylated nascent peptides in HeLa cells (David et al., 2012). My observation that puromycin is incorporated at most transcription sites on the polytene chromosome along with other data we have published, strongly indicates the presence of translating 80S in the nucleolus and at transcription sites (Al-Jubran et al., 2013), it has been argued that puromycylation is an indicator of peptidyl transferase activity, but not necessarily of translation (Dahlberg and Lund, 2012). Whether RPM can be used to visualise translation needs to be further investigated.

6.1.4 UPF1 recruitment at transcription sites indicates possible nuclear function

Consistent with the view that translating ribosomes are present at transcription sites, in a parallel project during my PhD, I found that the NMD factor UPF1 binds to such sites. There is both direct and indirect evidence showing that proteins involved in NMD are at transcription sites. Additionally, whole salivary gland staining shows signal both in the cytoplasm and nucleus. Based on the current NMD model, unlike UPF3, UPF1 is a cytoplasmic protein and key component of NMD factor. However, from my data, association of UPF1 at the transcription sites might indicate possible nuclear function. This includes the observation that nonsense mutation are linked to abnormal polyadenylation of Adh pre-mRNA in *Drosophila* (Brogna, 1999). Earlier studies also proposed that NMD thus occurs in

the nuclear fraction, or that the scanning of mRNAs occur while they are still associated with the nucleus before entering into the cytoplasm (Maquat and Carmichael, 2001; Urlaub et al., 1989). A recent study in mammalian cells also reported enrichment of the NMD factor UPF1 at transcription sites, further supporting the possibility of NMD occurring at the chromosomes. However, the association of UPF1 with these sites does not necessarily indicate the occurrence of NMD and therefore that translation is occurring there. There could be another function which is unrelated to NMD. Moreover, it has been also reported that UPF1 has a role in the replication of telomeres, which consequently aids in the stability of the genome (Azzalin, 2012). Therefore, it will be interesting to determine whether UPF1 recruitment at transcription sites occurs either with nascent RNA, DNA or with other proteins. This is an aspect that should be investigated further in the future to better understand the function of UPF1 at the chromosomes.

6.1.5 Transgenic reporter constructs provide an effective model to visualize splicing

The association of the EJC at transcription sites does not depend on the specific features of genes (intron-containing and intron-less), allowing me to further investigate its splicing independent association by using transgenic reporter constructs. In chapter five, I have described the experimental system that allows visualization of splicing at the transcription sites of *Drosophila* polytene chromosome. I have demonstrated that Adh-MS2 and a split Adh-MS2 reporter construct containing tagged with MS2 sequence and subsequently crossing with MCP-GFP or MCP-RFP lines is a preferable method to visualize nascent mRNA and splicing cotranscriptionally. Further, I also described a system that can be used to confirm that spliced or nascent MS2-mRNA corresponds to the transgenic reporter construct. MS2-GFP system considered as an appropriate method to localize and detect the reporter mRNA in

the cell and was successfully applied before (Querido and Chartrand, 2008). However, due to time constraints, this last stage of the project could not be completed. Future works involve crossing the *lacI* GFP transgenic lines with both intron containing (Adh-MS2) and intron-less transgenic reporters (available in Dr. Brogna lab). In parallel, staining of EJC proteins will allow further investigation of the mechanism of splicing-independent EJC deposition. However, this system can also be used in the future to investigate how pre-mRNP decoration is affected by splicing signals or how EJC protein recruitment is affected due to specific features of genes such as long or short introns.

6.2 Conclusion

My data demonstrate that EJC proteins, particularly eIF4AIII, associate with most of the transcription sites. However, the association was observed at both intron-containing and intron-less genes on polytene chromosomes. The binding patterns of Y14 and MAGO are similar, yet apparently different from that of eIF4AIII. Additionally, the association of EJC proteins with transcription sites seems to be RNase-insensitive, and that of Y14/MAGO shows no correlation with splicing markers or with nascent RNA. Chromatin immunoprecipitation coupled with high-throughput sequencing (ChIP-seq) indicates that the association of EJC protein peaks at transcription start sites in *Drosophila* cells. These observations are inconsistent both with constitutive splicing-dependent EJC deposition and with eIF4AII forming a stable complex with Y14 and MAGO in *Drosophila*; instead they suggest that eIF4AIII and Y14/MAGO have separate splicing-independent roles at transcription sites. Consistent with this prediction, RNAi of Y14/MAGO altered transcription induction of ecdysone responsive genes. My study also demonstrates that there are ribosomal proteins and functional ribosome at transcription sites, which further indicates translation

might be occurring at these sites. Although it is not clear yet whether translation at this sites produces functional proteins, will be an interesting question to investigate in future. I also observed that UPF1 is recruited at most of the transcription sites, suggesting that NMD can occur co-transcriptionally. Moreover, the MS2-GFP system I have described also can be used to study further splicing independent recruitment of EJC protein at transcription sites.

References

Abruzzi, K.C., Lacadie, S., and Rosbash, M. (2004). Biochemical analysis of TREX complex recruitment to intronless and intron-containing yeast genes. EMBO J *23*, 2620-2631.

Adelman, K., and Lis, J.T. (2012). Promoter-proximal pausing of RNA polymerase II: emerging roles in metazoans. Nature reviews Genetics *13*, 720-731.

Al-Jubran, K., Wen, J., Abdullahi, A., Roy Chaudhury, S., Li, M., Ramanathan, P., Matina, A., De, S., Piechocki, K., Rugjee, K.N., *et al.* (2013). Visualization of the joining of ribosomal subunits reveals the presence of 80S ribosomes in the nucleus. RNA *19*, 1669-1683.

Alexander, R.D., Innocente, S.A., Barrass, J.D., and Beggs, J.D. (2010). Splicing-dependent RNA polymerase pausing in yeast. Molecular cell *40*, 582-593.

Alexandrov, A., Colognori, D., Shu, M.D., and Steitz, J.A. (2012). Human spliceosomal protein CWC22 plays a role in coupling splicing to exon junction complex deposition and nonsense-mediated decay. Proc Natl Acad Sci U S A *109*, 21313-21318.

Amrani, N., Ganesan, R., Kervestin, S., Mangus, D.A., Ghosh, S., and Jacobson, A. (2004). A faux 3'-UTR promotes aberrant termination and triggers nonsense-mediated mRNA decay. Nature *432*, 112-118.

Ashton-Beaucage, D., Udell, C.M., Lavoie, H., Baril, C., Lefrancois, M., Chagnon, P., Gendron, P., Caron-Lizotte, O., Bonneil, E., Thibault, P., *et al.* (2010). The exon junction complex controls the splicing of MAPK and other long intron-containing transcripts in Drosophila. Cell *143*, 251-262.

Azzalin, C.M. (2012). UPF1: a leader at the end of chromosomes. Nucleus *3*, 16-21.

Baguet, A., Degot, S., Cougot, N., Bertrand, E., Chenard, M.P., Wendling, C., Kessler, P., Le Hir, H., Rio, M.C., and Tomasetto, C. (2007). The exon-junction-complex-component metastatic lymph node 51 functions in stress-granule assembly. J Cell Sci *120*, 2774-2784.

Ballut, L., Marchadier, B., Baguet, A., Tomasetto, C., Seraphin, B., and Le Hir, H. (2005). The exon junction core complex is locked onto RNA by inhibition of eIF4AIII ATPase activity. Nat Struct Mol Biol *12*, 861-869.

Barbosa, I., Haque, N., Fiorini, F., Barrandon, C., Tomasetto, C., Blanchette, M., and Le Hir, H. (2012). Human CWC22 escorts the helicase eIF4AIII to spliceosomes and promotes exon junction complex assembly. Nature structural & molecular biology *19*, 983-990.

Beelman, C.A., and Parker, R. (1995). Degradation of mRNA in eukaryotes. Cell *81*, 179-183.

Behm-Ansmant, I., Branlant, C., and Motorin, Y. (2007). The Saccharomyces cerevisiae Pus2 protein encoded by YGL063w ORF is a mitochondrial tRNA:Psi27/28-synthase. Rna *13*, 1641-1647.

Belgrader, P., Cheng, J., Zhou, X., Stephenson, L.S., and Maquat, L.E. (1994). Mammalian nonsense codons can be cis effectors of nuclear mRNA half-life. Molecular and cellular biology *14*, 8219-8228.

Berget, S.M., Moore, C., and Sharp, P.A. (2000). Spliced segments at the 5' terminus of adenovirus 2 late mRNA. 1977. Rev Med Virol *10*, 356-362; discussion 355-356.

Bessonov, S., Anokhina, M., Krasauskas, A., Golas, M.M., Sander, B., Will, C.L., Urlaub, H., Stark, H., and Luhrmann, R. (2010). Characterization of purified human Bact spliceosomal complexes reveals compositional and morphological changes during spliceosome activation and first step catalysis. Rna *16*, 2384-2403.

Beyer, A.L., and Osheim, Y.N. (1988). Splice site selection, rate of splicing, and alternative splicing on nascent transcripts. Genes & development *2*, 754-765.

Biyasheva, A., Do, T.V., Lu, Y., Vaskova, M., and Andres, A.J. (2001). Glue secretion in the Drosophila salivary gland: a model for steroid-regulated exocytosis. Developmental biology *231*, 234-251.

Bono, F., Cook, A.G., Grunwald, M., Ebert, J., and Conti, E. (2010). Nuclear import mechanism of the EJC component Mago-Y14 revealed by structural studies of importin 13. Molecular cell *37*, 211-222.

Bono, F., Ebert, J., Lorentzen, E., and Conti, E. (2006). The crystal structure of the exon junction complex reveals how it maintains a stable grip on mRNA. Cell *126*, 713-725.

Bono, F., and Gehring, N.H. (2011). Assembly, disassembly and recycling: the dynamics of exon junction complexes. RNA biology *8*, 24-29.

Brodsky, A.S., and Silver, P.A. (2000). Pre-mRNA processing factors are required for nuclear export. Rna *6*, 1737-1749.

Brogna, S. (1999). Nonsense mutations in the alcohol dehydrogenase gene of Drosophila melanogaster correlate with an abnormal 3' end processing of the corresponding pre-mRNA. Rna *5*, 562-573.

Brogna, S., Sato, T.A., and Rosbash, M. (2002). Ribosome components are associated with sites of transcription. Mol Cell *10*, 93-104.

Buratowski, S. (2009). Progression through the RNA polymerase II CTD cycle. Molecular cell *36*, 541-546.

Burtis, K.C., Thummel, C.S., Jones, C.W., Karim, F.D., and Hogness, D.S. (1990). The Drosophila 74EF early puff contains E74, a complex ecdysone-inducible gene that encodes two ets-related proteins. Cell *61*, 85-99.

Carrillo Oesterreich, F., Bieberstein, N., and Neugebauer, K.M. (2011). Pause locally, splice globally. Trends in cell biology *21*, 328-335.

Carrillo Oesterreich, F., Preibisch, S., and Neugebauer, K.M. (2010). Global analysis of nascent RNA reveals transcriptional pausing in terminal exons. Mol Cell, *4*, 571-581.

Carter, M.S., Li, S., and Wilkinson, M.F. (1996). A splicing-dependent regulatory mechanism that detects translation signals. EMBO J *15*, 5965-5975.

Chang, J.C., and Kan, Y.W. (1979). beta 0 thalassemia, a nonsense mutation in man. Proceedings of the National Academy of Sciences of the United States of America *76*, 2886-2889.

Chang, W.Y., Winegarden, N.A., Paraiso, J.P., Stevens, M.L., and Westwood, J.T. (2000). Visualization of nascent transcripts on Drosophila polytene chromosomes using BrUTP incorporation. BioTechniques *29*, 934-936.

Chang, Y.F., Imam, J.S., and Wilkinson, M.F. (2007). The nonsense-mediated decay RNA surveillance pathway. Annu Rev Biochem *76*, 51-74.

Chuang, T.W., Chang, W.L., Lee, K.M., and Tarn, W.Y. (2013). The RNA-binding protein Y14 inhibits mRNA decapping and modulates processing body formation. Mol Biol Cell *24*, 1-13.

Colgan, D.F., and Manley, J.L. (1997). Mechanism and regulation of mRNA polyadenylation. Genes & development *11*, 2755-2766.

Conti, E., and Izaurralde, E. (2005). Nonsense-mediated mRNA decay: molecular insights and mechanistic variations across species. Current opinion in cell biology *17*, 316-325.

Cui, Y., Hagan, K.W., Zhang, S., and Peltz, S.W. (1995). Identification and characterization of genes that are required for the accelerated degradation of mRNAs containing a premature translational termination codon. Genes & development *9*, 423-436.

Cummins, C.M., Gaber, R.F., Culbertson, M.R., Mann, R., and Fink, G.R. (1980). Frameshift suppression in Saccharomyces cerevisiae. III. Isolation and genetic properties of group III suppressors. Genetics *95*, 855-879.

Custodio, N., Carvalho, C., Condado, I., Antoniou, M., Blencowe, B.J., and Carmo-Fonseca, M. (2004). In vivo recruitment of exon junction complex proteins to transcription sites in mammalian cell nuclei. RNA *10*, 622-633.

Dahlberg, J., and Lund, E. (2012). Nuclear translation or nuclear peptidyl transferase? Nucleus *3*, 320-321.

Das, R., Dufu, K., Romney, B., Feldt, M., Elenko, M., and Reed, R. (2006). Functional coupling of RNAP II transcription to spliceosome assembly. Genes & development *20*, 1100-1109.

David, A., Dolan, B.P., Hickman, H.D., Knowlton, J.J., Clavarino, G., Pierre, P., Bennink, J.R., and Yewdell, J.W. (2012). Nuclear translation visualized by ribosome-bound nascent chain puromycylation. The Journal of cell biology *197*, 45-57.

de la Mata, M., Lafaille, C., and Kornblihtt, A.R. (2010). First come, first served revisited: factors affecting the same alternative splicing event have different effects on the relative rates of intron removal. Rna *16*, 904-912.

De, S., Varsally, W., Falciani, F., and Brogna, S. (2011). Ribosomal proteins' association with transcription sites peaks at tRNA genes in Schizosaccharomyces pombe. Rna *17*, 1713-1726.

de Turris, V., Nicholson, P., Orozco, R.Z., Singer, R.H., and Muhlemann, O. (2011). Cotranscriptional effect of a premature termination codon revealed by live-cell imaging. Rna *17*, 2094-2107.

Degot, S., Le Hir, H., Alpy, F., Kedinger, V., Stoll, I., Wendling, C., Seraphin, B., Rio, M.C., and Tomasetto, C. (2004). Association of the breast cancer protein MLN51 with the exon junction complex via its speckle localizer and RNA binding module. J Biol Chem *279*, 33702-33715.

Duffy, J.B. (2002). GAL4 system in Drosophila: a fly geneticist's Swiss army knife. Genesis *34*, 1-15.

Fribourg, S., Gatfield, D., Izaurralde, E., and Conti, E. (2003). A novel mode of RBD-protein recognition in the Y14-Mago complex. Nature structural biology *10*, 433-439.

Gatfield, D., Unterholzner, L., Ciccarelli, F.D., Bork, P., and Izaurralde, E. (2003). Nonsense-mediated mRNA decay in Drosophila: at the intersection of the yeast and mammalian pathways. EMBO J *22*, 3960-3970.

Gehring, N.H., Lamprinaki, S., Kulozik, A.E., and Hentze, M.W. (2009). Disassembly of exon junction complexes by PYM. Cell *137*, 536-548.

Ghosh, S., Obrdlik, A., Marchand, V., and Ephrussi, A. (2014). The EJC binding and dissociating activity of PYM is regulated in Drosophila. PLoS genetics *10*, e1004455.

Gornemann, J., Kotovic, K.M., Hujer, K., and Neugebauer, K.M. (2005). Cotranscriptional spliceosome assembly occurs in a stepwise fashion and requires the cap binding complex. Molecular cell *19*, 53-63.

Hachet, O., and Ephrussi, A. (2001). Drosophila Y14 shuttles to the posterior of the oocyte and is required for oskar mRNA transport. Current biology : CB *11*, 1666-1674.

Hall, S.L., and Padgett, R.A. (1996). Requirement of U12 snRNA for in vivo splicing of a minor class of eukaryotic nuclear pre-mRNA introns. Science *271*, 1716-1718

Hayashi, R., Handler, D., Ish-Horowicz, D., and Brennecke, J. (2014). The exon junction complex is required for definition and excision of neighboring introns in Drosophila. Genes & development *28*, 1772-1785.

Henderson, K.D., and Andrew, D.J. (2000). Regulation and function of Scr, exd, and hth in the Drosophila salivary gland. Developmental biology *217*, 362-374.

Hochstrasser, M., and Sedat, J.W. (1987). Three-dimensional organization of Drosophila melanogaster interphase nuclei. I. Tissue-specific aspects of polytene nuclear architecture. The Journal of cell biology *104*, 1455-1470.

Hui, J. (2009). Regulation of mammalian pre-mRNA splicing. Sci China C Life Sci *52*, 253-260.

Iborra, F.J., Jackson, D.A., and Cook, P.R. (2001). Coupled transcription and translation within nuclei of mammalian cells. Science *293*, 1139-1142.

Ishigaki, Y., Li, X., Serin, G., and Maquat, L.E. (2001). Evidence for a pioneer round of mRNA translation: mRNAs subject to nonsense-mediated decay in mammalian cells are bound by CBP80 and CBP20. Cell *106*, 607-617.

Ji, X., Zhou, Y., Pandit, S., Huang, J., Li, H., Lin, C.Y., Xiao, R., Burge, C.B., and Fu, X.D. (2013). SR proteins collaborate with 7SK and promoter-associated nascent RNA to release paused polymerase. Cell *153*, 855-868.

Johansen, K.M., Cai, W., Deng, H., Bao, X., Zhang, W., Girton, J., and Johansen, J. (2009). Polytene chromosome squash methods for studying transcription and epigenetic chromatin modification in Drosophila using antibodies. Methods *48*, 387-397.

Kadener, S., Cramer, P., Nogues, G., Cazalla, D., de la Mata, M., Fededa, J.P., Werbajh, S.E., Srebrow, A., and Kornblihtt, A.R. (2001). Antagonistic effects of T-Ag and VP16 reveal a role for RNA pol II elongation on alternative splicing. EMBO J *20*, 5759-5768.

Kataoka, N., Yong, J., Kim, V.N., Velazquez, F., Perkinson, R.A., Wang, F., and Dreyfuss, G. (2000). Pre-mRNA splicing imprints mRNA in the nucleus with a novel RNA-binding protein that persists in the cytoplasm. Mol Cell *6*, 673-682.

Khodor, Y.L., Menet, J.S., Tolan, M., and Rosbash, M. (2012). Cotranscriptional splicing efficiency differs dramatically between Drosophila and mouse. Rna *18*, 2174-2186.

Khodor, Y.L., Rodriguez, J., Abruzzi, K.C., Tang, C.H., Marr, M.T., 2nd, and Rosbash, M. (2011). Nascent-seq indicates widespread cotranscriptional pre-mRNA splicing in Drosophila. Genes & development *25*, 2502-2512.

Kim, V.N., Kataoka, N., and Dreyfuss, G. (2001). Role of the nonsense-mediated decay factor hUpf3 in the splicing-dependent exon-exon junction complex. Science *293*, 1832-1836.

Klinge, S., Voigts-Hoffmann, F., Leibundgut, M., and Ban, N. (2012). Atomic structures of the eukaryotic ribosome. Trends Biochem Sci *37*, 189-198.

Lakhotia, S.C., and Tapadia, M.G. (1998). Genetic mapping of the amide response element(s) of the hsr omega locus of Drosophila melanogaster. Chromosoma *107*, 127-135.

Lau, C.K., Diem, M.D., Dreyfuss, G., and Van Duyne, G.D. (2003). Structure of the Y14-Magoh core of the exon junction complex. Current biology : CB *13*, 933-941.

Le Hir, H., Gatfield, D., Izaurralde, E., and Moore, M.J. (2001). The exon-exon junction complex provides a binding platform for factors involved in mRNA export and nonsense-mediated mRNA decay. EMBO J *20*, 4987-4997.

Le Hir, H., Izaurralde, E., Maquat, L.E., and Moore, M.J. (2000a). The spliceosome deposits multiple proteins 20-24 nucleotides upstream of mRNA exon-exon junctions. EMBO J *19*, 6860-6869.

Le Hir, H., Moore, M.J., and Maquat, L.E. (2000b). Pre-mRNA splicing alters mRNP composition: evidence for stable association of proteins at exon-exon junctions. Genes & development *14*, 1098-1108.

Leeds, P., Peltz, S.W., Jacobson, A., and Culbertson, M.R. (1991). The product of the yeast UPF1 gene is required for rapid turnover of mRNAs containing a premature translational termination codon. Genes & development *5*, 2303-2314.

Leeds, P., Wood, J.M., Lee, B.S., and Culbertson, M.R. (1992). Gene products that promote mRNA turnover in Saccharomyces cerevisiae. Molecular and cellular biology *12*, 2165-2177.

Lejeune, F., Ishigaki, Y., Li, X., and Maquat, L.E. (2002). The exon junction complex is detected on CBP80-bound but not eIF4E-bound mRNA in mammalian cells: dynamics of mRNP remodeling. EMBO J *21*, 3536-3545.

LeMaire, M.F., and Thummel, C.S. (1990). Splicing precedes polyadenylation during Drosophila E74A transcription. Molecular and cellular biology *10*, 6059-6063.

Lin, S., and Fu, X.D. (2007). SR proteins and related factors in alternative splicing. Advances in experimental medicine and biology *623*, 107-122.

Lis, J.T., Neckameyer, W., Dubensky, R., and Costlow, N. (1981). Cloning and characterization of nine heat-shock-induced mRNAs of Drosophila melanogaster. Gene *15*, 67-80.

Macchi, P., Kroening, S., Palacios, I.M., Baldassa, S., Grunewald, B., Ambrosino, C., Goetze, B., Lupas, A., St Johnston, D., and Kiebler, M. (2003). Barentsz, a new component of the Staufen-containing ribonucleoprotein particles in mammalian cells, interacts with Staufen in an RNA-dependent manner. The Journal of neuroscience : the official journal of the Society for Neuroscience *23*, 5778-5788.

Maniatis, T., and Reed, R. (2002). An extensive network of coupling among gene expression machines. Nature *416*, 499-506.

Maquat, L.E., and Carmichael, G.G. (2001). Quality control of mRNA function. Cell *104*, 173-176.

Maquat, L.E., Tarn, W.Y., and Isken, O. (2010). The pioneer round of translation: features and functions. Cell *142*, 368-374.

Martin, R.M., Rino, J., Carvalho, C., Kirchhausen, T., and Carmo-Fonseca, M. (2013). Live-cell visualization of pre-mRNA splicing with single-molecule sensitivity. Cell reports *4*, 1144-1155.

Marygold, S.J., Roote, J., Reuter, G., Lambertsson, A., Ashburner, M., Millburn, G.H., Harrison, P.M., Yu, Z., Kenmochi, N., Kaufman, T.C., *et al.* (2007). The ribosomal protein genes and Minute loci of Drosophila melanogaster. Genome Biol *8*, R216.

Matsumoto, K., Wassarman, K.M., and Wolffe, A.P. (1998). Nuclear history of a pre-mRNA determines the translational activity of cytoplasmic mRNA. EMBO J *17*, 2107-2121.

Matunis, E.L., Matunis, M.J., and Dreyfuss, G. (1993). Association of individual hnRNP proteins and snRNPs with nascent transcripts. The Journal of cell biology *121*, 219-228.

McCracken, S., Fong, N., Yankulov, K., Ballantyne, S., Pan, G., Greenblatt, J., Patterson, S.D., Wickens, M., and Bentley, D.L. (1997). The C-terminal domain of RNA polymerase II couples mRNA processing to transcription. Nature *385*, 357-361.

Mohr, S.E., Dillon, S.T., and Boswell, R.E. (2001). The RNA-binding protein Tsunagi interacts with Mago Nashi to establish polarity and localize oskar mRNA during Drosophila oogenesis. Genes Dev *15*, 2886-2899.

Morin, X., Daneman, R., Zavortink, M., and Chia, W. (2001). A protein trap strategy to detect GFP-tagged proteins expressed from their endogenous loci in Drosophila. Proc Natl Acad Sci U S A *98*, 15050-15055.

Morris, D.P., and Greenleaf, A.L. (2000). The splicing factor, Prp40, binds the phosphorylated carboxyl-terminal domain of RNA polymerase II. J Biol Chem *275*, 39935-39943.

Muhlemann, O., Eberle, A.B., Stalder, L., and Zamudio Orozco, R. (2008). Recognition and elimination of nonsense mRNA. Biochim Biophys Acta *1779*, 538-549.

Nathanson, L., Xia, T., and Deutscher, M.P. (2003). Nuclear protein synthesis: a re-evaluation. Rna *9*, 9-13.

Neugebauer, K.M. (2002). On the importance of being co-transcriptional. J Cell Sci *115*, 3865-3871.

Nilsen, T.W. (2003). The spliceosome: the most complex macromolecular machine in the cell? Bioessays *25*, 1147-1149.

Nott, A., Le Hir, H., and Moore, M.J. (2004). Splicing enhances translation in mammalian cells: an additional function of the exon junction complex. Genes Dev *18*, 210-222.

O'Brien, T., Hardin, S., Greenleaf, A., and Lis, J.T. (1994). Phosphorylation of RNA polymerase II C-terminal domain and transcriptional elongation. Nature *370*, 75-77.

Ohbayashi, N., Taira, N., Kawakami, S., Togi, S., Sato, N., Ikeda, O., Kamitani, S., Muromoto, R., Sekine, Y., and Matsuda, T. (2008). An RNA biding protein, Y14 interacts with and modulates STAT3 activation. Biochem Biophys Res Commun *372*, 475-479.

Palacios, I.M., Gatfield, D., St Johnston, D., and Izaurralde, E. (2004). An eIF4AIII-containing complex required for mRNA localization and nonsense-mediated mRNA decay. Nature *427*, 753-757.

Parma, D.H., Bennett, P.E., Jr., and Boswell, R.E. (2007). Mago Nashi and Tsunagi/Y14, respectively, regulate Drosophila germline stem cell differentiation and oocyte specification. Developmental biology *308*, 507-519.

Perales, R., and Bentley, D. (2009). "Cotranscriptionality": the transcription elongation complex as a nexus for nuclear transactions. Molecular cell *36*, 178-191.

Perlick, H.A., Medghalchi, S.M., Spencer, F.A., Kendzior, R.J., Jr., and Dietz, H.C. (1996). Mammalian orthologues of a yeast regulator of nonsense transcript stability. Proceedings of the National Academy of Sciences of the United States of America *93*, 10928-10932.

Peterlin, B.M., and Price, D.H. (2006). Controlling the elongation phase of transcription with P-TEFb. Molecular cell *23*, 297-305.

Phatnani, H.P., and Greenleaf, A.L. (2006). Phosphorylation and functions of the RNA polymerase II CTD. Genes & development *20*, 2922-2936.

Proshkin, S., Rahmouni, A.R., Mironov, A., and Nudler, E. (2010). Cooperation between translating ribosomes and RNA polymerase in transcription elongation. Science *328*, 504-508.

Querido, E., and Chartrand, P. (2008). Using fluorescent proteins to study mRNA trafficking in living cells. Methods Cell Biol *85*, 273-292.

Roignant, J.Y., and Treisman, J.E. (2010). Exon junction complex subunits are required to splice Drosophila MAP kinase, a large heterochromatic gene. Cell *143*, 238-250.

Rugjee, K.N., Roy Chaudhury, S., Al-Jubran, K., Ramanathan, P., Matina, T., Wen, J., and Brogna, S. (2013). Fluorescent protein tagging confirms the presence of ribosomal proteins at Drosophila polytene chromosomes. PeerJ *1*, e15.

Ruiz-Echevarria, M.J., Gonzalez, C.I., and Peltz, S.W. (1998). Identifying the right stop: determining how the surveillance complex recognizes and degrades an aberrant mRNA. EMBO J *17*, 575-589.

Sauliere, J., Haque, N., Harms, S., Barbosa, I., Blanchette, M., and Le Hir, H. (2010). The exon junction complex differentially marks spliced junctions. Nature structural & molecular biology *17*, 1269-1271.

Sauliere, J., Murigneux, V., Wang, Z., Marquenet, E., Barbosa, I., Le Tonqueze, O., Audic, Y., Paillard, L., Roest Crollius, H., and Le Hir, H. (2012). CLIP-seq of eIF4AIII reveals transcriptome-wide mapping of the human exon junction complex. Nature structural & molecular biology *19*, 1124-1131.

Schmid, M., and Jensen, T.H. (2010). Nuclear quality control of RNA polymerase II transcripts. Wiley interdisciplinary reviews RNA *1*, 474-485.

Schneider, I. (1972). Cell lines derived from late embryonic stages of Drosophila melanogaster. Journal of embryology and experimental morphology *27*, 353-365.

Schroder, P.A., and Moore, M.J. (2005). Association of ribosomal proteins with nascent transcripts in S. cerevisiae. Rna *11*, 1521-1529.

Segraves, W.A., and Hogness, D.S. (1990). The E75 ecdysone-inducible gene responsible for the 75B early puff in Drosophila encodes two new members of the steroid receptor superfamily. Genes & development *4*, 204-219.

Sharma, S., Kohlstaedt, L.A., Damianov, A., Rio, D.C., and Black, D.L. (2008). Polypyrimidine tract binding protein controls the transition from exon definition to an intron defined spliceosome. Nature structural & molecular biology *15*, 183-191.

Shatkin, A.J., and Manley, J.L. (2000). The ends of the affair: capping and polyadenylation. Nature structural biology *7*, 838-842.

Shibuya, T., Tange, T.O., Sonenberg, N., and Moore, M.J. (2004). eIF4AIII binds spliced mRNA in the exon junction complex and is essential for nonsense-mediated decay. Nature structural & molecular biology *11*, 346-351.

Shuman, S. (2001). Structure, mechanism, and evolution of the mRNA capping apparatus. Prog Nucleic Acid Res Mol Biol *66*, 1-40.

Silver, D.L., Watkins-Chow, D.E., Schreck, K.C., Pierfelice, T.J., Larson, D.M., Burnetti, A.J., Liaw, H.J., Myung, K., Walsh, C.A., Gaiano, N., *et al.* (2010). The exon junction complex component Magoh controls brain size by regulating neural stem cell division. Nature neuroscience *13*, 551-558.

Singh, G., Kucukural, A., Cenik, C., Leszyk, J.D., Shaffer, S.A., Weng, Z., and Moore, M.J. (2012). The cellular EJC interactome reveals higher-order mRNP structure and an EJC-SR protein nexus. Cell *151*, 750-764.

Steckelberg, A.L., Boehm, V., Gromadzka, A.M., and Gehring, N.H. (2012). CWC22 connects pre-mRNA splicing and exon junction complex assembly. Cell reports *2*, 454-461.

Su, A.A., and Randau, L. (2011). A-to-I and C-to-U editing within transfer RNAs. Biochemistry (Mosc) *76*, 932-937.

Tange, T.O., Nott, A., and Moore, M.J. (2004). The ever-increasing complexities of the exon junction complex. Current opinion in cell biology *16*, 279-284.

Truman, J.W., and Riddiford, L.M. (2002). Endocrine insights into the evolution of metamorphosis in insects. Annu Rev Entomol *47*, 467-500.

Tscherne, J.S., and Pestka, S. (1975). Inhibition of protein synthesis in intact HeLa cells. Antimicrob Agents Chemother *8*, 479-487.

Urlaub, G., Mitchell, P.J., Ciudad, C.J., and Chasin, L.A. (1989). Nonsense mutations in the dihydrofolate reductase gene affect RNA processing. Mol Cell Biol *9*, 2868-2880.

Wang, J., Chang, Y.F., Hamilton, J.I., and Wilkinson, M.F. (2002). Nonsense-associated altered splicing: a frame-dependent response distinct from nonsense-mediated decay. Molecular cell *10*, 951-957.

Wang, Z., Murigneux, V., and Le Hir, H. (2014). Transcriptome-wide modulation of splicing by the exon junction complex. Genome Biol *15*, 551

Warner, J.R., and McIntosh, K.B. (2009). How common are extraribosomal functions of ribosomal proteins? Mol Cell *34*, 3-11.

Weil, T.T., Parton, R.M., and Davis, I. (2010). Making the message clear: visualizing mRNA localization. Trends Cell Biol *20*, 380-390.

Wilkinson, M.F., and Shyu, A.B. (2002). RNA surveillance by nuclear scanning? Nat Cell Biol *4*, E144-147.

Will, C.L., and Luhrmann, R. (2001). Spliceosomal UsnRNP biogenesis, structure and function. Curr Opin Cell Biol *13*, 290-301.

Yarmolinsky, M.B., and Haba, G.L. (1959). Inhibition by Puromycin of Amino Acid Incorporation into Protein. Proc Natl Acad Sci U S A *45*, 1721-1729.

Zhang, J., Sun, X., Qian, Y., LaDuca, J.P., and Maquat, L.E. (1998). At least one intron is required for the nonsense-mediated decay of triosephosphate isomerase mRNA: a possible link between nuclear splicing and cytoplasmic translation. Molecular and cellular biology *18*, 5272-5283.

Zhou, Z., Licklider, L.J., Gygi, S.P., and Reed, R. (2002). Comprehensive proteomic analysis of the human spliceosome. Nature *419*, 182-185.

Appendices

Appendix I

Protocol for ChIP

1. Grow the S2 cells in a complete medium for two days to get a $10x10^6$ cells.

2. Started with $10x10^6$ S2 cells.

3. Mix, and add formaldehyde (10%) to 1% v/v final concentration.

4. Incubate at 25^0C for 15 minutes.

5. Add glycine to 125mM and mix incubate 5 min at 25°C.

6. Centrifuge 3000 rpm/ 835 g (Eppendorf) 5 min at 4°C in a benchtop centrifuge

7. Remove supernatant.

8. Resuspend in 500 µl of 1X PBS + 1X Protease inhibitors (Roche EDTA free mini protease inhibitor).

9. Repeat 2X.

10. Remove supernatant and store as cell pellet at -80^0C.

11. The day before the ChIP prepare antibody coated Dynal beads (Protein-G for rabbit IgG). Resuspend beads by gentle vortexing. Per ChIP prepares 40 µl of beads. Split into two tubes, 25 µl for ChIP (+Ab) and 15 µl for pre-absorb (-Ab). Wash beads in a low-bind tube 4x with 1 ml of 1XPBS, 5mg/ml BSA. Wash the beads in a magnetic rack by moving 6 times each. Pull-down beads using magnetic rack and discard supernatant completely.

12. After the final wash resuspend the beads in 500 all of 1XPBS, 5mg/ml BSA. Leave Pre-absorb (-Ab) beads as its. To antibody coated beads add at least 2 µg of antibody.

13. Incubate ChIP (+Ab), and pre-absorb (-Ab) beads overnight at 4°C on a

Rotator.

14. On the day of the ChIP. Thaw cells on ice. Resuspend cell pellets in 100 µl

Of SDS Lysis Buffer. Sonicate at high intensity for 12 min with 15 Sec on/off.

15. Dilute sample to 1 ml using ChIP dilution buffer.

16. Centrifuge at 13000 rpm/ 15682 g (Eppendorf) for 10 minutes in a microcentrifuge at 18°C (NB. SDS will precipitate at 4°C) to the pellet insoluble material.

17. Remove supernatant to a fresh DNA lobind tube.

18. While sonication is being performed, wash ChIP (+Ab), and pre-absorb (-Ab) beads. Pellet in a magnetic rack and wash with 1 ml of 1XPBS, 5mg/ml BSA 4 times to remove unbound antibody. During the wash mix it properly by vortex and spin briefly. Resuspend beads finally in 40 µl of 1 ml of 1XPBS, 5mg/ml BSA.

19. Pre-absorb (-Ab) beads slurry resuspend in a 25 µl of 1 ml of 1XPBS, 5mg/ml BSA. And add to the soluble chromatin prepared in 17.

20. Incubate 15 min at R.T by using a rotating rotator.

21. Spin briefly and Pellet beads using magnetic rack and transfer cleared supernatant to a fresh lobind tube.

22. Remove 100 µl of soluble chromatin from 21 to use as input sample. Reserve in a lobind tube in -20°C.

23. To remaining chromatin add 40 µl ChIP (+Ab) bead slurry from step 18.

24. Incubate 2.30 hrs at room temperature, on a rotator to form immune complexes on beads.

25. Spin briefly and Pull-down beads on magnetic rack and discard supernatant.

26. Wash 5 minutes each on rotating rotor at R.T with 1 ml of the following. During the wash mix it properly by vortex and spin briefly. Wash the beads in a magnetic rack by moving 6 times each and discard the supernatant.

26.1 Low salt wash-1x

26.2 High salt wash-1x

26.3 LiCl wash-1x

27. Then wash twice with 1 ml of TE buffer.

28. Elute protein-DNA complexes by two washes with 75 µl of freshly prepared 1% v/v SDS 0.1M NaHC03 solution. Vortex, spin and then incubate at RT in a rotating rotor for 15 min. Spin briefly and put on magnetic rack, transfer the supernatant on to new lobind tubes. Repeat the above process again with 75 µl of elution buffer so the total volume at the end 150 µl.

29. Combine the elutes.

30. To the input DNA reserved in step 22 add 50 µl of elution buffer (28) to make an equal volume with chip sample (150 µl).

31. Add protease K to all samples (2 µl of 50 mg/ml) including input and Chip sample and incubate at 65°C on the dry heat block overnight to digest protein and reverse crosslinks.

32. The following morning purifies DNA using AMPure XP beads (both the input and chip sample). Basically add 1.8volumes of AMPure XP bead slurry to DNA. Mix it properly by vortexing. Allow Bind for 10 minutes in rotating rotor at RT, spin briefly and then pellet beads in a magnetic rack and discard the supernatant. Wash 3X with 300 µl of freshly prepared 70% v/v ethanol, each time vortex, spin it puts on magnetic rack and rotate 6 times and discard the supernatant. After the final wash, spin it again and put on a magnetic rack to make sure there is no ethanol. Air-dry in the magnetic stand until the beads are dry and show visible cracking. Elute DNA using 30 µl of 10 mM Tris (8.0). Transfer elute 3 times into new lobind tubes by placing in magnetic rack to remove magnetic beads completely.

33. Use DNA in SOLiD library preparation procedure.

Standard Protocol for Salivary glands squashing and immunostaining

1. *D. melaonogaster* larvae were grown at 18^0C in bottles containing dry yeast.

2. Larvae were collected from bottles and placed in a dissecting glass dish filled with water to wash and put them on ice to sleep for 5 minutes.

3. Larvae were then dissected in a dissection buffer of 20µl solutions A, using sharp tweezers. For the fixation, salivary glands were transferred in a 20µl of solution B and kept for 1 minute.

4. Salivary glands were washed in 20µl solutions G for a few seconds and then transfer to siliconized glass coverslip containing 13µl solutions G. Glands were allowed to incubate in solution G for 3 minutes.

5. After that frozen end microscopic slide touch on the top of the coverslip and make sure that liquid evenly spread throughout the coverslip and slide.

6. Salivary glands were first spread with the blunt tip of the brush by tapping a few times on top of the coverslip. After that folded tissue paper kept on top of coverslip and squashed vertically using the thumb.

7. Check the spreading of the polytene chromosome by placing under the phase contrast microscope.

8. The position of the coverslip marked by diamond pencil on both sides of the coverslip and the sample were freeze on the slide by dipping into liquid nitrogen for 60 seconds.

9. Coverslip were removed from the slide using a razor blade and then put in a coplin jar filled with 95% ethanol and stored at -20°C for next day immunostaining.

10. Next day polytene chromosome spread slides were first washed in a coplin jar with 1X TBST (150 Mm NaCl, 10 mM Tris-Cl pH 7.0-7.5, 0.05% v/v Tween) two times for 10 minutes each at room temperature.

11.Slides were transferred in a coplin jar filled with blocking solution TBS, 10% Fetal Bovine Serum (FBS) and 0.05% v/w sodium azide (NaN3) for 30 minutes at room temperature.

12. Primary antibody diluted (1: 100, depend on the concentration of antibody) with blocking solution and proceed for immunostaining.

13. 20µl drops of diluted antibody put on the coverslip and the slides were touch on top of the drop carefully make sure there was no air bubbles between the slide and coverslip.

14. Humid chamber was made by TBS and slides were then placed in a humid chamber and incubate overnight at 4^0C.

15. Next day morning slides were removed from the chamber and placed in a beaker with TBST to displace the coverslip from slide. Slides were then washed with TBST two times 10 minutes each at room temperature.

16. Secondary antibody staining was carried out in a same way as primary antibody but the dilution of secondary antibody was (1: 250) with blocking solution and incubated at room temperature for 1 hour in a humid chamber.

17. Slides were first washed with TBST containing DAPI (1: 10,000 dilutions) 0.1 µg /ml to stain DNA followed by a second wash with TBST for 10 minutes.

18. Slides were dried in a room temperature about 20 minutes, and covered with aluminium foil to protect from light.

19. Once the slides were dried out, a drop of mountaining medium were places on the coverslip and carefully touch with the dried slides on top of mountaining medium.

20. Slides were now ready to examine in fluorescence microscope or kept at 4^0C.

Appendix II

List of Primers

Code	Name	Sequence
S38	Y14 RNAi F	**TTAATACGACTCACTATAGGGGAGA**CG ATGTGTTGGACATTGACA
S39	Y14 RNAi R	**TTAATACGACTCACTATAGGGGAGA**GA CGCTTTTCGGACTTTTT
S40	MAGO RNAi F	**TTAATACGACTCACTATAGGGGAGA**CA CGGAGGACTTTTACCTAC
S41	MAGO RNAi R	**TTAATACGACTCACTATAGGGGAGA**AT ATGGGCTTGATCTTGAAATG
S42	eIF4AIII RNAi F	**TTAATACGACTCACTATAGGGGAGA**GA CGAATTGACACTGGAAGG
S43	eIF4AIII RNAi R	**TTAATACGACTCACTATAGGGGAGA**AG AATATTAGTTTAGATCAAGTCAG
S50	74EF Sense	TGGTGCAGGGAATGATAGCCATTG
S51	74EF Anti-sense	GGGCACCTTTCTGCATCCGAATTT
S52	75B Sense	TCGCATCACCTGGCCATTTAGACA
S53	75B Anti-Sense	CTGTGAGTTCACCAAGGAGAAGGT
S54	BR-C Sense	TCTTAAGGAAGGACTGCAGGGACT
S55	BR-C Anti-Sense	AGATGGACGACACACAGCACTTCT
S 78	Y14 left	ATTGACAATGCGGAGGAGTTCGAGG
S 79	Y14 Right	CGGTGCTTCGCCTTTTCCTTCAG

S 80	MAGO Left	CGTGATGGAAGAACTGAAGCGAATCA
S 81	MAGO Right	TCGAGGTGGTGAACGAGATGTGC
S 86	RpL41 Forward	CTAAATGCACAGCGACGGAT
S 87	RpL41 Reverse	CTGCGCTTACTTGGACCTTG
S 88	RpL10Ab Forward	ATGCACAGCGACGGATTC
S 89	RpL10Ab Reverse	CTAGTAAAGACGCTGGGGC
S 90	RpS9034 Forward	CGGATTCGCGCTATTTAGAAAG
S 91	RpS9034 Reverse	AGTCTGCGCCATGTATTTGTC

Appendix III

List of Fly stocks

ID name	Lines	Origin
FKH- GAL4	Fork head -GAL4	Brogna Lab
Double Balancer stock	w+; IF; MKRS Cyo; TM6B	Hidalgo Lab
S-240 MCP-GFP , ID-7278	P{w[+mC]=Hsp83-MCP-GFP}11, y[1] w[*]	Bloomington Drosophila Stock Center
S-241 MCP-GFP ID-7279	y[1] w[*]; P{w[+mC]=Hsp83-MCP-GFP}5A	Bloomington Drosophila Stock Center
S-242 MCP-GFP ID-7280	y[1] w[*]; P{w[+mC]=Hsp83-MCP-GFP}3	Bloomington Drosophila Stock Center
S-243 MCP-RFP ID-27418	y[1] w[*]; P{w[+mC]=UAS-MCP-RFP}8A	Bloomington Drosophila Stock Center
S-244 MCP-RFP ID-27419	y[1] w[*]; P{w[+mC]=UAS-MCP-RFP}12A	Bloomington Drosophila Stock Center
S-245 MCP-RFP ID-9939	y[1] w[67c23]; P{w[+mC]=Hsp83-MCP-RFP}12a/TM3, Sb[1]	Bloomington Drosophila Stock Center
S-246 MCP-RFP ID-9940	y[1] w[67c23]; P{w[+mC]=Hsp83-MCP-RFP}4a/CyO	Bloomington Drosophila Stock Center
S-247 RpS9 ID-115034	w[1118]; PBac{602.P.SVS-1}RpS9[CPTI000493]	DGRC, Kyoto stock centre
S-249 RPpL41 ID-115344	w[1118]; PBac{754.P.FSVS-0}RpL41[CPTI002881]	DGRC, Kyoto stock centre

S-250 RpL10Ab ID-115462	w[1118]; PBac{802.P.SVS-2}RpL10Ab[CPTI003957]	DGRC, Kyoto stock centre
S-251 RpS9 ID-115504	w[1118]; PBac{602.P.SVS-1}RpS9[CPTI000785]	DGRC, Kyoto stock centre
S-253 pUAST-Y14/TM3	8069-14.2- pUAST-Y14/TM3 C-terminal 2X HA and 2X Flag tag	Marco Blanchette
S-254 pUAST-Y14/TM3	8069-14.3- pUAST-Y14/TM3 C-terminal 2X HA and 2X Flag tag	Marco Blanchette
S-259 pUAST-eIF4AIII/TM3	8069-13.4- pUAST-eIF4AIII/TM3 C-terminal 2X HA and 2X Flag tag	Marco Blanchette
S-260 pUAST-eIF4AIII/TM3	8069-13.5- pUAST-eIF4AIII/TM3 C-terminal 2X HA and 2X Flag tag	Marco Blanchette
S-308 Upf1 RNAi	y[1] v[1]; P{y[+t7.7] v[+t1.8]=TRiP.GL01485}attP2	Bloomington Drosophila Stock Center (FBgn0030354)
S-310 Y14 RNAi, ID-36024	(w1118; P{GD14025}v36024)	VDRC RNAi stock centre
S-311 eIF4AIII RNAi, ID-108580	(P{KK101462}VIE-260B)	VDRC RNAi stock centre
S-252 Mago RNAi, ID-28132	w[1118]; P{GD12556}v28132	VDRC RNAi stock centre
S-305 Y14 RNAi, ID-36585	y[1] sc[*] v[1]; P{y[+t7.7] v[+t1.8]=TRiP.GL00545}attP2	Bloomington Drosophila Stock Center
S-306 Mago RNAi, ID-35453	y[1] sc[*] v[1]; P{y[+t7.7] v[+t1.8]=TRiP.GL00378}attP2	Bloomington Drosophila Stock Center
S-307 eIF4AIII RNAi, ID-32444	y[1] sc[*] v[1]; P{y[+t7.7] v[+t1.8]=TRiP.HMS00442}attP2	Bloomington Drosophila Stock Center
S-308 UPF1 RNAi, ID 43144	y[1] v[1]; P{y[+t7.7] v[+t1.8]=TRiP.GL01485}attP2	Bloomington Drosophila

		Stock Center
lac O (S-133)	P [W^+= Lac O repeat] (E2)	Brogna Lab
lac I-GFP (S-205)	6(4.1)/CyO hsp83::Gfp-lacI	J.Vasquez
Lac I-GFP (S-206)	6(4:1)/ Cyo hsp83.GFP-lac I	J.Vasquez
MIN-4 (S-118)	ERE-Adh1-MS2	Brogna Lab
Split MS2 (S-90)	ERE-Adh1-split MS2 (K_{15}-M_7)	Brogna Lab

Appendix IV

List of plasmid

Name	**Description**	**Origin**
UPF1-GFP (B 306)	pAGW.N-termGFP.UPF1	Brogna lab
FLAG/HA-Y14	pUAST-attB-Y14-2XHF	Marco Blanchette
FLAG/HA-eIF4AIII	pUAST-attB-eIF4A3-2XHF	Marco Blanchette

Appendix V

DNA sequencing and BLAT search were matched with tagging construct of RpL41-YFP and RpL10Ab-YFP and RpS9-YFP (034)

RpL41 (DNA sequence)

ANCATATTTCNGAATGCATGCGTCAATTTTACGCAGACTATCTTTCTAGGGTTAAACGCGAGTGAA
CAACAACTAACAGTGATTTTTATCGTTTGCAGTGGCGTAAGAAGCGTATGCGTAGGTTGAAGCGTA
AGCGCAGAAAGATGCGTGCAAGGTCCAAGTAAGCGCAG

BLAST

Drosophila melanogaster ribosomal protein L41 (RpL41), mRNA

Sequence ID: ref|NM_001014551.3| **Length:** 320 **Number of Matches:** 1

Range 1: 54 to 127 GenBank Graphics ▼ Next Match ▲ Previous Match

Score	Expect	Identities	Gaps	Strand
137 bits(74)	4e-29	74/74(100%)	0/74(0%)	Plus/Plus

```
Query  80   AGTGGCGTAAGAAGCGTATGCGTAGGTTGAAGCGTAAGCGCAGAAAGATGCGTGCAAGGT  139
           ||||||||||||||||||||||||||||||||||||||||||||||||||||||||||||
Sbjct  54   AGTGGCGTAAGAAGCGTATGCGTAGGTTGAAGCGTAAGCGCAGAAAGATGCGTGCAAGGT  113

Query  140  CCAAGTAAGCGCAG  153
           ||||||||||||||
Sbjct  114  CCAAGTAAGCGCAG  127
```

RpL10Ab (DNA sequence)

GCATGCGNCATTTTACGCAGACTATCTTTCTAGGGTTAATATGTAAAAGAAAGCAACTAAACATTG
GGTACATTAATGAAATTTGAATTCTAAGCGATCCTGTGATCAGTGGCAATCAGAAACCAGCTTTTT
AGACCTTTTCCATGTCCATATCAGTTTGGAAATGATTGCAAAAGAAAAACGTGGTTTTATGTGCCA
AATAAGCAACTAATATGTGGGCTGCCTTCATTTGCGCATTAGTCCGACAGTCAAAAAAAGATAAA
CAGCCAATGCTTGCAGTGTTCATTTGCCTTCCATTTGTTTGATAATTGGTTCAATCTTGCAGGTCGA
AGGTTTCGCGTGATACGCTGTATGAGGGCGTCAATGGACTCCTGGAGGCTTCGGCGAAGAAGAAG
CGCGGCTTCCTCGAGACGGTGGAACTGCAGATCGGCCTGAAGAACTACGATCCCCAGAAGGACAA
GCGTTTCTCCGGCACCGTCAAGTACGTTGGCTAAGTCACCTGCGCACGTGCTTGGATAGAAGCTCC
CATGGGAGTTGAGTTCATCACGTCATCAGGTAGTCGAGGACATGTGGCTGTCACATCTCGACGGAC
CTGCACTCAGGGTCTTTAAAATTTGAGTAGGTCTCCAGCAATGGACACCGAACCCCCATTTTCTTA
ATAACTATGAAAACGTGCTCCTCTGAGAGCCTTGTAAGTTTTCCATGAGGCCCCACTTATATCTAC
ATCTATTTGAATCCACAAAGCACTGGCTAATTTATGGTTACTTTCTTGTCATCCCACAGGTTGAAGC
ACATTCCTCGTCCCAAGATGAAGGTGTGCATCCTTGGCGATCAGCAGCATTGCGACGAAGCCAAG
GCCAACAACGTCGACNTCATGGATGCCGAGGCTCTGAAGAAGCTGAACAAGAACAAGAAGCTGGT
GAAGAAGCTGGCCAAGTCCTATGATGCCTTCCTGGCCTCTGAGTCGCTGATCAAGCAGATTCCTCG
TTTGCTTGGCCCTGGCTTGAACAAGGCCGGCAAGTTCCCTGCCCTGCTGTCGCATCAGGAGTCTAT
GATTGGCAAGATCGANGNGGTTAAGTCGACCATCAAGTTCCAGATGAANAAGGTGCTCTGCCTGT
CCGTCGCCGTCGGCCACGTTGGCATGAAGTCCGANNANCTTGCCCAAAACGTCAACTTGTCGATCA
ACTTCTTNGGTGTCCCNTT

BLAST

Drosophila melanogaster ribosomal protein L10Ab (RpL10Ab), transcript variant F, mRNA

Sequence ID: ref|NM_168480.2| **Length:** 960 **Number of Matches:** 1

Range 1: 41 to 408 GenBank Graphics ▼ Next Match ▲ Previous Match

Score	Expect	Identities	Gaps	Strand
680 bits(368)	0.0	368/368(100%)	0/368(0%)	Plus/Plus

```
Query  163  GTCGAAGGTTTCGCGTGATACGCTGTATGAGGGCGTCAATGGACTCCTGGAGGCTTCGGC  222
            ||||||||||||||||||||||||||||||||||||||||||||||||||||||||||||
Sbjct  41   GTCGAAGGTTTCGCGTGATACGCTGTATGAGGGCGTCAATGGACTCCTGGAGGCTTCGGC  100

Query  223  GAAGAAGAAGCGCGGCTTCCTCGAGACGGTGGAACTGCAGATCGGCCTGAAGAACTACGA  282
            ||||||||||||||||||||||||||||||||||||||||||||||||||||||||||||
Sbjct  101  GAAGAAGAAGCGCGGCTTCCTCGAGACGGTGGAACTGCAGATCGGCCTGAAGAACTACGA  160

Query  283  TCCCCAGAAGGACAAGCGTTTCTCCGGCACCGTCAAGTACGTTGGCTAAGTCACCTGCGC  342
            ||||||||||||||||||||||||||||||||||||||||||||||||||||||||||||
Sbjct  161  TCCCCAGAAGGACAAGCGTTTCTCCGGCACCGTCAAGTACGTTGGCTAAGTCACCTGCGC  220

Query  343  ACGTGCTTGGATAGAAGCTCCCATGGGAGTTGAGTTCATCACGTCATCAGGTAGTCGAGG  402
            ||||||||||||||||||||||||||||||||||||||||||||||||||||||||||||
Sbjct  221  ACGTGCTTGGATAGAAGCTCCCATGGGAGTTGAGTTCATCACGTCATCAGGTAGTCGAGG  280

Query  403  ACATGTGGCTGTCACATCTCGACGGACCTGCACTCAGGGTCTTTAAAATTTGAGTAGGTC  462
            ||||||||||||||||||||||||||||||||||||||||||||||||||||||||||||
Sbjct  281  ACATGTGGCTGTCACATCTCGACGGACCTGCACTCAGGGTCTTTAAAATTTGAGTAGGTC  340

Query  463  TCCAGCAATGGACACCGAACCCCCATTTTCTTAATAACTATGAAAACGTGCTCCTCTGAG  522
            ||||||||||||||||||||||||||||||||||||||||||||||||||||||||||||
Sbjct  341  TCCAGCAATGGACACCGAACCCCCATTTTCTTAATAACTATGAAAACGTGCTCCTCTGAG  400

Query  523  AGCCTTGT  530
            ||||||||
Sbjct  401  AGCCTTGT  408
```

RpS9 (034) (DNA sequence)

GCGTCATTTNANGCAGACTATCTTTCTAGGGTTAAATGTCTAGACAGTATGTATATGCGAAGGAAG
TTCGACTGCATAATCCAATTAGTTGCCCTGACCTGATGAACTGTATTAAAAAATATATTCTGACAC
TTCTTGTCTGATAAAATACGTTGACGTTAACAAATACACACTGAAGAGAATTCTTCGCTAGAACTA
GCGATTGCATTTTGAAACTTCCATTGATTGTGTACCCATTTTACCCACAGGTAATGCCCTGCTGCGC
CGTCTGGTCCGTATCGGTGTCCTGGACGAGTCCCGCATGAAGCTCGATTACGTGCTGGGTCTGAAG
ATTGAGGACTTCTTGGAGCGTCGTCTGCAGACGCAGGTGTTCAAGCTGGGACTTGCCAAGTCCATC
CATCATGCTCGCGTCCTGATCCGTCAGCGTCACATTCGGTAAATATCGCTTGGACAGGCGACAACA
TCGTCGCCAGGCTCTCTCAGATATAAACTCTGTTCTGTTCAGTAAGACCACTTGGGAGTCGAACAG
GCGCCAATGCTTGTACCGACTCTCAACGTCTGTAGATTGCGCATGTGACTCCGTTCACACCAATCG
AAAATGCAAAATGCCCGCCTAGCGTAAGTTGCACTGAACGTTTTTTGTTGAACCCAACATACATAG
CAGCCACCATTCCGATGGTTATCATAAAGCAGAGCTTAACTAATCCAAATATGGTGTTCTTCTTCC
GTTTGTTTTCACAGTGTCCGCAAGCAGGTGGTCAACATCCCGTCGTTCGTCGTGCGCCTGGACTCCC
AGAAGCACATCGACTTCTCCCTGAAGTCGCCCTTCGGCGGCGGCCGTCCCGGTCGCGTCAAGAGG
AAGAACCTGAAGAAGAACCAGGGCGGTGGCGGTGGAGCTGCTGAAGAGGAGGAGGACTAAGCAG
TGGTAGCCAGCTGTAGCCAAGACAA

BLAST

Drosophila melanogaster ribosomal protein S9 (RpS9), transcript variant E, mRNA

Sequence ID: ref|NM_001300079.1| **Length:** 803 **Number of Matches:** 2

Range 1: 437 to 644 GenBank Graphics ▼ Next Match ▲ Previous Match

Score	Expect	Identities	Gaps	Strand
385 bits(208)	1e-102	208/208(100%)	0/208(0%)	Plus/Plus

```
Query  714  GTGTCCGCAAGCAGGTGGTCAACATCCCGTCGTTCGTCGTGCGCCTGGACTCCCAGAAGC  773
            ||||||||||||||||||||||||||||||||||||||||||||||||||||||||||||
Sbjct  437  GTGTCCGCAAGCAGGTGGTCAACATCCCGTCGTTCGTCGTGCGCCTGGACTCCCAGAAGC  496

Query  774  ACATCGACTTCTCCCTGAAGTCGCCCTTCGGCGGCGGCCGTCCCGGTCGCGTCAAGAGGA  833
            ||||||||||||||||||||||||||||||||||||||||||||||||||||||||||||
Sbjct  497  ACATCGACTTCTCCCTGAAGTCGCCCTTCGGCGGCGGCCGTCCCGGTCGCGTCAAGAGGA  556

Query  834  AGAACCTGAAGAAGAACCAGGGCGGTGGCGGTGGAGCTGCTGAAGAGGAGGAGGACTAAG  893
            ||||||||||||||||||||||||||||||||||||||||||||||||||||||||||||
Sbjct  557  AGAACCTGAAGAAGAACCAGGGCGGTGGCGGTGGAGCTGCTGAAGAGGAGGAGGACTAAG  616

Query  894  CAGTGGTAGCCAGCTGTAGCCAAGACAA  921
            ||||||||||||||||||||||||||||
Sbjct  617  CAGTGGTAGCCAGCTGTAGCCAAGACAA  644
```

Appendix VI

None of the UPF2 monoclonal antibodies could recognize UPF2 protein by Western blotting

The 15 ascites samples corresponding to hybridoma against the 12 UPF2 epitopes (see Appendix VII (B) for the list of all ascites and clone ID number) were tested by Western blotting as before. Unlike for the UPF1 antibodies, none of the ascites samples detected a band of the size expected for UPF2, and some give extensive background (see figure below). All clones were renamed to distinguish from each other like UPF1 based on their lane number in Western blot from UPF2-1 to UPF2-15. It was therefore decided not to proceed with UPF2 with further purification or testing.

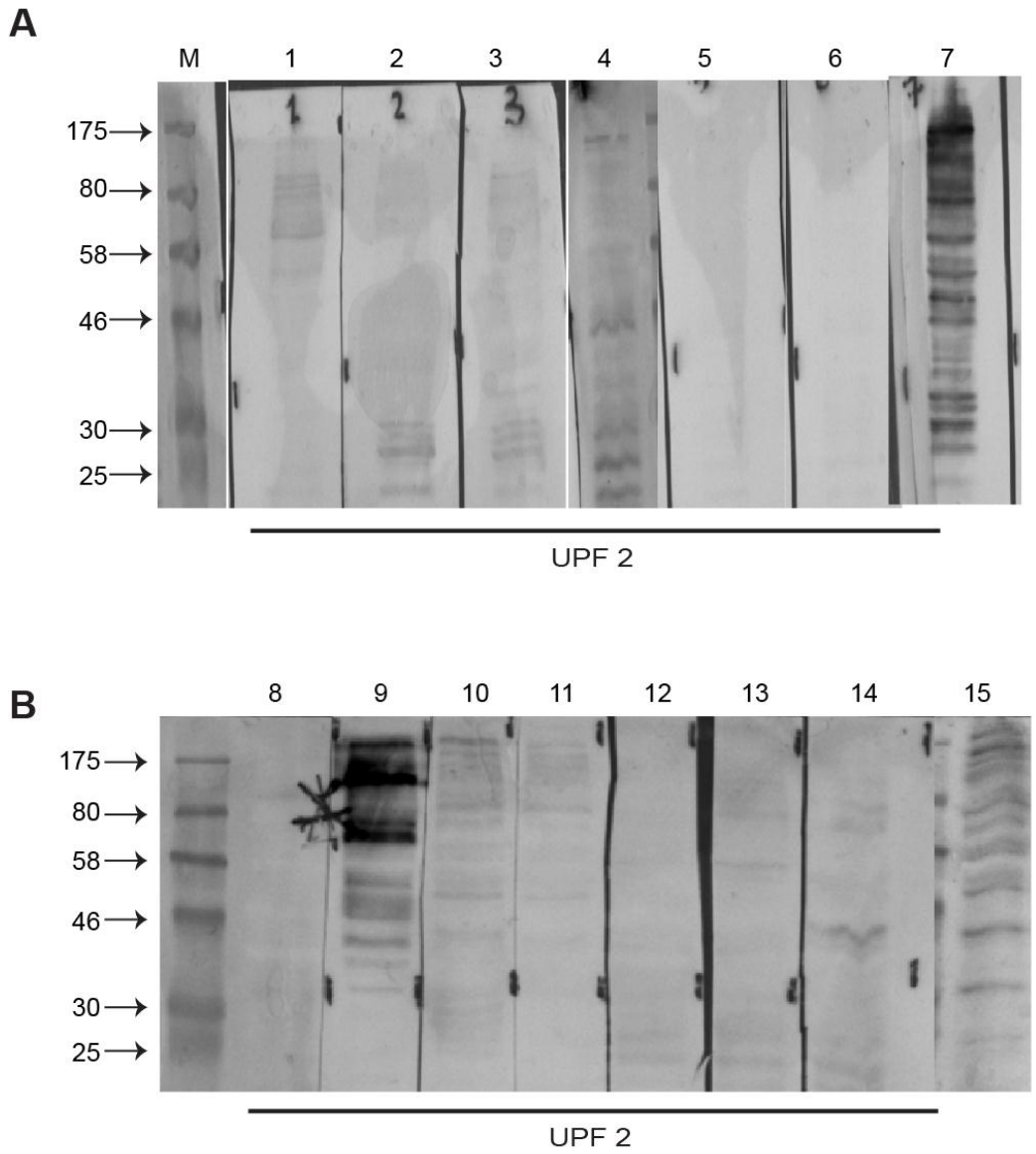

Western blot of S2 cell extract to test the specificity of each clone correspond to endogenous UPF2

(A) & (B) S2 cell extract immunoblot with UPF2-1 to UPF2-15 ascites, in which none of the clones able to detect the right molecular size (140.08 kDa) against the endogenous UPF2. All the ascites shows much background signal in the Western blot.

Appendix VII

(A) List of UPF1 Ascites

Project ID	Target protein	Product name	Ig type	Antibody type	Company
10108-1	UPF1-1	10108-1-1M1/1C13-2_121113	Mouse IgG Monoclonal	Ascites	Abmart Inc
10108-1	UPF1-2	10108-1-1M1/1B16-1_121113	Mouse IgG Monoclonal	Ascites	Abmart Inc
10108-1	UPF1-3	10108-1-7M1/7D17-11_121114	Mouse IgG Monoclonal	Ascites	Abmart Inc
10108-1	UPF1-4	10108-1-1M1/1I23-2_121113	Mouse IgG Monoclonal	Ascites	Abmart Inc
10108-1	UPF1-5	10108-1-7M1/7F3-11_121113	Mouse IgG Monoclonal	Ascites	Abmart Inc
10108-1	UPF1-6	10108-1-3M1/3B21-6_121113	Mouse IgG Monoclonal	Ascites	Abmart Inc
10108-1	UPF1-7	10108-1-1M1/1E23-2_121113	Mouse IgG Monoclonal	Ascites	Abmart Inc
10108-1	UPF1-8	10108-1-1M1/1D7-1_121113	Mouse IgG Monoclonal	Ascites	Abmart Inc
10108-1	UPF1-9	10108-1-3M1/3M14-6_121113	Mouse IgG Monoclonal	Ascites	Abmart Inc
10108-1	UPF1-10	10108-1-5M1/5F1-8_121115	Mouse IgG Monoclonal	Ascites	Abmart Inc
10108-1	UPF1-11	10108-1-1M1/1A21-2_121117	Mouse IgG Monoclonal	Ascites	Abmart Inc
10108-1	UPF1-12	10108-1-5M1/5I1-9_121119	Mouse IgG Monoclonal	Ascites	Abmart Inc
10108-1	UPF1-13	10108-1-1M1/1F16-1_121119	Mouse IgG Monoclonal	Ascites	Abmart Inc
10108-1	UPF1-14	10108-1-1M1/1C23-2_121119	Mouse IgG Monoclonal	Ascites	Abmart Inc
10108-1	UPF1-15	10108-1-1M1/1G20-	Mouse IgG Monoclonal	Ascites	Abmart Inc

		1_121119			
10108-1	UPF1-16	10108-1-7M1/7B12-12_121120	Mouse IgG Monoclonal	Ascites	Abmart Inc
10108-1	UPF1-17	10108-1-3M1/3E22-5_121120	Mouse IgG Monoclonal	Ascites	Abmart Inc
10108-1	UPF1-18	10108-1-7M1/7I4-11_121129	Mouse IgG Monoclonal	Ascites	Abmart Inc

(B) List of UPF2 Ascites

Project ID	Target protein	Product name	Ig type	Antibody type	Company
10109-1	UPF2-1	10109-1-1M1/1D4-2_121113	Mouse IgG Monoclonal	Ascites	Abmart Inc
10109-1	UPF2-2	10109-1-7M1/7K13-12_121113	Mouse IgG Monoclonal	Ascites	Abmart Inc
10109-1	UPF2-3	10109-1-5M1/5J4-9_121113	Mouse IgG Monoclonal	Ascites	Abmart Inc
10109-1	UPF2-4	10109-1-5M1/5N18-7_121113	Mouse IgG Monoclonal	Ascites	Abmart Inc
10109-1	UPF2-5	10109-1-7M1/7M2-12_121114	Mouse IgG Monoclonal	Ascites	Abmart Inc
10109-1	UPF2-6	10109-1-7M1/7K5-12_121114	Mouse IgG Monoclonal	Ascites	Abmart Inc
10109-1	UPF2-7	10109-1-5M1/5A5-8_121113	Mouse IgG Monoclonal	Ascites	Abmart Inc
10109-1	UPF2-8	10109-1-7M1/7E12-11_121113	Mouse IgG Monoclonal	Ascites	Abmart Inc
10109-1	UPF2-9	10109-1-7M1/7O6-11_121115	Mouse IgG Monoclonal	Ascites	Abmart Inc
10109-1	UPF2-10	10109-1-1M1/1M14-2_121115	Mouse IgG Monoclonal	Ascites	Abmart Inc
10109-1	UPF2-11	10109-1-1M1/1P22-2_121119	Mouse IgG Monoclonal	Ascites	Abmart Inc
10109-1	UPF2-12	10109-1-7M1/7H1-12_121119	Mouse IgG Monoclonal	Ascites	Abmart Inc
10109-1	UPF2-13	10109-1-7M1/7H21-12_121120	Mouse IgG Monoclonal	Ascites	Abmart Inc
10109-1	UPF2-14	10109-1-	Mouse IgG	Ascites	Abmart Inc

		5M1/5H2-8_121123	Monoclonal		
10109-1	UPF2-15	10109-1-1M1/1K7-2_121202	Mouse IgG Monoclonal	Ascites	Abmart Inc

Appendix VIII

Y14 ChIP-seq genes list (top 20 based on their Wig peak height)

flanking genes within 300bp upstream and downstream	wig peak height
MED30|Rev1	704
klar|klar|CG17180	492
roX1|roX1	468
bocksbeutel|bocksbeutel|CG8312	462
Kul	456
S|ast|S	400
Bsg|Bsg|Bsg|Bsg	400
eEF1delta|eEF1delta	385
Vti1	383
CG8498	382
vlc|vlc|vlc|vlc|vlc	378
CG33967	371
RpL23A	363
mad2	361
CG16903|Unc-76|Unc-76	356
RpL15|RpL15|RpL15|RpL15	337
CG34200	335
cue|Psa|Psa|Psa|Psa|Psa	330
RpL3|CG6693|RpL3|RpL3	330

Appendix IX

Published articles

1. Rugjee, K.N., **Roy Chaudhury, S.**, Al-Jubran, K., Ramanathan, P., Matina, T., Wen, J., and Brogna, S. (2013). Fluorescent protein tagging confirms the presence of ribosomal proteins at Drosophila polytene chromosomes. PeerJ *1*, e15.

2. Al-Jubran, K., Wen, J., Abdullahi, A., **Roy Chaudhury, S.**, Li, M., Ramanathan, P., Matina, A., De, S., Piechocki, K., Rugjee, K.N., *et al.* (2013). Visualization of the joining of ribosomal subunits reveals the presence of 80S ribosomes in the nucleus. RNA *19*, 1669-1683.